frontiers | Research Topics

Crustose coralline red algae frameworks and rhodoliths: Past and present

Edited by
Ana Cristina Rebelo, Sebastian Teichert, Valentina Alice Bracchi, Michael Rasser and Daniela Basso

Published in
Frontiers in Earth Science
Frontiers in Marine Science

ISSN 1664-8714
ISBN 978-2-83251-024-7
DOI 10.3389/978-2-83251-024-7

About Frontiers

Frontiers is more than just an open access publisher of scholarly articles: it is a pioneering approach to the world of academia, radically improving the way scholarly research is managed. The grand vision of Frontiers is a world where all people have an equal opportunity to seek, share and generate knowledge. Frontiers provides immediate and permanent online open access to all its publications, but this alone is not enough to realize our grand goals.

Frontiers journal series

The Frontiers journal series is a multi-tier and interdisciplinary set of open-access, online journals, promising a paradigm shift from the current review, selection and dissemination processes in academic publishing. All Frontiers journals are driven by researchers for researchers; therefore, they constitute a service to the scholarly community. At the same time, the *Frontiers journal series* operates on a revolutionary invention, the tiered publishing system, initially addressing specific communities of scholars, and gradually climbing up to broader public understanding, thus serving the interests of the lay society, too.

Dedication to quality

Each Frontiers article is a landmark of the highest quality, thanks to genuinely collaborative interactions between authors and review editors, who include some of the world's best academicians. Research must be certified by peers before entering a stream of knowledge that may eventually reach the public - and shape society; therefore, Frontiers only applies the most rigorous and unbiased reviews. Frontiers revolutionizes research publishing by freely delivering the most outstanding research, evaluated with no bias from both the academic and social point of view. By applying the most advanced information technologies, Frontiers is catapulting scholarly publishing into a new generation.

What are Frontiers Research Topics?

Frontiers Research Topics are very popular trademarks of the *Frontiers journals series*: they are collections of at least ten articles, all centered on a particular subject. With their unique mix of varied contributions from Original Research to Review Articles, Frontiers Research Topics unify the most influential researchers, the latest key findings and historical advances in a hot research area.

Find out more on how to host your own Frontiers Research Topic or contribute to one as an author by contacting the Frontiers editorial office: frontiersin.org/about/contact

Crustose coralline red algae frameworks and rhodoliths: Past and present

Topic editors

Ana Cristina Rebelo — Instituto Hidrográfico, Portugal
Sebastian Teichert — Friedrich-Alexander-Universität Erlangen-Nürnberg, Germany
Valentina Alice Bracchi — University of Milano-Bicocca, Italy
Michael Rasser — Staatliches Museum für Naturkunde Stuttgart, Germany
Daniela Basso — University of Milano-Bicocca, Italy

Citation

Rebelo, A. C., Teichert, S., Bracchi, V. A., Rasser, M., Basso, D., eds. (2022). *Crustose coralline red algae frameworks and rhodoliths: Past and present*.
Lausanne: Frontiers Media SA. doi: 10.3389/978-2-83251-024-7

Table of contents

frontiers | Frontiers in Earth Science

TYPE Editorial
PUBLISHED 28 November 2022
DOI 10.3389/feart.2022.1090091

OPEN ACCESS

EDITED AND REVIEWED BY
Bruce S. Lieberman,
University of Kansas, United States

*CORRESPONDENCE
Ana Cristina Rebelo,
acfurtadorebelo@gmail.com

SPECIALTY SECTION
This article was submitted to Paleontology, a section of the journal Frontiers in Earth Science

RECEIVED 04 November 2022
ACCEPTED 21 November 2022
PUBLISHED 28 November 2022

CITATION
Rebelo AC, Teichert S, Bracchi VA, Rasser MW and Basso D (2022), Editorial: Crustose coralline red algae frameworks and rhodoliths: Past and present.
Front. Earth Sci. 10:1090091.
doi: 10.3389/feart.2022.1090091

Editorial: Crustose coralline red algae frameworks and rhodoliths: Past and present

Ana Cristina Rebelo[1,2,3,4,5]*, Sebastian Teichert[6], Valentina A. Bracchi[7], Michael W. Rasser[5] and Daniela Basso[7]

[1]Divisão De Geologia Marinha, Instituto Hidrográfico, Lisboa, Portugal, [2]CIBIO–Centro De Investigação Em Biodiversidade e Recursos Genéticos, InBio Laboratório Associado, Ponta Delgada, Portugal, [3]BIOPOLIS–Program in Genomics, Biodiversity and Land Planning, CIBIO, Vairão, Portugal, [4]MPB–Marine Palaeontology and Biogeography Lab, University of the Azores, Ponta Delgada, Portugal, [5]SMNS–Staatliches Museum für Naturkunde Stuttgart, Stuttgart, Germany, [6]GeoZentrum Nordbayern, Department Geographie und Geowissenschaften, Naturwissenschaften Fakultät, Friedrich-Alexander-Universität Erlangen-Nürnberg, Erlangen, Germany, [7]Department of Earth and Environmental Sciences, University of Milano-Bicocca, Milano, Italy

KEYWORDS

calcareous algae, algal lithofacies, bioconstructions, palaeobiogeography, palaeoenvironments, maerl, coralline framework, ecosystem engineers

Editorial on the Research Topic
Crustose coralline red algae frameworks and rhodoliths: Past and present

Crustose Coralline red Algae (CCA) have a long and vast fossil record and continue to be significant components in recent ecosystems (Bosence, 1983). They can produce extensive carbonate sediments, either as simple crusts, free-living forms known as rhodoliths, as entire reef frameworks, or on break down, as coralline algal sands and gravels (Bosence, 1983; Rasser and Piller, 2004; Basso and Granier, 2012). CCA are autogenic ecosystem engineers, providing living space for other organisms, particularly in areas where other habitat providers, such as corals, are lacking. At microscopic scale CCA build crusts and branches providing substratum for microborers, encrusters and several other invertebrates. At macroscopic scale they form successive crusts as well as rhodoliths and their accretions, providing shelter for larger invertebrates and vertebrates, such as nurseries for fishes (Steneck, 1986; Foster, 2001). Furthermore, at a megascale CCA can form entire reef bodies, rhodolith beds and maerl megadunes, controlling extensive marine areas (Adey, 1986; Steneck, 1986; Rasser and Piller, 2004; Bracchi et al., 2015). The longevity of CCA, together with their ecological restrictions and plasticity of growth-forms in relation to environmental parameters, makes them excellent ecological indicators for recent and palaeo-environments (Bosence, 1991; Basso, 1998; Barattolo et al., 2007 and references therein). Regardless of the abundance and ecological importance in time and space, CCA frameworks and rhodoliths are still poorly understood.

Several subjects are covered by the nine research articles of this Research Topic which add greatly to advance our scientific knowledge on CCA.

Abundance and richness of the macrofauna (>500 μm) associated with a rhodolith bed at Isla del Coco National Park in Costa Rica was studied by Solano-Barquero et al. This study showed that moderate aggregation in rhodolith beds favours a greater diversity of associated taxa, as the different physical aggregation levels and morphological characteristic variation of the rhodoliths influence the faunal communities. This adds evidence to the role of rhodolith beds in providing background heterogeneity suitable for a myriad of organisms. Solano-Barquero et al. manifest the importance of rhodolith beds for biodiversity and highlight the need to preserve such ecologically relevant habitats.

Another assessment of rhodolith diversity was done by Richards et al. on the Northwestern Gulf of Mexico, including the description of a new species of *Sporolithon* (Sporolithales, Rhodophyta) and three new species of *Roseolithon* (Hapalidiales, Rhodophyta). The northwestern Gulf of Mexico is a hotspot for CCA and this study stresses the continuation of assessment in the identification and description of new species which are of critical importance to conservation efforts in the region.

Mills et al. provide an update of the CCA diversity of Guam (Mariana Islands) based on a recent DNA barcoding effort where taxa is compared to 1) the most current species inventories for Guam based on morphological identifications and 2) similar floristic accounts of CCA from other regions. Phenotypic plasticity and convergent morphologies of corallines complicate taxonomic identification. For this reason CCA have often been overlooked by phycologists and ecologists, despite their abundance and ecological importance on reefs. This study contributes to a better understanding of Guam's CCA diversity and highlights the importance of DNA-based identification in examining corallines.

Rebelo et al. report on the distribution of rhodolith-forming species and consider the factors controlling rhodolith beds around the shores of Fuerteventura Island (Canary Islands, Spain). Their study adds to a better understanding of insular rhodolith formation and deposition. They also highlight the importance of preserving rhodolith beds as biodiversity hotspots and call for a conscientious effort in the protection and maintenance of these valuable biological resources.

In the Mediterranean, Del Río et al. give a detailed analysis of the structure and morphospecies composition of a shallow rhodolith bed at Punta de la Mona, Granada (southern Spain). The rhodolith bed extends for 16,000 square meters from 9 to 24 m water depth in oligotrophic waters off Almuñecar in the Alborán Sea. While *Lithophyllum incrustans* and *Lithophyllum dentatum* dominate at shallow depths (9–12 m), *Lithothamnion valens* is the dominant species at intermediate and greater depths. This study also contradicts the common assumption in the geological literature that rhodolith beds are indicative of oligophotic environments with high nutrient levels.

Continuing in the Mediterranean, Bracchi et al. use image analysis and computed axial tomography to distinguish and quantify the different components both on the surface and inside of a Coralligenous framework. Coralligenous (reefs made of red algae) are considered the most important ecosystems in the Mediterranean Sea due to their extent, complexity, and heterogeneity, supporting very high levels of biodiversity. Their study confirms the primary role of CCA as major builders in the Mediterranean and also confirms matching evidence from the Quaternary fossil record. Their study also emphasizes the importance of monitoring, maintenance, and restoration.

Basso et al. assess the contribution of calcareous autogenic engineers to the present-day Ligurian Coralligenous on rocky walls vs. sub-horizontal substrates, to define its age and mean accumulation rate, and to explore the response of Coralligenous structural composition and major calcareous bio-engineers to Holocene climate and oceanographic changes recorded in the build-ups. Our knowledge on Coralligenous accumulation rate and age, although very fragmentary, suggests that present-day exposed algal build-ups require thousands of years to form, depending on favourable combinations of carbonate precipitation by algal engineers, persistence of compatible oceanographic conditions, and sedimentation rate, in turn controlled by the overarching geological setting. The correct temporal and spatial frame has important implications for our understanding of the history and fate of marine temperate/cold biogenic habitats under ongoing human impacts, ocean warming, and acidification (Basso et al.).

Moving on to the fossil rhodoliths Braga and Aguirre describe a cross-bedded rhodolith limestone, up to 20 m thick, which forms a mesa on which the Roman town of Acinipo was settled. This limestone is part of the infill of the Ronda Basin, a Neogene basin at the southern margin of the Atlantic-linked Guadalquivir Basin in southern Spain. This study shows how rhodoliths grew on submarine dunes in a sheltered bay episodically affected by storms.

Lastly, a study on fossil rhodoliths and coralline algal debris by Aguirre and Braga examines the Serravallian limestones at the southern margin of the Guadalquivir Basin that crop out in the vicinity of Jimena, Bedmar, and Jódar (Jaén Province, SE Spain). The coralline algae are major biotic components in these carbonates, occurring in densely packed rhodolith beds and as dispersed fragments together with other bioclasts. Here rhodoliths and coralline algal debris are preserved *in situ* or very close to their growth habitats (autochthonous–parautochthonous assemblages) and also as reworked remains (allochthonous assemblages).

This study is a key to understand the significance of this type of deposit in carbonate production within the western Mediterranean.

In summary, this Research Topic focuses on the diverse scientific questions on the crustose coralline red algae frameworks and rhodoliths through different time slices, the factors controlling species distribution and the reconstruction of their palaeoenvironments. The research developed in this Research Topic helps advance on scientific knowledge of CCA and their sensitivity to ecological parameters.

Author contributions

All authors listed have made a substantial, direct, and intellectual contribution to the work and approved it for publication.

Funding

AR was supported by a Post-doctoral grant SFRH/BPD/117810/2016 from the Portuguese Science Foundation (FCT) and project NORTE-01-0246-FEDER-000063, supported by Norte Portugal Regional Operational Programme (NORTE2020), under the PORTUGAL 2020 Partnership Agreement, through the European Regional Development Fund (ERDF).

Acknowledgments

We thank all the contributing authors, reviewers, editors and the Frontiers in Marine Science Editorial staff for their support in producing this Research Topic. AR acknowledges research support from National Funds through FCT - Foundation for Science and Technology under the project UIDB/50027/2020 and through DRCT under the project ACORES-01-0145_FEDER-000078 - VRPROTO: Virtual Reality PROTOtype: the geological history of "Pedra-que-pica, and under DRCTM1.1.a/005/ 519 Funcionamento-C-/2016 (CIBIOA) project. DB and VB acknowledge the research funding provided by MIUR FISR2019-04543.

Conflict of interest

The authors declare that the research was conducted in the absence of any commercial or financial relationships that could be construed as a potential conflict of interest.

Publisher's note

All claims expressed in this article are solely those of the authors and do not necessarily represent those of their affiliated organizations, or those of the publisher, the editors and the reviewers. Any product that may be evaluated in this article, or claim that may be made by its manufacturer, is not guaranteed or endorsed by the publisher.

References

Adey, W. H. (1986). "Coralline algae as indicators of sea-level," in *Sea-level research*. Editor O. van de Plassche (Dordrecht: Springer). doi:10.1007/978-94-009-4215-8_9

Barattolo, F., Bassi, D., and Romano, R. (2007). Upper Eocene larger foraminiferal–coralline algal facies from the Klokova Mountain (southern continental Greece). *Facies* 53, 361–375. doi:10.1007/s10347-007-0108-2

Basso, D., and Granier, B. (2012). Calcareous algae and global change: from identification to quantification/Algues calcaires et changement global : de l'identification à la quantification. *Geodiversitas* 34 (1), 1–12. Available at: https://sciencepress.mnhn.fr/en/periodiques/geodiversitas/34/1

Basso, D. (1998). Deep rhodolith distribution in the pontian Islands, Italy: A model for the paleoecology of a temperate sea. *Palaeogeogr. Palaeoclimatol. Palaeoecol.* 137, 173–187. doi:10.1016/s0031-0182(97)00099-0

Bosence, D. W. J. (1983). Coralline algae from the miocene of Malta. *Palaeontology* 26, 147–173.

Bosence, D. W. J. (1991). Coralline algae: mineralization, taxonomy, and palaeoecology," in *Calcareous Algae and Stromatolites*. Editor R. Riding. Berlin, Heidelberg: Springer doi:10.1007/978-3-642-52335-9_5

Bracchi, V., Savini, A., Marchese, F., Palamara, S., Basso, D., and Corselli, C. (2015). Coralligenous habitat in the Mediterranean Sea: A geomorphological description from remote data. *Italian J. Geosci.* 134, 32–40. doi:10.3301/ijg.2014.16

Foster, M. S. (2001). Rhodoliths: between rocks and soft places. *J. Phycol.* 37, 659–667. doi:10.1046/j.1529-8817.2001.00195.x

Rasser, M. W., and Piller, W. E. (2004). Crustose algal frameworks from the eocene alpine foreland. *Palaeogeogr. Palaeoclimatol. Palaeoecol.* 206, 21–39. doi:10.1016/j.palaeo.2003.12.018

Steneck, R. S. (1986). The ecology of coralline algal crusts: convergent patterns and adaptative strategies. *Annu. Rev. Ecol. Syst.* 17, 273–303. doi:10.1146/annurev.es.17.110186.001421

frontiers | Frontiers in Marine Science

ORIGINAL RESEARCH
published: 25 April 2022
doi: 10.3389/fmars.2022.858416

Macrofauna Associated With a Rhodolith Bed at an Oceanic Island in the Eastern Tropical Pacific (Isla del Coco National Park, Costa Rica)

Alberto Solano-Barquero[1,2†], *Jeffrey A. Sibaja-Cordero*[1,3†] *and Jorge Cortés*[1,3*†]

[1] Centro de Investigación en Ciencias del Mar y Limnología (CIMAR), Universidad de Costa Rica, San José, Costa Rica,
[2] Departamento de Parasitología, Facultad de Microbiología, Universidad de Costa Rica, San José, Costa Rica,
[3] Escuela de Biología, Universidad de Costa Rica, San José, Costa Rica

OPEN ACCESS

Edited by:
Ana Cristina Rebelo, Instituto Hidrográfico, Portugal

Reviewed by:
Scott Gabara, University of Alaska System, United States
Guilherme Henrique Pereira-Filho, Universidade Federal de São Paulo, Brazil

***Correspondence:**
Jorge Cortés
jorge.cortes@ucr.ac.cr

†ORCID:
Alberto Solano-Barquero
orcid.org/0000-0002-8800-1205
Jeffrey A. Sibaja-Cordero
orcid.org/0000-0001-5323-356X
Jorge Cortés
orcid.org/0000-0001-7004-8649

Specialty section:
This article was submitted to Marine Ecosystem Ecology, a section of the journal Frontiers in Marine Science

Received: *19 January 2022*
Accepted: *18 March 2022*
Published: *25 April 2022*

Citation:
Solano-Barquero A, Sibaja-Cordero JA and Cortés J (2022) Macrofauna Associated With a Rhodolith Bed at an Oceanic Island in the Eastern Tropical Pacific (Isla del Coco National Park, Costa Rica). Front. Mar. Sci. 9:858416. doi: 10.3389/fmars.2022.858416

Rhodoliths are round calcareous red algae that form extensive beds and associated with them are a diverse suite of species. Rhodolith beds are among the least known coastal–marine ecosystems, and even less is understood about their associated flora and fauna. Here, we present an evaluation of the biodiversity larger than 500 μm associated with rhodoliths at Isla del Coco National Park, Costa Rica, an oceanic island in the Eastern Tropical Pacific, 500 km offshore of the mainland. This research determined the influence of rhodolith degree of aggregation (distance among individual rhodolith) as well as rhodolith complexity, volume, and mass in relation to the diversity, composition, and biomass of the associated fauna. A total of 145 taxa were collected in 60 rhodolith samples. Arthropods, polychaetes, and mollusks were the dominant taxa in terms of richness, and crustaceans + acari represented >50% of the total abundance. Five potentially new species were collected in this study. Collections identified 31 new records, with 20 of them being newly reported genera for Isla del Coco. Many of the organisms found were juveniles as well as adult stages bearing eggs, demonstrating the importance of this ecosystem. The faunal composition changed along the gradient of rhodolith aggregation. Moderately aggregated rhodoliths (separated by 5 to 10 cm) had the highest diversity, with the highest averages of taxon richness and total numerical abundance and the highest faunal biomass. There were more organisms in more complex rhodoliths; nevertheless, the complexity of the rhodolith did not affect the number of taxa or total organism biomass. Larger rhodoliths, in size and mass, favored higher amounts of taxa and organisms. The rhodolith bed studied is an example of the intermediate disturbance hypothesis because the highest value of biodiversity of invertebrates was at the moderate aggregation level of rhodoliths. In this density of rhodoliths, the fauna was less exposed to hard environmental conditions and prevented dominant species.

Keywords: rhodoliths, intermediate disturbance, epifauna, red algae, aggregation effects

INTRODUCTION

Rhodolith bed-forming algae are considered habitat modifiers or "bioengineering species" since they provide three-dimensional shelter for recruits as well as refuge and foraging habitat for a diversity of species (Riosmena-Rodríguez and Medina-López, 2010). Live rhodoliths can sustain a higher richness of invertebrate species than dead rhodoliths or coarse-grained (sand–gravel) sediment habitats (De Grave and Whitaker, 1999; Steller et al., 2003; Riosmena-Rodríguez et al., 2017; Stelzer et al., 2021). Rhodoliths are also biodiversity hotspots of micro- and macroalgae and are important for the establishment and maintenance of biodiversity (Fredericq et al., 2019; Stelzer et al., 2021). Rhodoliths influence the density and diversity of the sediments by providing carbonate material and organic matter (Stelzer et al., 2021).

Multiple authors have identified the fragility of the rhodolith-dominated ecosystems (Steller et al., 2003; Gabara et al., 2018). Rhodolith beds can be disturbed by a myriad of factors. Human activity, rhodolith bed characteristics (nodule density, nodule size, depth, trapped sediment), macroalgal epiphytism, and the presence of other ecosystem engineers have been described as drivers of the rhodolith-associated macrofauna (Steller et al., 2003; Veras et al., 2020; Sánchez-Latorre et al., 2020; Stelzer et al., 2021).

Rhodoliths form extensive beds between 15 and 35 m depth and have been observed as deep as 90 m at Isla del Coco National Park in Costa Rica (Cortés, 2016). There is a need for better understanding rhodolith beds as faunal habitat at Isla del Coco, because of the known fragility of these ecosystems and their importance for the maintenance of marine biodiversity. The primary goal of the present study was to determine the abundance and richness of fauna, greater than 500 μm, associated with a rhodolith bed at an oceanic island in the Eastern Tropical Pacific Ocean (Isla del Coco, Costa Rica). The secondary goal was to test if rhodolith bed structure, based on the degree of aggregation of rhodoliths, affected the diversity, abundance, richness, composition, and biomass of the associated fauna. The final goal was to determine if the structure of each rhodolith (complexity, volume, and mass) was associated with species richness, abundance, and composition of organisms that inhabit them.

MATERIALS AND METHODS

Collection Site

Sampling was conducted at around 20 m depth off Punta Ulloa in Isla del Coco National Park, Costa Rica, during May of 2008 (**Figure 1**). This oceanic island is located about 500 km off the Central American coast in the Eastern Tropical Pacific (Cortés, 2012). The island has a diversity of shallow subtidal habitats including coral reef, rock outcrop and boulder–cobble, coarse sand, and rhodolith beds (Cortés, 2016). The bottom at the site of the study consisted mainly of coarse sand with isolated, hard substrates and coral colonies. The rhodolith bed from which the samples were taken extends for several hundred meters. More dispersed rhodoliths are found in the border of the sampling area, closest to the coast, followed by a zone with aggregated rhodoliths, separated by 5 to 10 cm, and an area of several hundred meters with rhodoliths highly aggregated (**Figure 1**).

Sampling Methods and Sample Processing

Sixty rhodoliths and their associated fauna were collected from the rhodolith bed. The rhodoliths to be collected were chosen based on three spatial distribution categories. Twenty were

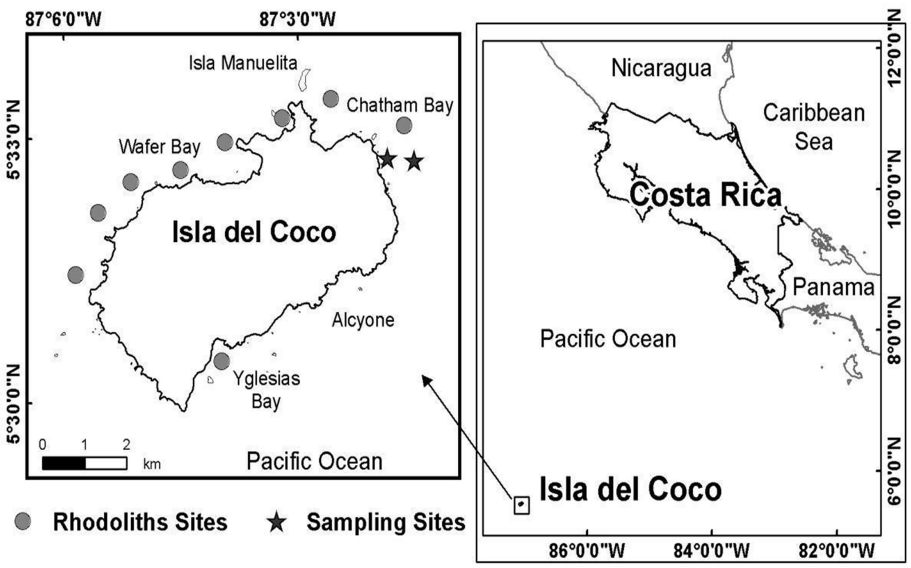

FIGURE 1 | Isla del Coco, Costa Rica (Eastern Tropical Pacific). Circles are rhodolith beds and the stars correspond to the rhodolith bed sampled (two areas: one with more dispersed rhodoliths nearest to the coastline and the other with more grouped rhodoliths).

highly aggregated rhodoliths (in direct contact with each other), and these were extracted one from each of the 20 points separated at least 1 m one from each other, all of them within an area of 50 m^2; 20 moderately aggregated rhodoliths (separated by 5 to 10 cm one from another) were extracted from each of the 20 patches meeting that definition of separation along a transect of about 150 m; and 20 other rhodoliths were extracted from each of the 20 isolated patches (rhodoliths were separated more than 10 cm one from another) along a transect of about 150 m. During scuba dives, samples were carefully collected by hand and placed individually in plastic bags (no sediments). They were washed in a 500-µm sieve in the laboratory to retain benthic fauna that could be easily extracted from the rhodolith by a thorough, albeit superficial, mechanical washing. This process extracted most of the vagile fauna, those organisms with the ability to move from one site to another on their own, such as wandering polychaetes, arthropods, most mollusks, echinoderms, and some of the fish caught in internal crevices in rhodolith nodules. After that, each rhodolith was thoroughly examined in search for sessile individuals and vagile organisms kept trapped between the branches or crevices of the rhodolith nodules to pick them up directly from each rhodolith, very carefully, using tweezers. Subsequently, the elements of the macrofauna found attached to the rhodolith nodule were counted. This included sessile hydrozoans, anemones, ascidian tunicates, bryozoans, and sponges. Rhodolith nodule-attached hydrozoans, bryozoans, and sponges, all of which present a modular growth, were counted as single units (one colonial unit counted as "one individual") to prevent counting the same organism more than once. When fragments of each morphotype of any of the organisms were found in the material retained in the sieve, if the same morphotype was not present yet attached to the rhodolith (e.g., sponges, sessile cnidarians, bryozoans), it was counted as a single unit even if more fragments of it appeared in the sieved material. Fragments of polychaetes and arthropods were not counted at least they had the anterior parts used for identification. Echinoderms were counted only when the oral disc was nearly complete (at least >60% of the oral disc present). Fragments of mollusks or empty mollusk shells were not counted.

Weight in grams of each rhodolith was recorded, as well as length, height, and width measures in centimeters to calculate the volume of the rhodolith using the approximation to an ellipsoid as explained in Duerr (1994). Rhodoliths were sawed in halves; one-half of each rhodolith was dissolved immediately in dilute HCl to collect boring organism specimens, while the other half was thoroughly checked in the internal holes, grooves, and crevices for the presence of these boring organisms. This half was then placed in a digital scanner to preserve a flat image to determine the rhodolith surface rugosity (complexity) (**Figure 2**). The surface rugosity (complexity) of each of the 60 rhodoliths was measured by calculating the ratio of rugose line distance (perimeter) to a straight line distance (circumference), as explained by Fuad (2010).

The associated organisms were classified to the lowest possible taxonomic category and the number of individuals and their relative abundance were recorded.

Statistical Analysis

Testing for the Effects of Rhodolith-Forming Species on the Faunal Response Variables

A linear model (analysis of variance: ANOVA) was used to verify the existence of mean differences in species richness, total abundance, or total biomass of the fauna between the algal species of the rhodoliths. A squared root of the species richness and a cubic root of the total abundance were the transformed responses used to avoid overdispersions in each model. The analysis determines whether algae species affect faunal variables, which could modify the effect of the aggregation factor. Finally, the fitted values, residuals, and residual deviance inspection indicated that each linear model in this study follows the required assumptions of normality of residuals and homogeneity of variances (Crawley, 2007).

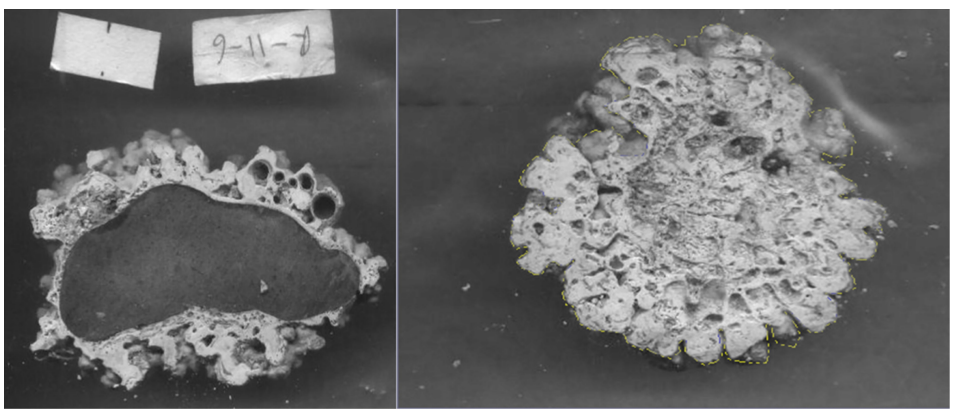

FIGURE 2 | Scanned halves of sawed rhodolith from Isla del Coco to determine complexity.

Evaluation of Differences in Rhodolith Nodule Characteristics (Complexity, Mass, Volume) Between the Three Levels of Aggregation

A linear model (ANOVA) was used to evaluate for the existence of mean differences in complexity, mass, or volume of the rhodoliths between the three aggregation levels (highly aggregated, moderately aggregated, and isolated patches, $n = 20$ in each level).

Effects of Rhodolith Aggregation Level on Faunal Response Variables (Total Biomass, Total Abundance, Species Richness)

The command "glm" in R was used to create generalized linear models (analysis of covariance: ANCOVA) (Crawley, 2007), to investigate how the aggregation factor ($n = 20$ in each level), rhodolith characteristics as covariates, and their interaction affect each faunal response variable: total biomass (ln transformed), total abundance (cubic-root transformed), or overall species richness (square root transformed). Previously, a Pearson index was used to identify highly correlated covariates (>0.65) to avoid the singularity in the model. The natural logarithm (ln) of the volume and the square root of the mass of the rhodoliths were highly correlated ($r = 0.80$). Only the ln (volume) and complexity squared of the rhodoliths were introduced in the model as covariables.

The models for these variables were fitted using the Gaussian distribution (with the identity-link function). The total biomass model was done with Gamma distribution (with the log-link function) to avoid overdispersion. Subsequent model simplification was done with the command step. It retained only the significant terms that explain mean differences or relation to the parameters.

Effects of Rhodolith Bed Structure (Level of Aggregation) Over the Macrofaunal Species Diversity and Species Composition

Species diversity was calculated for each category of aggregation with the Shannon–Wiener (H) index (ln based and compared by t-test for diversity index) and Pielou equitability (J) in the package PAST (Hammer et al., 2001).

Species composition was compared with a principal coordinates analysis (PCoA) based on the Bray–Curtis similarity index with the aggregation of rhodoliths (with three levels) as the principal factor in the package "labdsv" in R and tested with an analysis of similarities (ANOSIM, $n = 20$ in each aggregation level). Internal variation of faunal composition on each of these levels of aggregation was quantified with the multivariate index of dispersion using the command betadisper in R in the library "vegan."

The contribution of particular species to differences between aggregation levels was determined using a similarity percentage routine (overall multigroup and crossed-groups SIMPER) test in the package PAST (Hammer et al., 2001; Quinn and Keough, 2002).

Mantel tests were used to identify the individual correlations of the factors of the rhodoliths (aggregation, complexity, and volume) with the species composition (Bray–Curtis matrix). Additionally, partial Mantel tests were calculated to determine if significant factors (from the previous Mantel test) are independent or partially explain the correlation with the faunal composition (Zar, 1996; Quinn and Keough, 2002). The significant factors were plotted over the PCoA ordination in labdsv in R.

RESULTS

Taxonomic Composition of Rhodoliths

The taxonomic composition of the rhodoliths varied, with *Sporolithon* present in 23 of the samples, the genus *Lithothamnion* in 13 of the samples, an indeterminate species of rhodolith in 7 of the specimens, and a mixture of these species and *Sporolithon* in 16 samples. *Hydrolithon onkodes* was found building one sample. Rhodoliths were mainly spherical or compact (50%) or compact-platy-bladed (25%) based on Sneed and Folk classes assigned by triplot analysis for lithic materials (Graham and Midgley, 2000).

Rhodolith species presented similar mean faunal species richness (ANOVA: $F = 0.30$, $df = 3/55$, $p = 0.828$), similar mean faunal abundance (ANOVA: $F = 0.16$, $df = 3/55$, $p = 0.942$), and similar mean faunal biomass (ANOVA: $F = 1.46$, $df = 3/55$, $p = 0.236$). A single specimen of *H. onkodes* was excluded from the linear models.

Rhodolith-Associated Macrofauna

A total of 5,483 organisms and 145 taxa of fauna were found in the 60 rhodoliths sampled. Crustaceans, polychaetes, and mollusks were the dominant taxa, with crustaceans accounting for more than half of total abundance and 25.5% of total richness. Gammaridean amphipods and tanaidaceans (*Leptochelia* sp. and *Apseudomorpha* sp.) were the most abundant crustacean species inhabiting rhodoliths; amphipods, isopods, and decapods, together, constituted up to 58% of the crustacean species found. Syllidae (11 spp.), Phyllodocidadae (6 spp.), and Nereididae (1 sp.) were the best-represented polychaete families. *Ceratonereis singularis* was the only nereid polychaete found, but that species alone was by far the most abundant polychaete species (45% of the total polychaete species). Molluscan fauna were mainly gastropods with 34% of all mollusks represented by the pyramidellid gastropod *Odostomia grijalvae*, which was recorded from 53% of all samples. *Cerithiopsina adamsi* and *Cerithiopsina* sp. together with *Turbo saxosus* and *Eulithidium diantha* were also very common. Among bivalves, the most abundant was an unidentified species of *Lithophaga* boring in 31.6% of rhodoliths. Two species of ophiuroids dominated the echinoderm fauna: *Ophiactis savigny* (found in 90% of the samples) and *Ophiocoma* cf. *alexandri* (found in 66.6% of the samples) (**Figure 3**, and **Table 1**). At least five new species were found in this study, two tanaidaceans and three Paranthurid isopods, as well as 14 species, 20 genera, and 12 families newly reported for Isla del Coco and the Eastern Tropical Pacific (**Table 1** and **Appendix 1**).

During the sampling collections, many small fishes were seen swimming back to the rhodolith shelter while we were scuba diving. Nine out of 60 rhodoliths had fish, almost all of them found inside crevices or tunnels in the rhodolith nodule (eight hollow rhodoliths had fishes). These fishes were represented by five species, and one of them, *Emblemaria piratica*, is a new report for Isla del Coco. Additionally, two species of snapper fish (genus *Lutjanus*) and one species of *Cirrhitichthys* (*C. oxycephalus*) were encountered in the rhodoliths. Other sessile fauna found on rhodoliths included two species of sponges, two species of ascidians, and several hydrozoans and anthozoans (**Appendix 1**).

Although sex and maturity of macrofaunal elements were not thoroughly investigated, many of the rhodoliths sampled had one or more immature specimens, many of them being isopod and amphipod crustaceans, but also decapods, fishes, tube polychaetes, and mollusks. In 78.1% of rhodolith samples having crustaceans, there were several females of at least one species carrying eggs or embryos, and these species were mainly gammarid amphipods (8 spp., 87 females carrying eggs or

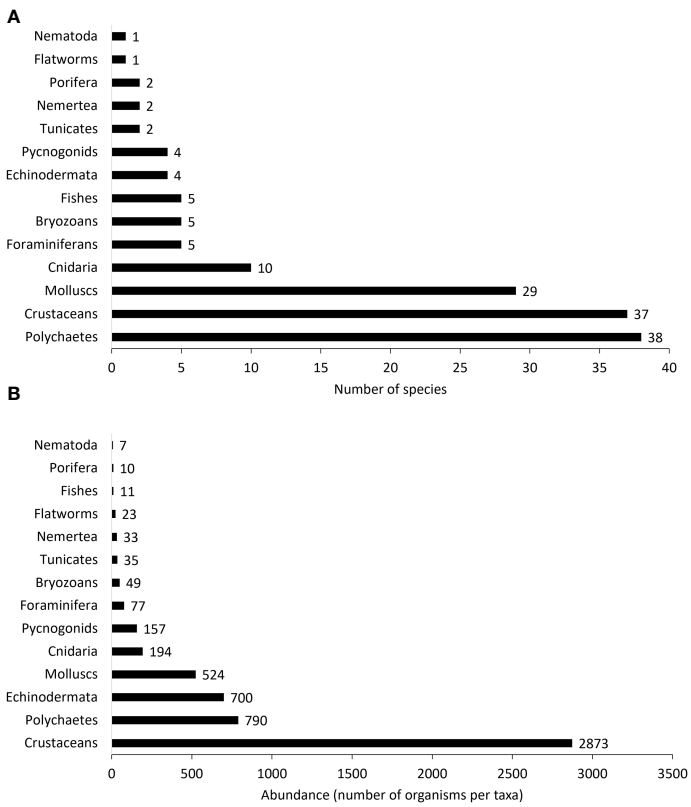

FIGURE 3 | Number of morphospecies per taxon **(A)** and number of individuals **(B)** per taxon found among all the rhodolith samples.

TABLE 1 | Richness (number of morphospecies), abundance (number of organisms), and biomass per group of organisms associated with rhodoliths at Isla del Coco; taxa with fewer than 100 organisms (with the exception of fish, see note below) were included in "other fauna".

Taxon	Richness	%	Abundance	%	%
Crustaceans	37	25.5	2,873	52.4	22.8
Polychaetes	38	26.2	790	14.4	4.1
Mollusks	29	20	524	9.6	9.9
Echinoderms	4	2.8	700	12.8	20.1
Cnidarians	10	6.9	194	3.5	–
Pycnogonids	4	2.8	157	2.8	–
Fish	5	3.4	11	0.2	27.5
Other fauna[a]	18	12.4	234	4.3	15.6[b]

[a]*Except for fish, which contribute a significant amount of biomass despite having only 11 individuals collected, taxa with few organisms (100) were included in "other fauna" (tunicates, bryozoans, nemerteans, nematodes, foraminiferans, and flatworms).*

[b]*Other fauna biomass and biomass percentage include pycnogonids and cnidarians which were not separately measured.*

embryos), isopods (4 spp., 23 carrying eggs or embryos), and tanaidaceans (11 *Leptochelia* sp. and 9 *Apseudomorpha* sp. are egg-carrying females) (**Supplementary Figure S1**). The number of females of each species carrying eggs or embryos as well as the average number of eggs carried by each species was recorded (**Appendix 2**). Additionally, eight hollow rhodoliths had fish in crevices or tunnels inside the rhodolith nodule. The two species of snapper fish and *C. oxycephalus* were juveniles. Adults of the mantis shrimp *Neogonodactylus zacae* and adults of the crabs *Paractea sulcata* and *Micropanope maculatus* were discovered in pairs of male and female, protected inside crevices of some hollow rhodolith nodules, with the female of *M. maculatus* having several hundreds of eggs.

Effects of Rhodolith Bed Structure (Level of Aggregation) on Rhodolith Physical Characteristics

Rhodolith complexity and volume were similar in their mean value between the three aggregation levels (**Table 2**). The mean value of rhodolith mass varied depending on the aggregation level. The Tukey pairwise comparisons test showed that isolated rhodoliths had a lower mean mass than the moderate aggregation level, but there were no differences between isolated and high aggregation levels nor between high and moderate aggregation levels in terms of rhodolith mass. The range of variation of each characteristic was well represented within each aggregation level of the rhodoliths.

Effects of the Rhodolith Bed Structure (Levels of Aggregation) and Covariates on the Macrofauna Richness and Abundance

Effects on the Richness

The ANCOVA shows that the mean value of species richness was higher in moderately aggregated rhodoliths, followed by highly aggregated rhodoliths (**Figure 4A**). Both levels of aggregation had a higher taxon richness than the isolated rhodoliths (**Table 3** and **Figure 4A**). No interaction was found between these covariates and aggregation level over these faunal variables, but as additive factors, the complexity and volume of rhodoliths produced a linear increase of the faunal species richness within each level of rhodolith aggregation (**Table 3** and **Figures 4B, C**).

Effects on the Abundance

Similarly, the highest mean abundance occurs in the moderately aggregated rhodoliths (**Table 4** and **Figure 5A**). The mean abundance of fauna in highly aggregated and isolated rhodoliths was similar (**Figure 5A**). Only an additive effect of the complexity and volume of rhodoliths to increase the abundance of fauna was found (**Table 4** and **Figures 5B, C**).

Effects of Rhodolith Bed Structure (Levels of Aggregation) and Rhodolith Nodule Volume on the Total Biomass

The ANCOVA shows that faunal biomass depends on the interaction between the aggregation level and the volume of the rhodoliths. The higher the volume of the rhodolith, the more the biomass of the fauna. The relationship changes between moderate rhodoliths where the slope is less steep than the same relationship at isolated or highly aggregated rhodoliths (**Table 5** and **Figure 6**). This differentiated effect means a higher average of the biomass/volume ratio in the moderate rhodoliths than in the other two levels (**Figure 6**).

In addition to the moderate aggregation level of the rhodoliths, larger and more voluminous rhodoliths had a higher number of taxa, individual organisms, and total biomass of associated fauna based on these linear models.

Some groups contributed more to total biomass than others. Together, the most abundant groups (e.g., crustaceans, polychaetes, mollusks, and echinoderms) contributed 56.9% to total biomass. Crustaceans and echinoderms (primarily ophiuroids) were the invertebrates that contributed the most to this parameter (22.8% and 20.1%, respectively). Even though only 11 individuals of fish were collected, they accounted for 27.5% of total biomass. Given that fish were found in only a small number of rhodoliths (9 out of 60), and because it was frequently observed that the biomass of a single fish contributed significantly more than the combined biomass of other taxa for the same rhodolith, fish biomass was not included in the analyses.

TABLE 2 | Mean value and their upper and lower limits of 95% of confidence for the rhodolith characteristics by the three levels of aggregation of rhodoliths at Isla del Coco.

Variable	Parameter	Aggregation			Linear model (ANOVA)
		Isolated	Moderately	Highly	*F*, *p*-value
Complexity	Upper limit	0.74	0.68	0.68	
	Mean	**0.68**	**0.64**	**0.64**	0.95, **0.392**
	Lower limit	0.62	0.59	0.6	
Volume (cm^3)	Upper limit	1,085.19	1,432	1,194.61	
	Mean	**810.51**	**1,138.52**	**947.58**	1.74, **0.184**
	Lower limit	605.36	905.19	751.63	
Mass (g)	Upper limit	122.39	177.69	160.32	
	Mean	**93.87**	**147.83**	**129.1**	3.70, **0.031***
	Lower limit	69.13	120.72	101.27	

The p-value of the linear model is presented. The symbol (*) indicates a significant p-value. Mean values and p values are highlighted.

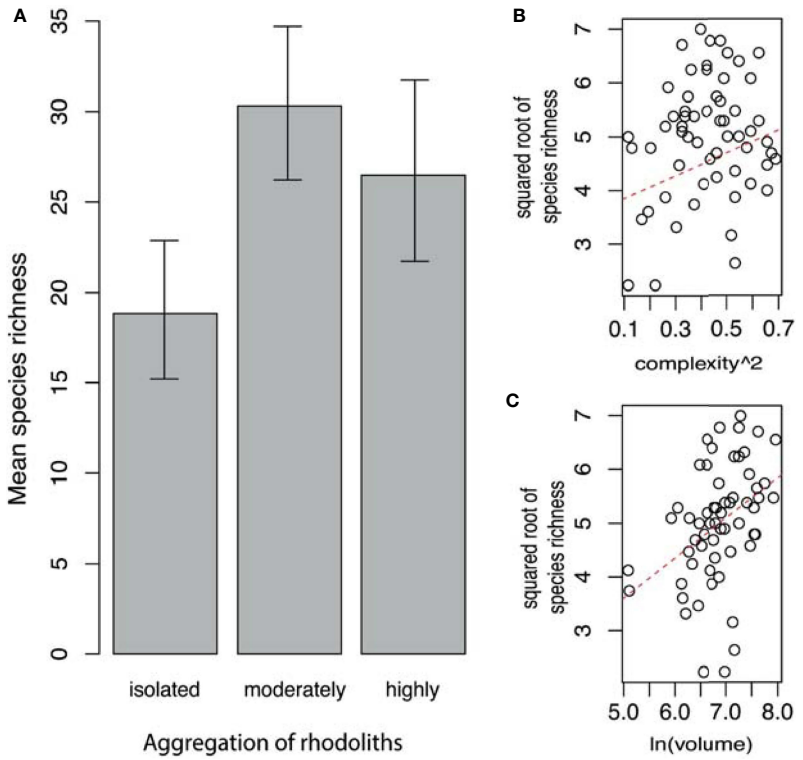

FIGURE 4 | **(A)** Mean of fauna species richness (with 95% confidence limits) by aggregation of rhodoliths. **(B)** Relationship between faunal species richness and complexity of rhodoliths. **(C)** Relationship between faunal species richness and volume of rhodoliths (Isla del Coco, Costa Rica).

Effects of Rhodolith Bed Structure (Levels of Aggregation) on Overall Diversity and Species Composition

The Shannon–Wiener diversity index was lower in isolated rhodoliths than in moderately aggregated rhodoliths (t: −7.59, df = 3,350.7, p = 0.001), and moderately aggregated rhodoliths were also more diverse than highly aggregated rhodoliths (t: 1.98, df = 3,430.6, p = 0.047). The equitability results are similar between moderately and highly aggregated rhodoliths; however, the former had greater abundance and better distribution in a greater number of species (**Table 6**).

The taxon composition was different from isolated to highly aggregated rhodoliths (**Figure 7A**, ANOSIM, R = 0.25, p < 0.001). Within groups, faunal similarity was higher among highly aggregated rhodoliths, while isolated rhodoliths presented greater variation from one rhodolith to another (**Figures 7A–C** and **Table 7**). Abundant and well-distributed taxa like Amphipoda indet. 1 and the ophiuroid *O. savigny* contributed importantly to this similarity within each level of aggregation and to the overall similarity, and those species were typical of all levels of aggregation (**Table 7**). The nereid polychaete *C. singularis* was a typical species in highly and moderately aggregated rhodoliths but not in isolated rhodoliths, where the ophiuroid *O. savigny* was the most typical species and contributed more to the similarity in isolated patches (**Table 7**). Few taxa made the highest contribution to the dissimilarity between pairs of aggregation levels (**Table 8**). The taxon with the highest contribution to the dissimilarity

TABLE 3 | Simplified generalized linear model (ANCOVA) for faunal species richness in the rhodoliths (Isla del Coco, Costa Rica).

Coefficients:	Estimate	Std. error	*t* value	*p*
(Intercept)	−0.143	1.447	−0.1	0.921
Moderately vs. isolated	1.094	0.304	3.6	<0.001
Highly vs. isolated	0.818	0.296	2.77	0.008
Complexity squared	1.892	0.828	2.28	0.026
ln (volume)	0.539	0.212	2.54	0.014

Simplified model: squared root (species) ~ aggregation + complexity squared + ln (volume), family = Gaussian.
Null deviance: 71.459 on 59 degrees of freedom.
Residual deviance: 46.296 on 55 degrees of freedom.
AIC: 166.71.

TABLE 4 | Simplified generalized linear model (ANCOVA) for total abundance of fauna in the rhodoliths (Isla del Coco, Costa Rica).

Coefficients:	Estimate	Std. error	*t* value	*p*
(Intercept)	1.069	1.016	1.05	0.297
Moderately vs. isolated	0.468	0.214	2.19	0.033
Highly vs. isolated	0.101	0.208	0.49	0.629
Complexity squared	1.263	0.581	2.17	0.034
ln (volume)	0.378	0.149	2.54	0.014

Simplified model: Cubic root (Abundance) ~ aggregation + complexity squared + ln (volume), family = Gaussian.
Null deviance: 31.042 on 59 degrees of freedom.
Residual deviance: 22.811 on 55 degrees of freedom.
AIC: 124.25.

between categories of aggregation was Amphipoda indet. 1, which increased in abundance from isolated to highly aggregated rhodoliths (**Table 8**). The taxa making the next highest level of contribution to dissimilarity between pairs of groups were the tanaidaceans *Leptochelia* sp. (isolated vs. moderately) and *Apseudomorpha* sp. (moderately vs. highly aggregated). *Leptochelia* was more abundant in isolated rhodoliths, while *Apseudomorpha* was more abundant in moderately aggregated rhodoliths (**Table 8**). The major groups that contributed to dissimilarity between groups were crustaceans (mainly peracarids), followed by ophiuroids and polychaetes (mobile predators). There is a higher dissimilarity percentage between isolated and highly aggregated rhodoliths, and that difference is lowest between moderately and highly aggregated rhodoliths (**Table 8**). The nereid polychaete *C. singularis* was very abundant, mainly in moderately aggregated rhodoliths, and was uncommon in isolated rhodoliths, and the relative abundances of *C. singularis* were very consistent along with the levels of aggregation, so its diss/SD ratio is among the highest in all levels (**Table 8**).

The mean abundance of each taxon by the levels of aggregation is also presented. Only the highest contributors are presented. Average abundances in which each species dominates as well as the highest diss/SD ratios are highlighted.

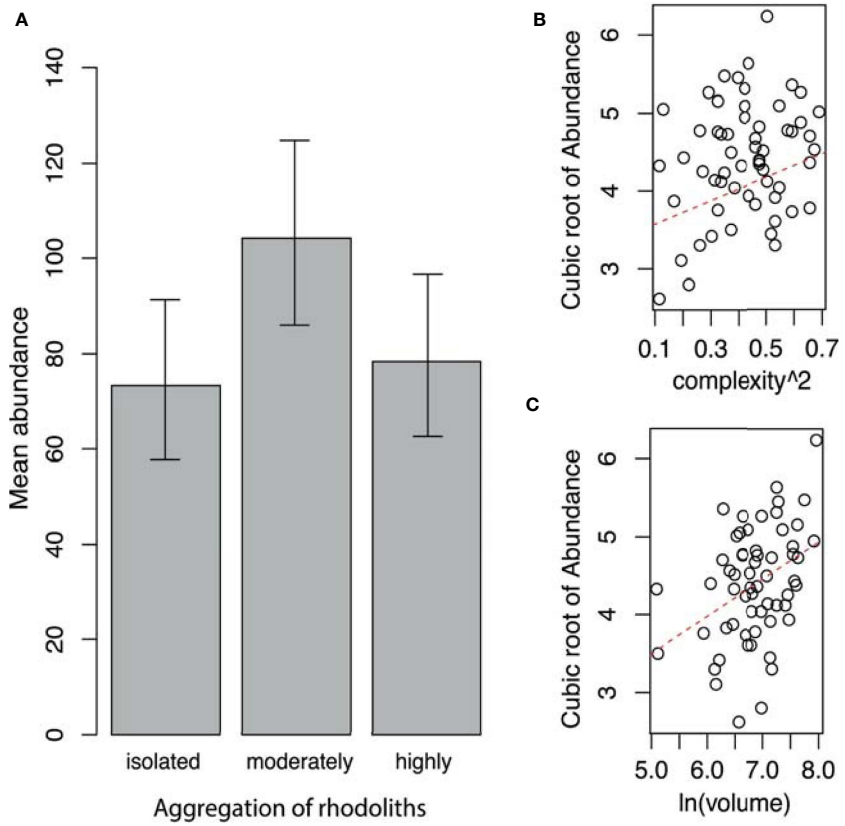

FIGURE 5 | **(A)** Mean abundance of fauna (with 95% confidence limits) by aggregation of rhodoliths. **(B)** Relationship between the abundance of fauna and complexity of rhodoliths. **(C)** Relationship between the abundance of fauna and volume of rhodoliths (Isla del Coco, Costa Rica).

TABLE 5 | Simplified generalized linear model (ANCOVA) for total biomass of fauna in the rhodoliths (Isla del Coco, Costa Rica).

Coefficients:	Estimate	Std. Error	*t* value	*p*
(Intercept)	–9.346	1.41	–6.63	0
Moderately vs. isolated	6.088	2.351	2.59	0.012
Highly vs. isolated	1.477	2.298	0.64	0.523
Log(volume)	1.212	0.21	5.78	0
Moderately * log(volume) vs. isolated * log(volume)	–0.809	0.339	–2.39	0.021
Highly * log(volume) vs. isolated * log(volume)	–0.174	0.337	–0.52	0.607

*Simplified model: total biomass ~ aggregation + ln (volume) + aggregation * ln (volume), family = Gamma(link = log).*
Null deviance: 38.793 on 59 degrees of freedom.
Residual deviance: 20.781 on 55 degrees of freedom.
AIC: 6.5618.

Effects of Rhodolith Complexity on the Faunal Composition

In addition to the effect of aggregation levels, an effect of rhodolith complexity on the composition of fauna species was observed (**Table 9** and **Figure 7B**). The correspondence pattern of rhodolith complexity with faunal similarity differs from the pattern by aggregation levels. Based on the small change in the *r*-value with the partial Mantel test (**Table 9**), both predictors are additive effects in determining the faunal composition of the rhodoliths. Other factors, such as volume or rhodolith species, had no effect on fauna composition (**Table 9**).

DISCUSSION

Rhodolith-Associated Macrofauna

This is the first time that rhodolith-associated fauna has been systematically studied in low latitudes in the Neotropical Pacific region. As a result, multiple taxa are new records for the region and five specimens found in this study are possibly new species. Rhodoliths in Isla del Coco National Park show particularly high levels of diversity with 145 taxa from 60 rhodoliths sampled, compared with the well-studied regions in the Gulf of California and Brazil. Steller et al. (2003) found 52 species of rhodolith-associated fauna based on three 30-m transects and five 1-m^2 quadrats in the Gulf of California. In the same region, Hinojosa-Arango and Riosmena-Rodríguez (2004) found 104 species of macrofauna in 120 rhodoliths, and Neill et al. (2015) found less than 110 species of epibenthic fauna following a methodology similar to Steller et al. (2003). In northeast Brazil, Paraíba State, Costa et al. (2021) found 60 rhodolith-associated macrofaunal species with a method based on three 100-m^2 quadrats placed each in three different beaches (there was no mention on the total number of rhodoliths sampled). Prata et al. (2017) reported, from the same state, 12 species of just echinoderms (we reported here only four species). Stelzer et al. (2021) sampled the eastern ecoregion of Brazil (more than 140 rhodoliths sampled) and reported 148 macrofaunal taxa, a value similar to Isla del Coco, but in more rhodoliths sampled. Taxa groups that dominated the faunal communities found in this study were crustaceans, polychaetes, and mollusks. Similarly, previous research has revealed that the abundance and diversity (richness) of crustaceans, polychaetes, and mollusks makes them dominant taxa in the rhodolith-associated benthic communities (Hinojosa-Arango and Riosmena-Rodríguez, 2004; Neill et al., 2015; Stelzer et al., 2021; Costa et al., 2021). Although more research on the rhodolith-associated communities in Isla del Coco is needed, these numbers could indicate that Isla del Coco rhodoliths have been altered only slightly by human activity and can therefore be used in future research as a reference for an unimpacted habitat.

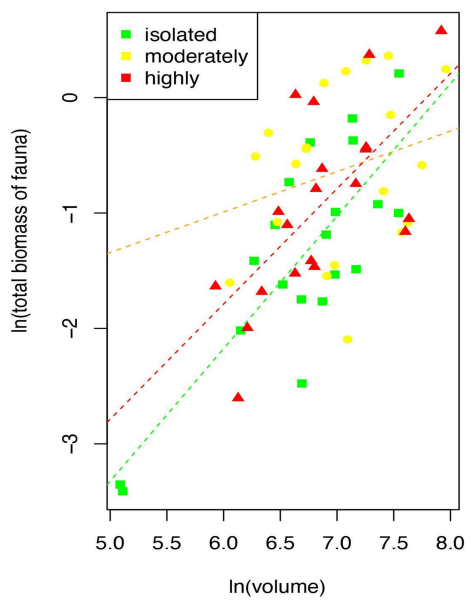

FIGURE 6 | Relationship of the total biomass of fauna and volume of rhodoliths by each level of aggregation of rhodoliths (Isla del Coco, Costa Rica).

Regarding the faunal composition, Isla del Coco rhodoliths harbor, in general terms, a similar faunal assemblage in comparison with major tropical marine environments having a similar temperature, depth, and substrate type, with the same taxon subgroups (gammarid amphipods, isopods, tanaidaceans, syllid, phyllodocid, and nereid polychaetes; gastropod mollusks; and ophiuroids) being the most abundant and diverse (Steller et al., 2003; Hinojosa-Arango and Riosmena-Rodríguez, 2004; Costa et al., 2021).

Some fishes found in rhodoliths were juveniles, which included two species of the economically important genus *Lutjanus* (snapper fish). *Lutjanus argentiventris* is known to have ontogenetic habitat shifts, with juveniles migrating from

TABLE 6 | Summary of faunal species and abundance, diversity index (*H*), and equitability (*J*) by each level of aggregation of rhodoliths.

	Aggregation	Isolated	Moderately	Highly
Species	Total	104	119	115
Abundance	Total	1,591	2,206	1,686
Shannon–Wiener	Upper limit 95%	3.39	3.72	3.65
	H	3.31	3.67	3.57
	Lower limit 95%	3.26	3.61	3.51
Pielou equitability	Upper limit 95%	0.73	0.78	0.77
	J	0.71	0.77	0.75
	Lower limit 95%	0.7	0.76	0.74

mangroves to continue their growth in shallow rocky reefs. Rhodoliths can have a similar role as those rocky reefs in the life history of these *Lutjanus* species, as a suitable habitat that offers protection to these fish (Aburto-Oropeza et al., 2009). Several amphipod and decapod crustaceans were found in reproductive pairs or had eggs or larvae (**Appendix 2**). These results support the role of rhodoliths as breeding and nursery sites for the species found in nearby environments as it has been found in several studies (Cudney-Bueno et al., 2008; Gagnon et al., 2012; Teichert, 2014; Jørgensbye and Halfar, 2017; Navarro-Mayoral et al., 2020). It also leads to questions about how the drivers of rhodolith-associated organism diversity affect reproduction in those organisms. Rhodolith structural complexity, rhodolith size, and intactness have been found to influence larval settlement and growth of some species (e.g., scallops) (Steller and Cáceres-Martínez, 2009). Certainly, further research on faunal reproduction and ontogenetic events in rhodolith beds is needed.

Rhodolith Bed Structure Effects on Macrofauna Richness, Abundance, and Total Biomass

Values of total biomass, richness, and abundance of the macrofauna were higher in moderately aggregated rhodoliths than in the other extremes of aggregation. These results suggest a

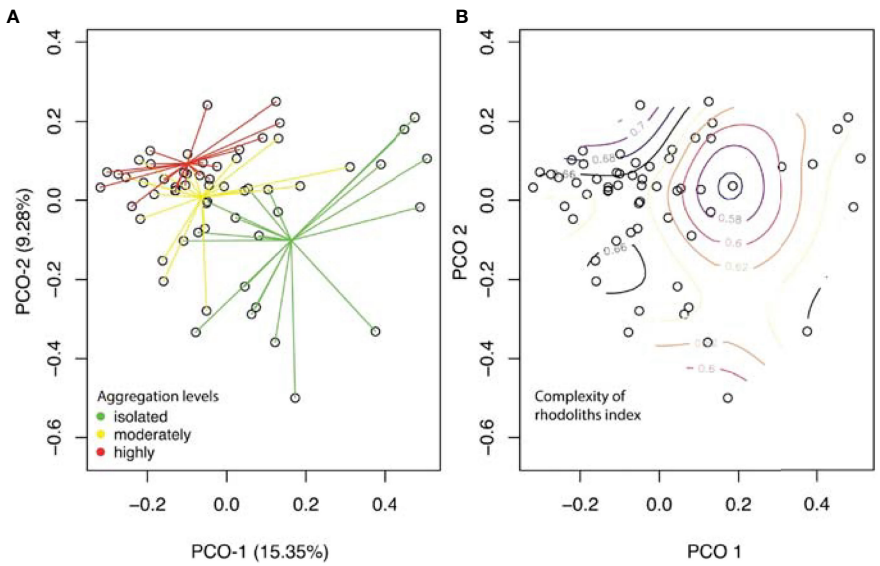

C

Level of aggregation	Multivariate dispersion index	ANOSIM (Bray-Curtis based)
Isolated	0.47	Permutations : 9999 Mean rank within : 757.1 Mean rank between 946.5 *R : 0.25* *P < 0.001*
moderately	0.44	
Highly	0.43	

FIGURE 7 | Principal coordinate analysis based on Bray–Curtis of the abundance of invertebrates in rhodolith samples by **(A)** the level of aggregation of the rhodolith bed and **(B)** the value of complexity of the rhodoliths (Isla del Coco). **(C)** Comparison of multivariate dispersion indexes generated by betadisper (R, library "vegan") and PERMANOVA analysis of internal variation in species composition.

TABLE 7 | Results of the SIMPER analysis for within-group similarity.

Group III					
Average similarity: 37.53					
Species	**Av. abund**	**Av. sim**	**Sim/SD**	**Contrib%**	**Cum%**
Amphipoda indet. 1	18.70	15.04	1.75	40.08	40.08
Ceratonereis singularis	7.05	5.18	1.69	13.81	53.89
Ophiactis savigny	7.40	4.29	0.98	11.44	65.33
Synalpheus sp.	2.10	1.29	1.11	3.44	68.77
Ophiocoma cf. *alexandri*	2.30	0.79	0.49	2.11	70.88
Group II					
Average similarity: 35.85					
Species	**Av. abund**	**Av. sim**	**Sim/SD**	**Contrib%**	**Cum%**
Amphipoda indet. 1	16.1	8.9	1.44	24.84	24.84
Ophiactis savigny	8.15	4.86	1.19	13.56	38.4
Ceratonereis singularis	8.7	4.41	1.45	12.32	50.72
Apseudomorpha sp.	9.45	2.93	0.82	8.19	58.9
Amphipoda indet. 3	6	1.88	0.81	5.23	64.13
Leptochelia sp.	4.55	1.11	0.75	3.09	67.22
Odostomia grijalvae	4.05	1.03	0.55	2.86	70.08
Group I					
Average similarity: 32.13					
Species	**Av. abund**	**Av. sim**	**Sim/SD**	**Contrib%**	**Cum%**
Ophiactis savigny	10.6	10.16	1.28	31.63	31.63
Amphipoda indet. 1	12.5	6.04	0.85	18.81	50.44
Leptochelia sp.	8.4	3.86	0.65	12.03	62.47
Amphipoda indet. 3	6.9	1.71	0.48	5.34	67.8
Pseudotanais sp.	3.4	1.54	0.63	4.79	72.59

I: isolated, II: moderately, and III: highly aggregated rhodoliths.

Av, abund, average abundance; Av, sim, average similarity; Sim/SD, similarity/standard deviation ratio; Contrib%, contribution percentage to similarity for each species; Cum%, cumulative percentage contribution to similarity for each species.

similar pattern to that proposed by the intermediate disturbance hypothesis according to which the highest values of biodiversity are reached in habitats at intermediate scales of disturbance (Connell, 1978; Wilson, 1994).

Rhodolith density is known as one of the main drivers of biodiversity associated with rhodolith beds (Veras et al., 2020; Stelzer et al., 2021). When compared, high rhodolith nodule density supports higher biodiversity than those rhodoliths in less density (Stelzer et al., 2021). In tightly packed beds, rhodoliths are in contact with each other, and there is little room to grow or to have extensive branching which limits the heterogeneity of the nodule and its associated biodiversity. Patches composed of rhodoliths far apart from each other are exposed to more perturbations of the patch, which could lead to less diversity of associated fauna. Dispersed rhodoliths could have a higher chance of being buried by sediments for a longer period than aggregated ones and could be more susceptible to tidal wave disruption and foraging of big animals (e.g., rays). In experiments in which the stability of a rhodolith patch was artificially controlled (tied vs. untied rhodoliths), windier conditions (which led to bigger effects of waves on the rhodolith beds) significantly reduced the abundance and total biomass of motile rhodolith-associated fauna, although it had neutral effects on species richness, and rhodolith densities were not controlled in those experiments (Hinojosa-Arango et al., 2009). Dispersed and unstable rhodoliths that are subject to tidal changes have a lower overall abundance of organisms and lower species richness than more stable rhodoliths under the same controlled conditions. Interestingly, this effect is specifically on motile species, while sessile species, on the contrary, increase their abundance (Hinojosa-Arango et al., 2009). This pattern of changes in species richness and abundance due to shifts in substrate stability has also been noticed in other macrophytic-dominated systems, and mobile fauna is greatly affected by these shifts (Christie et al., 2009). Under the assumptions of the intermediate disturbance hypothesis, settlement of a great diversity of new organisms would be limited in isolated rhodoliths given the distance that larvae or other dispersion forms should travel to arrive in the next rhodolith (Dial and Roughgarden, 1998). Although there is evidence that rhodolith beds play an important role in the recruitment of larval forms of invertebrate species (Riosmena-Rodríguez and Medina-López, 2010), the effects of rhodolith aggregation degree on this recruitment have received little attention. Although in this study depth was a controlled variable, other relevant rhodolith-associated macrofaunal biodiversity drivers like macroalgal biomass, bioengineers, and bioerosion, and water motion, current velocity, light, or sedimentation were not measured or controlled, and they might influence the abundance, species richness, and total biomass (Pereira-Filho et al., 2015).

TABLE 8 | Results of the SIMPER analysis with the percentage of contribution by taxon to the dissimilarity between pairs of aggregation levels—I: isolated, II: moderately, and III: highly aggregated.

Dissimilarity I vs. II	**Average dissimilarity 71%**		**Av. dissim**	**Diss/SD**	**Contrib%**	**Cumul%**
Taxon	**Av. abund I**	**Av. abund II**				
Amphipoda indet. 1	12.50	**16.10**	7.09	**1.21**	9.98	9.98
Leptochelia sp.	**8.40**	4.55	4.61	**1.04**	6.50	16.49
Amphipoda indet. 3	**6.90**	6.00	4.45	0.93	6.28	22.76
Apseudomorpha sp.	1.15	**9.45**	4.41	0.95	6.21	28.98
Ceratonereis singularis	2.00	**8.70**	3.98	**1.29**	5.61	34.58
Ophiactis savigny	**10.60**	8.15	3.83	**1.19**	5.39	39.97
Actiniaria indet. 1	**3.80**	1.85	2.41	0.67	3.40	43.37
Amphipoda indet. 3	0.00	**3.90**	2.15	0.55	3.04	46.41
Odostomia grijalvae	0.95	**4.05**	2.08	0.83	2.92	49.33
Pseudotanais sp.	**3.40**	1.40	1.87	0.85	2.63	51.96
Amphipoda indet. 2	**2.55**	1.90	1.74	0.79	2.45	54.41
Pycnogonida indet. 1	**3.40**	0.50	1.67	0.43	2.36	56.77
Jaeropsis sp.	1.60	**1.80**	1.21	1.03	1.70	58.47
Ophiocoma cf. *alexandri*	**2.05**	1.65	1.19	0.96	1.67	60.14
Dissimilarity III vs. II	**Average dissimilarity 65.61%**					
Taxon	**Av. abund III**	**Av. abund II**	**Av. dissim**	**Diss/SD**	**Contrib%**	**Cumul%**
Amphipoda indet. 1	**18.70**	16.10	6.50	**1.34**	9.91	9.91
Apseudomorpha sp.	2.05	**9.45**	4.20	0.96	6.40	16.31
Ophiactis savigny	7.40	**8.15**	3.71	**1.15**	5.66	21.96
Ceratonereis singularis	7.05	**8.70**	3.28	**1.28**	4.99	26.96
Amphipoda indet. 3	0.45	**6.00**	2.87	0.79	4.37	31.33
Odostomia grijalvae	3.90	**4.05**	2.76	0.78	4.21	35.54
Amphipoda indet. 5	0.90	**3.90**	2.11	0.57	3.21	38.75
Leptochelia sp.	1.15	**4.55**	2.05	0.70	3.13	41.88
Ophiocoma cf. *alexandri*	**2.30**	2.05	1.50	1.01	2.28	44.16
W. heterocirrata	**1.95**	1.15	1.31	0.64	2.00	46.16
Amphipoda indet. 2	1.35	**1.90**	1.24	0.65	1.89	48.08
Paranthura sp.	1.10	**2.05**	1.16	0.68	1.77	49.83
Caprellidae indet. 1	1.30	**1.60**	1.10	1.03	1.68	51.50
Actiniaria indet. 1	0.70	**1.85**	1.01	0.88	1.55	53.05
Synalpheus sp.	**2.10**	1.65	1.00	0.42	1.52	56.10
Colanthura sp.	0.85	**2.00**	0.97	1.06	1.47	57.57
Amphipoda indet. 4	0.65	**1.80**	0.90	0.91	1.38	58.95
Jaeropsis sp.	1.25	**1.40**	0.87	0.91	1.33	60.28
Dissimilarity III vs. I	**Average dissimilarity = 72.50**					
Taxon	**Av. abund II**	**Av. abund I**	**Av. dissim**	**Diss/SD**	**Contrib%**	**Cumul%**
Amphipoda indet. 1	**18.70**	12.50	9.23	**1.23**	12.73	12.73
Ophiactis savigny	7.40	**10.60**	5.01	**1.16**	6.91	19.64
Leptochelia sp.	1.15	**8.40**	4.97	0.92	6.85	26.50
Amphipoda indet. 3	0.45	**6.90**	3.71	0.69	5.11	31.61
Ceratonereis singularis	**7.05**	2.00	3.66	**1.51**	5.05	36.66
Actiniaria indet. 1	0.70	**3.80**	2.61	0.57	3.60	40.26
Pseudotanais sp.	1.25	**3.40**	2.07	0.79	2.86	43.11
Odostomia grijalvae	**3.90**	0.95	2.06	0.55	2.84	45.95
Pycnogonida indet. 1	0.80	**3.40**	2.00	0.45	2.76	48.71
Amphipoda indet. 2	1.35	**2.55**	1.77	0.81	2.44	51.15
Ophiocoma cf. *alexandri*	**2.30**	1.65	1.62	1.00	2.23	53.38
Apseudomorpha sp.	**2.05**	1.15	1.45	0.85	2.00	55.39
W. heterocirrata	**1.95**	0.15	1.26	0.52	1.74	59.12
Synalpheus sp.	**2.10**	0.65	1.21	**1.27**	1.66	58.79
Colanthura sp.	**1.65**	0.10	1.16	0.38	1.60	60.39

Only the highest contributors are presented. Average abundances in which each species dominates as well as the highest diss/SD ratios are highlighted.

Rhodolith Bed Structure Effects on Total Faunal Biomass

Total biomass was also higher in the moderately aggregated rhodoliths. Our findings indicated that faunal biomass depends on the interaction between the aggregation level and the volume of the rhodoliths, with a higher average biomass/volume ratio in the moderately aggregated rhodoliths than in the two other levels. Regarding the volume effect, densely packed rhodoliths are limited in their growing capacity, leading to less voluminous rhodolith nodules, while moderately aggregated rhodoliths have

TABLE 9 | Mantel and partial Mantel test to determine the relationship of fauna and characteristics and aggregation of the rhodoliths (Isla del Coco).

Relationship of fauna composition with	**Mantel test (*r*)**	***p*-value**
Aggregation levels	0.176	0.001
Complexity	0.134	0.026
Volume	0.001	0.466
Species of rhodolith	0.031	0.193
Relationship of fauna composition with	**Partial Mantel test**	***p*-value**
Aggregation levels controlled by complexity	0.175	0.001
Complexity controlled by aggregation levels	0.132	0.033

sufficient space to grow and be more voluminous. The size of rhodolith has been recognized as another rhodolith-associated fauna biodiversity driver and as a factor that influences the total biomass (Veras et al., 2020). Why isolated rhodoliths in this study had the lowest average volume is more complex to explain. Isolated rhodoliths had a significantly lower mass, and they are lighter and may be more easily affected by water motion. Other factors, such as bioengineering damage, bioerosion, or sedimentation, that could hinder their growth could also play a role in affecting rhodolith size in these isolated patches, but these were not measured.

Rhodolith Bed Structure Effects on Overall Diversity and Faunal Composition

Macrofaunal diversity measured by the Shannon–Wiener index was higher in the moderately aggregated rhodoliths when this level of aggregation was compared with either of the two other levels. This was expected given the relationships found between the level of aggregation and the abundance and richness of macrofauna species. Moderately aggregated rhodoliths had a higher and better-distributed abundance in a greater number of species.

In this study, the SIMPER and ANOSIM analyses show how motile fauna is the one that contributes the most to the difference between aggregation levels, mainly highly motile fauna such as small crustaceans. This change in the faunal composition according to the density of rhodoliths also was found by Veras et al. (2020) in Fernando de Noronha Archipelago, Brazil, and by Stelzer et al. (2021) in the Eastern Marine Ecoregion of Brazil, and in these studies, a marked change in the faunal composition was detected between the macrofaunal assemblages of highly dense and low-density rhodolith nodules. In our study, the overall dissimilarity between each pair of aggregation levels shows the highest dissimilarity between the isolated and highly aggregated rhodoliths than between either combination of moderately aggregated rhodoliths (moderately vs. isolated or moderately vs. highly aggregated). This difference in the faunal composition, higher between the extremes (isolated vs. highly aggregated), is also noticed in the PCoA plot (**Figure 7A**). Rhodolith density has previously been demonstrated as a significant factor influencing the composition of macrofauna associated with rhodoliths, though it appears that not all taxa are equally affected. Certain groups of polychaetes, such as eunicids and phyllodocids, and gastropod mollusks, as well as most crustaceans and ophiuroids, in rhodoliths were better predicted by this factor (Costa et al., 2021).

The highest diversity occurs at moderate levels of rhodolith aggregation. The density of moderately aggregated rhodoliths is such that, despite being influenced by the movement or burial of the rhodoliths, they are not so far apart that continuous arrival of motile organisms is possible. In rhodolith beds in the Gulf of California, the increase in stability beyond a certain point results in a lower number of species (Hinojosa-Arango and Riosmena-Rodríguez, 2004). A rhodolith bed can be in different successional stages depending on the time and degree of previous alterations, as it occurs in other marine systems (Connell, 1978; Wilson, 1994). We hypothesize that rolling rhodoliths could cause disruption and instability for the epibionts, causing many of them to die and making room for new colonizers. When a rhodolith is buried for an extended period, the number of epibionts decreases. Unbranched bryozoans and boring mollusks, on the other hand, may survive despite such disturbances. There is a higher probability that forceful enough water movements (e.g., during storms) move more regularly low-density rhodoliths and that those highly aggregated rhodoliths are less affected by those water movements, but the mass and volume of rhodoliths are also implied in these probabilities (Bosellini and Ginsburg, 1971; Marrack, 1999; Basso et al., 2009).

Isolated rhodoliths present the dominance of just a few species. The migration of organisms commonly associated with hard substrates, such as many mollusks and polychaetes, from one rhodolith to another, can be too risky, and isolated rhodoliths are surrounded by sandy substrate. These organisms would need to embark on a relatively long path through the sandy seafloor, exposed to predators before encountering another suitable hard substrate.

In very aggregated rhodolith beds, there is the potential for a rapid and continuous interchange of organisms that soon reaches a dynamic equilibrium typical of a climax community. It has been proposed that good competitors displace good dispersers in rhodolith beds in stable zones, but good dispersers are dominant in unstable zones where usually good competitors cannot tolerate disturbance (Hinojosa-Arango et al., 2009). It has been found that densely aggregated rhodoliths could limit the amount of growth of branches and bioerosion in the external surfaces of rhodoliths and that a low density of rhodoliths would permit these rhodoliths to roll more easily and suffer more erosion and branch breaking, making them less complex in the outer surfaces (Hinojosa-Arango et al., 2009).

Effects of Rhodolith Complexity on Rhodolith-Associated Macrofauna Diversity

Eight hollow rhodoliths had fishes (only one additional fish was found in a non-hollow rhodolith). Extensive branching and crevices within the rhodoliths or hollow rhodoliths (rhodoliths with little cave-like spaces inside) are known to be relevant to small fishes (Teichert, 2014). The hollows can increase the rhodolith volume and complexity, providing small fish and other taxa with suitable habitats (Gagnon et al., 2012).

In the present study, no difference in the average complexity was found according to the levels of aggregation. There are rhodoliths within the entire range of complexity within each level of aggregation. During the dives, we observed that the rhodoliths at the highest aggregation remain within an immobile matrix. Their branches are intertwined. Rhodoliths with fewer branches remain within this array. In the less-dense bed zone, there is greater freedom for some disturbance (currents or macropredators) to mobilize, bury, or unearth them. Rhodoliths might represent a mix of early to later successional stages in the moderate density zone, in contrast with the pioneer colonized or opportunist species in isolated rhodoliths and dominant or stable species in the dense bed (Johnson, 1972). The moderate aggregation level is possibly more dynamic in the species turnover in the course of time, with migration into and out to the rhodolith bed as pointed out by Hinojosa-Arango et al. (2009). This pattern is similar to a dense forest that supports greater diversity when clear patches are formed (Connell, 1978); in the case of the moderately aggregated rhodoliths, there can be both soft bottom and hard bottom fauna, while in highly dense rhodoliths, species adapted to hard substrates dominated (Otero-Ferrer et al., 2019).

Rhodolith structure has proven to be relevant for the biodiversity of associated organisms (Steller et al., 2003; Gabara et al., 2018; Fredericq et al., 2019). In this study, within each aggregation level, more complex rhodoliths had a higher species richness and abundance of organisms, concordant with the results of Steller et al. (2003) that used branch density instead of perimeter variation as an indicator of complexity. The gradient in the complexity of rhodoliths also changes the composition of macrofauna additionally to the density of the rhodolith bed, similar to the experimental results by Otero-Ferrer et al. (2019).

The biomass of macrofauna was higher in more voluminous rhodoliths because they can harbor a higher number of organisms or animals of higher body size. Moderately aggregated rhodoliths had higher biomass per volume than in the other levels. Less voluminous isolated rhodoliths can be more easily disturbed or have less probability to be colonized within the sandy bottom, i.e., insufficient niche requirements (Grinnell, 1917; Hutchinson, 1959; Schoener, 1974). To explain the differences between moderately and highly aggregated relationships with the volume of the rhodoliths and biomass, more detailed methods of measuring the complexity and availability of outer and inner space of rhodoliths are needed. Otero-Ferrer et al. (2019) found that complexity and habitat source influence the colonizers in the assemblages in different rhodolith aggregations. Interspace can allow sediment retention in the sandy bottom and animals used them for food sources, but in dense rhodolith beds, the main use is to avoid predation. Novel computerized techniques, like microtomography, offer three-dimensional models of the outer and inner complexity of a rhodolith and may be an option for future research (Torrano-Silva et al., 2015).

CONCLUSIONS

Rhodolith beds of Isla del Coco display a rich and diverse associated fauna. Our results demonstrate that moderate aggregation in rhodolith beds favors a greater diversity of associated taxa as that density permits some variation in the successional stages on rhodoliths. Physical aggregation levels and morphological characteristic variation of rhodoliths influence faunal communities adding evidence to the role of these beds in providing background heterogeneity suitable for a myriad of organisms. Because of the presence of active reproduction, adults, and juvenile stages of several of the species associated with rhodoliths, future research could use these communities as models to study the aspects of reproduction and dispersal processes.

Research on rhodolith beds of Isla del Coco is a promising source of discoveries since only a small portion of these beds has been investigated in search of their associated fauna and their ecology. This research contributes to making evident the importance of rhodolith beds for biodiversity and the need to preserve such ecologically relevant habitats.

DATA AVAILABILITY STATEMENT

The original contributions presented in the study are included in the article/**Supplementary Material**. Further inquiries can be directed to the corresponding author.

ETHICS STATEMENT

Ethical review and approval was not required for the animal study.

AUTHOR CONTRIBUTIONS

AS-B, JS-C, and JC contributed to the conception and design of the study. JC collected the samples. AS-B analyzed the samples and organized the database. AS-B and JS-C performed the statistical analysis. AS-B and JC wrote the first draft of the manuscript. AS-B, JS-C, and JC wrote sections of the manuscript. All authors contributed to manuscript revision and read and approved the submitted version.

ACKNOWLEDGMENTS

This project was funded by the Vicerrectoría de Investigación, Universidad de Costa Rica (projects 808-A6-155 and 808-B0-654) and the Consejo Nacional de Rectores de las Universidades Públicas de Costa Rica (CONARE, National Council of Public University Rectors). The authors thank Peter J. Auster (University of Connecticut) for his critical review of the manuscript.

SUPPLEMENTARY MATERIAL

The Supplementary Material for this article can be found online at: https://www.frontiersin.org/articles/10.3389/fmars.2022.858416/full#supplementary-material

Supplementary Appendix 1 | List of organisms found in rhodoliths from Parque Nacional Isla del Coco, Costa Rica. Indet., Indertemined taxonomy; IC, Isla del Coco.

REFERENCES

Aburto-Oropeza, O., Dominguez-Guerrero, I., Cota-Nieto, J., and Plomozo-Lugo, T. (2009). Recruitment and Ontogenetic Habitat Shifts of the Yellow Snapper (*Lutjanus Argentiventris*) in the Gulf of California. *Mar. Biol.* 156 (12), 2461–2472. doi: 10.1007/s00227-009-1271-5

Basso, D., Nalin, R., and Nelson, C. S. (2009). Shallow-Water Sporolithon Rhodoliths From North Island (New Zealand). *Palaios* 24 (2), 92–103. doi: 10.2110/palo.2008.p08-048r

Bosellini, A., and Ginsburg, R. N. (1971). Form and Internal Structure of Recent Algal Nodules (Rhodolites) From Bermuda. *J. Geol.* 79 (6), 669–682. doi: 10.1007/978-90-481-2639-2_249

Christie, H., Norderhaug, K. M., and Fredriksen, S. (2009). Macrophytes as Habitat for Fauna. *Mar. Ecol. Prog. Ser.* 396, 221–233. doi: 10.3354/meps08351

Connell, J. H. (1978). Diversity in Tropical Rain Forests and Coral Reefs. *Science* 199, 1302–1310. doi: 10.1126/science.199.4335.1302

Cortés, J. (2012). Marine Biodiversity of an Eastern Tropical Pacific Oceanic Island, Isla Del Coco, Costa Rica. *Rev. Biol. Trop.* 60 (3), 131–185. doi: 1015517/RBT.V6013.28356

Cortés, J. (2016). "Isla Del Coco: Coastal and Marine Ecosystems," in *Costa Rican Ecosystems*. Ed. M. Kappelle (Chicago and London: University of ChicagoPress), 162–191. doi: 10.1126/science.199.4335.1302

Costa, D. A., de Lucena, R. F. P., da Silva, F. D. A., da Silva, G. M. B., Massei, K., Christoffersen, M. L., et al. (2021). Importance of Rhodoliths as Habitats for Benthic Communities in Impacted Environments. *Reg. Stud. Mar. Sci.* 48, 102055. doi: 10.1016/j.rsma.2021.102055

Crawley, M. J. (2007). *The R Book* (Hoboken, New Jersey: John Wiley & Sons).

Cudney-Bueno, R., Prescott, R., and Hinojosa-Huerta, O. (2008). The Black Murex Snail, *Hexaplex Nigritus* (Mollusca, Muricidae), in the Gulf of California, Mexico: I. Reproductive Ecology and Breeding Aggregations. *Bull. Mar. Sci.* 83, 285–298.

De Grave, S., and Whitaker, A. (1999). A Census of Maërl Beds in Irish Waters. *Aquat. Conserv. Mar. Freshw. Ecosyst.* 9, 303–311.

Dial, R., and Roughgarden, J. (1998). Theory of Marine Communities: The Intermediate Disturbance Hypothesis. *Ecology* 79, 1412–1424. doi: 10.2307/176752

Duerr, S. B. (1994). Quick Estimation of Pebble Volumes. *J. Sediment. Res.* 64, 677–679. doi: 10.1306/D4267E56-2B26-11D7-8648000102C1865D

Fredericq, S., Krayesky-Self, S., Sauvage, T., Richards, J., Kittle, R., Arakaki, N., et al. (2019). The Critical Importance of Rhodoliths in the Life Cycle Completion of Both Macro- and Microalgae, and as Holobionts for the Establishment and Maintenance of Marine Biodiversity. *Front. Mar. Sci.* 5. doi: 10.3389/fmars.2018.00502

Fuad, M. A. Z. (2010). Coral Reef Rugosity and Coral Biodiversity: Bunaken National Park-North Sulawesi, Indonesia. *Tourism* 60, 14–18.

Gabara, S. S., Hamilton, S. L., Edwards, M. S., and Steller, D. L. (2018). Rhodolith Structural Loss Decreases Abundance, Diversity, and Stability of Benthic Communities at Santa Catalina Island, CA. *Mar. Ecol. Prog. Ser.* 595, 71–88. doi: 10.3354/MEPS12528

Gagnon, P., Matheson, K., and Stapleton, M. (2012). Variation in Rhodolith Morphology and Biogenic Potential of Newly Discovered Rhodolith Beds in Newfoundland and Labrador (Canada). *Bot. Mar.* 55, 85–99. doi: 10.1515/bot-2011-0064

Graham, D. J., and Midgley, N. G. (2000). Graphical Representation of Particle Shape Using Triangular Diagrams: An Excel Spreadsheet Method. *Earth Surf. Process. Landforms* 25 (13), 1473–1477. doi: 10.1002/1096-9837(200012)25:13<1473::AID-ESP158>3.0.CO;2-C

Grinnell, J. (1917). The Niche-Relationships of the California Thrasher. *Auk* 34, 427–433. doi: 10.2307/4072271

Hammer, Ø., Harper, D. A. T., and Ryan, P. D. (2001). PAST: Paleontological Statistics Software Package for Education and Data Analysis. *Palaeont. Electr.* 4, 1–9.

Hinojosa-Arango, G., Maggs, C. A., and Johnson, M. P. (2009). Like a Rolling Stone: The Mobility of Maerl (Corallinaceae) and the Neutrality of the Associated Assemblages. *Ecology* 90, 517–528. doi: 10.1890/07-2110.1

Hinojosa-Arango, G., and Riosmena-Rodríguez, R. (2004). Influence of Rhodolith-Forming Species and Growth-Form on Associated Fauna of Rhodolith Beds in the Central-West Gulf of California, México. *Mar. Ecol.* 25, 109–127. doi: 10.1111/j.1439-0485.2004.00019.x

Hutchinson, G. E. (1959). Homage to Santa Rosalia, or Why are There So Many Kinds of Animals? *Amer. Natural.* 93, 145–159. doi: 10.1086/282070

Jørgensbye, H. I. Ø., and Halfar, J. (2017). Overview of Coralline Red Algal Crusts and Rhodolith Beds (Corallinales, Rhodophyta) and Their Possible Ecological Importance in Greenland. *Polar Biol.* 40, 517–531. doi: 10.1007/s00300-016-1975-1

Johnson, R. G. (1972). "Conceptual Models of Benthic Marine Communities," in *Models in Paleobiology*. Ed. T. J. M. Schopf (San Francisco, California: Freeman, Cooper & Co), 148–159.

Marrack, E. C. (1999). The Relationship Between Water Motion and Living Rhodolith Beds in the Southwestern Gulf of California, Mexico. *Palaios* 14, 159–171. doi: 10.2307/3515371

Navarro-Mayoral, S., Fernandez-Gonzalez, V., Otero-Ferrer, F., and Tuya, F. (2020). Spatio-Temporal Variability of Amphipod Assemblages Associated With Rhodolith Seabeds. *Mar. Freshwat. Res.* 72 (1), 76–83. doi: 10.1071/mf19360

Neill, K. F., Nelson, W. A., D'Archino, R., Leduc, D., and Farr, T. J. (2015). Northern New Zealand Rhodoliths: Assessing Faunal and Floral Diversity in Physically Contrasting Beds. *Mar. Biodiv.* 45, 63–75. doi: 10.1007/s12526-014-0229-0

Otero-Ferrer, F., Mannarà, E., Cosme, M., Falace, A., Montiel-Nelson, J. A., Espino, F., et al. (2019). Early-Faunal Colonization Patterns of Discrete Habitat Units: A Case Study With Rhodolith-Associated Vagile Macrofauna. *Estuar. Coast. Shelf Sci.* 218, 9–22. doi: 10.1016/j.ecss.2018.11.020

Prata, J., Costa, D. A., Manso, C. L. C., Crispim, M. C., and Christoffersen, M. L. (2017). Echinodermata Associated to Rhodoliths From Seixas Beach, State of Paraíba, Northeast Brazil. *Biota Neotrop.* 17 (3), e20170363. doi: 10.1590/1676-0611-BN-2017-0363

Pereira-Filho, G. H., Francini-Filho, R. B., Pierozzi, I. Jr., Pinheiro, H. T., Bastos, A. C., Leão de Moura, R., et al. (2015). Sponges and Fish Facilitate Succession from Rhodolith Beds to Reefs. *Bull. Mar. Sci.* 91, 45–46. doi: 10.5343/bms.2014.1067

Quinn, J., and Keough, M. J. (2002). *Experimental Design and Data Analysis for Biologists* (Cambridge and New York: Cambridge University Press).

Riosmena-Rodríguez, R., and Medina-López, M. A. (2010). *The Role of Rhodolith Beds in the Recruitment of Invertebrate Species in the Southwestern Gulf of Mexico. All Flesh is Green, Plant-Animal.* Eds. J. Seckbach and Z. Dubinsk (New York: Springer), 417–428.

Riosmena-Rodríguez, R., Nelson, W., and Aguirre, J. (2017). *Rhodolith/Maërl Beds: A Global Perspective* (Cham, Switzerland: Springer Int. Publ). 319 p.

Sánchez-Latorre, C., Triay-Portella, R., Cosme, M., Tuya, F., and Otero-Ferrer, F. (2020). Brachyuran Crabs (Decapoda) Associated With Rhodolith Beds: Spatio-Temporal Variability at Gran Canaria Island. *Diversity* 12, 223. doi: 10.3390/d12060223

Schoener, T. W. (1974). Resource Partitioning in Ecological Communities. *Science* 185, 27–39. doi: 10.1126/science.185.4145.27

Steller, D. L., and Cáceres-Martínez, C. (2009). Coralline Algal Rhodoliths Enhance Larval Settlement and Early Growth of the Pacific Calico Scallop *Argopecten Ventricosus*. *Mar. Ecol. Prog. Ser.* 396, 49–60. doi: 10.3354/meps08261

Steller, D. L., Riosmena-Rodríguez, R., Foster, M. S., and Roberts, C. A. (2003). Rhodolith Bed Diversity in the Gulf of California: The Importance of Rhodolith Structure and Consequences of Disturbance. *Aquat. Conserv. Mar. Freshwat. Ecosyst.* 13, S5–S20. doi: 10.1002/aqc.564

Stelzer, P. S., Mazzuco, A. C. A., Gomes, L. E., Martins, J., Netto, S., and Bernardino, A. F. (2021). Taxonomic and Functional Diversity of Benthic Macrofauna Associated With Rhodolith Beds in SE Brazil. *PeerJ* 9, e11903. doi: 10.7717/peerj.11903

Teichert, S. (2014). Hollow Rhodoliths Increase Svalbard´s Shelf Biodiversity. *Nat. Scient. Rep.* 4, 1–5. doi: 10.1038/srep06972

Torrano-Silva, B. N., Gomes-Ferreira, S., and Oliveira, M. C. (2015). Unveiling Privacy: Advances in Microtomography of Coralline Algae. *Micron* 72, 34–38. doi: 10.1016/j.micron.2015.02.004

Veras, P., de, C., Pierozzi, I. Jr., Lino, J. B., Amado-Filho, G. M., de Senna, A. R., et al. (2020). Drivers of Biodiversity Associated With Rhodolith Beds From Euphotic and Mesophotic Zones: Insights for Management and Conservation. *Perspect. Ecol. Conserv.* 18, 37–43. doi: 10.1016/j.pecon.2019.12.003

Wilson, J. B. (1994). The 'Intermediate Disturbance Hypothesis' of Species Coexistence is Based on Patch Dynamics. *New Z. J. Ecol.* 18, 176–181.

Zar, J. H. (1996). *Biostatistical Analysis. 3rd Edition* (New Jersey: Prentice-Hall). 716 p.

Conflict of Interest: The authors declare that the research was conducted in the absence of any commercial or financial relationships that could be construed as a potential conflict of interest.

frontiers | Frontiers in Earth Science

ORIGINAL RESEARCH
published: 22 June 2022
doi: 10.3389/feart.2022.884685

The Punta de la Mona Rhodolith Bed: Shallow-Water Mediterranean Rhodoliths (Almuñecar, Granada, Southern Spain)

Jesús Del Río[1], *Dino Angelo Ramos*[2], *Luis Sánchez-Tocino*[3], *Julio Peñas*[4] *and Juan Carlos Braga*[2]*

[1]Departamento de Geodiversidad y Biodiversidad, Delegación Territorial de Desarrollo Sostenible de Granada, Junta de Andalucía, Granada, Spain, [2]Departamento de Estratigrafía y Paleontología, Universidad de Granada, Granada, Spain, [3]Departamento de Zoología, Universidad de Granada, Granada, Spain, [4]Departamento de Botánica, Universidad de Granada, Granada, Spain

Shallow-water rhodolith beds are rare in the Mediterranean Sea and generally poorly known. The Punta de la Mona rhodolith bed extends for 16,000 square meters in shallow and oligotrophic waters at the southern coast of Spain, off Almuñecar in the Alborán Sea. We present a detailed analysis of the structure (rhodolith cover and density, rhodolith size and shape, sediment granulometry) and morphospecies composition of the bed along a depth gradient. A stratified sampling was carried out at six depths (9, 12, 15, 18, 21, and 24 m), estimating rhodolith cover and abundance; rhodoliths were collected from one 30 by 30 cm quadrat for each transect, resulting in 18 samples and a total of 656 rhodoliths. The collected rhodoliths were measured and the coralline algal components identified morphoanatomically through a stereomicroscope and SEM. Sediment on the seafloor mainly consisted of pebbles and cobbles; the highest rhodolith cover occurred between 15 and 18 m, and the lowest at the shallowest and deepest transects (9 and 24 m). Mean Rhodolith size was similar throughout the depth range (23–35 mm) with a slight increase at 24 m, although the largest rhodoliths occurred at 21 m. In monospecific rhodoliths, size depended more on the forming species than on depth. We found 25 non-geniculate coralline morphospecies, nearly all rhodolith-forming morphospecies reported in the Mediterranean Sea in recent accounts. The highest morphospecies richness (18–19) and proportional abundance were found at intermediate depths (15–18 m), where rhodolith cover is also highest. *Lithophyllum incrustans* and *Lithophyllum dentatum* dominated at shallow depths (9–12 m), whereas *Lithothamnion valens* was the dominant species at intermediate and greater depths. Overall, the latter species was the most common in the rhodolith bed. The shallow-water rhodolith bed in Punta de la Mona is probably the most diverse in the Mediterranean Sea. This highlights the importance of the conservation of this habitat and, in general, emphasizes the role of the Alborán Sea as a diversity center of coralline algae. The Punta de la Mona example contradicts the common assumption in the geological literature that rhodolith beds are indicative of oligophotic environments with high nutrients levels.

Keywords: coralline red algae, depth-gradient patterns, rhodolith cover and size, rhodolith diversity, Alboran sea

OPEN ACCESS

Edited by:
Daniela Basso,
University of Milano-Bicocca, Italy

Reviewed by:
Nadine Schubert,
University of Algarve, Portugal
Salvatore Giacobbe,
University of Messina, Italy

***Correspondence:**
Juan Carlos Braga
jbraga@ugr.es

Specialty section:
This article was submitted to Paleontology, a section of the journal Frontiers in Earth Science

Received: *14 March 2022*
Accepted: *30 May 2022*
Published: *22 June 2022*

Citation:
Del Río J, Ramos DA, Sánchez-Tocino L, Peñas J and Braga JC (2022) The Punta de la Mona Rhodolith Bed: Shallow-Water Mediterranean Rhodoliths (Almuñecar, Granada, Southern Spain). Front. Earth Sci. 10:884685. doi: 10.3389/feart.2022.884685

INTRODUCTION

Rhodolith beds are living or fossil concentrations of free-living coralline algae (Riosmena-Rodríguez, 2017). The largest rhodolith beds occur in Brazil, where they cover a substantial part of the continental shelf, with some extending for more than 20,000 km^2 (Amado-Filho et al., 2012). They are also widespread around islands and capes, and on seamounts in Baja California,

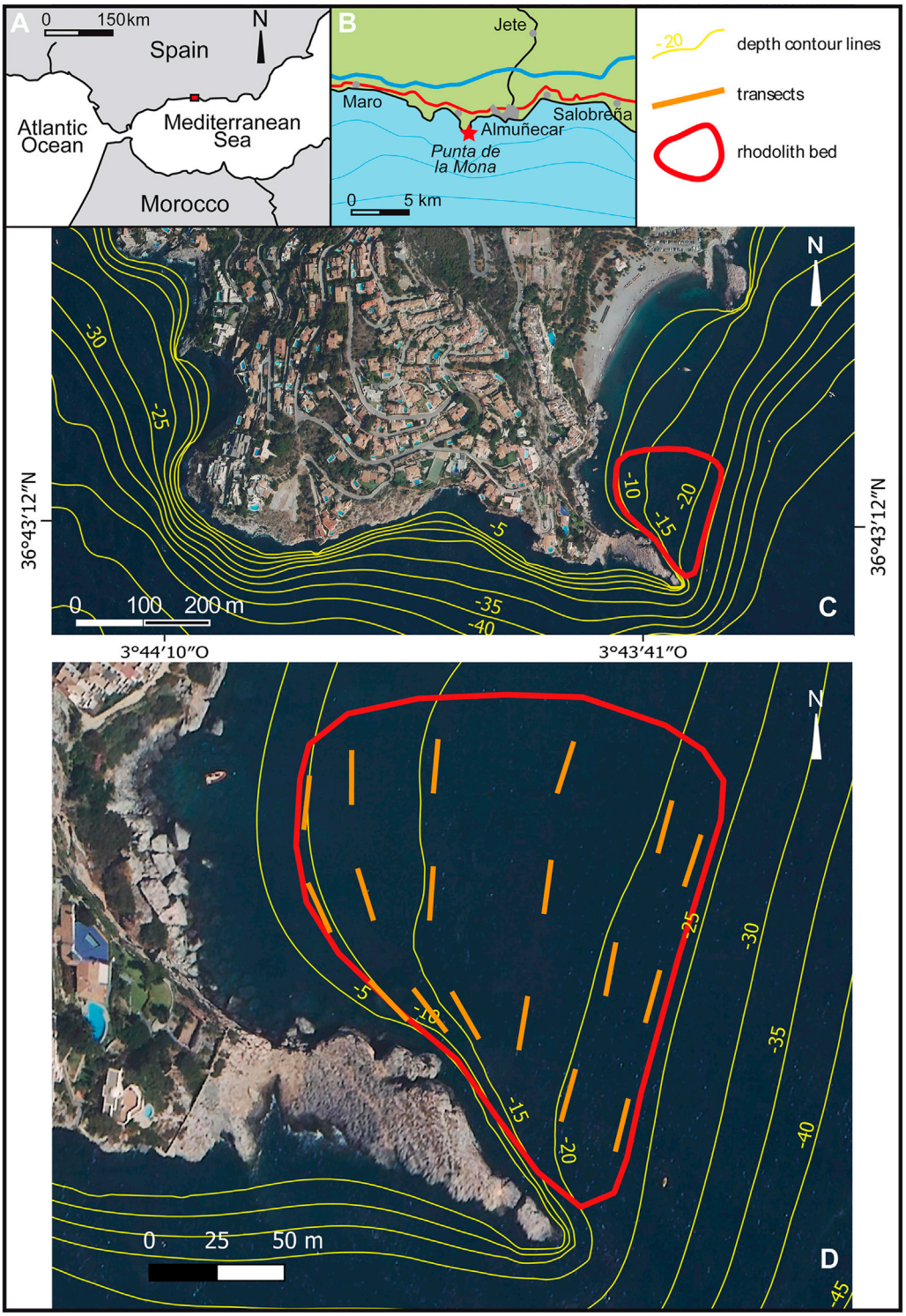

FIGURE 1 | Study area east of Punta de la Mona in southern Spain.

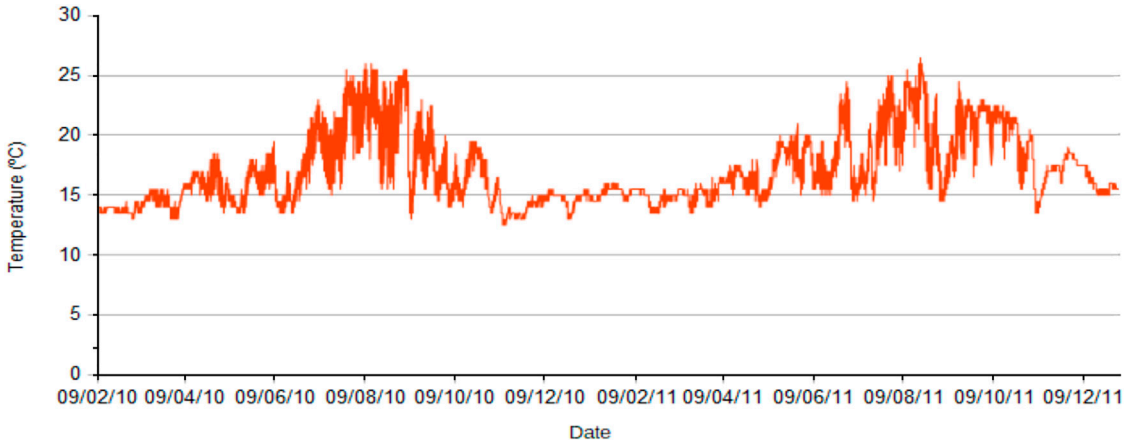

FIGURE 2 | Water temperature at 16 m in the Punta de la Mona between February 2010 and December 2011.

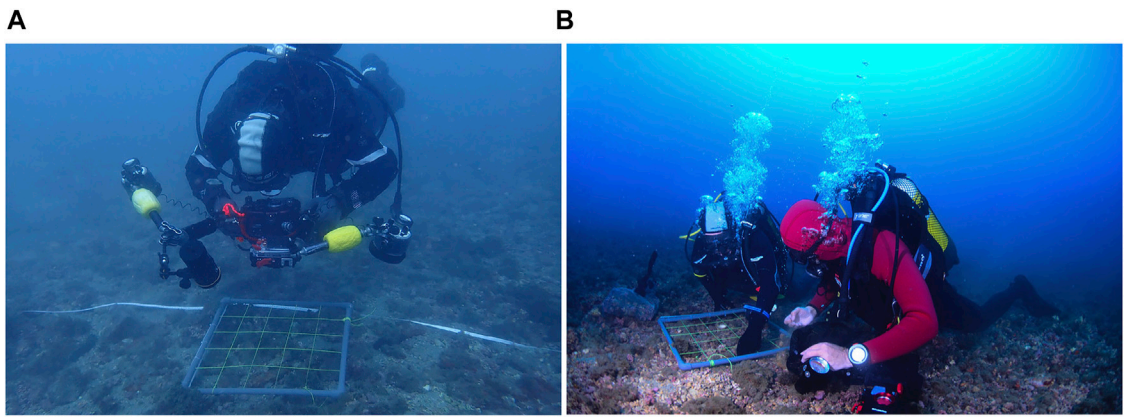

FIGURE 3 | (A) Line transect and quadrat (50 × 50-cm) for living-rhodolith cover estimation. **(B)** Quadrat (30 × 30-cm) for rhodolith collection.

northern Atlantic, Mediterranean Sea, and Australia (Foster, 2001; Steller et al., 2003; Harvey et al., 2016; Basso et al., 2017; Hernández-Kantún et al., 2017; Kamenos et al., 2017). Fragkopoulou et al. (2021) estimate that rhodolith beds might cover up to 4.1×10^6 km^2 on the seafloor, being one of the largest benthic communities dominated by macrophytes, together with seagrass beds, kelp forests and coralligènes. The main environmental factors that condition the development of rhodolith beds are light, temperature, nutrients, and currents or bioturbation phenomena that avoid the rhodoliths being buried by sediments (Jacquotte, 1962; Birkett et al., 1998; Marrack, 1999; Carvalho et al., 2020).

Rhodolith beds are considered critical ecosystems for marine biodiversity (Fredericq et al., 2019), which depends on their structural complexity (Bordehore et al., 2003; Teichert et al., 2014). In fact, rhodoliths are ecosystem engineers (Nelson, 2009), which generate structural complexity and hard substrates on detrital sea floors (Cabioch, 1969), fostering biodiversity by providing habitat to species of both hard and mobile bottoms (Keegan, 1974; Barberá et al., 2003), from microfauna (Steller et al., 2003; Foster et al., 2007) to macroalgae (Peña et al., 2014), and to species of commercial interest (Hall-Spencer et al., 2003; Kamenos et al., 2004; Steller and Cáceres-Martínez, 2009). Rhodolith beds are vulnerable to changes in the environment, especially those resulting from human activities, which result in reduced complexity and biodiversity (Peña and Bárbara, 2010). Moreover, rhodolith beds provide environmental services, such as carbonate sequestration and habitat complexity with unique benthic diversity and associated fish assemblages, thus justifying urgent actions to protect them (Amado-Filho et al., 2017). The knowledge of their distribution, structure and composition is, therefore, necessary to preserve the ecosystem services of rhodolith beds (Salomidi et al., 2012; Basso et al., 2016).

Reported rhodolith beds are scarce in the Alborán Sea, the southwestern sector of the Mediterranean (Robles, 2010). The largest one occurs on the Alborán island shelf, with several square kilometers extending from 20 to 100 m depth (Betzler et al., 2011; Gofas et al., 2014). Twenty-one species of coralline algae were

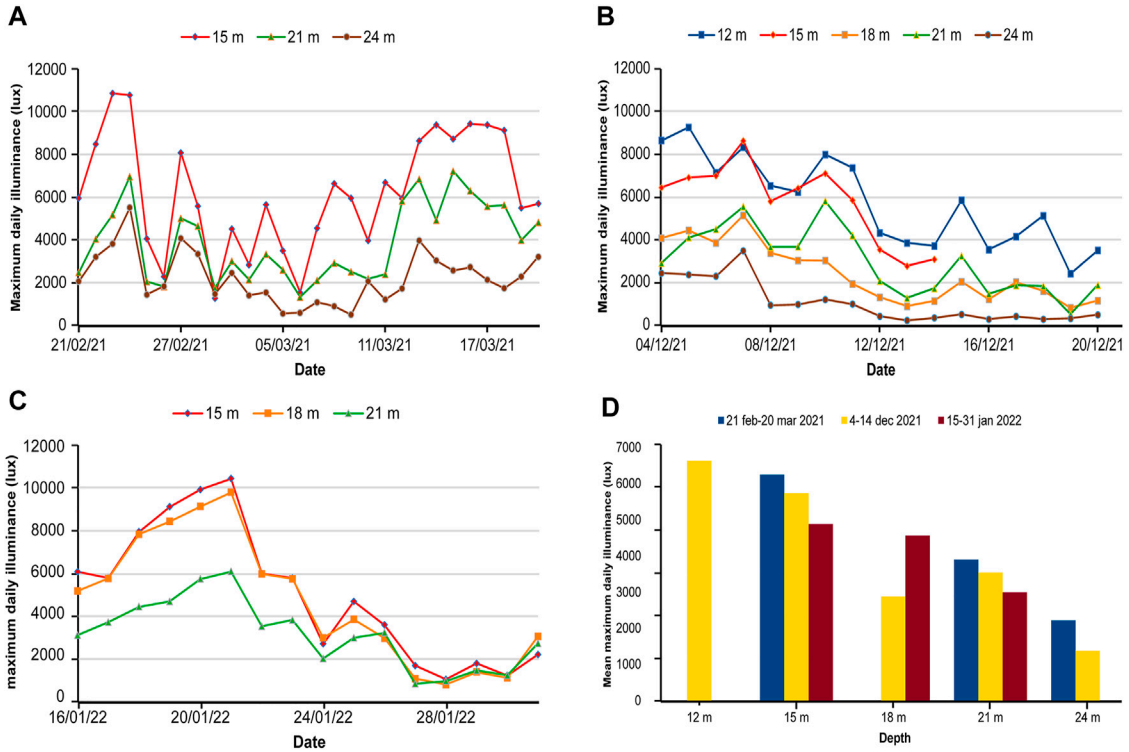

FIGURE 4 | Daily maximum illuminance from **(A)** 21 February to 21 March2021 and **(B)** 4 to 20 December 2021, **(C)** 15 to 31 January 2022 and **(D)** variation of mean maximum illuminances by depth.

recognized by molecular analysis in this bed, ten of which remain unnamed (Gofas et al., 2014). Rhodolith beds have also been recorded in the Tres Forcas cape, in Morocco (CAR/ASP-PNUE/PAM, 2013), Gibraltar Straits (García-Gómez et al., 2003), Ceuta (Ocaña et al., 2009) and the Almería shelf, in southeastern Spain (Ministerio de Agricultura, Alimentación y Medio Ambiente, 2012), although their structure and composition were not reported. The composition of coralline algal assemblages, including those forming rhodoliths, was described at the northeastern limit of the Alborán Sea, in the waters of the Cabo de Gata Natural Park in Almería (Braga et al., 2009; Bassi et al., 2020).

This work aims to describe a shallow-water rhodolith bed located off the Punta de la Mona, Granada, (southern Spain) in the northern shelf of the Alborán Sea. We assess the rhodolith cover, size, shape, morphospecies composition and diversity along a depth range from 9 to 24 m, and relate the observed patterns to environmental variables, such as temperature and illuminance. We stress the uniqueness and originality of this bed and the need for conservation of marine biodiversity reserves.

MATERIAL AND METHODS

Study Area

The study area is located at the southern coast of Spain, near Almuñecar in the province of Granada. The area encompasses a rhodolith bed of 16,000 m^2 extending from 9 to 24 m depth in a small bay east of Punta de la Mona (36°41′13′′ N, 3°43′39′′ W). This is a cape running N-S for approximately 1,000 m and then bending to a E-ESE direction. As a result, the small bay in which the rhodoliths occur is protected from the westerlies (**Figure 1**).

According to the wave modeling SIMAR for the Punta de la Mona (site 2039080), during the period January 1958-July 2021, dominant wave directions were from E-ESE (41.8%) and W-WSW (30.3%). Waves had heights above 2 m only 4.5% of the time, and calms and waves <0.5 m occurred 55% of the time (Puertos del Estado, 2021a).

The levels of chlorophyll A from 2000 to 2020 obtained from the AQUA MODIS satellite indicate an oligotrophic environment, with mean values of 1–1.5 mg/cm^3, peaking in spring (1.5–2 mg/cm^3) and dropping in autumn-winter (>0.01 mg/cm^3) (REDIAM, 2021).

Sea surface temperature (SST) in 2020–2021, estimated by the satellite Sentinel (site 2039080), ranged between 27.1°C in summer and 13.3°C in winter (Puertos del Estado, 2021b). Measuring every 30 min at 16 m depth, in 2010–2011 the average temperature was 17°C, ranging from 26.5°C in summer to 12.5°C in winter. The summer temperatures underwent strong fluctuations due to upwelling events related to storms from the west, whilst winter temperatures were more stable around 15°C (**Figure 2**). New temperature measurements were carried out for this study (see below).

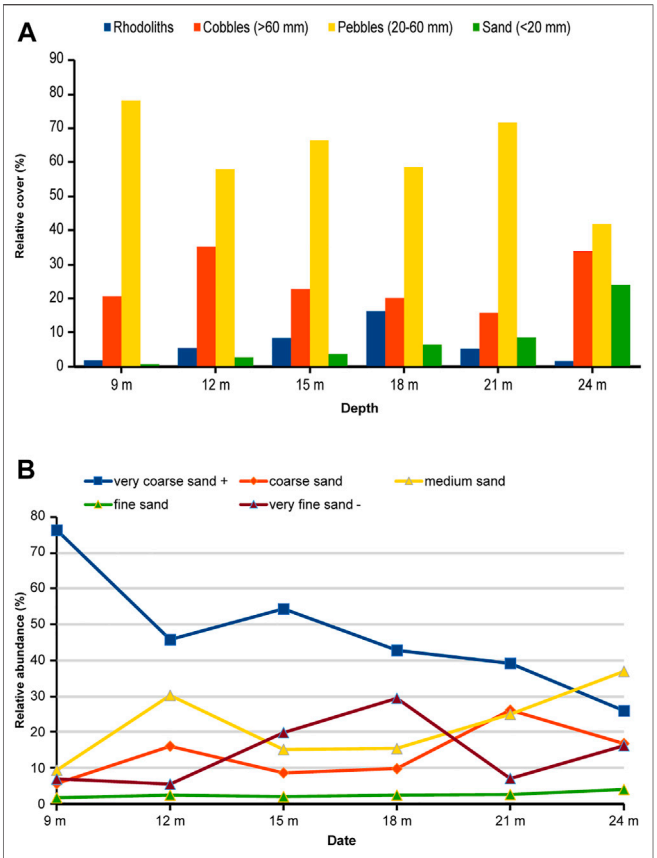

FIGURE 5 | (A) Proportion of rhodoliths and grain-size classes (% cover) at different depths. **(B)** Proportion of sand-sized fractions (<2 mm) at different depths.

Sampling Design and Sample Collection

The extent of the rhodolith bed was delimited by mapping the seafloor by SCUBA diving. A stratified sampling design at six depths (9, 12, 15, 18, 21 and 24 m) was used to analyze distribution and density of rhodoliths. Three 20 m long line transects were placed at each depth. To estimate the living (coloured) rhodolith cover, photographs of ten 50x50 cm quadrats were taken in each transect, i.e., 30 photographs in each depth and 180 photos in total (**Figure 3A**). The pictures were processed with the software ImageJ (National Institutes of Health, United States, https://imagej.nih.gov) to obtain the area covered by living-rhodoliths, cobbles, pebbles, and sand in each quadrat. The proportion of dead rhodoliths was negligible. All rhodoliths in a randomly placed 30 × 30 cm quadrat were collected in each transect, i.e., 3 collections from each depth and 18 in total for measuring and identification of coralline algal composition. Collections were done between May and December 2020 (**Figure 3B**). Both unattached coralline growths and pebbles coated by corallines (independently of coating proportion) were collected and air dried for at least 2 days.

Environmental Variables

Six dataloggers (HOBO Pendant® MX, Temp/Light, www.onsensetcomp.com) were installed for data acquisition of temperature (°C) and illumination (lux) at each sampling depth, using the maximum daily illuminance by depth from measurements taken every 10 min (Otero-Ferrer et al., 2020). Two 50-ml samples of sediment smaller than pebbles were collected in each sampling depth to estimate granulometry. The samples were dried and then sieved in >1, 0.5, 0.250, and <0.125 mm fractions.

Size, Shape and Morphology of Rhodoliths

The long, intermediate and short axes of all collected rhodoliths (n= 656) were measured to estimate size, using the mean of the three axes $(L + I + S)/3$ (Bosellini and Ginsburg, 1971) and the sphericity $\psi_p = \sqrt[3]{\frac{S^2}{LS}}$ and shape classes according to Sneed and Folk (1958) and Bosence (1976, 1983). The Microsoft Excel triangular diagram plotting spreadsheet (TRI-PLOT) of Graham and Midgley (2000) was used to illustrate the representation of the shape classes. Collected rhodoliths were classified according to their morphology in four morphotypes. Three of them (pralines, branches, and boxwork rhodoliths) followed the classification scheme proposed by Basso (1998, 2012) and Basso et al. (2016); the additional class (other) comprised coatings (less than 50% of coralline algal volume, Steneck, 1986) on lithoclasts and bioclasts, and compact rhodoliths of encrusting corallines, which are difficult to distinguish without sectioning them (Aguirre et al., 2017).

Taxonomic Identification

Identification of coralline algae forming the rhodoliths was performed with a stereomicroscope and ESEM (FEG-ESEM QuemScan650F). The morphospecies identification followed the available literature on Atlantic and Mediterranean coralline algae and the taxonomy proposed by Cormaci et al. (2017) and AlgaeBase (Guiry and Guiry, 2022). Once the component species in each rhodolith were identified, a visual estimation of their relative proportions on the rhodolith surface was performed. Vouchers of the rhodoliths will be deposited at the University of Granada Herbarium (GDA).

Diversity Indexes

The diversity indexes based in abundance models allow us to compare the diversity of rhodoliths taking into consideration the relative abundance of species in an ecosystem (Magurran, 2004), that is, in our study the relative species-cover (i.e., relative proportions of individual species on the rhodolith surface) or species-frequency (i.e., relative abundance of species) that form the rhodoliths in different depths. The calculation of the Shannon-Wiener index (Magurran, 2004) was made through the formula $H' = -\sum p_i ln$, where p_i is the proportion of cover or frequency of the i^{th} species in each depth.

Data Analysis

Statistical comparisons between groups were performed on R Studio 2021.09.1+372 (RStudio Team, 2020) running R 4.1.2 (R Core Team, 2021). Data manipulation was facilitated by the dplyr 2.1.1, tidyverse 1.3.1, and broom 0.7.10 packages. Plots and

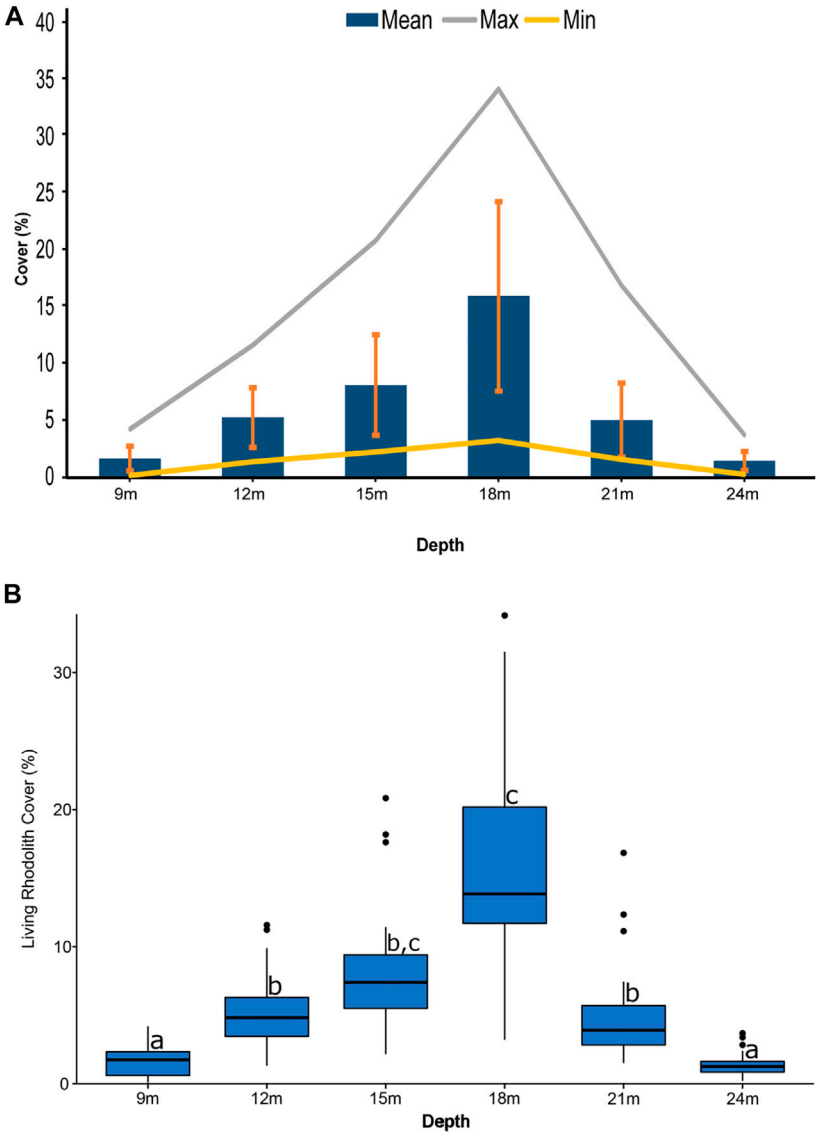

FIGURE 6 | (A) Rhodolith cover (mean and SD) and **(B)** boxplots of rhodolith cover illustrating significant differences detected across depths.

graphs were generated by the ggplot2 3.3.5 package and finalized in Inkscape 1.1.1 (http://inkscape.org). All other statistical tests were from the base package of R.

The non-parametric Kruskal–Wallis rank sum test was used to compare the differences among groups since the data did not fulfill the assumptions of ANOVA. Dunn's test with Holm's correction was used as the post-hoc test when a significant difference resulted from Kruskal–Wallis tests. Comparisons across the sampled depths were made for the benthic cover of 1) living-rhodoliths, 2) different grain sizes (cobbles, pebbles, sand), and the sizes of 3) all rhodoliths, and 4) species of the monospecific rhodoliths, excluding encrusting species (*Lithophyllum incrustans*) and those with <5 samples. 5) Size differences among species of selected monospecific rhodoliths were also compared.

RESULTS

Environmental Data

Data on temperature and illumination were obtained from 21 February to 21 March 2021 at 15, 21 and 24 m depth, from 4 to 21 December 2021 at 12, 15, 18, 21 and 24 m, and from 15 to 31 January 2022 at 15, 18 and 21 m.

The average temperature at the end of the winter in 2021 ranged from 15.8°C at 15 m to 15.7°C at 24 m, whereas in December 2021 they were slightly lower ranging between 15.6°C at 12 m and 15.5°C at 24 m, with no significant differences among depths. In January 2022, the temperature was 15.1°C between the depths of 15–21 m (**Supplementary Table S1**).

Illuminance measured every 10 min showed that the daily maxima was highly variable from 21 February to 21 March 2021,

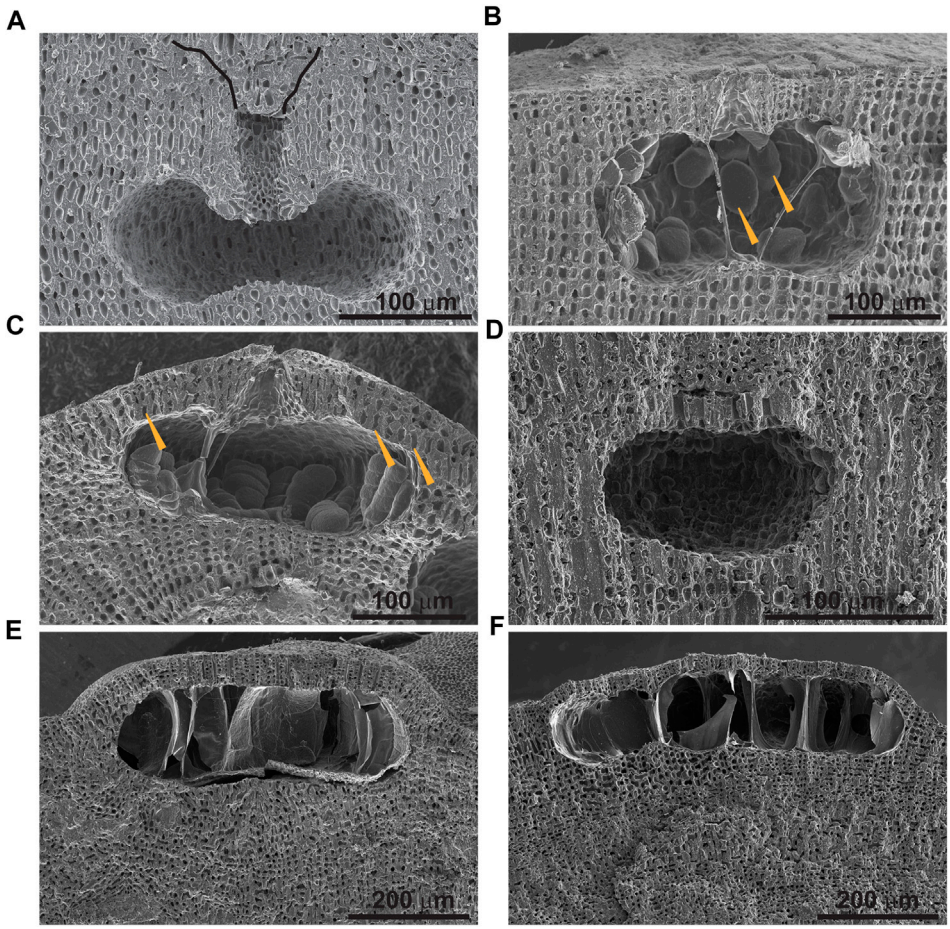

FIGURE 7 | SEM images of selected examples of identified morphospecies: **(A)** Sporangial conceptacle of *Lithophyllum hibernicum*. Black lines mark the contour of funnel-like depression on top of conceptacle pore filled by overgrowing filaments; **(B)** Bisporangial conceptacle of *Lithophyllum orbiculatum*. Arrowheads point to bispores; **(C)** Tetrasporangial conceptacle of *Lithophyllum nitorum*. Arrowheads point to elongated cells at the base of conceptacle roof; **(D)** Tetrasporangial conceptacle of *Phymatolithon calcareum*; **(E)** Tetrasporangial conceptacle of *Lithothamnion corallioides*; **(F)** Tetrasporangial conceptacle of *Lithothamnion valens*.

with a maximum value of 10,875 lux at 15 m and a minimum of 486 lux at 24 m (**Figure 4A**). The average maximum illuminance at the end of the winter showed a marked gradient with depth (**Figure 4D**). In a similar way, in December 2021 the daily maximum illuminance ranged from 9,224 lux at 12 m and 170 lux at 24 m (**Figure 4B**). The decreasing gradient with depth showed a reversal at 18 m where the values were lower than at 21 m (**Figure 4D**). In January 2022, the maximum daily illuminance ranged between 10,416 and 827 lux at 15 m (**Figure 4C**), with a reduction in mean illuminance to 93.6% at 18 m and 61.4% at 21 m with respect to at 15 m (**Supplementary Table S2**). In the three periods, the reduction in maximum illuminance between 15 and 21 m was similar, with values of 62.5, 61.8 = (3543.7/5734.6); 53.5% in **Supplementary Table S2** because the basis was the lux at 12 m, and 61.4% (**Figure 4D**; **Supplementary Table S2**).

Regarding grain size on the seafloor, pebbles were the commonest grains at all depths, followed by cobbles (**Supplementary Table S3**). Significant differences were found across depths for cobbles (p-value < 0.001), pebbles (p-value = $1.72e^{-12}$), and sand (p-value < $2.2e^{-16}$), but only sand cover exhibited a clear pattern with depth. The proportion of sand-sized grains increased from 0.5% at 9 m to 23.7% at 24 m. (**Figure 5A**). Within the sand-sized particles, the proportion of very coarse grains decreased with depth, whereas other fractions tended to increase, except very fine sand and mud which showed the highest percentage at 18 m (**Figure 5B**, **Supplementary Table S3**). A weak current was perceived at this depth while sampling.

Living-Rhodolith Cover

The average cover of living-rhodolith (mean ± SD) ranged between 1.6% (±1.1) and 1.4% (±0.8) at 24 and 9 m, respectively, and 15.9% (±8.3) at 18 m (p-value < $2.2e^{-16}$). Highest rhodolith cover in sampling quadrats ranged between 3.7% at 24 m and 34.7% at 18 m. Rhodolith distribution was heterogeneous with dispersed nodules at the bed margins at 9 and 24 m and density increased towards intermediate depths from 12 to 21 m, where rhodoliths occurred in patches whose average cover ranged from 5% (±3.3) to 15.2% (±8.3) and maximum cover from 11.58 to 34.2% (**Figure 6**).

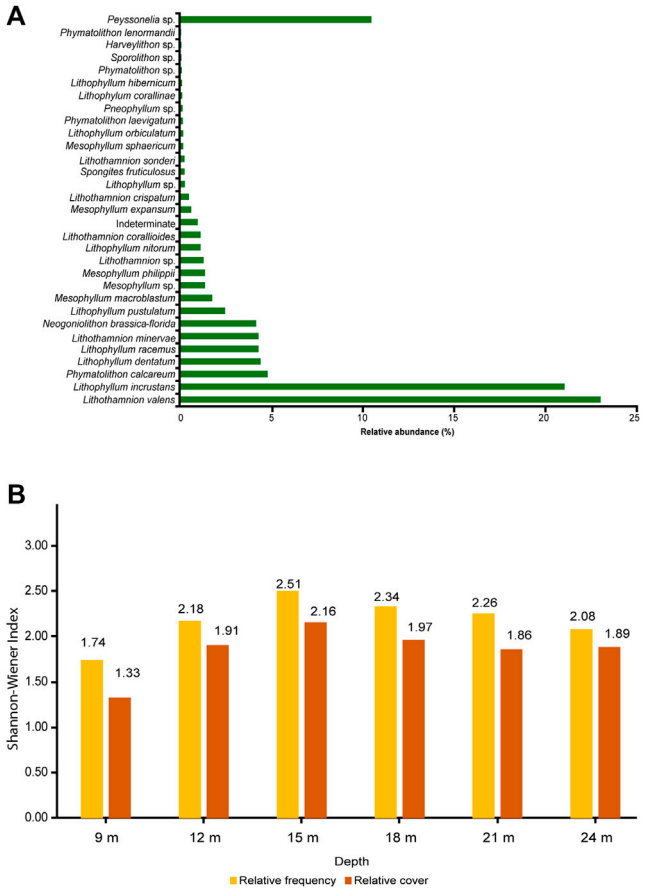

FIGURE 8 | (A) Relative abundance of the identified taxa at the sampling depths. **(B)** Shannon-Wiener index diversity measures (based on species frequency or cover) at the sampling depths.

Species Composition

Twenty-two morphospecies belonging to 6 genera (*Lithophyllum, Spongites, Neogoniolithon, Lithothamnion, Mesophyllum,* and *Phymatolithon*) were identified (**Figure 7**). Other thalli were only identified at the genus level, due to the lack of diagnostic characters. In three genera no individual species were recognised (*Pneophyllum* sp., *Sporolithon* sp., and *Harveylithon* sp.), for a total of 9 genera. Seven species dominated the assemblages, with occurrence proportions higher than 4%: *Lithothamnion valens* Foslie (23.1%), *Lithophyllum incrustans* Philippi (21.1%), *Phymatolithon calcareum* (Pallas) W.H. Adey et D.L. McKibbin ex Woelkerling et L.M. Irvine (4.8%), *Lithophyllum dentatum* (Kützing) Foslie (4.4%), *Lithophyllum racemus* (Lamarck) Foslie (4.3%), *Lithothamnion minervae* Basso (4.3%) and *Neogoniolithon brassica-florida* (Harvey) Setchell et L.R. Mason (4.1%). (**Figure 8A**; **Table 1**).

Depth distribution of morphospecies was heterogeneous. The relative abundance of *Lithophyllum incrustans* decreased with depth from 58.5% of the algal assemblage at 9 m to 5.9% at 21 m. In contrast, the proportion of *Lithothamnion valens* increased with depth from being absent at 9 m to 38.3% at 21 m. Other species showed limited depth ranges: *Lithophyllum orbiculatum* (Foslie) Foslie only occurred at shallow depths (9–12 m), *Lithophyllum dentatum* was most abundant around 12 m, *Lithothamnion minervae* and *Phymatolithon calcareum* were more abundant at 15 m, and *Mesophyllum macroblastum* (Foslie) W.H. Adey, only occurred below 15 m, with the highest counts at 24 m. Other morphospecies, such as *Lithophyllum pustulatum* (J.V. Lamouroux) Foslie, *Lithophyllum nitorum* W.H. Adey et PJ Adey, and *Lithothamnion corallioides* (P.Crouan et H. Crouan) P. Crouan et H. Crouan had homogeneous relative abundance at all depths (**Table 1**).

Monospecific rhodoliths comprised 34% of the analyzed nodules, varying from 17.9% at 9 m to 39.8% at 21 m. *Lithothamnion valens* was the most common species building monospecific rhodoliths (44.4%), followed by *Lithophyllum incrustans* (15.2%), *Phymatolithon calcareum* (10.3%) and *Lithothamnion minervae* (8.1%). Two nodules of *Lithophyllum pustulatum* and *Lithothamnion sonderi* Hauck, encrusting bioclastic and lithic nuclei, respectively, were monospecific as well (**Table 2**).

Size and Shape of Rhodoliths

Mean size of rhodoliths (mean ± SD) ranges from 23.7 mm (±9.5) at 18 m to 35.8 mm (±12.3) at 24 m, where the rhodoliths were significantly bigger than in the other depths (p-value = $2.31e^{-09}$).

TABLE 1 | Species distribution by depth (%).

Species	9 m	12 m	15 m	18 m	21 m	24 m	Total
Lithothamnion valens	0.0	8.6	25.6	32.1	38.3	23.3	23.1
Lithophyllum incrustans	58.5	37.7	14.3	9.0	5.9	13.2	21.1
Phymatolithon calcareum	0.1	0.3	8.5	6.7	4.8	2.2	4.8
Lithophyllum dentatum	2.2	18.2	4.8	0.0	1.6	0.0	4.4
Lithophyllum racemus	3.7	5.1	7.5	3.8	1.1	0.0	4.3
Lithothamnion minervae	0.9	2.0	8.4	4.1	4.2	0.0	4.3
Neogoniolithon brassica-florida	6.1	5.3	3.7	4.1	0.0	11.6	4.1
Lithophyllum pustulatum	2.4	1.6	1.0	3.9	3.5	1.1	2.4
Mesophyllum macroblastum	0.0	0.0	1.3	1.3	3.4	10.6	1.7
Mesophyllum sp.	0.0	0.0	1.0	1.2	4.2	1.9	1.3
Mesophyllum philippii	0.0	1.8	0.6	0.6	4.7	0.0	1.3
Lithothamnion sp.	0.0	4.7	0.1	1.6	1.0	0.0	1.3
Lithophyllum nitorum	0.9	0.0	2.6	0.7	0.5	0.6	1.1
Lithothamnion corallioides	0.0	1.3	0.5	1.2	2.4	1.7	1.1
Indeterminate	0.1	0.8	0.8	1.3	1.0	2.4	0.9
Mesophyllum expansum	0.8	0.0	0.0	0.8	1.6	0.0	0.6
Lithothamnion crispatum	0.0	0.0	0.5	0.0	0.0	6.6	0.4
Lithophyllum sp.	0.1	0.4	0.4	0.2	0.0	0.0	0.2
Spongites fruticulosus	0.0	0.3	0.6	0.1	0.0	0.0	0.2
Lithothamnion sonderi	1.3	0.0	0.1	0.0	0.0	0.0	0.2
Mesophyllum sphaericum	0.0	0.0	0.2	0.4	0.0	0.0	0.1
Lithophyllum orbiculatum	0.1	0.8	0.0	0.0	0.0	0.0	0.1
Phymatolithon laevigatum	0.0	0.0	0.4	0.0	0.0	0.0	0.1
Pneophyllum sp.	0.0	0.1	0.3	0.0	0.0	0.0	0.1
Lithophylum corallinae	0.0	0.0	0.0	0.2	0.2	0.0	0.1
Lithophyllum hibernicum	0.0	0.4	0.0	0.0	0.0	0.0	0.1
Phymatolithon sp.	0.0	0.0	0.1	0.1	0.1	0.0	0.1
Sporolithon sp.	0.3	0.0	0.0	0.0	0.0	0.0	0.0
Harveylithon sp.	0.0	0.0	0.0	0.1	0.0	0.0	0.0
Phymatolithon lenormandii	0.0	0.0	0.0	0.0	0.0	0.0	0.0
Peyssonelia sp.	12.7	8.3	10.7	14.1	6.1	5.8	10.5
Biogenic and lithic remains	9.6	2.4	5.8	12.3	15.3	19.1	9.7

TABLE 2 | Counts of monospecific rhodoliths by depth.

	9 m	12 m	15 m	18 m	21 m	24 m	Total	%
Lithophyllum incrustans	16	7	3	4	3	1	34	15.2
Lithophyllum dentatum	0	5	2	0	1	0	8	3.6
Lithophyllum pustulatum	0	0	0	1	0	0	1	0.4
Lithophyllum racemus	0	2	4	2	0	0	8	3.6
Lithothamnion corallioides	0	0	0	2	0	0	2	0.9
Lithothamnion minervae	0	2	9	4	2	1	18	8.1
Lithothamnion sp.	0	4	0	2	1	0	7	3.1
Lithothamnion sonderi	1	0	0	0	0	0	1	0.4
Lithothamnion valens	0	6	24	37	28	4	99	44.4
Mesophyllum macroblastum	0	0	1	1	1	0	3	1.3
Mesophyllum philippii	0	1	0	1	2	0	4	1.8
Neogoniolithon brassica-florida	0	3	2	2	0	1	8	3.6
Peyssonnelia sp.	0	1	2	4	0	0	7	3.1
Phymatolithon calcareum	0	0	12	8	3	0	23	10.3
Total	17	31	59	68	41	7	223	100.0
% of total rhodoliths	17.9	34.4	35.8	37.6	39.8	31.8	34.0	—

Maximum size of rhodoliths increased from 49 mm at 9 m to 101 mm at 21 m and decreased to 53 mm at 24 m (**Figure 9**). The number of large rhodoliths (>50 mm) also increased from 0 at 9 m to 9 at 21 m and decreased to 2 at 24 m (**Table 3**).

Monospecific rhodoliths of the most abundant species (see below) were grouped in two size classes (p-value = $9.58e^{-09}$). Based on the size ranges, *Lithophyllum dentatum* (**Figure 10A**), *Lithothamnion valens* (**Figure 10D**) and *Neogoniolithon brassica-florida* form the larger

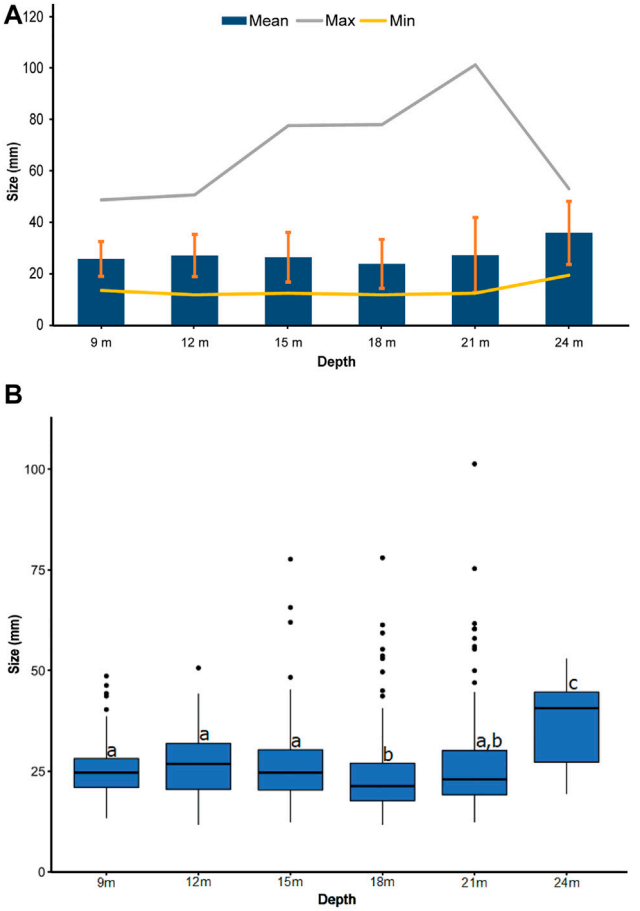

FIGURE 9 | (A) Rhodolith sizes and **(B)** boxplots illustrating significant differences detected across depths.

rhodoliths with mean sizes of 34.7 mm (±8.3), 28.8 mm (±11.7), and 27.1 mm (±8.2), respectively, whereas rhodoliths of *Lithophyllum racemus* (**Figure 10B**), *Lithothamnion minervae* (**Figure 10C**) and *Phymatolithon calcareum* were smaller, with mean sizes of 21.4 mm (±4.7 mm), 18.1 mm (±4.3 mm) and 18.4 mm (±3.8 mm) (**Figure 11A**), respectively. No significant differences were observed in the mean sizes of monospecific rhodoliths at the different depths in which they occur (p-value > 0.05, **Figure 11B**).

The maximum sphericity projection (Ψ) ranged between 0.65 at 9 m and 0.74 at 21 m, with similar values from 12 to 24 m (**Supplementary Table S4**). Most rhodoliths were spheroidal (62.5%), with lesser proportions of discoidal (19.9%) and ellipsoidal (17.6%) nodules. Proportions of shape classes were similar at all depths from 12 to 21, with a dominance of spheroidal nodules. In contrast, at 9 m, discoidal (33.7%) and ellipsoidal (28.4%) were more common (**Figure 12A**).

Most collected rhodoliths were pralines (47.7%, **Figure 12B**; **Supplementary Table S5**). This morphotype is the most abundant below 9 m. The proportion of boxwork rhodoliths increased with depth, whereas coatings and compact rhodoliths built by encrusting corallines (as other in **Figure 12B**), which were the most abundant at 9 m, tended to be less common in deeper transects. Branches were rare from 15 to 21 m and absent in the rest of depths (**Supplementary Table S5**).

Diversity of Rhodoliths

The diversity of rhodoliths (Shannon-Wiener index, H'), both based on species frequency and cover, was highest at medium depths (15 and 18 m). The maximum rhodolith diversity was 2.51 for species frequency and 2.16 for species cover at 15 m, and the minimum rhodolith diversity was 1.74 for species frequency and 1.33 for species cover at 9 m (**Figure 8B**).

DISCUSSION

Bed Structure and Rhodolith Characteristics

The Punta de la Mona rhodolith bed occupies a small surface and a narrow depth range, showing that good conditions for rhodolith growth are limited to the eastern side of a small cape enclosing a small embayment. In this small area, bottom currents generated by storms from the east hit the submarine cliff and flow out of the embayment (**Figure 1**). The generally coarse grain size on the seafloor, dominated by cobbles and pebbles (**Figure 5**), indicates that currents sweep away fine sediment. Above the upper limit of the bed, the seafloor is covered by boulders and cobbles derived from rock fall from the cliff, and high turbulence seems to prevent rhodolith development, although boulders and cobbles are partially covered by coralline algae. Below 24 m, fine-grained sediments bury the rhodoliths hindering their significant development (Steller and Foster, 1995; Wilson et al., 2004; Villas-Bôas et al., 2014).

The highest average cover of living-rhodoliths occurs at 18 m, where the values are three times higher than those at 12 and 21 m (**Figure 6**). The optimum conditions for rhodolith growth might be due to a flatter seafloor between 15 and 20 m (**Figure 1**).

TABLE 3 | Rhodolith cover (%) and size (mm) by depth.

Depth (m)	Mean cover ± SD (%)	Max cover	No. rhodoliths	No. rhodoliths >50 mm and %	Mean size ± SD (mm)	Max size	Min size
9	1.6 ± 1.1	4.2	95	0 (0%)	25.7 ± 6.8	48.7	13.3
12	5.2 ± 2.6	11.6	90	1 (1.1%)	27.0 ± 8.2	50.7	11.7
15	8.1 ± 4.4	20.8	165	3 (1.8%)	26.4 ± 9.7	77.7	12.3
18	15.9 ± 8.4	34.2	181	6 (3.3%)	23.8 ± 9.5	78.0	11.7
21	5.0 ± 3.3	16.8	103	9 (8.7%)	27.2 ± 14.6	101.3	12.3
24	1.4 ± 0.9	3.7	22	2 (9.1%)	35.8 ± 12.3	53.0	19.3

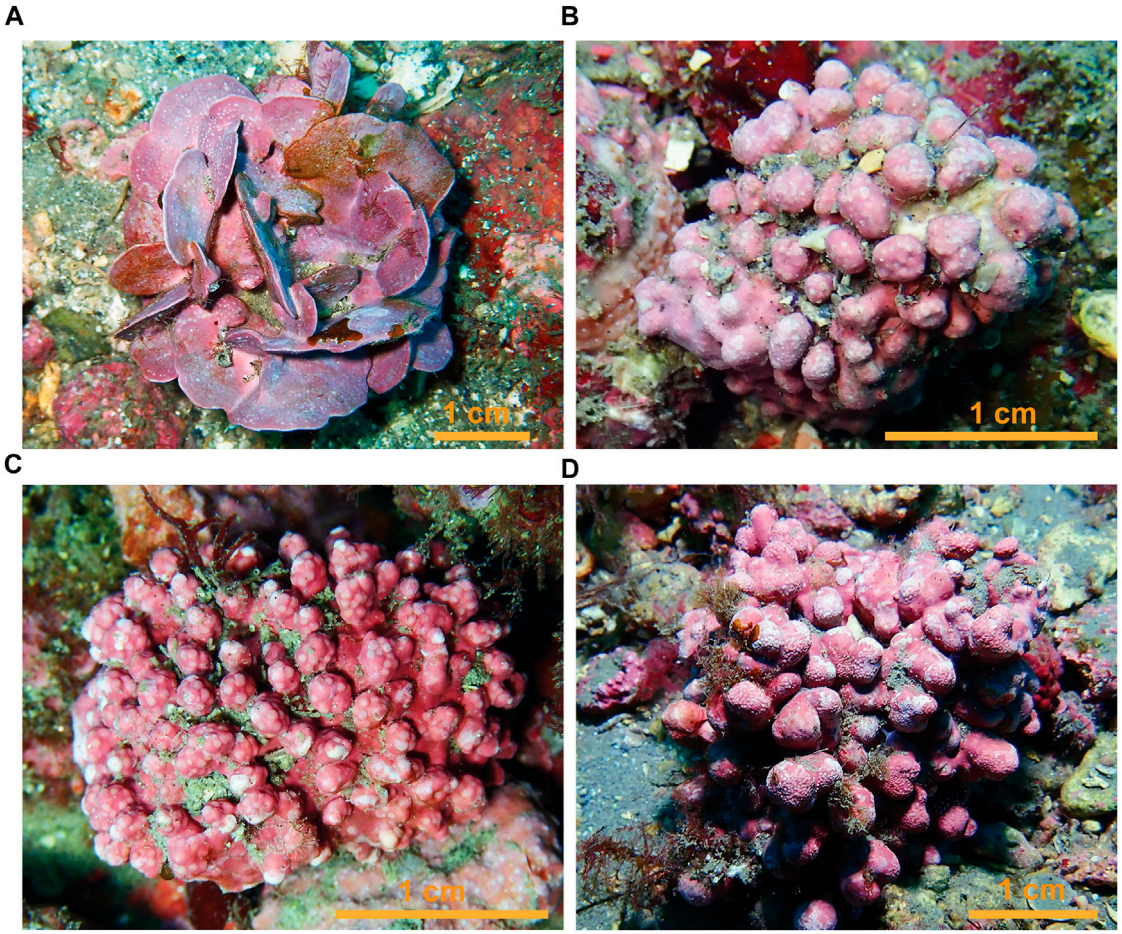

FIGURE 10 | Monospecific rhodoliths: **(A)** *Lithophyllum dentatum*; **(B)** *Lithopyllum racemus*; **(C)** *Lithothamnion minervae*; **(D)** *Lithothamnion valens.*

Despite the weak current perceived, the highest proportion of very fine sand and mud occurs at 18 m. This can be due to the well-known baffling effect of dense concentrations of branching rhodoliths, which stabilize fine-grained sediment below them (Bassi et al., 2009; Millar and Gagnon, 2018; O'Connell et al., 2021).

The mean rhodolith size is relatively small (23.7 mm). The maximum size and the number of rhodoliths larger than 50 mm increases with depth (**Figure 9**), probably related to the turbulence gradient (Amado-Filho et al., 2007; Gagnon et al., 2012; Sañé et al., 2016). The size of monospecific rhodoliths is species-dependent. Two size classes can be distinguished for monospecific rhodoliths: *Lithophyllum dentatum* and *Lithothamnion valens,* build relatively large rhodoliths, whereas the rhodoliths of *Lithothamnion minervae* and *Phymatolithon calcareum* are significantly smaller (**Figure 11**). Rhodolith sizes within individual species do not show significant differences among depths, suggesting that genetic signatures control the sizes of monospecific rhodoliths rather than environmental conditions, at least at the small scale of the Punta de la Mona bed.

The high abundance of discoidal rhodoliths at 9 m (**Figure 12A**) reflects the flat, discoidal shape of lithoclastic nuclei, commonly coated by *Lithophyllum incrustans* at this depth. In contrast with their distribution in the Punta de la Mona, discoidal rhodoliths tend to be more common at deeper depths, because of reduced overturning due to lower energy (Bosellini and Ginsburg, 1971; Bosence, 1976; Peña and Bárbara, 2009). This is an additional example confirming that other factors, such as nucleus shape and building species, influence rhodolith shape, which is not exclusively controlled by hydrodynamic energy (Aguirre et al., 2017; Braga, 2017; O'Connell et al., 2021).

Coatings and compact rhodoliths made of encrusting corallines are the most abundant morphotype at 9 m (**Figure 12B**), reflecting the dominance of encrusting *Lithophyllum* morphospecies at this depth. The general decrease of this morphotype with increasing depth parallels the decrease of encrusting plants of this genus. In a similar way, the increase of the relative proportion of boxwork rhodoliths with depth parallels the increase of *Mesophyllum*. The dominance of mono or paucispecific pralines formed by different species and the scarcity of

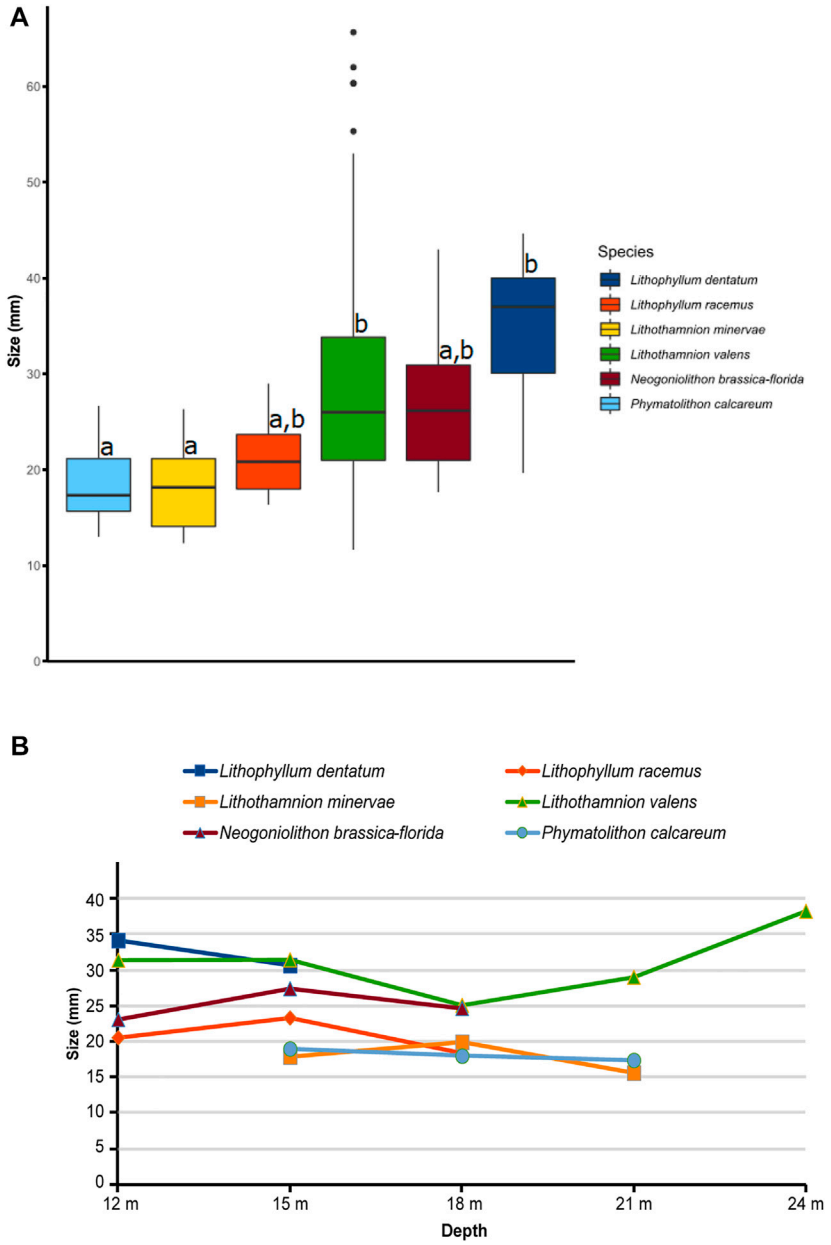

FIGURE 11 | (A) Boxplots of sizes of monospecific rhodoliths illustrating significant differences detected across species and **(B)** their mean size at different depths.

branches (**Figure 12B**) probably reflect a strong to intermediate hydrodynamic regime (Bracchi et al., 2022) suggested by the coarse grain size.

Species Composition and Diversity

The morphospecies richness in the Punta de la Mona bed (25 morphospecies, 22 of them identified at the species level, in 9 genera) is the highest described in the Mediterranean so far in a single bed. Traditionally, the Mediterranean rhodolith beds have been considered richer than those of the eastern Atlantic at similar latitudes (Basso et al., 2017), although only 4–13 species have been reported from beds in the western Mediterranean (Ballesteros, 1989; Basso, 1998; Lanfranco et al., 1999; Mannino et al., 2002; Sciberras et al., 2009; Barberá et al., 2012; Basso et al., 2014; Nitsch et al., 2015; Sañé et al., 2016; Bracchi et al., 2019; Rendina et al., 2020b; Chimienti et al., 2020). The majority of rhodolith-forming species living in the Mediterranean (Basso et al., 2017; Rindi et al., 2019) have been recorded in the Punta de la Mona bed, except for *Phymatolithon lusitanicum* V. Peña (Peña et al., 2015), and *Neogoniolithon hauckii* (Rothpletz) RA Townsend & Huisman (Townsend and Huisman, 2018). Although we were not able to identify the recently described *Lithophyllum pseudoracemus* Caragnano, Rodondi and Rindi separately from *Lithophyllum racemus*, the former taxon was collected in the Punta de la Mona bed (Caragnano et al., 2020). This exemplifies that the cryptic

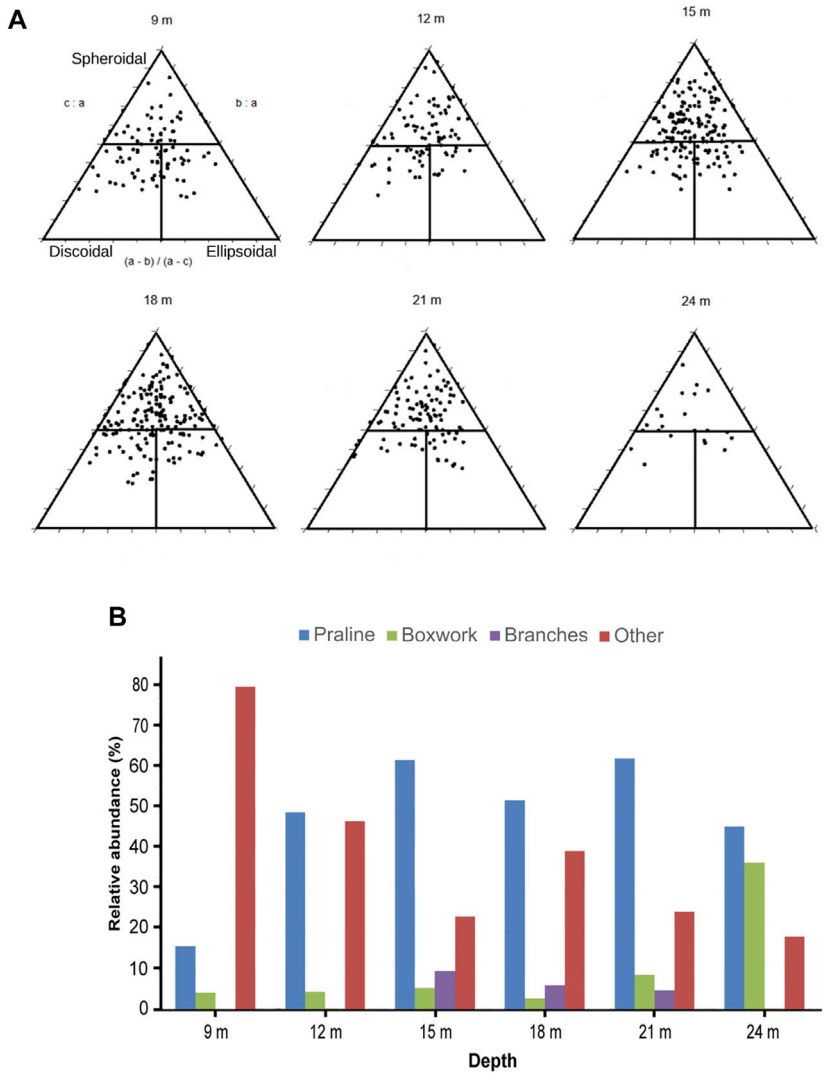

FIGURE 12 | (A) Triangular diagrams of rhodolith shape classes at each sampling depth (Sneed and Folk, 1958; Bosence, 1983; Graham and Midgley, 2000) and **(B)** relative proportions of rhodolith morphotypes at each sampling depth. Other includes coatings on lithoclasts and bioclasts, and compact rhodoliths of encrusting coralline algae.

molecular diversity is probably higher than the morphospecies richness assessed in our study (Gabrielson et al., 2018; De Jode et al., 2019; Pezzolesi et al., 2019; Caragnano et al., 2020; Kato et al., 2022).

Lithothamnion valens, the dominant species in the Punta de la Mona bed, is a Mediterranean endemic (Guiry and Guiry, 2022), which was considered a major structural component of a type of detrital bottom, called "facies de *Lithothamnion valens*," since the early descriptions of Mediterranean benthic habitats (Pérès and Picard, 1964). Rhodolith beds dominated by this species have been reported off Murcia in Spain (Aguado-Giménez and Ruiz-Fernández, 2012) and several locations, such as the Balearic Islands (Barberá et al., 2012), Tyrrhenian Sea (Basso, 1995; Bracchi et al., 2019; Rendina et al., 2020b) and Adriatic Sea (Chimienti et al., 2020). The composition of Mediterranean rhodolith beds, however, is heterogeneous even in small areas (Chimienti et al., 2020). No clear pattern of species dominance can be observed at the regional scale, since *Lithophyllum racemus* (Sañé et al., 2016; Chimienti et al., 2020), *Lithothamnion minervae* (Rendina et al., 2020b), *Spongites fruticulosus* (Ballesteros, 1989; Joher et al., 2015), and *Lithothamnion corallioides* (Barberá et al., 2017) have been reported as dominant species in different beds. Nevertheless, despite the heterogeneity, these species, together with *Lithothamnion valens, Phymatolithon calcareum* and *Neogoniolithon brassica-florida* are the rhodolith-forming species characteristic of the Mediterranean. Within the Punta de la Mona bed, the identified morphospecies show patterns of depth distribution probably related to illuminance gradients. *Lithophyllum dentatum* is rare below 15 m and the abundance of *Lithophyllum incrustans* markedly decreases with depth. In contrast, *Mesophyllum macroblastum* does not occur at shallow depths (9–12 m) and has higher relative abundance at 24 m where the maximum illuminance is only 21% of that at 12 m.

Among the small and rare species identified in the multispecific rhodoliths, *Lithophyllum orbiculatum* (Foslie) Foslie, *Lithothamnion crispatum* Hauck, and *Lithothamnion sonderi* Hauck have not been reported in the Alborán Sea so far (Gallardo et al., 2016).

The Shannon-Wiener index (H') values are higher than those obtained in deeper (40–60 m) Mediterranean enclaves (Rendina et al., 2017). In maërl communities of shallow European Atlantic beds, Peña and Bárbara (2010) obtained similar H' indexes (1.98–2.96), but for all associated species, not just for coralline algae. Likewise, our results are similar to those obtained by Costa et al. (2019) in a tropical environment and at depths shallower than our study. The coralline algae diversity, as the proportional distribution of species in the ecosystem, is remarkable due to its high values, and the Punta de la Mona can be considered as a "nano-hotspot" (in the sense of Cañadas et al., 2014 for terrestrial regions) of rhodolith biodiversity in the biogeographical context of the Alborán Sea.

Uniqueness and Conservation of the Punta de la Mona Rhodolith Bed

The Punta de la Mona rhodolith bed is unique due to the scarcity of this kind of formation in the Alborán Sea, and its shallow depth range, contrasting with the generally deeper depth distribution of rhodolith beds in the Mediterranean (Basso et al., 2017). In this sea, the majority of rhodolith beds occur at 30–75 m, although in oligotrophic clear waters may reach depths close to 150 m, such as in the Balearic Islands (Massutí et al., 2022). Beds shallower than 25 m are scarce, although they occur from 2 m depth in Tunisia (CAR/ASP-PNUE/PAM, 2011), at 9–10 m in Israel (Ramos-Esplá et al., 2012), and in the Apulian shelf in southern Italy (Chimienti et al., 2020). In addition, the Punta de la Mona bed develops in oligotrophic waters, challenging the simplistic assumption, widespread in the geological literature, that rhodolith beds are indicative of oligophotic, mesotrophic to eutrophic environments.

The Punta de la Mona rhodolith bed is protected as a special conservation area (SCA) with the Natura 2000 network. Despite this protection, this habitat is threatened by nautical and fishing activities, affecting the seafloor by the frequent anchoring of boats that use the area as a refuge (Dolinar et al., 2020), the tangling of large branching rhodoliths in fishing nets (Borg et al., 1998), abandoned fishing nets and lines (Rendina et al., 2020a), and the disruption of trophic networks due to intense sport fishing with uncertain consequences on coralline algal communities (O'Leary and McClanahan, 2010). Appropriate regulations for the SCA should be imposed to prevent all these impacts in the future. Restrictions to fishing activities in marine protected areas resulted in increasing rhodolith covers (Barberá et al., 2017). This improved the environmental services provided by the rhodolith beds, including higher biodiversity (Barberá et al., 2003) and larger fish populations (Ordines et al., 2015). Nevertheless, the main threat for the rhodolith bed is the Asian alga *Rugulopteryx okamurae* (E.Y. Dawson) I.K.Hwang, W.J.Lee & H.S.Kim (Altamirano-Jeschke et al., 2016) first detected in 2020, which is quickly expanding from the Gibraltar straits and nearly completely covering the rocky substrates between 5 and 30 m (García-Gómez et al., 2020), displacing the native algal communities and disturbing the associated invertebrate communities (Navarro-Barranco et al., 2019; Sempere-Valverde et al., 2021). In the first weeks of 2022, the occurrence of many rhodoliths settled by *Rugulopterix okamurae* makes the future of the rhodolith bed uncertain, and needs to be monitored in the following years. This exemplifies that it is necessary to be cautious and incorporate the knowledge of these communities into the spatial planning framework of Punta de la Mona and other marine protected areas.

DATA AVAILABILITY STATEMENT

The original contributions presented in the study are included in the article/**Supplementary Material**, further inquiries can be directed to the corresponding author.

AUTHOR CONTRIBUTIONS

JD: Research design, sampling, underwater pictures, taxonomic identification, writing the manuscript; DR: Taxonomic identification, statistics, editing the manuscript; LS-T: Sampling, underwater pictures; JP: Sampling, statistics, editing the manuscript; JB: Taxonomic identification, editing the manuscript.

FUNDING

This work was partly funded by the Junta de Andalucía Research Group RNM 190.

ACKNOWLEDGMENTS

DAR work was funded by EU Horizon 2020 research and innovation program Marie Sklodowska-Curie Grant Agreement No. 813360. We would like to thank Isabel Sánchez for facilitating the SEM imaging remotely. We are grateful to two reviewers whose comments helped to improve the article.

SUPPLEMENTARY MATERIAL

The Supplementary Material for this article can be found online at: https://www.frontiersin.org/articles/10.3389/feart.2022.884685/full#supplementary-material

REFERENCES

Aguado-Giménez, F., and Ruiz-Fernández, J. M. (2012). Influence of an Experimental Fish Farm on the Spatio-Temporal Dynamic of a Mediterranean Maërl Algae Community. *Mar. Environ. Res.* 74, 47–55. doi:10.1016/j.marenvres.2011.12.003

Aguirre, J., Braga, J. C., and Bassi, D. (2017). "Rhodoliths and Rhodolith Beds in the Rock Record," in Rhodolith/Maërl Beds: A Global Perspective *Coastal Research Library*. Editors R. Riosmena-Rodríguez, W. Nelson, and J. Aguirre (Cham:

Springer International Publishing), 105–138. doi:10.1007/978-3-319-29315-8_5

Altamirano Jeschke, M., De la Rosa Álamos, J., and Martínez Medina, F. J. (2016). Arribazones de la Especie Exótica *Rugulopteryx Okamurae* (E.Y. Dawson) I.K. Hwang, W.J. Lee and H.S. Kim (Dictyotales, Ochrophyta) en el Estrecho de Gibraltar: Primera Cita Para el Atlántico y España. *Algas* 52, 20.

Amado-Filho, G., Maneveldt, G., Manso, R., Marins-Rosa, B., Pacheco, M., and Guimarães, S. (2007). Structure of Rhodolith Beds from 4 to 55 Meters Deep along the Southern Coast of Espírito Santo State, Brazil. *Cienc. Mar.* 33, 399–410. doi:10.7773/cm.v33i4.1148

Amado-Filho, G. M., Bahia, R. G., Pereira-Filho, G. H., and Longo, L. L. (2017). "South Atlantic Rhodolith Beds: Latitudinal Distribution, Species Composition, Structure and Ecosystem Functions, Threats and Conservation Status," in Rhodolith/Maërl Beds: A Global Perspective *Coastal Research Library*. Editors R. Riosmena-Rodríguez, W. Nelson, and J. Aguirre (Cham: Springer International Publishing), 299–317. doi:10.1007/978-3-319-29315-8_12

Amado-Filho, G. M., Moura, R. L., Bastos, A. C., Salgado, L. T., Sumida, P. Y., Guth, A. Z., et al. (2012). Rhodolith Beds Are Major CaCO3 Bio-Factories in the Tropical South West Atlantic. *PLOS ONE* 7, e35171. doi:10.1371/journal.pone.0035171

Ballesteros, E. (1989). Composición y estructura de los fondos de maërl de Tossa de Mar (Gerona, España). *Collect. Bot.* 17, 161–182. doi:10.3989/collectbot.1989.v17.137

Barberá, C., Bordehore, C., Borg, J. A., Glemarec, M., Grall, J., Hall-Spencer, J. M., et al. (2003). Conservation and Management of Northeast Atlantic and Mediterranean Maerl Beds. *Aquat. Conserv. Mar. Freshw. Ecosyst.* 13, S65–S76. doi:10.1002/aqc.569

Barberá, C., Moranta, J., Ordines, F., Ramón, M., de Mesa, A., Díaz-Valdés, M., et al. (2012). Biodiversity and Habitat Mapping of Menorca Channel (Western Mediterranean): Implications for Conservation. *Biodivers. Conserv.* 21, 701–728. doi:10.1007/s10531-011-0210-1

Barberá, C., Mallol, S., Vergés, A., Cabanellas-Reboredo, M., Díaz, D., and Goñi, R. (2017). Maerl Beds inside and outside a 25-Year-Old No-take A-rea. *Mar. Ecol. Prog. Ser.* 572, 77–90. doi:10.3354/meps12110

Bassi, D., Nebelsick, J. H., Checconi, A., Hohenegger, J., and Iryu, Y. (2009). Present-day and Fossil Rhodolith Pavements Compared: Their Potential for Analysing Shallow-Water Carbonate Deposits. *Sediment. Geol.* 214, 74–84. doi:10.1016/j.sedgeo.2008.03.010

Bassi, D., Braga, J. C., Owada, M., Aguirre, J., Lipps, J. H., Takayanagi, H., et al. (2020). Boring Bivalve Traces in Modern Reef and Deeper-Water Macroid and Rhodolith Beds. *Prog. Earth Planet. Sci.* 7 (1), 1–17. doi:10.1186/s40645-020-00356-w

Basso, D., Babbini, L., Kaleb, S., Bracchi, V. A., and Falace, A. (2016). Monitoring Deep Mediterranean Rhodolith Beds. *Aquat. Conserv. Mar. Freshw. Ecosyst.* 26, 549–561. doi:10.1002/aqc.2586

Basso, D., Babbini, L., Ramos-Esplá, A. A., and Salomidi, M. (2017). "Mediterranean Rhodolith Beds," in Rhodolith/Maërl Beds: A Global Perspective *Coastal Research Library*. Editors R. Riosmena-Rodríguez, W. Nelson, and J. Aguirre (Cham: Springer International Publishing), 281–298. doi:10.1007/978-3-319-29315-8_11

Basso, D. (1995). Living Calcareous Algae by a Paleontological Approach: the Genus *Lithothamnion* Heydrich Nom. Cons. From the Soft Bottoms of the Tyrrhenian Sea (Mediterranean). *Riv. Ital. Paleontol. Stratigr.* 101, 349–366. doi:10.13130/2039-4942/8592

Basso, D. (1998). Deep Rhodolith Distribution in the Pontian Islands, Italy: a Model for the Paleoecology of a Temperate Sea. *Palaeogeogr. Palaeoclimatol. Palaeoecol.* 137, 173–187. doi:10.1016/S0031-0182(97)00099-0

Basso, D. (2012). Carbonate Production by Calcareous Red Algae and Global Change. *Geodiversitas* 34, 13–33. doi:10.5252/g2012n1a2

Basso, D., Rodondi, G., and Caragnano, A. (2014). "Coralline Species Composition of Tyrrhenian Maerl Beds (Western Mediterranean)," in *UNEP/MAP - RAC/SPA Proceedings of the 2nd Mediterranean Symposium on the Conservation of Coralligenous and Other Calcareous Bio-Concretions*. Editors f. C. Bouafi, H. Langar, and A. Ouerghi (Portorož, Slovenia, 197–198.

Betzler, C., Braga, J. C., Jaramillo-Vogel, D., Römer, M., Hübscher, C., Schmiedl, G., et al. (2011). Late Pleistocene and Holocene Cool-Water Carbonates of the Western Mediterranean Sea. *Sedimentology* 58, 643–669. doi:10.1111/j.1365-3091.2010.01177.x

Birkett, D. A., Maggs, C. A., and Dring, M. J. (1998). An Overview of Dynamic and Sensitivity Characteristics for Conservation Management of Marine SACs (Vol. 5. Maerl, [UK Marine SACs Project]). *Scott. Assoc. Mar. Sci. (SAMS)* 5, 1–90.

Bordehore, C., Ramos-Esplá, A. A., and Riosmena-Rodríguez, R. (2003). Comparative Study of Two Maerl Beds with Different Otter Trawling History, Southeast Iberian Peninsula. *Aquat. Conserv. Mar. Freshw. Ecosyst.* 13, S43–S54. doi:10.1002/aqc.567

Borg, J. A., Lanfranco, E., Mifsud, J. R., Rizzo, M., and Schembri, P. J. (1998). in *Does Fishing Have an Impact on Maltese Maerl Grounds?* Heraklion, Crete, 18.

Bosellini, A., and Ginsburg, R. N. (1971). Form and Internal Structure of Recent Algal Nodules (Rhodolites) from Bermuda. *J. Geol.* 79, 669–682. doi:10.1086/627697

Bosence, D. W. J. (1983). "Description and Classification of Rhodoliths (Rhodoids, Rhodolites)," in *Coated Grains*. Editor T. M. Peryt (Berlin: Springer-Verlag), 217–224. doi:10.1007/978-3-642-68869-0_19

Bosence, D. W. J. (1976). Ecological Studies on Two Unattached Coralline Algae from Western Ireland. *Paleontology* 19, 365–395.

Bracchi, V. A., Angeletti, L., Marchese, F., Taviani, M., Cardone, F., Hajdas, I., et al. (2019). A Resilient Deep-Water Rhodolith Bed off the Egadi Archipelago (Mediterranean Sea) and its Actuopaleontological Significance. *Alp. Mediterr. Quat.* 32, 131–150. doi:10.26382/AMQ.2019.09

Bracchi, V. A., Caronni, S., Meroni, A. N., Burguett, E. G., Atzori, F., Cadoni, N., et al. (2022). Morphostructural Characterization of the Heterogeneous Rhodolith Bed at the Marine Protected Area "Capo Carbonara" (Italy) and Hydrodynamics. *Diversity* 14 (1), 51. doi:10.3390/d14010051

Braga, J. C., Aguirre, J., and Esteban, J. (2009). "Calcareous algae of Cabo de Gata-Níjar Nature Park. Field guide/Algas calcáreas del Parque Natural de Cabo de Gata. Guía de campo (Bilingual English/Spanish)," in *ACUMEN y Consejería de Medio Ambiente (Junta de Andalucía=*. Editors M. Villalobos and A. B. Pérez-Muñoz (Madrid: Aguas de las Cuencas Mediterráneas).

Braga, J. C. (2017). "Neogene Rhodoliths in the Mediterranean Basins," in Rhodolith/Maërl Beds: A Global Perspective *Coastal Research Library*. Editors R. Riosmena-Rodríguez, W. Nelson, and J. Aguirre (Cham: Springer International Publishing), 169–193. doi:10.1007/978-3-319-29315-8_7

Cabioch, J. (1969). Les fonds de Maerl de la Baie de Morlaix et leur peuplement végétal. *Cah. Biol. Mar.* 10, 139–161.

Cañadas, E. M., Fenu, G., Peñas, J., Lorite, J., Mattana, E., and Bacchetta, G. (2014). Hotspots within Hotspots: Endemic Plant Richness, Environmental Drivers, and Implications for Conservation. *Biol. Conserv.* 170, 282–291. doi:10.1016/j.biocon.2013.12.007

Caragnano, A., Rodondi, G., Basso, D., Peña, V., le Gall, L., and Rindi, F. (2020). Circumscription of Lithophyllum Racemus (Corallinales, Rhodophyta) from the Western Mediterranean Sea Reveals the Species Lithophyllum Pseudoracemus Sp. Nov. *Phycologia* 59, 584–597. doi:10.1080/00318884.2020.1829348

Carvalho, V. F., Assis, J., Serrão, E. A., Nunes, J. M., Anderson, A. B., Batista, M. B., et al. (2020). Environmental Drivers of Rhodolith Beds and Epiphytes Community along the South Western Atlantic Coast. *Mar. Environ. Res.* 154, 104827. doi:10.1016/j.marenvres.2019.104827

Chimienti, G., Rizzo, L., Kaleb, S., Falace, A., Fraschetti, S., Giosa, F. D., et al. (2020). Rhodolith Beds Heterogeneity along the Apulian Continental Shelf (Mediterranean Sea). *J. Mar. Sci. Eng.* 8, 813. doi:10.3390/jmse8100813

Cormaci, M., Furnari, G., and Alongi, G. (2017). Flora marina bentonica del Mediterraneo: Rhodophyta (*Rhodymeniophycidae* escluse). *Boll. Accad. Gioenia Sci. Nat.* 50, 1–391.

Costa, D. d. A., Da Silva, F. d. A., Silva, J. M. d. L., Pereira, A. R., Dolbeth, M., Christoffersen, M. L., et al. (2019). Is Tourism Affecting Polychaete Assemblages Associated with Rhodolith Beds in Northeastern Brazil? *Rev. Biol. Trop.* 67, S1–S15. doi:10.15517/rbt.v67is5.38922

CAR/ASP - PNUE/PAM (2013). in *Communautés biologiques marines du Cap des Trois Fourches (Mediterranée, Maroc): caractérisation, cartographie et orientations de gestion*. Editors H. Par Bazairi, A. Limam, A. Benhoussa, C. Navarro-Barrancoa, A. R. González, M. Maestre, et al. (Tunis: CAR/ASP-Projet MedMPAnet).

CAR/ASP - PNUE/PAM (2011). in *Habitats marins et principales espèces des îles Kuriat (Tunisie) – Etude complémentaire: Formations naturelles d'intérêt pour la conservation*. Editors H. Par Langar, C. Bouafif, A. Charfeddine, S. El Asmi, A. Limam, A. Ouerghi, et al. (Tunis: CAR/ASP-Projet MedMPAnet).

De Jode, A., David, R., Haguenauer, A., Cahill, A. E., Erga, Z., Guillemain, D., et al. (2019). From Seascape Ecology to Population Genomics and Back. Spatial and Ecological Differentiation Among Cryptic Species of the Red Algae *Lithophyllum Stictiforme/L. Cabiochiae*, Main Bioconstructors of Coralligenous Habitats. *Mol. Phylogenetics Evol.* 137, 104–113. doi:10.1016/j.ympev.2019.04.005

Dolinar, D., Steller, D., Gabara, S., Beckley, B., Kim, J.-H., and Edwards, M. (2020). Impacts of Boat Mooring Disturbance on Productivity and Respiration in Rhodolith Beds from Catalina Island, USA. *Cienc. Mar.* 46, 253–267. doi:10.7773/cm.v46i4.3135

Foster, M., McConnico, L., Lundsten, L., Wadsworth, T., Kimball, T., Brooks, L., et al. (2007). Diversity and Natural History of a *Lithothamnion Muelleri-Sargassum Horridum* Community in the Gulf of California. *Cienc. Mar.* 33, 367–384. doi:10.7773/cm.v33i4.1174

Foster, M. S. (2001). Rhodoliths: Between Rocks and Soft Places. *J. Phycol.* 37, 659–667. doi:10.1046/j.1529-8817.2001.00195.x

Fragkopoulou, E., Serrão, E. A., Horta, P. A., Koerich, G., and Assis, J. (2021). Bottom Trawling Threatens Future Climate Refugia of Rhodoliths Globally. *Front. Mar. Sci.* 7, 594537(Accessed January 21, 2022). doi:10.3389/fmars.2020.594537

Fredericq, S., Krayesky-Self, S., Sauvage, T., Richards, J., Kittle, R., Arakaki, N., et al. (2019). The Critical Importance of Rhodoliths in the Life Cycle Completion of Both Macro- and Microalgae, and as Holobionts for the Establishment and Maintenance of Marine Biodiversity. *Front. Mar. Sci.* 5, 502. doi:10.3389/fmars.2018.00502

Gabrielson, P. W., Hughey, J. R., and Diaz-Pulido, G. (2018). Genomics Reveals Abundant Speciation in the Coral Reef Building Alga *Porolithon Onkodes* (*Corallinales, Rhodophyta*). *J. Phycol.* 54, 429–434. doi:10.1111/jpy.12761

Gagnon, P., Matheson, K., and Stapleton, M. (2012). Variation in Rhodolith Morphology and Biogenic Potential of Newly Discovered Rhodolith Beds in Newfoundland and Labrador (Canada). *Bot. Mar.* 55, 85–99. doi:10.1515/bot-2011-0064

Gallardo, T., Bárbara, I., Alfonso-Carrillo, J., Bermejo, R., Altamirano, M., Gómez-Garreta, A., et al. (2016). Nueva lista crítica de las algas bentónicas marinas de España. *Algas* 51, 7–52.

García-Gómez, J. C., Corzo, J. R., López-Fé de la Cuadra, C. M., Sánchez Moyano, J. E., Corzo, M., Rey, J., et al. (2003). Metodología cartográfica submarina orientada a la gestión y conservación del medio litoral: mapa de las comunidades bentónicas del frente litoral norte del estrecho de Gibraltar. *Bol. Inst. Esp. Oceanogr.* 19, 149–163.

García-Gómez, J. C., Sempere-Valverde, J., González, A. R., Martínez-Chacón, M., Olaya-Ponzone, L., Sánchez-Moyano, E., et al. (2020). From Exotic to Invasive in Record Time: The Extreme Impact of *Rugulopteryx Okamurae* (Dictyotales, Ochrophyta) in the Strait of Gibraltar. *Sci. Total Environ.* 704, 135408. doi:10.1016/j.scitotenv.2019.135408

Gofas, S., Goutayer, J., Luque, Á. A., Salas, C., and Templado, J. (2014). Espacio Marino de Alborán. *Proyecto LIFE+ INDEMARES Fundación Biodiversidad del Ministerio de Agricultura, Alimentación y Medio Ambiente*.

Graham, D. J., and Midgley, N. G. (2000). Graphical Representation of Particle Shape Using Triangular Diagrams: an Excel Spreadsheet Method. *Earth Surf. Process. Landforms* 25, 1473–1477. doi:10.1002/1096-9837(200012)25:13<1473::aid-esp158>3.0.co;2-c

Guiry, M. D., and Guiry, G. M. (2022). AlgaeBase. World-wide Electronic Publication, National University of Ireland, Galway. Available at: https://www.algaebase.org (Accessed January 20, 2022).

Hall-Spencer, J. M., Grall, J., Moore, P. G., and Atkinson, R. J. A. (2003). Bivalve Fishing and Maerl-Bed Conservation in France and the UK?retrospect and Prospect. *Aquat. Conserv. Mar. Freshw. Ecosyst.* 13, S33–S41. doi:10.1002/aqc.566

Harvey, A. S., Harvey, R. M., Merton, E., Harvey, A. S., Harvey, R. M., and Merton, E. (2017). The Distribution, Significance and Vulnerability of Australian Rhodolith Beds: a Review. *Mar. Freshw. Res.* 68, 411–428. doi:10.1071/MF15434

Hernández-Kantún, J. J., Hall-Spencer, J. M., Grall, J., Adey, W., Rindi, F., Maggs, C. A., et al. (2017). "North Atlantic Rhodolith Beds," in Rhodolith/Maërl Beds: A Global Perspective *Coastal Research Library*. Editors R. Riosmena-Rodríguez, W. Nelson, and J. Aguirre (Cham: Springer International Publishing), 265–279. doi:10.1007/978-3-319-29315-8_10

Jacquotte, R. (1962). Étude des fonds de maërl de Méditerranée. *Rec. Trav. St. Mar. End.* 26, 141–235.

Joher, S., Ballesteros, E., and Rodrigues-Prieto, C. (2015). Contribution to the Study of Deep Coastal Detritic Bottoms: the Algal Communities of the Continental Shelf off the Balearic Islands, Western Mediterranean. *Medit. Mar. Sci.* 16, 573–590. doi:10.12681/mms.1249

Kamenos, N. A., Burdett, H. L., and Darrenougue, N. (2017). "Coralline Algae as Recorders of Past Climatic and Environmental Conditions," in Rhodolith/Maërl Beds: A Global Perspective *Coastal Research Library*. Editors R. Riosmena-Rodríguez, W. Nelson, and J. Aguirre (Cham: Springer International Publishing), 27–53. doi:10.1007/978-3-319-29315-8_2

Kamenos, N., Moore, P., and Hall-Spencer, J. (2004). Nursery-area Function of Maerl Grounds for Juvenile Queen Scallops *Aequipecten Opercularis* and Other Invertebrates. *Mar. Ecol. Prog. Ser.* 274, 183–189. doi:10.3354/meps274183

Kato, A., Basso, D., Caragnano, A., Rodondi, G., Le Gall, L., Peña, V., et al. (2022). Morphological and Molecular Assessment of *Lithophyllum Okamurae* with the Description of *L. Neo-Okamurae* Sp. Nov. (Corallinales, Rhodophyta). *Phycologia* 61, 117–131. doi:10.1080/00318884.2021.2005330

Keegan, B. F. (1974). The Macrofauna of Maërl Substrates on the West Coast of Ireland. *Cah. Biol. Mar.* 15, 513–530. doi:10.1016/s0033-3182(74)71273-7

Lanfranco, E., Rizzo, M., Hall-Spencer, J., Borg, J. A., and Schembri, P. (1999). Maerl-forming Coralline Algae and Associated Phytobenthos from the Maltese Islands. *Cent. Mediterr. Nat.* 3, 1–6.

Magurran, A. E. (2004). *Measuring Biological Diversity*. Oxford: Blackwell Publishing.

Mannino, A. M., Castriota, L., Beltrano, A. M., and Sunseri, G. (2002). The Epiflora of a Rhodolith Bed from the Island of Ustica (Southern Tyrrhenian Sea). *Flora Mediterr.* 12, 11–28.

Marrack, E. C. (1999). The Relationship between Water Motion and Living Rhodolith Beds in the Southwestern Gulf of California, Mexico. *Palaios* 14, 159–171. doi:10.2307/3515371

Massutí, E., Sánchez-Guillamón, O., Farriols, M. T., Palomino, D., Frank, A., Bárcenas, P., et al. (2022). Improving Scientific Knowledge of Mallorca Channel Seamounts (Western Mediterranean) within the Framework of Natura 2000 Network. *Diversity* 14, 4. doi:10.3390/d14010004

Millar, K., and Gagnon, P. (2018). Mechanisms of Stability of Rhodolith Beds: Sedimentological Aspects. *Mar. Ecol. Prog. Ser.* 594, 65–83. doi:10.3354/meps12501

Ministerio de Agricultura, Alimentación y Medio Ambiente (2012). *Estrategia marina demarcación marina del Estrecho y Alborán. Parte IV: Descriptores del buen estado ambiental. Descriptor 1: Biodiversidad, evaluación inicial y buen estado ambiental.* Madrid.

Navarro-Barranco, C., Muñoz-Gómez, B., Saiz, D., Ros, M., Guerra-García, J. M., Altamirano, M., et al. (2019). Can Invasive Habitat-Forming Species Play the Same Role as Native Ones? the Case of the Exotic Marine Macroalga *Rugulopteryx Okamurae* in the Strait of Gibraltar. *Biol. Invasions* 21, 3319–3334. doi:10.1007/s10530-019-02049-y

Nelson, W. A. (2009). Calcified Macroalgae - Critical to Coastal Ecosystems and Vulnerable to Change: a Review. *Mar. Freshw. Res.* 60, 787–801. doi:10.1071/MF08335

Nitsch, F., Nebelsick, J. H., and Bassi, D. (2015). Constructional and Destructional Patterns-Void Classification of Rhodoliths from Giglio Island, Italy. *Palaios* 30, 680–691. doi:10.2110/palo.2015.007

O'Connell, L. G., James, N. P., Harvey, A. S., Luick, J., Bone, Y., and Shepherd, S. A. (2021). Reevaluation of the Inferred Relationship between Living Rhodolith Morphologies, Their Movement, and Water Energy: Implications for Interpreting Paleoceanographic Conditions. *Palaios* 35, 543–556. doi:10.2110/palo.2019.101

Ocaña, O., Ramos, A., and Templado, J. (2009). *Los paisajes sumergidos de la región de Ceuta y su biodiversidad*. Ceuta: Fundación Museo del Mar de Ceuta.

O'Leary, J. K., and McClanahan, T. R. (2010). Trophic Cascades Result in Large-Scale Coralline Algae Loss through Differential Grazer Effects. *Ecology* 91, 3584–3597. doi:10.1890/09-2059.1

Ordines, F., Bauzá, M., Sbert, M., Roca, P., Gianotti, M., and Massutí, E. (2015). Red Algal Beds Increase the Condition of Nekto-Benthic Fish. *J. Sea Res.* 95, 115–123. doi:10.1016/j.seares.2014.08.002

Otero-Ferrer, F., Cosme, M., Tuya, F., Espino, F., and Haroun, R. (2020). Effect of Depth and Seasonality on the Functioning of Rhodolith Seabeds. *Estuar. Coast. Shelf Sci.* 235, 106579. doi:10.1016/j.ecss.2019.106579

Peña, V., and Bárbara, I. (2009). Distribution of the Galician Maerl Beds and Their Shape Classes (Atlantic Iberian Peninsula): Proposal of Areas in Future Conservation Actions. *Cah. Biol. Mar.* 50, 353–368. doi:10.1080/09670261003586938

Peña, V., and Bárbara, I. (2010). Seasonal Patterns in the Maërl Community of Shallow European Atlantic Beds and Their Use as a Baseline for Monitoring Studies. *Eur. J. Phycol.* 45, 327–342. doi:10.1080/09670261003586938

Peña, V., Bárbara, I., Grall, J., Maggs, C. A., and Hall-Spencer, J. M. (2014). The Diversity of Seaweeds on Maerl in the NE Atlantic. *Mar. Biodiv* 44, 533–551. doi:10.1007/s12526-014-0214-7

Peña, V., Pardo, C., López, L., Carro, B., Hernández-Kantún, J., Adey, W. H., et al. (2015). Phymatolithon Lusitanicumsp. Nov. (Hapalidiales, Rhodophyta): The Third Most Abundant Maerl-Forming Species in the Atlantic Iberian Peninsula. *Cryptogam. Algol.* 36, 429–459. doi:10.7872/crya/v36.iss4.2015.429

Pérès, J. M., and Picard, J. (1964). Nouveau manuel de bionomie benthique de la Mer Méditerranée. *Rec. Trav. St. Mar. End.* 31, 5–137.

Pezzolesi, L., Peña, V., Le Gall, L., Gabrielson, P. W., Kaleb, S., Hughey, J. R., et al. (2019). MediterraneanLithophyllum stictiforme(Corallinales, Rhodophyta) Is a Genetically Diverse Species Complex: Implications for Species Circumscription, Biogeography and Conservation of Coralligenous Habitats. *J. Phycol.* 55, 473–492. doi:10.1111/jpy.12837

Puertos del Estado (2021a). *Clima medio de oleaje. Nodo SIMAR 2039080. Banco de datos oceánicos de Puertos del Estado. Visor Portus*. Madrid: Ministerio de Transporte, Movilidad y Agenda Urbana. Available at: https://portus.puertos.es.

Puertos del Estado (2021b). *Temperatura Agua. Punto Satélite Sentinel 2039080. Visor Portus*. Madrid: Ministerio de Transporte, Movilidad y Agenda Urbana. Available at: https://portus.puertos.es.

R Core Team (2021). *R: A Language and Environment for Statistical Computing*. Vienna, Austria: R Foundation for Statistical Computing. Available at: https://www.R-project.org/.

Ramos-Esplá, A. A., Riosmena-Rodríguez, R., and Galil, B. (2012). "Contribution to the Knowledge of Maerl Beds in the Levantine Basin," in *Eastern Mediterranean* (Granada, Spain: IV International Rhodolith Workshop), 63.

REDIAM (2021). *WMS Serie de imágenes de satélite AQUA MODIS. Clorofila-a medias estacionales filtradas de la serie histórica: Años 2000-2020, 1100 m. Océano Atlántico y Mar de Alborán. Red de Información Ambiental de Andalucía. Junta de Andalucía*. Available at: https://www.juntadeandalucia.es/medioambiente/mapwms/REDIAM_aquamodis_cl_a_estacional_filtrada_2000_2020?

Rendina, F., Donnarumma, L., Appolloni, L., Bruno, R., Ferrigno, F., Di Stefano, F., et al. (2017). First Description of a Rhodolith Bed off the Island of Capri and its Associated Benthic Fauna. *Biol. Mar. Mediterr.* 24, 126–127.

Rendina, F., Ferrigno, F., Appolloni, L., Donnarumma, L., Sandulli, R., and Fulvio, G. (2020a). Anthropic Pressure Due to Lost Fishing Gears and Marine Litter on Different Rhodolith Beds off the Campania Coast (Tyrrhenian Sea, Italy). *Ecol. Quest.* 31, 1–51. doi:10.12775/EQ.2020.027

Rendina, F., Kaleb, S., Caragnano, A., Ferrigno, F., Appolloni, L., Donnarumma, L., et al. (2020b). Distribution and Characterization of Deep Rhodolith Beds off the Campania Coast (SW Italy, Mediterranean Sea). *Plants* 9, 985. doi:10.3390/plants9080985

Rindi, F., Braga, J. C., Martin, S., Peña, V., Le Gall, L., Caragnano, A., et al. (2019). Coralline Algae in a Changing Mediterranean Sea: How Can We Predict Their Future, if We Do Not Know Their Present? *Front. Mar. Sci.* 6, 723. doi:10.3389/fmars.2019.00723

Riosmena-Rodríguez, R. (2017). "Natural History of Rhodolith/Maërl Beds: Their Role in Near-Shore Biodiversity and Management," in Rhodolith/Maërl Beds: A Global Perspective *Coastal Research Library*. Editors R. Riosmena-Rodríguez, W. Nelson, and J. Aguirre (Cham: Springer International Publishing), 3–26. doi:10.1007/978-3-319-29315-8_1

Robles, R. (2010). *Conservación y desarrollo sostenible del mar de Alborán = Conservation et développement durable de la mer d'Alboran*. Málaga, Spain: IUCN. Available at: https://portals.iucn.org/library/node/9542 (Accessed January 26, 2022).

RStudio Team (2020). *RStudio: Integrated Development for R*. Boston, MA: RStudio, PBC. Available at: http://www.rstudio.com.

Salomidi, M., Katsanevakis, S., Borja, A., Braeckman, U., Damalas, D., Galparsoro, I., et al. (2012). Assessment of Goods and Services, Vulnerability, and Conservation Status of European Seabed Biotopes: a Stepping Stone towards Ecosystem-Based Marine Spatial Management. *Medit. Mar. Sci.* 13, 49–88. doi:10.12681/mms.23

Sañé, E., Chiocci, F. L., Basso, D., and Martorelli, E. (2016). Environmental Factors Controlling the Distribution of Rhodoliths: An Integrated Study Based on Seafloor Sampling, ROV and Side Scan Sonar Data, Offshore the W-Pontine Archipelago. *Cont. Shelf Res.* 129, 10–22. doi:10.1016/j.csr.2016.09.003

Sciberras, M., Rizzo, M., Mifsud, J. R., Camilleri, K., Borg, J. A., Lanfranco, E., et al. (2009). Habitat Structure and Biological Characteristics of a Maerl Bed off the Northeastern Coast of the Maltese Islands (Central Mediterranean). *Mar. Biodiv.* 39, 251–264. doi:10.1007/s12526-009-0017-4

Sempere-Valverde, J., Ostalé-Valriberas, E., Maestre, M., González Aranda, R., Bazairi, H., and Espinosa, F. (2021). Impacts of the Non-indigenous Seaweed *Rugulopteryx Okamurae* on a Mediterranean Coralligenous Community (Strait of Gibraltar): The Role of Long-Term Monitoring. *Ecol. Indic.* 121, 107135. doi:10.1016/j.ecolind.2020.107135

Sneed, E. D., and Folk, R. L. (1958). Pebbles in the Lower Colorado River, Texas a Study in Particle Morphogenesis. *J. Geol.* 66, 114–150. doi:10.1086/626490

Steller, D., and Cáceres-Martínez, C. (2009). Coralline Algal Rhodoliths Enhance Larval Settlement and Early Growth of the Pacific Calico Scallop *Argopecten Ventricosus*. *Mar. Ecol. Prog. Ser.* 396, 49–60. doi:10.3354/meps08261

Steller, D. L., and Foster, M. S. (1995). Environmental Factors Influencing Distribution and Morphology of Rhodoliths in Bahía Concepción, B.C.S., México. *J. Exp. Mar. Biol. Ecol.* 194, 201–212. doi:10.1016/0022-0981(95)00086-0

Steller, D. L., Riosmena-Rodríguez, R., Foster, M. S., and Roberts, C. A. (2003). Rhodolith Bed Diversity in the Gulf of California: the Importance of Rhodolith Structure and Consequences of Disturbance. *Aquat. Conserv. Mar. Freshw. Ecosyst.* 13, S5–S20. doi:10.1002/aqc.564

Steneck, R. S. (1986). THE ECOLOGY of CORALLINE ALGAL CRUSTS: Convergent Patterns and Adaptative Strategies. *Annu. Rev. Ecol. Syst.* 17, 273–303. doi:10.1146/annurev.es.17.110186.001421

Teichert, S., Woelkerling, W., Rüggeberg, A., Wisshak, M., Piepenburg, D., Meyerhöfer, M., et al. (2014). Arctic Rhodolith Beds and Their Environmental Controls (Spitsbergen, Norway). *Facies* 60, 15–37. doi:10.1007/s10347-013-0372-2

Townsend, R. A., and Huisman, J. M. (2018). "Coralline Algae," in *Algae of Australia. Marine Benthic Algae of North-Western Australia. 2. Red Algae*. Editor J. M. Huisman (Canberra & Melbourne: ABRS & CSIRO Publishing), 143–146. 86–97, 105–137.

Villas-Bôas, A. B., Tâmega, F. T. D. S., Andrade, M., Coutinho, R., and Figueiredo, M. A. D. O. (2014). Experimental effects of sediment burial and light attenuation on two coralline algae of a deep water rhodolith bed in Rio de Janeiro, Brazil. *Cryptogam. Algol.* 35, 67–76. doi:10.7872/crya.v35.iss1.2014.67

Wilson, S., Blake, C., Berges, J. A., and Maggs, C. A. (2004). Environmental Tolerances of Free-Living Coralline Algae (Maerl): Implications for European Marine Conservation. *Biol. Conserv.* 120, 279–289. doi:10.1016/j.biocon.2004.03.001

Conflict of Interest: The authors declare that the research was conducted in the absence of any commercial or financial relationships that could be construed as a potential conflict of interest.

frontiers | Frontiers in Earth Science

ORIGINAL RESEARCH
published: 01 July 2022
doi: 10.3389/feart.2022.910522

The Main Builders of Mediterranean Coralligenous: 2D and 3D Quantitative Approaches for its Identification

Valentina Alice Bracchi[1,2], Pietro Bazzicalupo[1], Luca Fallati[1], Andrea Giulia Varzi[1], Alessandra Savini[1,2], Mauro Pietro Negri[1], Antonietta Rosso[2,3], Rossana Sanfilippo[2,3], Adriano Guido[4], Marco Bertolino[5], Gabriele Costa[1,5], Elena De Ponti[6], Riccardo Leonardi[3], Maurizio Muzzupappa[7] and Daniela Basso[1,2]*

[1]Department of Earth and Environmental Sciences, University of Milano-Bicocca, Milano, Italy, [2]CoNISMa – Consorzio Nazionale Interuniversitario per le Scienze del Mare, Roma, Italy, [3]Department of Biological, Geological and Environmental Sciences, University of Catania, Catania, Italy, [4]Department of Biology, Ecology and Earth Sciences, University of Calabria, Cosenza, Italy, [5]Department of Earth, Environmental and Life Sciences (DISTAV), University of Genoa, Genoa, Italy, [6]Department of Medical Physics, ASST Monza, University of Milano-Bicocca, Monza, Italy, [7]Department of Mechanical, Energy and Management Engineering (DIMEG), University of Calabria, Cosenza, Italy

OPEN ACCESS

Edited by:
Emily G. Mitchell, University of Cambridge, United Kingdom

Reviewed by:
Salvatore Giacobbe, University of Messina, Italy
Pierre Boissery, Agence de l'eau Rhône Méditerranée Corse, France

***Correspondence:**
Valentina Alice Bracchi
valentina.bracchi@unimib.it

Specialty section:
This article was submitted to Paleontology, a section of the journal Frontiers in Earth Science

Received: *01 April 2022*
Accepted: *11 May 2022*
Published: *01 July 2022*

Citation:
Bracchi VA, Bazzicalupo P, Fallati L, Varzi AG, Savini A, Negri MP, Rosso A, Sanfilippo R, Guido A, Bertolino M, Costa G, De Ponti E, Leonardi R, Muzzupappa M and Basso D (2022) The Main Builders of Mediterranean Coralligenous: 2D and 3D Quantitative Approaches for its Identification. Front. Earth Sci. 10:910522. doi: 10.3389/feart.2022.910522

Along the Mediterranean Sea shelf, algal reefs made of crustose coralline algae and Peyssonneliales are known as Coralligenous. It ranks among the most important ecosystems in the Mediterranean Sea because of its extent, complexity, and heterogeneity, supporting very high levels of biodiversity. Descriptive approaches for monitoring purposes are often aimed at assessing the surficial ephemeral canopy, which is sustained and controlled by the occurrence of the long-lasting rigid structure at the base. This practice led to the non-univocal definition of Coralligenous, sometimes indicated as "animal Coralligenous" because of the surficial dominance of these components. The quantitative assessment of the builders that actively build up the persistent structure through geological time is therefore a fundamental topic. We collected two discrete coralligenous samples in front of Marzamemi village (Sicily, Ionian Sea), the first from an area of a dense coralligenous cover (- 37 m) and the second one from an area with sparse build-ups (- 36 m). By using image analysis and computerized axial tomography, we distinguished and quantified the different components both on the surface and inside the framework. In both cases, our results confirm the primary role of crustose coralline algae as major builders of the Mediterranean Coralligenous, this aspect matching with the evidence from the Quaternary fossil record. We suggest that the role of encrusting calcareous red algae in the Coralligenous should be considered in conservation and management policies.

Keywords: algal reef, bioconstruction, crustose coralline algae, framework, Marzamemi

1 INTRODUCTION

Encrusting calcareous red algae, among which are crustose coralline algae (CCA) and mineralized Peyssonneliales, are one of the key elements of the benthic marine shelf communities.

According to Fagerström (1991), who defined "builder" as any organism that builds a structure that survives to the death of the organism itself, encrusting calcareous red algae play a fundamental role as reef builders, being one of the most important components of the tropical coral reefs

(Littler, 1972). In recent revisions of the Mediterranean bioconstructions along the Italian coast, builder organisms have been indicated also as constructors (Rosso and Sanfilippo, 2009) or bioconstructors (Ingrosso et al., 2018). Furthermore, encrusting calcareous red algae are also able to develop endemic primary algal-dominated frameworks known as Coralligenous in the temperate waters of the Mediterranean Sea (e.g., Ballesteros, 2006). Coralligenous is considered an organic reef made of in-place reef-building organisms (Riding, 2002).

Marion (1883) first used the term *coralligène* (= @Coralligenous) while referring to the hard bottom found by anglers from Marseille (France), where *Corallium rubrum* (Linnaeus, 1758) was often found; Coralligenous literally means "producer of coral," relating to the abundance of this red coral. Pruvot (1894, 1895) and Feldmann (1937) studied the Coralligenous of Banyuls-sur-Mer (France) and first identified the main CCA genera and species responsible for the development of such frameworks. In the fifties and sixties, a fundamental contribution to our knowledge of the Mediterranean benthos came from the Endoume School (Marseille, France), summarized in the *Nouveau Manuel de Bionomie marine benthique de la Mer Méditerranée* by Pérès and Picard (1964). They defined the Coralligenous as the climax biocoenosis of the circalittoral zone, where CCA and mineralized Peyssonneliales develop primary or secondary hard bottoms of biogenic origin, under sciaphilous conditions. In addition to encrusting calcareous red algae, a contribution as builders of other organisms such as bryozoans, serpulids, and sponges has been sometimes indicated (Pérès and Picard, 1964; Pérès, 1982; Hong, 1982; Bellan-Santini et al., 1994; Ballesteros, 2006; Bertolino et al., 2017a, 2019; Costa et al., 2019).

At the scale of geological time, the overgrowing of such algae along the shelves gives rise to a geomorphological unit (bank or discrete columns) which completely changes the nature of the seafloor substrate. In turn, coralligenous build-ups modify the seascape (Bracchi et al., 2015, 2017), increase the carbonate production (Marchese et al., 2020), and may be preserved in the fossil record (Bosence and Pedley 1982; Carannante and Simone 1996; Rasser 2000; Nalin et al., 2006; Basso et al., 2007, 2009; Titschack et al., 2008; Bracchi et al., 2014, 2016, 2019).

Despite this definition, there is currently no real consensus among the scientific community to give a unique definition of Coralligenous. Past and recent biocenotic studies have shown the structural complexity of this habitat and the difficulty of its precise definition. Owing to its heterogeneity, Coralligenous has been interpreted as an assembly of several communities rather than a single community (Ballesteros, 2006; La Rivière et al., 2021). Because of its extent and complexity, this habitat supports high levels of biodiversity (Ballesteros, 2006) and ranks among the most important ecosystems in the Mediterranean Sea. Moreover, its multi-scale crevices and cavities produced by the irregular growth of algal thalli and the destructive action of some boring organisms contribute to increasing its biodiversity (Laborel 1961; Laubier 1966; Sartoretto et al., 1996; Cerrano et al., 2001), among which sponges represent one of the most abundant taxa (Bertolino et al., 2013; Costa et al., 2019).

Pérès and Picard (1964) originally indicated the spatial heterogeneity of Coralligenous and its co-occurrence with other types of habitats. Ballesteros (2006) introduced the wording of "animal-dominated" Coralligenous to indicate circalittoral bioherms not apparently dominated by CCA and mineralized Peyssonneliales. Several authors, consequently, indicated the forests of the gorgonian *Paramuricea clavata* (Risso, 1826) as one of the most peculiar elements characterizing Mediterranean coralligenous (Musard et al., 2014; Ponti et al., 2018). Bertolino et al. (2017a), while studying the coralligenous of Porto Cesareo (Apulia, Italy), noted the presence of abundant tubes of the serpulid *Protula* sp. that contributed to the framework. Enrichetti et al. (2019) used the definition "coralligenous animal forest" to indicate a particular aspect of Coralligenous dominated by gorgonians. Corriero et al. (2019) reported the occurrence of a bioconstruction along the Apulian coast (Italy) mostly made up of scleractinians together with some auxiliary building species, while the contribution of the CCA appeared negligible. Chimienti et al. (2020) described a mesophotic black coral forest in the Adriatic Sea, settled on animal-dominated bioconstructions, which has been considered as Coralligenous despite the very scarce presence of CCA. A recent revision of the Mediterranean biocoenoses (La Rivière et al., 2021) indicated at least seven associations and five facies for the coralligenous biocoenosis, all characterizing the surficial canopy of the build-ups.

Understandably, all these findings, although undoubtedly increasing our knowledge on mesophotic reefs and provide detailed information about the canopy community, rarely address the nature of the biogenic substrate, namely, the bioherm supporting these surface communities. Nevertheless, physical builders (*sensu* Fagerström, 1991) play a crucial role in the long-term survival of the build-ups, and the identification and distinction of the role of specific taxa should be considered, together with the canopy communities.

Finally, direct and indirect human impacts and mass mortality events threaten coralligenous, affecting the stability of this precious ecosystem and, thus, strongly compromising its conservation because of its destruction and reduction of biodiversity (Ingrosso et al., 2018). Due to its critical importance, Coralligenous is listed among Mediterranean priority habitats by the EU Habitats Directive and included in the network of Natura 2000 sites (92/43/CE). It is also subject to specific conservation plans in the framework of the Barcelona Convention (UNEP-MAP-RAC/SPA, 2008; UNEP-MAP-RAC/SPA, 2017). Coralligenous is included among the habitats monitored under the Marine Strategy Framework Directive (MSFD, EC, 2008). Consequently, non-destructive approaches have been developed to assess the ecological quality and health status of coralligenous assemblages. Most of them are based on visual census methods (Remotely Operated Vehicle, ROV, photo-transects or quadrats by scuba divers) (Kipson et al., 2011; Deter et al., 2012; Zapata-Ramírez et al., 2013; Cecchi et al., 2014; Gatti et al., 2015; Piazzi et al., 2015, 2021; Cánovas-Molina et al., 2016; Ferrigno et al., 2017, 2018; Montefalcone et al., 2017; Sartoretto et al., 2017; Enrichetti et al., 2019).

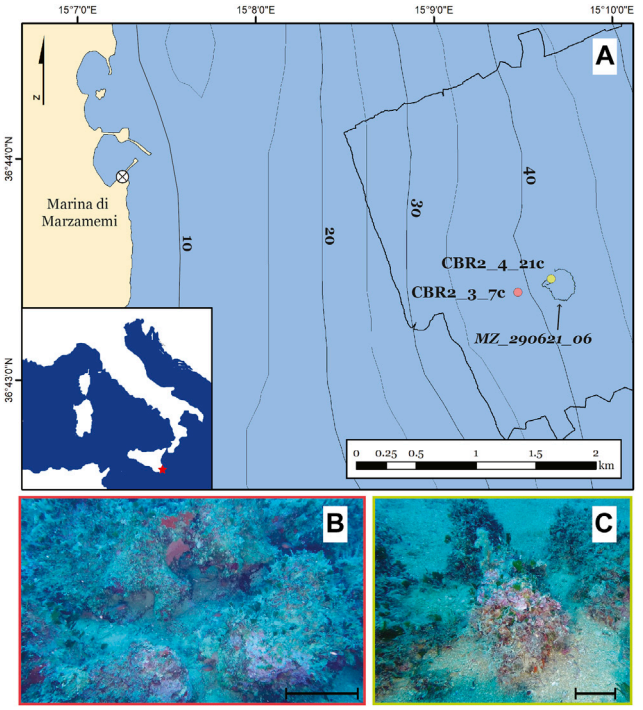

FIGURE 1 | Location of the study area and the sampling sites. **(A)** Bathymetric map of the study area, Marzamemi, Sicily, with the indication of the ROV_290621_06 track (black line) and the sampling sites (CBR2_3_7c, red dot and CBR2_4_21c, yellow dot). **(B)** Image from the ROV_290621_06 in a setting similar to the sampling site CBR2_3_7c. **(C)** Image from the ROV_290621_06 in a setting similar to the sampling site CBR2_4_21c. Scale bars = 10 cm for both **(C)** and **(D)**.

One of the main goals of the project "CRESCIBLUREEF - Grown in the blue: new technologies for knowledge and conservation of Mediterranean reefs" (project FISR 2019_04543) is to understand the *tempo* and the mode of the coralligenous inception and development, as well as the type of accretionary structures and their growth rate, also in the framework of the Holocene climate fluctuations.

Therefore, the appropriate identification of Coralligenous represents a fundamental starting point for this purpose. coralligenous build-ups indicated as pillars have already been identified in the sea bottom off south Marzamemi village (eastern Sicily, Ionian Sea, Italy) (Di Geronimo et al., 2001, 2002). In this context, we collected two coralligenous pillars at similar water depth but from different settings in terms of build-up density. The aim of this study is to identify and quantify the role of the different builders, both from the surface and from the inner structures by using photogrammetry and computed-tomography technology. This knowledge appears fundamental to properly addressing the efforts of monitoring, maintenance, and restoration of such types of submarine habitats in the long-term scenario, in the wider context of marine spatial planning.

2 MATERIALS AND METHODS

We collected direct observations of the seafloor offshore Marzamemi (**Figure 1A**) by using the ROV Steelhead SEAMORE, property of the University of Milano-Bicocca, during the first fieldwork survey of the CRESCIBLUREEF project (20–30 June 2021). The ROV is equipped with low- and high-quality cameras. Thanks to inspection ROV_290621_06, we were able to identify the proper sampling site, below the lower bathymetric limit of the *Posidonia oceanica* meadow (**Figure 1A**).

Two coralligenous samples were collected by scuba divers following the method of Bertolino et al. (2014) in the framework of the second field campaign of the project (1–7 August 2021) (**Figure 1A**). Samples have been marked with a spike on their north side before the collection.

CBR2_3_7c (36°43.394′ N; 15°09.469′ E, **Figure 1A**) was collected at a depth of 37 m, whereas CBR2_4_21c (36°43.454′ N; 15°09.657′ E, **Figure 1A**) was collected at a depth of 36 m.

2.1 Photogrammetric Reconstruction

Images were acquired all around the two samples in their original condition after recovery, to cover the entire surface with an adequate overlap between adjacent pictures (70%–80%). After the manual removal of the canopy with non-builder organisms, samples have been pictured again with the same scheme to produce a complete cover of the build-up.

All the images were processed using Agisoft Metashape®. This software performs 3D reconstruction of objects from overlapping images through a complete photogrammetric workflow (Anelli et al., 2019; Olinger et al., 2019; Casoli et al., 2021). After the alignment of the images, the obtained model has been scaled. Then, a textured mesh was generated. From this 3D model, six high-resolution scaled orthomosaics, representing all the sides of the Coralligenous (north, east, west, south, top, and bottom), were obtained and exported in TIFF format.

2.2 Object-Based Image Analysis and Classification of Orthomosaics

The analysis and classification of the orthomosaics obtained for each side of Coralligenous were performed using eCognition Developer 9.5® (Trimble). This software allowed carrying out an object-based image analysis (OBIA) to speed up the classification of the orthomosaics and estimate the extensions of the different classes (Blaschke, 2010; Fallati et al., 2020). As a first step, a multiresolution segmentation algorithm, based on homogeneity criteria, was applied to the orthomosaics. The image layer weights were set as identical for the three RGB bands, and the optimal scale parameter found was 350. A shape value of 0.3 and compactness of 0.7 were established for the homogeneity criteria. After the segmentation, a supervised classification was applied, taking advantage of the features calculated for each object such as the spectral value and size, shape, texture, and proximity. Thanks to these parameters and the high quality of orthomosaics, twelve classes were identified: CCA + Peyssonneliales; CCA framework; soft algae; foraminifera; sponges; cnidarians; mollusks (encrusting and boring); bryozoans;

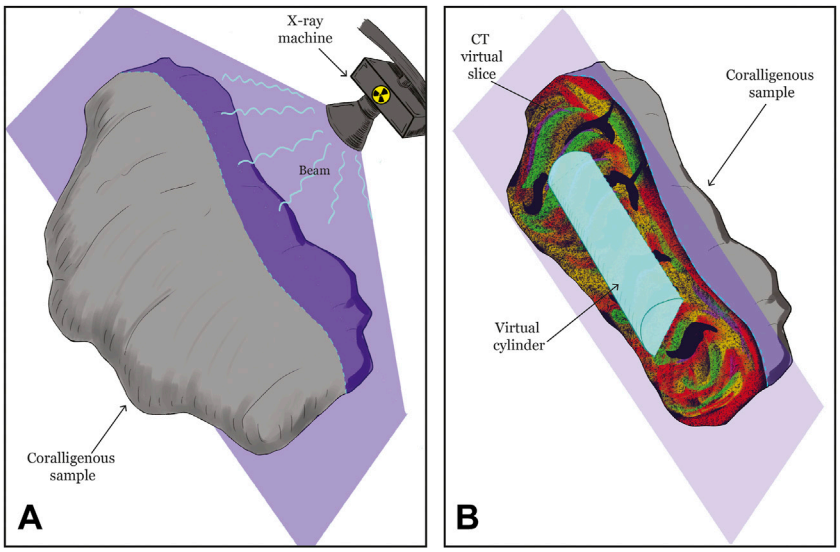

FIGURE 2 | Procedure scheme for the computed tomography and the volume calculation. **(A)** The acquisition phase, with the indication of one slice (in violet) as example. Inner structure is reconstructed by radiating using X-ray, in the three axes, adjacent slices of 0.625 mm thickness (step). The software then recomposed the complete structure in 3 dimensions. **(B)** Each slice is visualized and fragmented *via* thresholding by using AMIRA-Avizo software. In the inner structure, a virtual cylinder (light blue) for the volume calculation has been created.

annelids (polychaetes); arthropods (barnacles); sediment; and cavities on the surface. CCA + Peyssonneliales includes living CCA and both completely calcified and fleshy Peyssonneliales, whereas the fleshy Peyssonneliales were missing after the canopy removal. The CCA framework includes dead CCA.

After the classification, the extension of each class, expressed in cm^2, was automatically calculated in eCognition and exported. Extension represents the cover as the surface occupied by a single class, not considering overgrowing.

Principal component analyses (PCAs) were conducted on the cover percentage values to define the differences between the two samples using the software PAST 4.04 (Hammer et al., 2001). The first PCA was conducted on the whole dataset; both on the original and after the removal of the canopy cover values. Two further PCAs were conducted considering the two samples separately.

2.3 Computed Tomography

For computed tomography (CT), we used the model Revolution EVO integrated with the scanner PET/TC Discovery MI - General Electric, property of "Fondazione Tecnomed" of the University of Milano-Bicocca based at the Nuclear Medicine Department in Monza, Italy.

The acquisition protocol used the following set parameters: 140 kV and step 0.625 mm. Each sample was scanned along the three main axes (**Figure 2A**). Images were reconstructed by using the axial filter "bone plus" to obtain the best possible visualization of carbonate fraction.

The results were analyzed using AMIRA-Avizo software by Thermo Fisher Scientific, whereby threshold images were generated in order to clearly delineate skeletal material from empty space, as well as exclude sediment infilling. The results were visualized in three dimensions using the same software.

To compare the two Coralligenous in a more homogenous way, fragmentation *via* thresholding was quantified into two sub-volumes (two vertical cylinders, with a height of 30 and a diameter of 15 cm for CBR2_3_7c and a height of 22 and a diameter of 11 cm for CBR2_4_21c, **Figure 2B**). The difference in cylinder dimension is due to the real dimensions of coralligenous samples. Four density classes were identified using the multi-threshold tool: low-density (LD), medium-density (MD), high-density (HD), and ultrahigh-density (UHD). To validate the classes, we compared the identification with the samples. Void volume was measured and used to calculate the porosity of both samples, as the ratio between the total volume of the single cylinder and the total volume of its voids.

3 RESULTS

3.1 CBR2_3_7c

CBR2_3_7c was collected in an area characterized by high Coralligenous cover in the form of a hybrid bank (Bracchi et al., 2017), made of distinct coralligenous columns, sometimes coalescent, with a high cover of the seafloor (**Figure 1B**). Biogenic gravel occurs among coralligenous build-ups (**Figure 1B**). CBR2_3_7c is 56 cm high, with a circumference of 59 cm at the base, a circumference of 78 cm at the top and a maximum circumference of 116 cm (**Figure 3A**). The build-up was coalescent with a contiguous one, and therefore, it was broken not only at the base but also along its NE side. The weight of the sample is 35 kg.

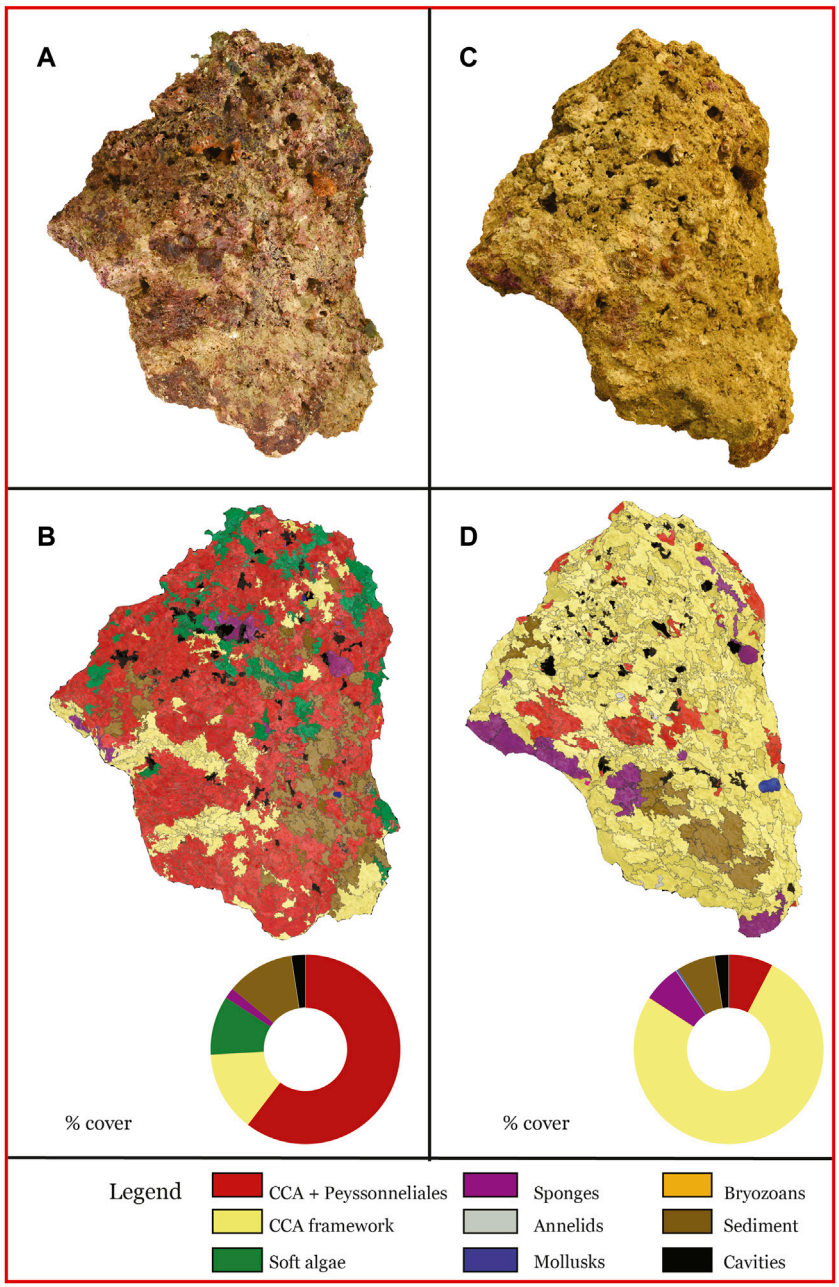

FIGURE 3 | East side of the sample CBR2_3_7c, pictured **(A,C)** and fragmented **(B,D)**. **(A)** Original east side; **(B)** results of the fragmentation of the east side with the ring chart of covers; **(C)** east side after the canopy removal; **(D)** results of the fragmentation of the east side after the canopy removal with the ring chart of covers. Among the 12 categories indicated in the Methods, only the ones actually detected have been reported in the legend.

3.1.1 Original Cover

The most abundant component is the CCA + Peyssonneliales class, with a cover ranging between 60.79% at the top and 38.69% at the bottom (**Figure 3A**; **Table 1**). Lateral cover ranges between 50.93% and 60.38% (**Figures 3A**,**B**, **4A**; **Table 1**). The CCA framework is the second component, with a cover ranging between 9.03% (south side) and 50.35% (bottom side) (**Figure 4A**; **Table 1**). Soft algae are also abundant, up to 20.29% in the south side (**Figure 4A**; **Table 1**). All the animal groups have negligible covers, whereas sediment ranges between 3.85% (north side) and 13.41% (south side) (**Figure 4A**; **Table 1**). Cavities range between 0.93% (top side) and 2.42% (east side) (**Figures 3B**, **4A**; **Table 1**).

TABLE 1 | Cover of the identified classes on the surfaces of coralligenous samples CBR2_3_7c and CBR2_4_21c, at time of collection (O = original) and after the canopy removal (R). Results expressed in cover percentages.

		CBR2_3_7c						CBR2_4_21c					
		Top	North	East	South	West	Bottom	Top	North	East	South	West	Bottom
CCA +Peyssonneliales	O	60.79	57.80	60.38	52.86	50.93	38.69	46.24	59.36	30.41	54.06	49.56	18.12
	R	21.53	14.43	7.58	9.47	25.99	2.26	17.91	17.80	9.16	23.96	22.17	5.58
CCA framework	O	15.31	21.05	13.74	9.03	22.91	50.35	5.64	14.50	18.42	5.53	3.07	63.48
	R	63.98	71.73	76.57	79.38	57.85	76.47	56.54	64.59	74.61	64.51	51.06	85.66
Soft algae	O	15.27	14.24	10.07	20.29	10.44	1.44	17.50	14.39	31.60	24.09	28.01	5.94
	R	1.40	0.47	0.00	1.48	2.28	1.01	0.27	0.67	0.12	0.07	0.02	0.00
Foraminifers	O	0.03	0.00	0.01	0.00	0.00	0.00	0.02	0.02	0.01	0.00	0.00	0.04
	R	0.00	0.00	0.05	0.00	0.00	0.04	0.08	0.13	0.18	0.15	0.07	0.05
Sponges	O	1.30	1.74	1.80	3.14	2.92	1.79	1.17	4.42	0.72	0.00	0.85	0.25
	R	1.51	3.38	6.35	2.30	3.35	4.28	1.14	3.84	0.92	2.19	1.71	1.93
Annelids	O	0.06	0.08	0.00	0.00	0.01	0.84	0.10	0.55	0.85	0.00	0.05	2.25
	R	0.13	0.21	0.17	0.00	0.07	0.75	0.03	1.54	0.27	0.54	0.57	1.12
Cnidarians	O	0.00	0.00	0.00	0.00	0.00	0.00	0.00	0.07	0.00	0.00	0.00	0.00
	R	0.00	0.00	0.00	0.00	0.00	0.00	0.08	0.00	0.00	0.00	0.00	0.00
Mollusks	O	0.00	0.00	0.07	0.05	0.00	0.00	0.31	0.02	0.00	0.00	0.00	0.06
	R	0.00	0.02	0.28	0.33	0.00	0.03	0.39	0.00	0.00	0.00	0.00	0.02
Bryozoans	O	0.14	0.09	0.06	0.11	0.09	0.11	12.30	3.71	8.05	3.25	7.75	6.09
	R	0.10	0.43	0.03	0.15	1.09	0.46	0.26	2.10	3.93	0.37	0.78	1.21
Arthropods	O	0.00	0.00	0.00	0.00	0.00	0.00	0.01	0.03	0.00	0.04	0.00	0.00
	R	0.00	0.00	0.00	0.00	0.00	0.00	0.00	0.00	0.00	0.00	0.00	0.00
Sediment	O	6.16	3.85	11.45	13.41	11.11	4.66	16.07	2.58	9.20	12.60	10.08	3.41
	R	8.86	6.08	6.56	4.86	5.72	11.56	22.67	8.45	8.51	7.15	22.51	3.18
Cavities	O	0.93	1.14	2.42	1.10	1.59	2.11	0.64	0.35	0.74	0.44	0.62	0.36
	R	2.49	3.26	2.40	2.03	3.64	3.14	0.62	0.87	2.29	1.06	1.11	1.24

3.1.2 Cover After the Canopy Removal

The most abundant component is the CCA framework, with a cover ranging between 57.85% (west side) and 79.38% (south side) (**Figure 4A**; **Table 1**). The CCA + Peyssonneliales class is still important (cover range 2.26%–25.99%), together with sediment (cover range 4.86%–11.56%) (**Figure 4A**; **Table 1**). Soft algae are negligible as well as all the animal groups except for sponges, which range between 1.51 and 6.35% (**Figure 4A**; **Table 1**). Cavities range between 2.03% (south side) and 3.26% (north side) (**Figure 4A**; **Table 1**).

3.1.3 CT Fragmentation

A volume corresponding to the 58.38% of the biocostruction is composed of a dense framework (HD + UHD classes) (**Figure 5A**; **Table 2**). The low-density class accounts for 22.06%, whereas medium density accounts for 10.03% (**Figure 5A**; **Table 2**). Voids account for 28.40% (**Figure 5A**; **Table 2**). Calculated porosity is 0.28 (**Table 2**). The validation of the identified classes with the sample reveals that UHD, HD, and MD classes correspond to the CCA framework with different levels of lithification, whereas the LD class corresponds to cavities filled by non-lithified sediments.

3.2 CBR2_4_21c

The CBR2_4_21c sample was collected in the middle of a submarine channel consisting of biogenic gravel and sand where distinct, small, and sparse columns of Coralligenous characterize the seascape (**Figure 1C**). CBR2_4_21c is 38 cm high, with a circumference of 71 cm at the base, a circumference of 52.5 cm at the top and a maximum circumference of 112 cm (**Figure 6**). The weight is 30 kg.

3.2.1 Original Cover

The most abundant component is the CCA + Peyssonneliales class, with a cover ranging between 18.12% (bottom side) and 59.36% (north side) (**Figures 4B**, **6B**; **Table 1**). Soft algae have important covers, ranging between 14.39% (north side) and 31.60% (east side), except for the bottom (5.94%) (**Figure 4B**; **Table 1**). The CCA framework is abundant only on the bottom side (63.48%), and it is relatively important in the north (14.50%) and east side (18.42%) (**Figures 4B**, **6B**; **Table 1**). All the animal groups are negligible except for the bryozoans (from 3.05% up to 12.30%). Sediment ranges between 2.58% (north side) and 16.07% (top side), whereas cavities are always less than 1% (**Figure 4B**; **Table 1**).

3.2.2 Cover After the Canopy Removal

The most abundant component is the CCA framework, with a cover ranging from 51.06% (west side) up to 85.66% (bottom side) (**Figure 4B**; **Table 1**). The CCA + Peyssonneliales class is still important (cover range 9.16%–23.96%), together with sediment (cover range 3.18%–22.67%) (**Figure 4B**; **Table 1**). All the animal groups are negligible, except for bryozoans and sponges, which range from 0.26% to 3.93% and from 0.92% and 3.84%, respectively (**Figure 4B**; **Table 1**). Sediment ranges between 3.18% (bottom side) and 22.67% (top side), whereas cavities range between 0.62% (top side) and 2.29% (east side) (**Figure 4B**; **Table 1**).

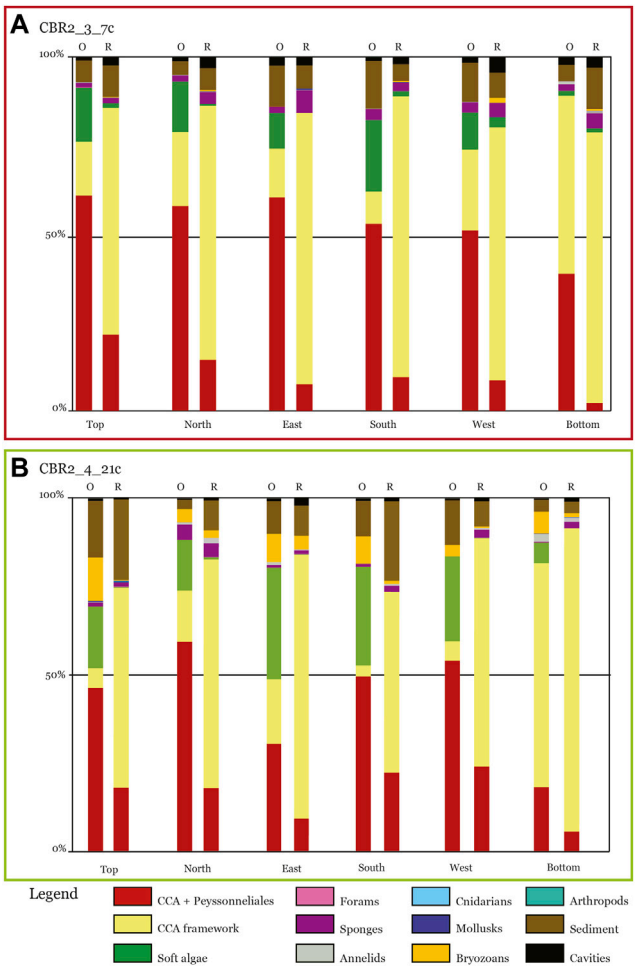

FIGURE 4 | Bar graphs with the cover percentage for each side of the samples (percentage). **(A)** Sample CBR2_3_7c. **(B)** Sample CBR2_4_21c. Values are expressed both for the original sample at the time of collection (O) and for the sample after the canopy removal (R).

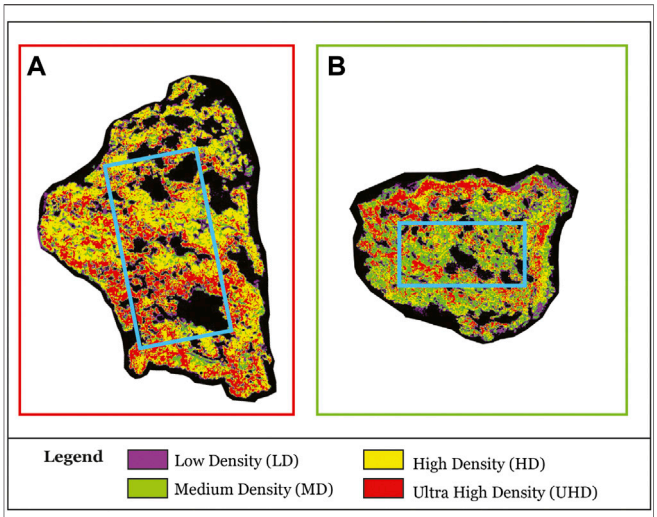

FIGURE 5 | Example of one slice per sample after the CT fragmentation *via* thresholding. **(A)** CBR2_3_7c fragmentation. **(B)** CBR2_4_21c f fragmentation. Light-blue lines indicate the sections of the cylindrical sub-volumes considered for the calculation.

3.2.3 CT Fragmentation

The most abundant class in the framework of the sample CBR2-4_21c is represented by the medium-density (31.09%) followed by the high-density (23.04%) class (**Figure 5B**; **Table 2**). Voids account for 21.04% and calculated porosity is 0.21 (**Table 2**). The validation of the identified classes with the sample reveals that UHD, HD, and MD classes correspond to the CCA framework with different levels of lithification, whereas the LD class corresponds to cavities filled by still unlithified sediments.

3.3 PCA Analyses

PCAs easily distinguish between original samples and the same after the canopy removal (**Figure 7**). **Figure 7A** shows the PCA plot considering both samples and all sides, whereas **Figures 7B,C** present the same results considering CBR2_3_7c and CBR2_4_21c separately. Component 1, representing the CCA framework, easily distinguishes between original and "after the removal" samples (**Figure 7A**). This is the reason why all the

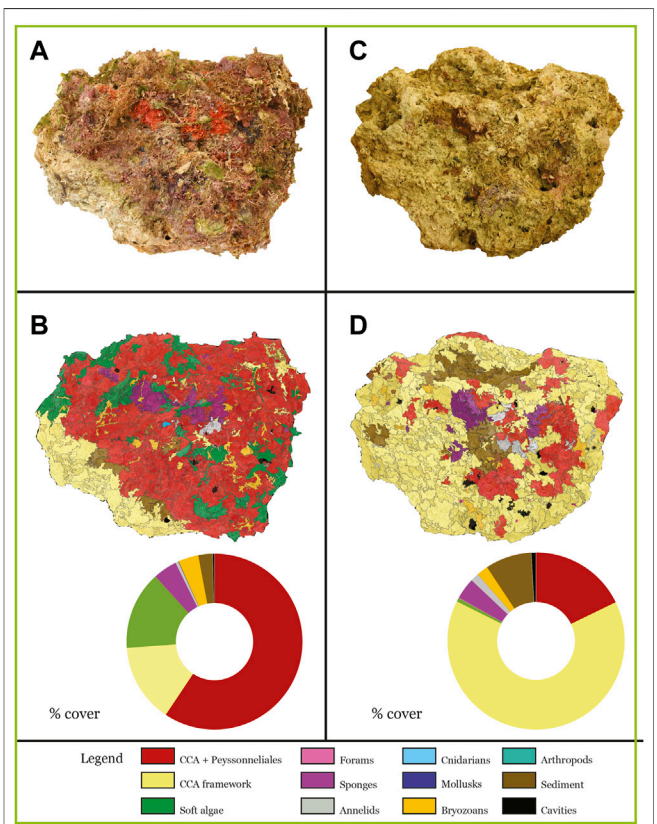

FIGURE 6 | North side of the sample CBR2_4_21c, pictured **(A,C)** and fragmented **(B,D)**. **(A)** Original north side; **(B)** results of the fragmentation of the north side with the ring chart of covers; **(C)** north side after the canopy removal; **(D)** results of the fragmentation of the north side after the canopy removal with the ring chart of covers.

TABLE 2 | Results of the fragmentation in density classes from the CT analysis. Volumes in mm^3 and percentage. LD, low-density; MD, medium-density; HD, high-density; UHD, ultrahigh-density.

		CBR2_3_7c	%	CBR2_4_21c	%
		mm^3		mm^3	
Volume	LD	535112	9.18	250512	9.42
	MD	584311	10.03	826887	31.09
	HD	1766900	30.32	612721	23.04
	UHD	1285660	22.06	399996	15.04
	Voids	1655197	28.40	569576	21.42
	Total volume	5827180		2659692	
	Porosity	0,28		0,21	

bottom sides are mixed (**Figure 7A**). Interestingly, in both CBR2_3_7c (**Figure 7B**) and CBR2_4_21c (**Figure 7C**), the two most different original surfaces are the north and south sides.

4 DISCUSSION

Several efforts have been made in the last decades to fill the gap in the knowledge of the so-called mesophotic biogenic reefs, also in the Mediterranean Sea. Coralligenous only partially overlaps with the wide range of the bioconstructions found in the mesophotic zone, developing at different depths and under different environmental factors (e.g., Cerrano et al., 2010, 2019; Bianchelli et al., 2013; Giusti et al., 2014; Cau et al., 2015; Grinyó et al., 2018).

Although the term coralligenous effectively identifies a heterogeneous bioconstruction (Pérès and Picard, 1964; Ballesteros, 2006; La Rivière et al., 2021), the use of this term for different types of bioherms and communities leads to possibly confusing different habitats/communities with each other, and consequently different mesophotic reefs, putting them all together under a unique definition.

Coralligenous samples examined in this study were collected below the bathymetric limit of the *Posidonia oceanica* meadow, as seen on the ROV (**Figures 1B,C**). The quantitative approach of this study confirms that the analyzed samples are dominated by CCA, in the form of living and dead CCA, and mineralized Peyssonneliales (**Figures 2**, **3**, **6**; **Table 1**), in agreement with the previous description of a coralligenous pillar in the area (Di Geronimo et al., 2002). We suggest that the CCA dominance, especially as primary substrate and in the inner structure, should identify the Coralligenous from all other different biogenic mesophotic reefs. This consideration finds a strong validation in the Quaternary fossil record, where analogous fossil reefs have been identified as Coralligenous, and they are mostly composed of CCA and lithified sediment, with a negligible contribution of all other components (Bosence and Pedley 1982; Carannante and Simone, 1996; Rasser, 2000; Nalin et al., 2006; Basso et al., 2007, 2009; Titschack et al., 2008; Bracchi et al., 2014, 2016, 2019). We consequently interpret our samples as true examples of Coralligenous circalittoral biocoenosis as originally defined by Pérès and Picard (1964). As supported by the results of PCA analyses (**Figure 7**), the different cover values clearly distinguish the original samples from those after the canopy removal (**Figures 2**, **5**; **Table 1**), showing that the surface often shows a high biodiversity because the solid substrate supports a wide range of communities. Nevertheless, we demonstrated that CCA are also abundant at the surface. Therefore, the appropriate identification of this class in visual methods, although applied only at surfaces, should be considered for the identification of the Coralligenous, when possible.

The CT revealed that the CCA framework, corresponding to classes from MD up to UHD, dominates the inner structure, although with different densities (**Figure 5**; **Table 2**). The framework represents a combination of algal thalli together with sediment that can fill the empty space among CCA crusts or inner voids. CCA surely represent the basic framework for the tridimensional development of the build-up, but also the role of sediment and lithification is crucial for its development. Two types of micrite are possibly present: detrital micrite and autochthonous micrite. The first type derives from physical processes, notably erosion, transport, and deposition. The lithification rate of this type of micrite is generally low and may take place over time after the primary framework is formed. The second type could derive from induced biomineralization, mediated by microbial metabolic activities, or influenced biomineralization, mediated by organic matter decay (Perry et al., 2007; Altermann et al., 2009; Dupraz et al., 2009; Anbu et al., 2016; Guido et al., 2019; Görgen et al., 2020; Riding and Virgone, 2020). The occurrence of autochthonous micrite allows hypothesizing a possible contribution of a non-skeletal carbonate component in the strengthening of the primary framework due to the sin-depositional cementation of this micrite type. Further specific micromorphological and biogeochemical analyses will allow elucidating the detrital *vs*. autochthonous origin of the micrite sediments and clarifying the role of the different types of micrites in terms of coralligenous density parameters.

The Coralligenous typically presents a cavernous structure (Ballesteros, 2006), and the occurrence of cavities and crevices at different scales contributes to the creation of several ecological niches that in turn enhance its values in term of biodiversity (Bertolino et al., 2013, 2017a; b; 2019, Costa et al., 2019). In our samples occur several surficial and internal cavities sometimes not in contact with the surface as inner voids. Interestingly, the surface shows few visible centimeter cavities (**Table 1**), whereas the CT shows a very porous framework, with centimetric voids (**Figure 5**).

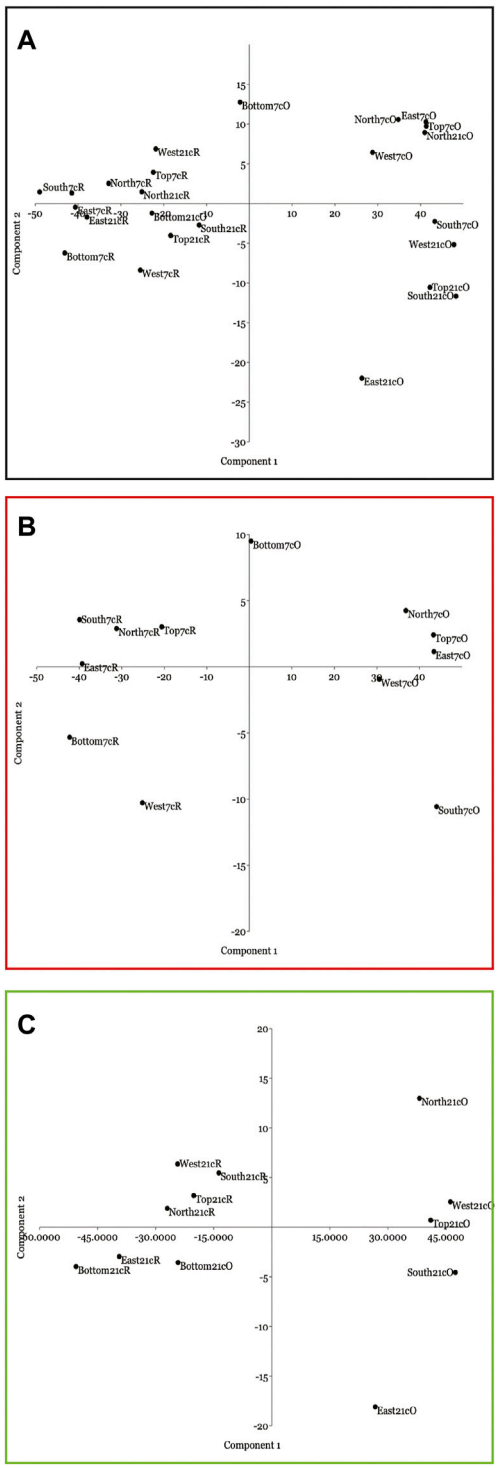

FIGURE 7 | Principal component analyses (PCAs) of the percentage cover of the coralligenous side, showing the scatter plot with the Component 1 and 2 axes. **(A)** PCA of all the sides, both original (O) and after the canopy removal (R); **(B)** only CBR2_3_7c; **(C)** only CBR2_4_21c.

CT shows that CBR2_3_7c has a more compact inner structure, and voids are generally coarser than CBR2_4_21c (**Figure 5A**; **Table 2**).

CBR2_4_21c is dominated by the MD to HD classes, actually showing a generally much more open framework with algal thalli separated by empty spaces, only sometimes filled by loose sediment, and generally fewer and smaller voids (**Figure 5B**; **Table 2**). The calculated porosity corresponds to 0.28 (CBR2_3_7c) and 0.21 (CBR2_4_21c) and these represent the first quantitative data about coralligenous porosity. The reported values suggest that a more compact material characterizes CBR2_3_7c with respect to CBR2_4_21c, despite the bigger inner voids. This variability can be related to the different density of Coralligenous at the habitat scale (**Figures 1B,C**). CBR2_4_21c developed in the middle of a submarine channel where transport of currents and sediments can generate much more turbidity with respect to CBR2_3_7c, which is instead more protected from sedimentation by its surroundings. This is also reflected in the cover percentage values, where the maximum sediment cover is observed on the top side of CBR2_4_21c (22.7%, **Table 1**). Further study will deeply investigate these aspects.

CCA in the Coralligenous have a growth rate ranging between 0.006 and 0.83 mm/yr (Ingrosso et al., 2018). Di Geronimo et al. (2002) specifically indicated 0.27 mm/year for samples collected in the same area. This extremely slow development is compatible with the scale of geological time, which is the appropriate scale of observation of the genetic process at the base of the persistent substrate of biogenic origin. Efforts in conservation and management should therefore consider this specific substrate for ensuring a proper management of the coralligenous habitat.

Multiscale remote and direct visual methods (pros and cons) applied to Coralligenous have been summarized in the study by Zapata-Ramírez et al. (2013). In our work, we applied both 2D (OBIA classification) and 3D (CT) techniques to quantitatively define the contribution of organisms, and among them, of the builders, in the Coralligenous at the scale of singular build-up with solid results. However, the orthomosaic fragmentation of the sample sides and subsequent OBIA classification present some limits like 1) the minimum dimension of the fragmentation setting and 2) the maximum resolution of the orthomosaic image. This translates in some limitations in the detection of some components of the fragmentation, if too small. Despite this apparent limitation, we were still able to depict high biodiversity at the surface and the contribution of all taxa, albeit with various degrees, to the surface cover (**Table 1**). These results confirm that coralligenous represents a hotspot of biodiversity, hosting highly diversified flora and fauna at its surface (**Figures 4**, **7**; **Table 1**) and that this technique is still appropriate. In addition, we were able to detect a good variability within the two samples and among sides of the same sample (**Figures 3**, **4**, **6**, **7**; **Table 1**), which suggests caution when comparing visual census observations from different sites for ecological status assessment and monitoring purposes.

CCA often serve as substrate for many different encrusting components, which means that the real CCA cover can be partially underestimated because CCA are not visible at the surface. Moreover, mineralized and unmineralized Peyssonneliales were not automatically distinguishable *via* fragmentation and OBIA classification. After the canopy

removal, the cover of the class CCA + Peyssonneliales no longer includes unmineralized Peyssonneliales. The comparison of the values of this class before and after the canopy removal is indicative of the contribution of unmineralized Peyssonneliales. As observed in **Table 1**, the values of this class before and after the canopy removal strongly decrease, suggesting that unmineralized Peyssonneliales are abundant and contribute to hiding the CCA on the bioconstruction surface. The risk of underestimating the CCA contributing to Coralligenous by surface observation is therefore an evident limit, and also, this aspect should be correctly considered for an adequate definition of Coralligenous.

5 CONCLUSION

The fine scale analysis of two discrete coralligenous build-ups collected offshore Marzamemi (Sicily, Ionian Sea) allowed univocally and quantitatively defining the role of different reef-builders in this type of Mediterranean bioconstruction. CCA dominate the surface of the structures, both in the original condition and after the removal of the canopy of fleshy and unmineralized organisms. Their skeletons, densely packed together with lithified sediments, form the primary framework of the bioconstruction attribuiting them a medium- to ultrahigh-density. Porosity in Coralligenous has been assessed as 0.21 and 0.28 for the first time. The present study approach enables us to confirm that the Marzamemi Coralligenous is a primary biogenic hard substrate dominated by CCA, which play a fundamental role as physical and permanent builders compared to all other taxonomic groups that provide negligible contributions. The long-time development of this primary substrate also supports important communities of high biodiversity value on its surface and into its crevices that, however, represent non-builder components.

Although Coralligenous shows a high heterogeneity, this term has been apparently applied to circalittoral mesophotic reefs different in respect to the original definition. Instead, the genetic nature of this specific substrate should be considered in order to develop appropriate measures for management and conservation to guarantee a future for this specific type of habitat.

DATA AVAILABILITY STATEMENT

The original contributions presented in the study are included in the article/Supplementary Material; further inquiries can be directed to the corresponding author.

AUTHOR CONTRIBUTIONS

Conceptualization: VB, AR, and DB; methodology: VB, PB, LF, RL, MN, and EP; formal analysis: VB, PB, and LF; investigation: VB, PB, LF, AV, AS, AR, RS, RL, and DB; data curation: VB, PB, and LF; writing—original draft preparation: VB and LF; writing—review and editing: VB, PB, LF, AV, AS, AR, RS, AG, MB, GC, and DB; supervision: DB and AR; project administration: DB, AR, and MM; funding acquisition: DB, AR, and MM. All authors have read and agreed to the published version of the manuscript.

FUNDING

Project "CRESCIBLUREEF - Grown in the blue: new technologies for knowledge and conservation of Mediterranean reefs," funded by the Italian Ministry of Research and University—Fondo Integrativo Speciale per la Ricerca (FISR), project number: FISR_04543.

ACKNOWLEDGMENTS

This is the Catania Palaeoecological Research Group contribution n. 486. Nunzio Pietralito and all the team of SUTTAKKUA diving school (Pachino, SR) are thanked for their support in the field activities. The Associate Editor Emily Mitchell and the two reviewers Salvatore Giacobbe and Pierre Boissery are thanked for their positive comments and fruitful suggestions on the article.

REFERENCES

Altermann, W., Böhmer, C., Gitter, F., Heimann, F., Heller, I., Läuchli, B., et al. (2009). Defining biominerals and organominerals: Direct and indirect indicators of life. Perry et al., Sedimentary Geology, 201, 157-179. *Sediment. Geol.* 213 (3-4), 150–151. doi:10.1016/j.sedgeo.2008.04.001

Anbu, P., Kang, C.-H., Shin, Y.-J., and So, J.-S. (2016). Formations of Calcium Carbonate Minerals by Bacteria and its Multiple Applications. *SpringerPlus* 5, 250. doi:10.1186/s40064-016-1869-2

Anelli, M., Julitta, T., Fallati, L., Galli, P., Rossini, M., and Colombo, R. (2019). Towards New Applications of Underwater Photogrammetry for Investigating Coral Reef Morphology and Habitat Complexity in the Myeik Archipelago, Myanmar. *Geocarto Int.* 34 (5), 459–472. doi:10.1080/10106049.2017.1408703

Ballesteros, E. (2006). "Mediterranean Coralligenous Assemblages," in *Oceanogr. Mar. Biol. Ann. Rev.* Editor H. Barners (London, EN: LTD Press), 123–195. doi:10.1201/9781420006391.ch4

Basso, D., Nalin, R., and Massari, F. (2007). Genesis and composition of the Pleistocene Coralligene de plateau of the Cutro Terrace (Calabria, southern Italy). *njgpa* 244 (2), 173–182. doi:10.1127/0077-7749/2007/0244-0173

Basso, D., Nalin, R., and Nelson, C. S. (2009). Shallow-water *Sporolithon* Rhodoliths from North Island (New Zealand). *Palaios* 24, 92–103. doi:10.2110/palo.2008.p08-048r

Bellan-Santini, D., Lacaze, J. C., and Poizat, C. (1994). *Les biocénoses marines et littorales de Méditerranée, Synthèse, menaces et perspectives*. Collect. Patrim. Nat., Paris: Muséum National d'Histoire Naturelle, Sécretariat de la Flore et de la Faune.

Bertolino, M., Cerrano, C., Bavestrello, G., Carella, M., Pansini, M., and Calcinai, B. (2013). Diversity of Porifera in the Mediterranean Coralligenous Accretions, with Description of a New Species. *Zookeys* 336, 1–37. doi:10.3897/zookeys.336.5139

Bertolino, M., Calcinai, B., Cattaneo-Vietti, R., Cerrano, C., Lafratta, C., Pansini, M., et al. (2014). Stability of the Sponge Assemblage of Mediterranean Coralligenous Concretions Along a Millennial Time Span. *Mar. Ecol.* 35, 149–158. doi:10.1111/maec.12063

Bertolino, M., Cattaneo-Vietti, R., Costa, G., Pansini, M., Fraschetti, S., and Bavestrello, G. (2017a). Have Climate Changes Driven the Diversity of a Mediterranean

Coralligenous Sponge Assemblage on a Millennial Timescale? *Palaeogeogr. Palaeoclimatol. Palaeoecol.* 487, 355–363. doi:10.1016/j.palaeo.2017.09.020

Bertolino, M., Costa, G., Carella, M., Cattaneo-Vietti, R., Cerrano, C., Pansini, M., et al. (2017b). The Dynamics of a Mediterranean Coralligenous Sponge Assemblage at Decennial and Millennial Temporal Scales. *PloS One* 12 (5), e0177945. doi:10.1371/journal.pone.0177945

Bertolino, M., Costa, G., Cattaneo-Vietti, R., Pansini, M., Quarta, G., Calcagnile, L., et al. (2019). Ancient and Recent Sponge Assemblages from the Tyrrhenian Coralligenous over Millennia (Mediterranean Sea). *Facies* 65 (3), 1–12. doi:10.1007/s10347-019-0573-4

Bianchelli, S., Pusceddu, A., Canese, S., Greco, S., and Danovaro, R. (2013). High Meiofaunal and Nematodes Diversity Around Mesophotic Coral Oases in the Mediterranean Sea. *PLoS One* 8, e66553. doi:10.1371/journal.pone.0066553

Blaschke, T. (2010). Object Based Image Analysis for Remote Sensing. *ISPRS J. Photogrammetry Remote Sens.* 65 (1), 2–16. doi:10.1016/j.isprsjprs.2009.06.004

Bosence, D. W. J., and Pedley, H. M. (1982). Sedimentology and Palaeoecology of a Miocene Coralline Algal Biostrome from the Maltese Islands. *Palaeogeogr. Palaeoclimatol. Palaeoecol.* 38, 9–43. doi:10.1016/0031-0182(82)90062-1

Bracchi, V. A., Basso, D., Marchese, F., Corselli, C., and Savini, A. (2017). Coralligenous Morphotypes on Subhorizontal Substrate: A New Categorization. *Cont. Shelf Res.* 144, 10–20. doi:10.1016/j.csr.2017.06.005

Bracchi, V. A., Basso, D., Savini, A., and Corselli, C. (2019). Algal Reefs (Coralligenous) from Glacial Stages: Origin and Nature of a Submerged Tabular Relief (Hyblean Plateau, Italy). *Mar. Geol.* 411, 119–132. doi:10.1016/j.margeo.2019.02.008

Bracchi, V. A., Nalin, R., and Basso, D. (2014). Paleoecology and Dynamics of Coralline Dominated Facies during a Pleistocene Transgressive-Regressive Cycle (Capo Colonna Marine Terrace, Southern Italy). *Palaeogeogr. Palaeoclimatol. Palaeoecol.* 414, 296–309. doi:10.1016/j.palaeo.2014.09.016

Bracchi, V. A., Nalin, R., and Basso, D. (2016). Morpho-structural Heterogeneity of Shallow-Water Coralligenous in a Pleistocene Marine Terrace (Le Castella, Italy). *Palaeogeogr. Palaeoclimatol. Palaeoecol.* 454, 101–112. doi:10.1016/j.palaeo.2016.04.014

Bracchi, V., Savini, A., Marchese, F., Palamara, S., Basso, D., and Corselli, C. (2015). Coralligenous Habitat in the Mediterranean Sea: a Geomorphological Description from Remote. *Ijg* 134, 32–40. doi:10.3301/IJG.2014.16

Cánovas-Molina, A., Montefalcone, M., Vassallo, P., Morri, C., Bianchi, C. N., and Bavestrello, G. (2016). Combining Literature Review, Acoustic Mapping and *In Situ* Observations: an Overview of Coralligenous Assemblages in Liguria (NW Mediterranean Sea). *Sci. Mar.* 80, 7–16. doi:10.3989/scimar.04235.23a

Carannante, G., and Simone, L. (1996). "Rhodolith Facies in the Central-southern Apennines Mountains, Italy," in *Models for Carbonate Stratigraphy from Miocene Reef Complexes of Mediterranean Regions*. Editors E. K. Franseen, M. Esteban, W. C. Ward, and J. M. Rouchy (Italy: SEPM Concepts in Sedimentology and Palaeontology), 5, 261–275. doi:10.2110/csp.96.01.0261

Casoli, E., Ventura, D., Mancini, G., Pace, D. S., Belluscio, A., and Ardizzone, G. (2021). High Spatial Resolution Photo Mosaicking for the Monitoring of Coralligenous Reefs. *Coral Reefs* 40 (4), 1267–1280. doi:10.1007/s00338-021-02136-4

Cau, A., Follesa, M. C., Moccia, D., Alvito, A., Bo, M., Angiolillo, M., et al. (2015). Deepwater corals biodiversity along roche du large ecosystems with different habitat complexity along the south Sardinia continental margin (CW Mediterranean Sea). *Mar. Biol.* 162, 1865–1878. doi:10.1007/s00227-015-2718-5

Cecchi, E., Gennaro, P., Piazzi, L., Ricevuto, E., and Serena, F. (2014). Development of a New Biotic Index for Ecological Status Assessment of Italian Coastal Waters Based on Coralligenous Macroalgal Assemblages. *Eur. J. Phycol.* 49, 298–312. doi:10.1080/09670262.2014.918657

Cerrano, C., Bastari, A., Calcinai, B., Di Camillo, C., Pica, D., Puce, S., et al. (2019). Temperate Mesophotic Ecosystems: Gaps and Perspectives of an Emerging Conservation Challenge for the Mediterranean Sea. *Eur. Zoological J.* 86 (1), 370–388. doi:10.1080/24750263.2019.1677790

Cerrano, C., Bavestrello, G., Bianchi, C. N., Calcinai, B., Cattaneo-Vietti, R., Morri, C., et al. (2001). "The Role of Sponge Bioerosion in Mediterranean Coralligenous Accretion," in *Mediterranean Ecosystems*. Editors F. M. Faranda, L. Guglielmo, and G. Spezie (Milano: Springer), 235–240. doi:10.1007/978-88-470-2105-1_30

Cerrano, C., Danovaro, R., Gambi, C., Pusceddu, A., Riva, A., and Schiaparelli, S. (2010). Gold Coral (*Savalia savaglia*) and Gorgonian Forests Enhance Benthic Biodiversity and Ecosystem Functioning in the Mesophotic Zone. *Biodivers. Conserv.* 19, 153–167. doi:10.1007/s10531-009-9712-5

Chimienti, G., De Padova, D., Mossa, M., and Mastrototaro, F. (2020). A Mesophotic Black Coral Forest in the Adriatic Sea. *Sci. Rep.* 10, 8504. doi:10.1038/s41598-020-65266-9

Corriero, G., Pierri, C., Mercurio, M., Nonnis Marzano, C., Onen Tarantini, S., Gravina, M. F., et al. (2019). A Mediterranean Mesophotic Coral Reef Built by Non-symbiotic Scleractinians. *Sci. Rep.* 9, 3601. doi:10.1038/s41598-019-40284-4

Costa, G., Bavestrello, G., Micaroni, V., Pansini, M., Strano, F., and Bertolino, M. (2019). Sponge Community Variation along the Apulian Coasts (Otranto Strait) over a Pluri-Decennial Time Span. Does Water Warming Drive a Sponge Diversity Increasing in the Mediterranean Sea? *J. Mar. Biol. Ass.* 99 (7), 1519–1534. doi:10.1017/s0025315419000651

Deter, J., Descamp, P., Ballesta, L., Boissery, P., and Holon, F. (2012). A Preliminary Study toward an Index Based on Coralligenous Assemblages for the Ecological Status Assessment of Mediterranean French Coastal Waters. *Ecol. Indic.* 20, 345–352. doi:10.1016/j.ecolind.2012.03.001

Di Geronimo, I., Di Geronimo, R., Improta, S., Rosso, A., and Sanfilippo, R. (2001). Preliminary Observations on a Columnar Coralline Build-Up from off SE Sicily in Proceedings of the Conference of the Society o Marine Biology, Sharm El Sheikh, May 13–20 2000. *Biol. Mar. Medit.* 8 (1), 1–10.

Di Geronimo, I., Di Geronimo, R., Rosso, A., and Sanfilippo, R. (2002). Structural and Taphonomic Analysis of a Columnar Coralline Algal Build-Up from SE Sicily. *Geobios* 35, 86–95. doi:10.1016/S0016-6995(02)00050-5

Dupraz, C., Reid, R. P., Braissant, O., Decho, A. W., Norman, R. S., and Visscher, P. T. (2009). Processes of Carbonate Precipitation in Modern Microbial Mats. *Earth-Science Rev.* 96, 141–162. doi:10.1016/j.earscirev.2008.10.005

Enrichetti, F., Bava, S., Bavestrello, G., Betti, F., Lanteri, L., and Bo, M. (2019). Artisanal Fishing Impact on Deep Coralligenous Animal Forests: A Mediterranean Case Study of Marine Vulnerability. *Ocean Coast. Manag.* 177, 112–126. doi:10.1016/J.OCECOAMAN.2019.04.021

Fagerström, J. A. (1991). Reef-building Guilds and a Checklist for Determining Guild Membership. *Coral Reefs* 10, 47–52. doi:10.1007/BF00301908

Fallati, L., Saponari, L., Savini, A., Marchese, F., Corselli, C., and Galli, P. (2020). Multi-temporal UAV Data and Object-Based Image Analysis (OBIA) for Estimation of Substrate Changes in a Post-bleaching Scenario on a Maldivian Reef. *Remote Sens.* 12 (13), 2093. doi:10.3390/rs12132093

Feldmann, J. (1937). *Recherches sur la Végétation Marine de la Méditerranée: la Côte des Albères*. Paris: Rouen: Wolf.

Ferrigno, F., Russo, G. F., and Sandulli, R. (2017). Coralligenous Bioconstructions Quality Index (CBQI): a Synthetic Indicator to Assess the Status of Different Types of Coralligenous Habitats. *Ecol. Indic.* 82, 271–279. doi:10.1016/j.ecolind.2017.07.020

Ferrigno, F., Russo, G. F., Semprucci, F., and Sandulli, R. (2018). Unveiling the State of Some Underexplored Deep Coralligenous Banks in the Gulf of Naples (Mediterranean Sea, Italy). *Regional Stud. Mar. Sci.* 22, 82–92. doi:10.1016/j.rsma.2018.05.006

Gatti, G., Bianchi, C. N., Morri, C., Montefalcone, M., and Sartoretto, S. (2015). Coralligenous Reefs State along Anthropized Coasts: Application and Validation of the COARSE Index, Based on a Rapid Visual Assessment (RVA) Approach. *Ecol. Indic.* 52, 567–576. doi:10.1016/j.ecolind.2014.12.026

Giusti, M., Innocenti, C., and Canese, S. (2014). Predicting Suitable Habitat for the Gold Coral *Savalia savaglia* (Bertoloni, 1819) (Cnidaria, Zoantharia) in the South Tyrrhenian Sea. *Cont. Shelf Res.* 81, 19–28. doi:10.1016/j.csr.2014.03.011

Görgen, S., Benzerara, K., Skouri-Panet, F., Gugger, M., Chauvat, F., and Cassier-Chauvat, C. (2020). The Diversity of Molecular Mechanisms of Carbonate Biomineralization by Bacteria. *Discov. Mat.* 1, 2. doi:10.1007/s43939-020-00001-9

Grinyó, J., Viladrich, N., Díaz, D., Muñoz, A., Mallol, S., Salazar, J., et al. (2018). Reproduction, Energy Storage and Metabolic Requirements in a Mesophotic Population of the Gorgonian Paramuricea Macrospina. *PLoS One* 13, e0203308. doi:10.1371/journal.pone.0203308

Guido, A., Gerovasileiou, V., Russo, F., Rosso, A., Sanfilippo, R., Voultsiadou, E., et al. (2019). Composition and Biostratinomy of Sponge-Rich Biogenic Crusts

in Submarine Caves (Aegean Sea, Eastern Mediterranean). *Palaeogeogr. Palaeoclimatol. Palaeoecol.* 534, 109338. doi:10.1016/j.palaeo.2019.109338

Hammer, Ø., Harper, D. A. T., and Ryan, P. D. (2001). Past: Paleontological Statistics Software Package for Education and Data Analysis. *Palaeontol. Electron.* 4 (4), 1–9.

Hong, J. S. (1982). Contribution a l'étude des Peuplements d'un Fond de Concrétionnement Corllaigène dans la Région Marsaillaise en Méditerranéee Nord-Occidentale. *Bull. Korea Oc. Res. Develop. Inst.* 4, 27–51.

Ingrosso, G., Abbiati, M., Badalamenti, F., Bavestrello, G., Belmonte, G., Cannas, R., et al. (2018). Mediterranean Bioconstructions along the Italian Coast. *Adv. Mar. Biol.* 79, 61–136. doi:10.1016/bs.amb.2018.05.001

Kipson, S., Fourt, M., Teixidó, N., Cebrian, E., Casas, E., Ballesteros, E., et al. (2011). Rapid Biodiversity Assessment and Monitoring Method for Highly Diverse Benthic Communities: A Case Study of Mediterranean Coralligenous Outcrops. *PLoS ONE* 6 (11), e27103. doi:10.1371/journal.pone.0027103

La Rivière, M., Michez, N., Delavenne, J., Andres, S., Fréjefond, C., Janson, A-L., et al. (2021). *Fiches descriptives des biocénoses benthiques de Méditerranée*. Paris: UMS PatriNat (OFB-CNRS-MNHN), 660.

Laborel, J. (1961). Le concrétionnement algal "Coralligene" et son importance géomorphologique en Méditerranée. *Rec. Trav. Stn. Mar. d'Endoume* 37 (27), 37–60.

Laubier, L. (1966). Le coralligène des Albères: monographie biocénotique. *Ann. l'Institut Océanogr. Monaco* 43, 139–316.

Littler, M. M. (1972). "The Crustose Corallinaceae," in *Oceanography and Marine Biology: An Annual Review*. Editor H. Barners (London, EN: LTD Press), 311–347.

Marchese, F., Bracchi, V. A., Lisi, G., Basso, D., Corselli, C., and Savini, A. (2020). Assessing Fine-Scale Distribution and Volume of Mediterranean Algal Reefs through Terrain Analysis of Multibeam Bathymetric Data. A Case Study in the Southern Adriatic Continental Shelf. *Water* 12, 157. doi:10.3390/w12010157

Marion, A. F. (1883). Esquisse d'une topographie zoologique du Golfe de Marseille. *Ann. Mus. Hist. Natur. Marseille* 1, 1–108.

Montefalcone, M., Morri, C., Bianchi, C. N., Bavestrello, G., and Piazzi, L. (2017). The Two Facets of Species Sensitivity: Stress and Disturbance on Coralligenous Assemblages in Space and Time. *Mar. Pollut. Bull.* 117, 229–238. doi:10.1016/j.marpolbul.2017.01.072

MSFD, EC (2008). *Directive 2008/56/EC of the European Parliament and of the Council of 17 June 2008 Establishing a Framework for Community Action in the Field of Marine Environmental Policy (Marine Strategy Framework Directive, Bruxelles)*.

Musard, O., Le Dû-Blayo, L., Francour, P., Beurier, J. P., Feunteun, E., and Talassinos, L. (2014). *Underwater Seascapes. From Geographical to Ecological Perspectives*. Berlin: Springer International Publishing.

Nalin, R., Basso, D., and Massari, F. (2006). Pleistocene coralline algal build-ups (coralligène de plateau) and associated bioclastic deposits in the sedimentary cover of Cutro marine terrace (Calabria, southern Italy). *Geol. Soc. Lond. Spec. Publ.* 255, 11–22. Cool-Water Carbonates: Depositional Systems and Palaeoenvironmental Controls, Editors H.M. Pedley, G. Carannante (London: The Geological Society of London). doi:10.1144/GSL.SP.2006.255.01.02

Olinger, L. K., Scott, A. R., McMurray, S. E., and Pawlik, J. R. (2019). Growth Estimates of Caribbean Reef Sponges on a Shipwreck Using 3D Photogrammetry. *Sci. Rep.* 9 (1), 1–12. doi:10.1038/s41598-019-54681-2

Pérès, J. M. (1982). "Major Benthic Assemblages," in *Marine Ecology*. Editor O. Kinne (London: John-Wiley Publ.), 5, 373–522.

Pérès, J. M., and Picard, J. (1964). Nouveau manuel de bionomie benthique de la Méditerranée. *Rec. Trav. Stat. Mar. Endoume* 31 (47), 1–37.

Perry, R. S., Mcloughlin, N., Lynne, B. Y., Sephton, M. A., Oliver, J. D., Perry, C. C., et al. (2007). Defining Biominerals and Organominerals: Direct and Indirect Indicators of Life. *Sediment. Geol.* 201, 157–179. doi:10.1016/j.sedgeo.2007.05.014

Piazzi, L., Gennaro, P., Cecchi, E., Bianchi, C. N., Cinti, M. F., Gatti, G., et al. (2021). Ecological Status of Coralligenous Assemblages: Ten Years of Application of the ESCA Index from Local to Wide Scale Validation. *Ecol. Indic.* 121, 107077. doi:10.1016/j.ecolind.2020.107077

Piazzi, L., Gennaro, P., Cecchi, E., and Serena, F. (2015). Improvement of the ESCA Index for the Evaluation of Ecological Quality of Coralligenous Habitat under the European Framework Directives. *Medit. Mar. Sci.* 16, 419–426. doi:10.12681/mms.1029

Ponti, M., Turicchia, E., Ferro, F., Cerrano, C., and Abbiati, M. (2018). The Understorey of Gorgonian Forests in Mesophotic Temperate Reefs. *Aquat. Conserv. Mar. Freshw. Ecosyst.* 28, 1153–1166. doi:10.1002/aqc.2928

Pruvot, G. (1895). Coup d'oeil sur la distribution générale des invertébrés dans la région de Banyuls (Golfe du Lion). *Arch. Zool. Exp. Gén.* 3, 629–658.

Pruvot, G. (1894). Sur les fonds sous-marins de la région de Banyuls et du cap de Creus. *Comp. Rend. Acad. Sci.* 118, 203–206.

Rasser, M. W. (2000). Coralline Red Algal Limestones of the Late Eocene Alpine Foreland Basin in Upper Austria: Component Analysis, Facies and Palecology. *Facies* 42 (1), 59–92. doi:10.1007/BF02562567

Riding, R. (2002). Structure and Composition of Organic Reefs and Carbonate Mud Mounds: Concepts and Categories. *Earth-Science Rev.* 58, 163–231. doi:10.1016/S0012-8252(01)00089-7

Riding, R., and Virgone, A. (2020). Hybrid Carbonates: *In Situ* Abiotic, Microbial and Skeletal Co-precipitates. *Earth-Science Rev.* 208, 103300. doi:10.1016/j.earscirev.2020.103300

Risso, A. (1826). "Histoire Naturelle des Principales Productions de l'Europe Méridionale et Particulièrement de Celles des Environs de Nice et des Alpes Maritimes,". Editor V. F.-G. Tome (Levrault, Paris), 400 pp.

Rosso, A., and Sanfilippo, R. (2009). "The Contribution of Bryozoans and Serpuloideans to Coralligenous Concretions From SE Sicily," in UNEM-MAP-RAC/SPA, Proceedings of the First Symposium on the Coralligenous and Other Calcareous Bio-Concretions of the Mediterranean Sea, Tabarka, January 15–16, 2009, pp. 123–128.

Sartoretto, S., Schohn, T., Bianchi, C. N., Morri, C., Garrabou, J., Ballesteros, E., et al. (2017). An Integrated Method to Evaluate and Monitor the Conservation State of Coralligenous Habitats: the INDEX-COR Approach. *Mar. Pollut. Bull.* 120, 222–231. doi:10.1016/j.marpolbul.2017.05.020

Sartoretto, S., Verlaque, M., and Laborel, J. (1996). Age of Settlement and Accumulation Rate of Submarine "coralligène" (−10 to −60 M) of the Northwestern Mediterranean Sea; Relation to Holocene Rise in Sea Level. *Mar. Geol.* 130, 317–331. doi:10.1016/0025-3227(95)00175-1

Titschack, J., Nelson, C. S., Beck, T., Freiwald, A., and Radtke, U. (2008). Sedimentary Evolution of a Late Pleistocene Temperate Red Algal Reef (Coralligène) on Rhodes, Greece: Correlation with Global Sea-Level Fluctuations. *Sedimentology* 55, 1747–1776. doi:10.1111/j.1365-3091.2008.00966.x

UNEP-MAP-RAC/SPA (2008). *Action Plan for the Conservation of the Coralligenous and Other Calcareous Bio-Concretions in the Mediterranean Sea*. Tunis: Rac/Spa, 1–21.

UNEP-MAP-RAC/SPA (2017). *Action Plan for the Conservation of the Coralligenous and Other Calcareous Bio-Concretions in the Mediterranean Sea*. Athens, Greece: Rac/Spa, 1–20.

Zapata-Ramírez, P. A., Scaradozzi, D., Scaradozzi, D., Sorbi, L., Palma, M., Pantaleo, U., et al. (2013). Innovative Study Methods for the Mediterranean Coralligenous Habitats. *Adv. Oceanogr. Limnol.* 4 (2), 102–119. doi:10.1080/19475721.2013.849758

Conflict of Interest: The authors declare that the research was conducted in the absence of any commercial or financial relationships that could be construed as a potential conflict of interest.

Publisher's Note: All claims expressed in this article are solely those of the authors and do not necessarily represent those of their affiliated organizations, or those of the publisher, the editors, and the reviewers. Any product that may be evaluated in this article, or claim that may be made by its manufacturer, is not guaranteed or endorsed by the publisher.

frontiers | Frontiers in Marine Science

ORIGINAL RESEARCH
published: 04 July 2022
doi: 10.3389/fmars.2022.906679

Assessment of Rhodolith Diversity in the Northwestern Gulf of Mexico Including the Description of *Sporolithon gracile* sp. nov. (Sporolithales, Rhodophyta), and Three New Species of *Roseolithon* (Hapalidiales, Rhodophyta)

Joseph Richards[1], Ronald P. Kittle III[1], William E. Schmidt[1], Thomas Sauvage[2,3], Carlos F. D. Gurgel[4], Daniela Gabriel[5] and Suzanne Fredericq[1]*

[1] Department of Biology, University of Louisiana at Lafayette, Lafayette, LA, United States, [2] Instituto de Biociências, Universidade Federal do Rio Grande do Sul, Porto Alegre, Brazil, [3] Ifremer, Centre Atlantique Ecosystèmes Microbiens et Molécules Marines pour les Biotechnologies (EM3B) Laboratory, Rue de l'Île d'Yeu, Nantes, France, [4] Centro de Ciências Biológicas, Departamento de Botânica, Universidade Federal de Santa Catarina, Florianópolis, Brazil, [5] School of Science and Technology (FCT), Research Center in Biodiversity and Genetic Resources (CIBIO), University of the Azores, Ponta Delgada, Portugal

OPEN ACCESS

Edited by:
Daniela Basso,
University of Milano-Bicocca, Italy

Reviewed by:
Gavin William Maneveldt,
University of the Western Cape, South Africa
Donatella Serio,
University of Catania, Italy

***Correspondence:**
Joseph Richards
joer207@gmail.com

Specialty section:
This article was submitted to Marine Ecosystem Ecology, a section of the journal Frontiers in Marine Science

Received: 28 March 2022
Accepted: 16 May 2022
Published: 04 July 2022

Citation:
Richards J, Kittle III RP, Schmidt WE, Sauvage T, Gurgel CFD, Gabriel D and Fredericq S (2022) Assessment of Rhodolith Diversity in the Northwestern Gulf of Mexico Including the Description of Sporolithon gracile sp. nov. (Sporolithales, Rhodophyta), and Three New Species of Roseolithon (Hapalidiales, Rhodophyta). Front. Mar. Sci. 9:906679. doi: 10.3389/fmars.2022.906679

In the past, non-geniculate coralline algae in the northwestern Gulf of Mexico have been identified based primarily on comparative morpho-anatomy. Recent studies employing DNA sequencing techniques combined with morpho-anatomical studies using SEM have revealed a wealth of previously undocumented diversity of rhodolith-forming non-geniculate coralline algae in the Corallinales, Hapalidiales and Sporolithales from mesophotic hard bank communities at 45-90 meters depth. Although many advances in the last decade have been made in clarifying species names and describing new species of corallines from offshore Louisiana and Texas, total diversity estimates are still incomplete and many species remain to be described. Collections from offshore Louisiana at Parker Bank in the newly expanded Flower Garden Banks National Marine Sanctuary yielded thin, finely branched rhodoliths. DNA sequence analyses of plastid-encoded *psb*A and *rbc*L loci, and nuclear-encoded LSU rDNA of these rhodolith-forming specimens revealed that some belong to an unnamed species of *Sporolithon* (Sporolithales) that we herein newly describe. Additionally, comparative DNA sequence analyses of rhodolith collections from Ewing Bank and other hard banks offshore Louisiana were conducted to assess rhodolith diversity in these mesophotic communities. The results revealed new reports of taxa for the region, including new rhodolith-forming species of *Roseolithon* (Hapalidiales) to be described herein as well. Our new biodiversity findings will be compared with historical studies from the NW Gulf of Mexico.

Keywords: CCA, coralline algae, FGBNMS, Gulf of Mexico, mesophotic, rhodoliths

INTRODUCTION

Previously, non-geniculate coralline algae (also known as crustose coralline algae or CCA) in the northwestern Gulf of Mexico have been identified based on morpho-anatomy (Minnery et al., 1985; Rezak et al., 1985; Minnery, 1990; Fredericq et al., 2009; Fredericq et al., 2014). Recent studies employing DNA sequencing techniques combined with morpho-anatomical studies have revealed a wealth of previously undocumented diversity of non-geniculate coralline algae in the Corallinales (Richards et al., 2014; Richards et al., 2021), Hapalidiales (Krayesky-Self et al., 2016; Richards et al., 2016; Richards et al., 2020) and Sporolithales (Richards and Fredericq, 2018; Fredericq et al., 2019; Richards et al., 2019) in the region.

Recently, Richards et al. (2017) performed comparative analyses of DNA sequences including sequences of type specimens and topotype specimens of *Sporolithon* spp., as well as morpho-anatomical studies using images generated with SEM. This foundational study clarified species names and helped resolve taxonomic problems in the order Sporolithales (Richards et al., 2017) and provided a foundation for describing new species of *Sporolithon* Heydrich from mesophotic habitats in the northwestern Gulf of Mexico, Brazil, and Bermuda, including *Sporolithon sinusmexicanum* J.L.Richards & Fredericq (Richards and Fredericq, 2018), *Sporolithon amadoi* J.L.Richards & R.G.Bahia (Richards et al., 2019), *Sporolithon franciscanum* L.A.S.Leão & R.G.Bahia (Leão et al., 2020) and *Sporolithon mesophoticum* J.Richards, P.W.Gabrielson & C.W.Schneider (Richards et al., 2018b). More recent advancements in Sporolithales taxonomy include the description of a new genus and species, *Roseapetra farriae* W.A.Nelson, Twist & K.F.Neil, a currently monotypic genus from New Zealand that includes the taxon previously treated as *Heydrichia woelkerlingii* R.ATownsend, Y.M.Chamberlain & Keats (Nelson et al., 2021).

Regarding the Hapalidiales, Richards et al. (2016) reported six species of *Lithothamnion* Heydrich from the northwestern Gulf of Mexico and demonstrated that *Lithothamnion* is a polyphyletic taxon. However, at the time of the 2016 study, there was a lack of DNA sequences available from the generitype species, *L. muelleri*, thus determining which clade corresponded to the true *Lithothamnion* was not possible at that time. Recently, the lectotype specimen of *L. muelleri* was sequenced (Jeong et al., 2021), which helped clarify the identification of the true *Lithothamnion*. The study by Jeong et al. (2021) in turn formed the foundation for describing a new genus, *Roseolithon* L.M.Coutinho and Barros-Barreto, which accommodated taxa previously included in the genus *Lithothamnion*. In their study, Coutinho et al. (2021) also described seven new species of *Roseolithon*.

Although many advances have been made in describing and clarifying the taxonomy of non-geniculate coralline algae offshore the northwestern Gulf of Mexico, many species remain to be described and further taxonomic issues remain unresolved. Herein, we describe the newly collected Sporolithales taxon from mesophotic depth at Parker Bank offshore Louisiana, as a new species of *Sporolithon* from offshore the northwestern Gulf of Mexico in the newly expanded Flower Garden Banks National Marine Sanctuary. Additionally, the diversity of the genus *Roseolithon* from offshore Louisiana will be assessed, and we herein describe three new species of *Roseolithon* from the northwestern Gulf of Mexico.

MATERIALS AND METHODS

Specimen Collection

Mesophotic specimens were collected aboard the R/V *Pelican*, the UNOLS (University National Oceanographic Laboratory System) research vessel stationed at LUMCON (Louisiana Universities Marine Consortium), using an hourglass design box dredge (Joyce and Williams, 1969) with minimum tows (usually 10 minutes or less) from offshore Louisiana in the Gulf of Mexico in the vicinity of Parker Bank (27° 58.189' N; 92° 02.80' W) at 92 m. depth. The rhodolith specimens were preserved in silica gel. Collection date was May 20, 2019, prior to the expansion of the Flower Garden Banks National Marine Sanctuary (the location was not part of the Marine Sanctuary at the time of collection). Additional newly collected Hapalidiales and Sporolithales specimens collected in the vicinity of Ewing Bank in May 2018-2019 were also included for comparative analyses, as well as a specimen collected from December 2010 following the Deepwater Horizon oil spill and a specimen collected from Campeche Bank in 2005. Specimens are housed at the University of Louisiana at Lafayette Herbarium (LAF). Herbarium abbreviations follow Thiers (2022, continuously updated). **Supplementary Table S1** provides a list of specimens and voucher information for taxa included in the analyses.

DNA Extraction and Sequencing

DNA was extracted from the newly collected specimens using the Quick-DNA Plant/Seed Miniprep Kit (Zymo Research, Irvine, CA, USA) and also using GenCatch™ Plant Genomic DNA Purification Kit (Epoch Life Science Inc., Missouri City, TX, USA). Markers chosen for PCR and sequencing included the plastid-encoded genes *psb*A (encodes photosystem II reaction center protein D1 gene) and *rbc*L (encodes the large subunit of the enzyme ribulose-1,5-bisphosphate carboxylase/oxygenase), and the nuclear-encoded LSU (partial 28S rDNA). PCR was performed following the protocols and primers described in Richards et al. (2014). PCR products were cleaned by the addition of 2 µl of ExoSAP-IT™ (USB, Cleveland, Ohio) per 5 µl of amplified DNA product. Reactions were incubated at 37°C for 15 min, followed by inactivation of ExoSAP-IT™ at 80°C for 15 min. Purified PCR products were subsequently cycle-sequenced using the BrightDye® Terminator Cycle Sequencing Kit (Molecular Cloning Laboratories [MCLAB], South San Francisco, CA, USA). Resulting cycle sequence reactions were purified with ETOH/EDTA precipitation and were sequenced in-house at the UL Lafayette campus on an ABI Model 3130xl Genetic Analyzer. The resulting chromatograms were assembled and edited using Sequencher 5.1 (Gene Codes Corp., Ann Arbor, MI, USA) and exported as individual ".FASTA" files. Newly generated sequences were accessed in GenBank (https://www.ncbi.nlm.nih.gov/genbank/) (**Supplementary Table S1**).

Phylogenetic Analysis

Single loci analyses were conducted for *psb*A, *rbc*L, and LSU. Available sequences were downloaded from GenBank (**Supplementary Table S1**) and aligned with newly generated sequences. Alignment was performed using MUSCLE in MEGA X (Stecher et al., 2020). Exploratory analyses were conducted in MEGA X using the Maximum Likelihood method and Tamura-Nei model (Tamura and Nei, 1993; Stecher et al., 2020). Final Maximum Likelihood analyses were conducted with CIPRES Science Gateway (Miller et al., 2010) using the RAxML-HPC2 program on XSEDE with 1,000 alternative runs on distinct starting trees and 1,000 bootstrap replicates.

Sequence Divergence Analysis

Single loci alignments of *psb*A and *rbc*L were constructed for *Sporolithon* spp. and *Roseolithon* spp. Alignments were cropped at the 5' and 3' ends to minimize missing data. For *Sporolithon* spp., a 472 bp alignment and a 366 bp alignment was constructed for *psb*A and *rbc*L, respectively. For *Roseolithon* spp., a 716 bp alignment was constructed for *psb*A, and both long and short alignments were constructed for *rbc*L and analyzed separately. The long *rbc*L alignment was 623 bp and did not include the sequence of LAF 7384; the short *rbc*L alignment included the sequence of LAF 7384 and was 366 bp in length. Sequence divergence values were calculated as the number of pairwise base pair differences in MEGA X (Kumar et al., 2018) and presented as a percentage (the number of base pair differences divided by the alignment length).

Microscopy

Thallus fragments were removed from the same specimens that were DNA-sequenced and fractured using a single edge razor blade. Specimens were mounted and viewed according to the protocol of Richards et al. (Richards et al., 2017; Richards et al., 2018b) using a Hitachi S-3000N Scanning Electron Microscope (SEM), and also using a Scios 2 Dual Beam Focused Ion Beam scanning electron microscope (FIB-SEM) at an accelerating voltage of 15 kV.

RESULTS

The *psb*A and *rbc*L analyses (**Figures 1**, **2**) showed a wealth of previously reported and newly reported diversity of non-geniculate corallines in the northwestern Gulf of Mexico, including 17 species. In the Sporolithales, two previously reported *Sporolithon* species were shown in the analyses, as well as a third species of *Sporolithon* that is described herein as a new species. In the Hapalidiales, the analyses revealed a newly reported range extension for *Roseolithon purii*, and showed that three taxa from the northwestern Gulf of Mexico previously reported as *Lithothamnion* spp. are members of *Roseolithon* as well, and are herein described as new species. The analyses also showed three species of *Lithothamnion* and *Mesophyllum erubescens* (Foslie) Me.Lemoine are present in the northwestern Gulf of Mexico. In the Corallinales, three species of *Harveylithon* A.Rösler, Perfectti, V.Peña & J.C.Braga were shown from the northwestern Gulf of Mexico, one species of *Lithophyllum* Philippi, and two species of *"Titanoderma"* Nägeli.

LSU analyses (**Figure 3**) showed at least three species of *Sporolithon* and a topology similar to the *psb*A and *rbc*L trees, with *Sporolithon gracile* J.Richards, Kittle & Fredericq sp. nov. (described below) sister to *S. sinusmexicanum*. The LSU tree revealed a putative fourth species of *Sporolithon* as well. This putative fourth species of *Sporolithon* included only one specimen, LAF 6726, that was sister to *Sporolithon amadoi*. The LSU tree also showed four clades of *Roseolithon*, that have a similar topology as shown in the *psb*A and *rbc*L trees.

The *psb*A sequence of *S. gracile* was 3.39% diverged from *S. sinusmexicanum*, and 6.99% and 7.63% diverged from *S. yoneshigueae* Bahia, Amado-Filho, Maneveldt & W.H.Adey and *S. mesophoticum*, respectively (**Supplementary Table S2**). The *rbc*L sequence of LAF 7255 was identical to the holotype sequence of *S. sinusmexicanum*, LAF 6956A (**Supplementary Tables S3**). The *rbc*L sequence of *S. gracile* was 2.46% diverged from sequences of *S. sinusmexicanum* and 11.46% and 8.47% diverged from sequences of *S. yoneshigueae* and *S. mesophoticum*, respectively (**Supplementary Table S3**). The *psb*A and *rbc*L sequences of *S. gracile* diverged 9.7% -12.3% from *Sporolithon amadoi* (**Supplementary Tables S2**, **S3**).

The *psb*A sequence of LAF 7384 was 0.0%-0.4% diverged from *psb*A sequences of Brazilian specimens of *Roseolithon purii* L.M.Coutinho & Barros-Barreto (**Supplementary Table S4**). Interspecific divergence for *psb*A sequences of *Roseolithon* spp. ranged from 1.49% - 5.46%. The *rbc*L sequence of LAF 7384 was identical to the sequence of *Roseolithon purii* IBC1886 from Brazil (**Supplementary Table S5**). Interspecific divergence for *rbc*L sequences of *Roseolithon* spp. ranged from 2.73% - 6.10% (**Supplementary Table S6**).

Sporolithon gracile J.L.Richards, Kittle & Fredericq sp. nov.

Holotype: LAF 7382 (field ID no. 5-20-19-5-1): Parker Bank, offshore Louisiana, U.S.A. (27° 58.180' N; 92° 02.80' W), Gulf of Mexico, western Atlantic Ocean, 20.v.2019, depth 92m, *leg.* S. Fredericq, R. P. Kittle III, W. E. Schmidt.,

Etymology: The specific epithet refers to the slender form of the protuberances that this rhodolith species is comprised of.

Description

DNA sequences: *psb*A and *rbc*L sequences (GB accessions ON365773, ON365775) diagnostic for this species. LSU sequence is also provided (GB accession ON427741) (**Supplementary Table S1**).

Habit and vegetative anatomy (**Figures 4**, **5**): Thallus non-geniculate, forming free-living biogenic rhodoliths that consist entirely of thin, branching protuberances. The habitat of this species is mesophotic rhodolith beds at a depth of 92 m. Protuberances with radial construction. Secondary hypothallus weakly developed with monomerous construction and 1-2 layers of rectangular hypothallial cells that formed new growth layers. Perithallus with cell fusions; secondary pit connections not observed. Perithallial cells 9-28 μm long x 8-15 μm wide. Pseudodichotomous branching was observed in the perithallus that contributed to protuberance widening. Intercalary meristem was observed with meristematic cells 5-9 μm long x 9-15 μm wide. Epithallus consisted of one layer of armored epithallial cells

FIGURE 1 | Maximum Likelihood analyses of *psb*A. Node values represent bootstrap values out of 1,000 replicates. Newly described species shown in bold. NWGMx, northwestern Gulf of Mexico.

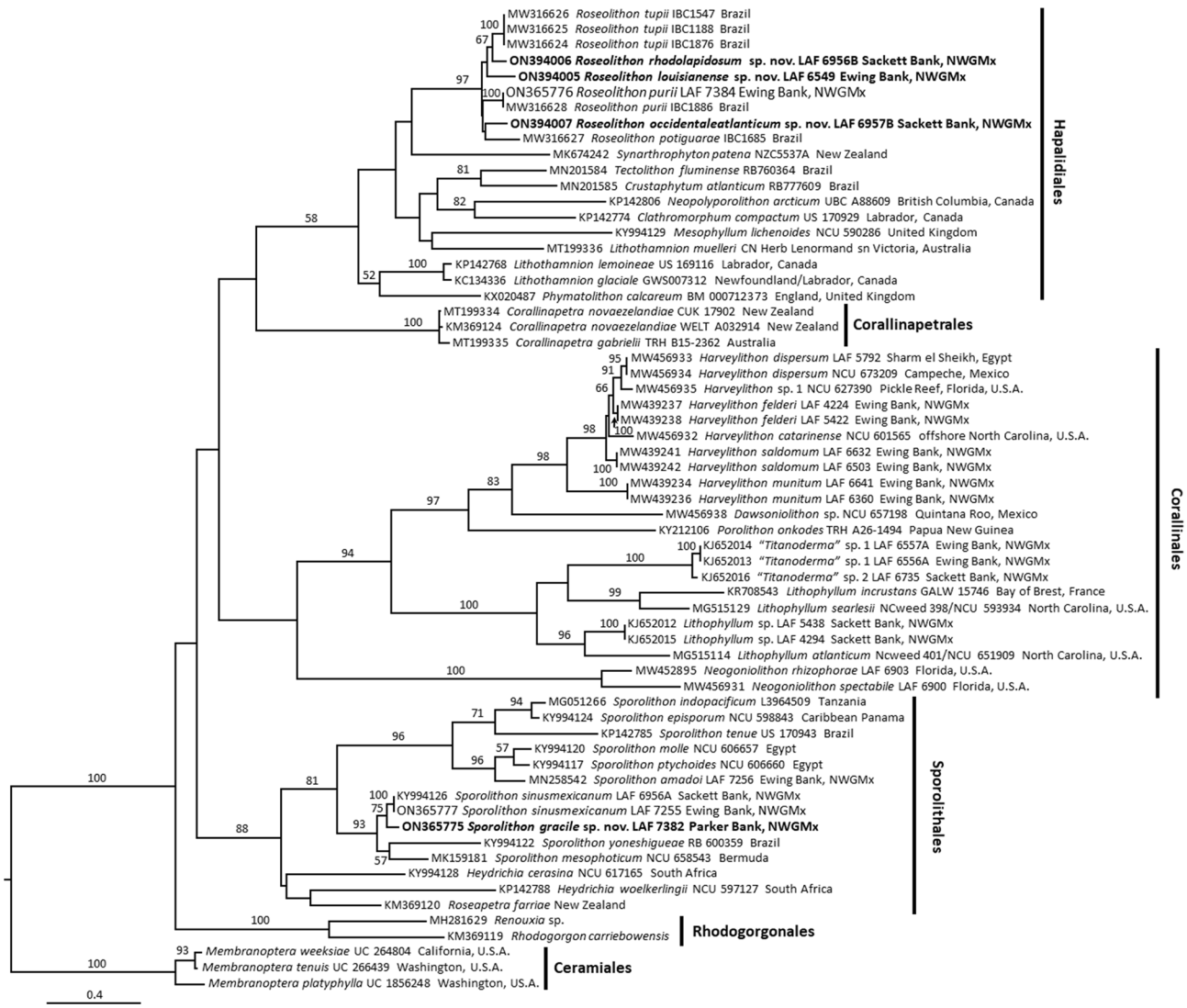

FIGURE 2 | Maximum Likelihood analyses of *rbc*L. Node values represent bootstrap values out of 1,000 replicates. Newly described species shown in bold. NWGMx, northwestern Gulf of Mexico.

2.9-4 μm long x 5-7 μm wide, with thick, heavily calcified cell walls and epithallial cell roof that was observed intact in some cells and missing in others.

Reproduction: No reproductive structures were observed.

Distribution: Known only from Parker Bank, offshore Louisiana, U.S.A.

Sporolithon sinusmexicanum J.L.Richards & Fredericq

DNA sequences: an *rbc*L sequence is herein provided for the newly collected specimen of this species (voucher no. LAF 7255, GB accession ON365777) (**Supplementary Table S1**).

Habit and vegetative anatomy (**Figure 6**): The specimen examined in this study was a biogenic rhodolith found growing inside of a marine sponge from mesophotic rhodolith beds at a depth of 75 m. Specimen was non-reproductive with a perithallus showing cell fusions and lacking secondary pit connections, an intercalary meristem, and an epithallus with armored epithallial cells.

Distribution: Ewing Bank and Sackett Bank, northwestern Gulf of Mexico, and the vicinity of the Dry Tortugas, southeastern Gulf of Mexico.

Sporolithon sp.

DNA sequence: An LSU sequence (GB accession ON427749) is provided for this taxon (**Supplementary Table S1**).

Habit and vegetative anatomy (**Figure 7**): This species was found epizoic on a *Naria acicularis* (Gmelin, 1791) shell. Hypothallus was incompletely shown in section view. Perithallus with cells linked by both secondary pit connections

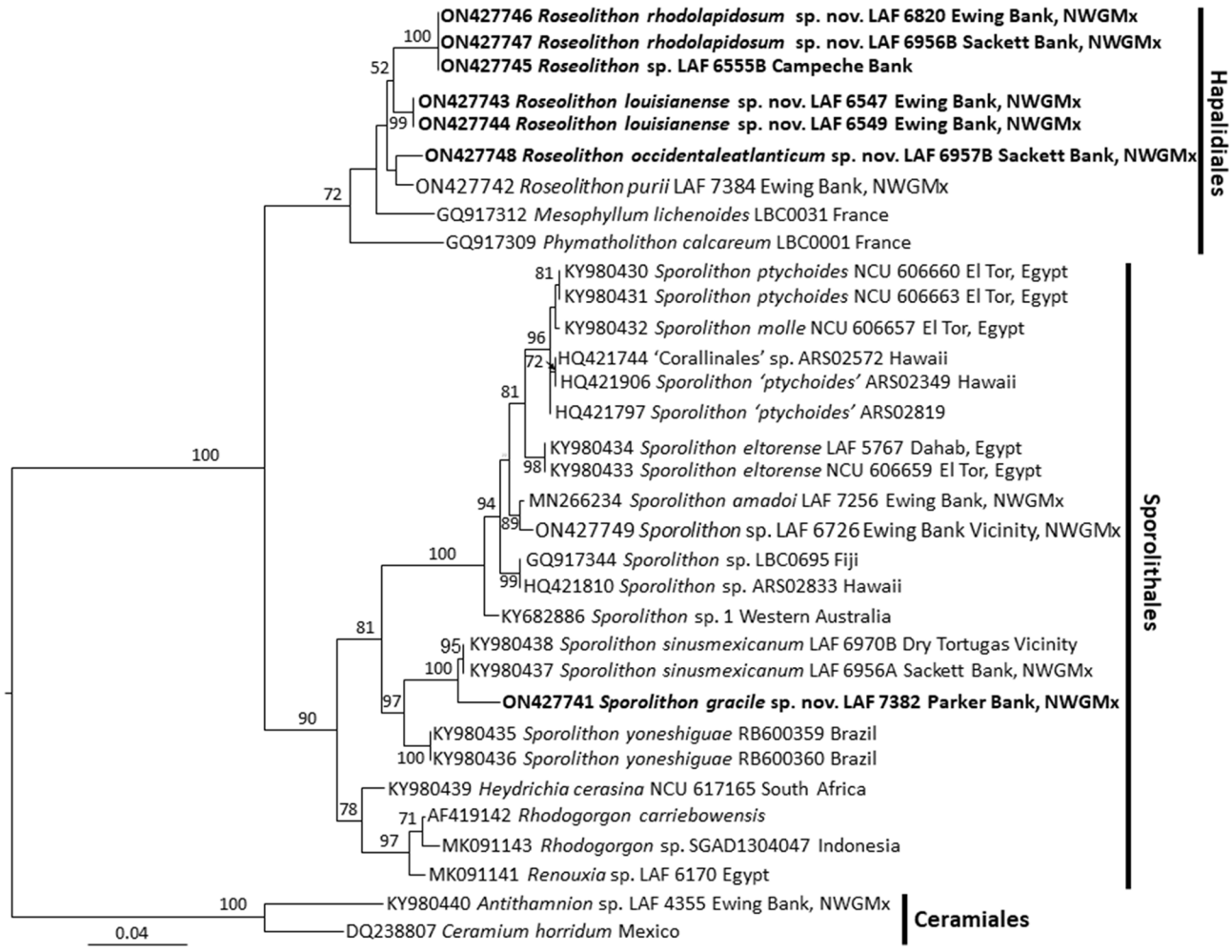

FIGURE 3 | Maximum Likelihood analyses of LSU. Node values represent bootstrap values out of 1,000 replicates. Newly described species shown in bold. NWGMx, northwestern Gulf of Mexico.

and cell fusions. Epithallus consisted of one layer of armored epithallial cells.

Reproduction: No reproductive structures were observed.

Note: A single specimen of this species was identified from collections taken shortly after the Deepwater Horizon oil spill and has not been found in any collections since.

Roseolithon purii L.M.Coutinho & Barros-Barreto

DNA sequences: *psb*A, *rbc*L, and LSU sequences herein provided for the Gulf of Mexico specimen of this species (GB accessions ON365774, ON365776, ON427742) (**Supplementary Table S1**).

Habit and vegetative anatomy of Gulf of Mexico specimen (**Figure 8**): Thallus forming biogenic rhodoliths with thin warty protuberances. Protuberances have radial construction; secondary hypothallus with monomerous construction and 3-8 layers of rectangular hypothallial cells observed grown over older growth layers. Perithallus with cell fusions and lacking secondary pit connections between adjacent filaments. Intercalary meristematic cells approximately as long as wide. Epithallus with a single layer of epithallial cells; epithallus sloughing was also observed.

Distribution: This species is currently distributed in Brazil and the Gulf of Mexico.

Roseolithon louisianense J.L.Richards & Fredericq sp. nov.

Holotype: LAF 6549 (field ID no. 11-16-12): Ewing Bank, offshore Louisiana, U.S.A. (28° 5.936'N; 91° 2.112'W), Gulf of Mexico, western Atlantic Ocean, 16.xi.12, depth 55-58 meters, *leg.* J. Richards & S. Fredericq.

Isotype: LAF 6547 (field ID no. 11-16-12).

Etymology: The specific epithet refers to the locality where it was collected offshore Louisiana.

Description

DNA sequences: *psb*A, *rbc*L, and COI sequences diagnostic for this species (GB accessions for the holotype: *psb*A = KU557497,

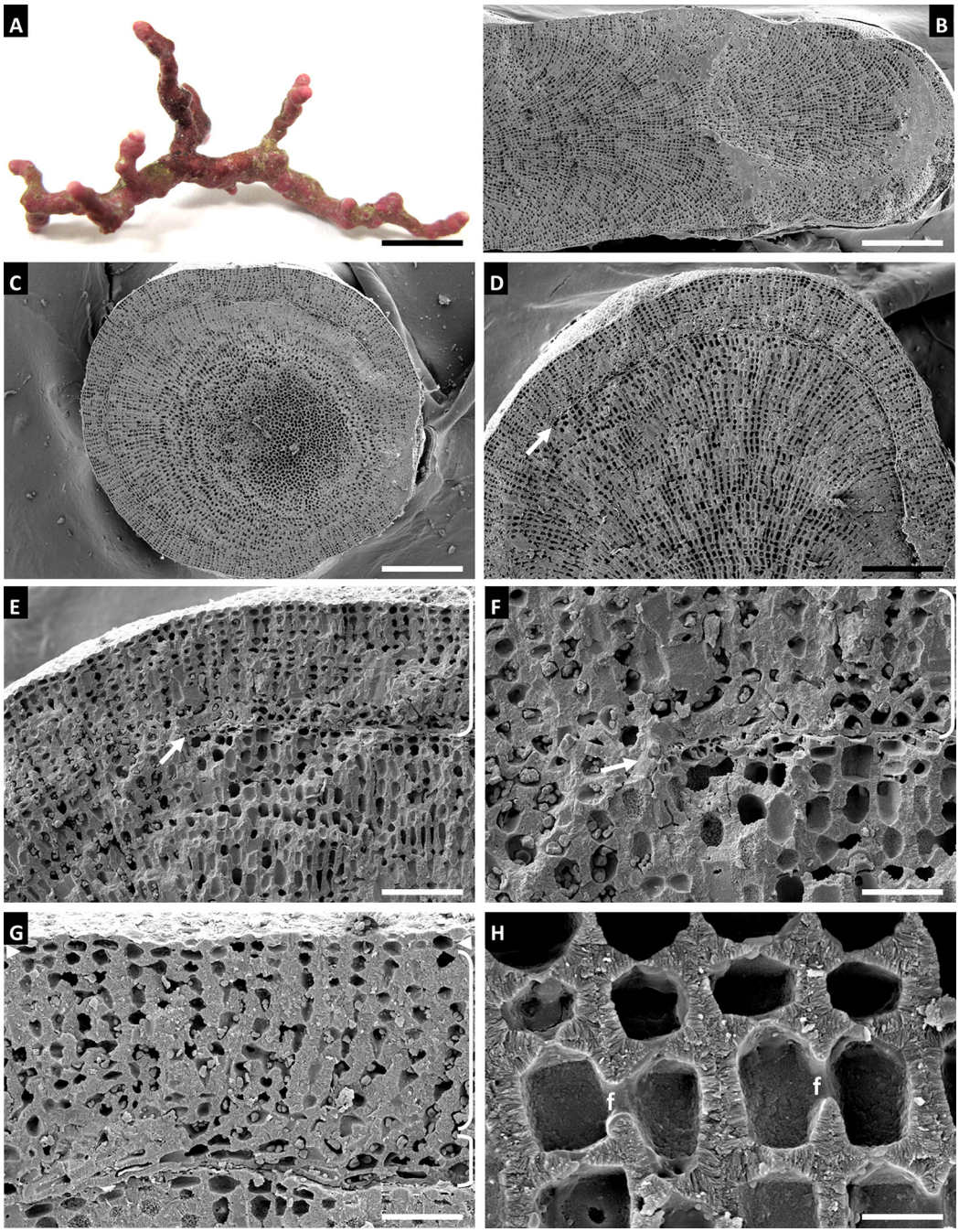

FIGURE 4 | *Sporolithon gracile* Holotype, voucher no. LAF 7382 **(A–H)**. **(A)** Habit of holotype. Scale bar = 0.4 cm. **(B)** Longitudinal section of thallus protuberance showing radial construction. Scale bar = 350 µm. **(C)** Cross section of thallus protuberance showing radial construction. Scale bar = 335 µm. **(D)** Longitudinal section showing origin of the new growth layer (arrow) over older portion of thallus. Scale bar = 225 µm. **(E, F)** Magnified views showing detail of new growth layer (arrow, bracket) over older portion of thallus. Scale bars = 90, 35 µm. **(G)** Detail of new growth layer showing secondary hypothallus with monomerous construction (lower bracket), perithallus (upper bracket), and intercalary meristem (arrowheads) over older thallus layer. Scale bar = 45 µm. **(H)** Perithallus with cell fusions (f). Scale bar = 11 µm.

*rbc*L = ON394005, COI = KU514420; GB accession for the isotype: *psb*A = KU557496). UPA and LSU sequences are also provided (GB accessions for the holotype: UPA = KU514426, LSU = ON427744; GB accessions for the isotype: UPA = KU514425, LSU = ON427743) (**Supplementary Table S1**; see also Richards et al. (2016).

Habit and vegetative anatomy: Vegetative anatomy as for the genus, including non-geniculate thallus habit with monomerous

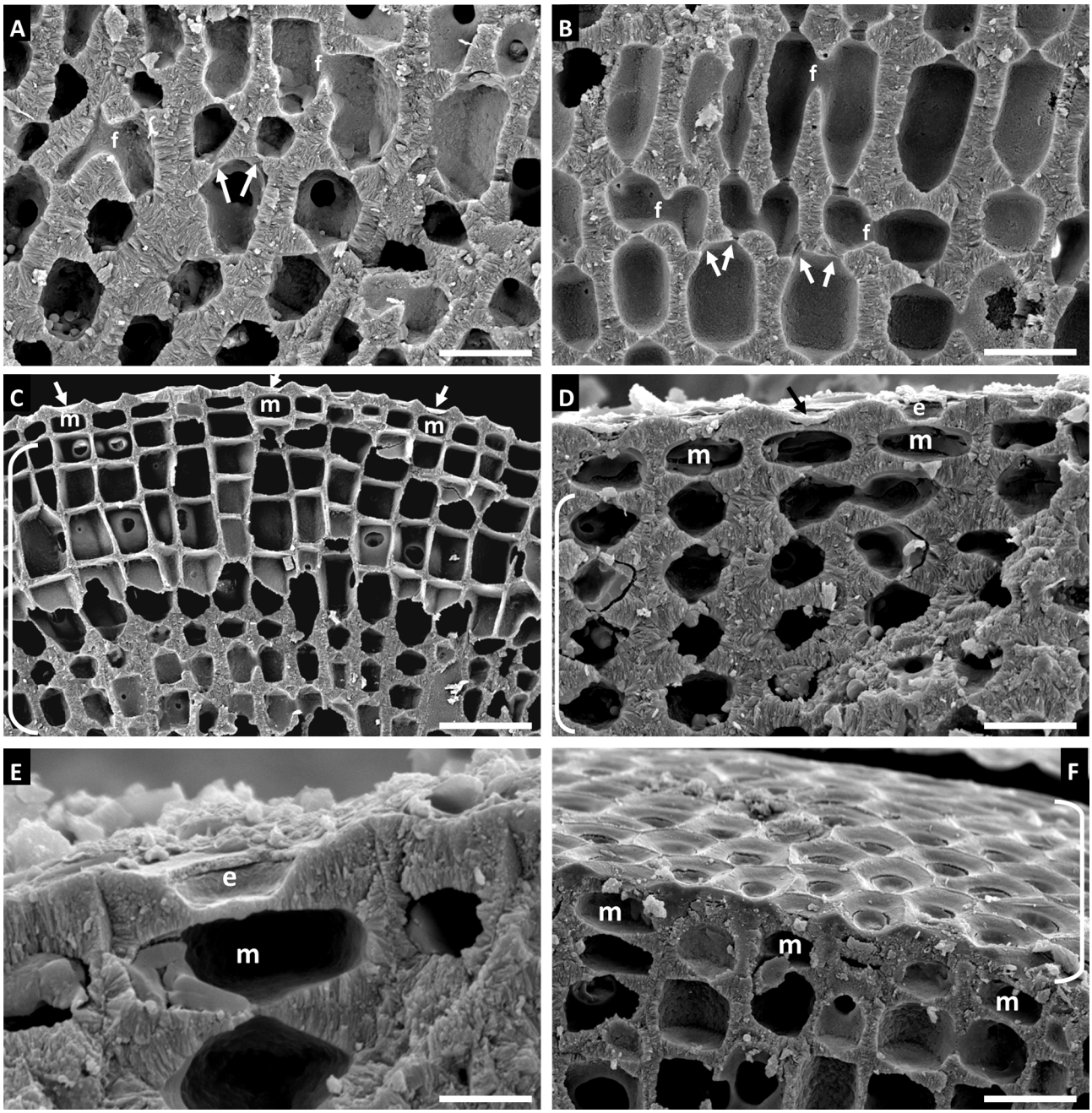

FIGURE 5 | *Sporolithon gracile* Holotype, voucher no. LAF 7382 **(A–F)**. **(A, B)** Perithallus showing locations of pesudodichotomous branching (arrows) and cell fusions (f). Scale bars = 18 µm. **(C)** Perithallus (bracket), meristematic cells (m), and epithallial cells (arrows). Scale bar = 37 µm. **(D)** Epithallus showing epithallial cells with roof intact (arrow) and with roof missing (e), intercalary meristematic cells (m), and perithallus (lower bracket). Scale bar = 15 µm. **(E)** Magnified view of epithallial cell lacking epithallial cell roof (e) and intercalary meristematic cell (m). Scale bar = 5.5 µm. **(F)** Surface view of epithallial cells (bracket) and partial section view showing intercalary meristematic cells (m). Scale bar = 18 µm.

thallus construction, hypothallus growing parallel to substratum, adjacent perithallial cells linked by cell fusions, secondary pit connections and trichocytes absent, and a single layer of armored (i.e. flared) epithallial cells. See Richards et al. (2016) for detailed habit and vegetative anatomy description ("as *Lithothamnion* sp. A"), as well as thallus habit image and SEM images.

Reproduction: This species produces multiporate tetrasporangial conceptacles with pores surrounded by 5-7

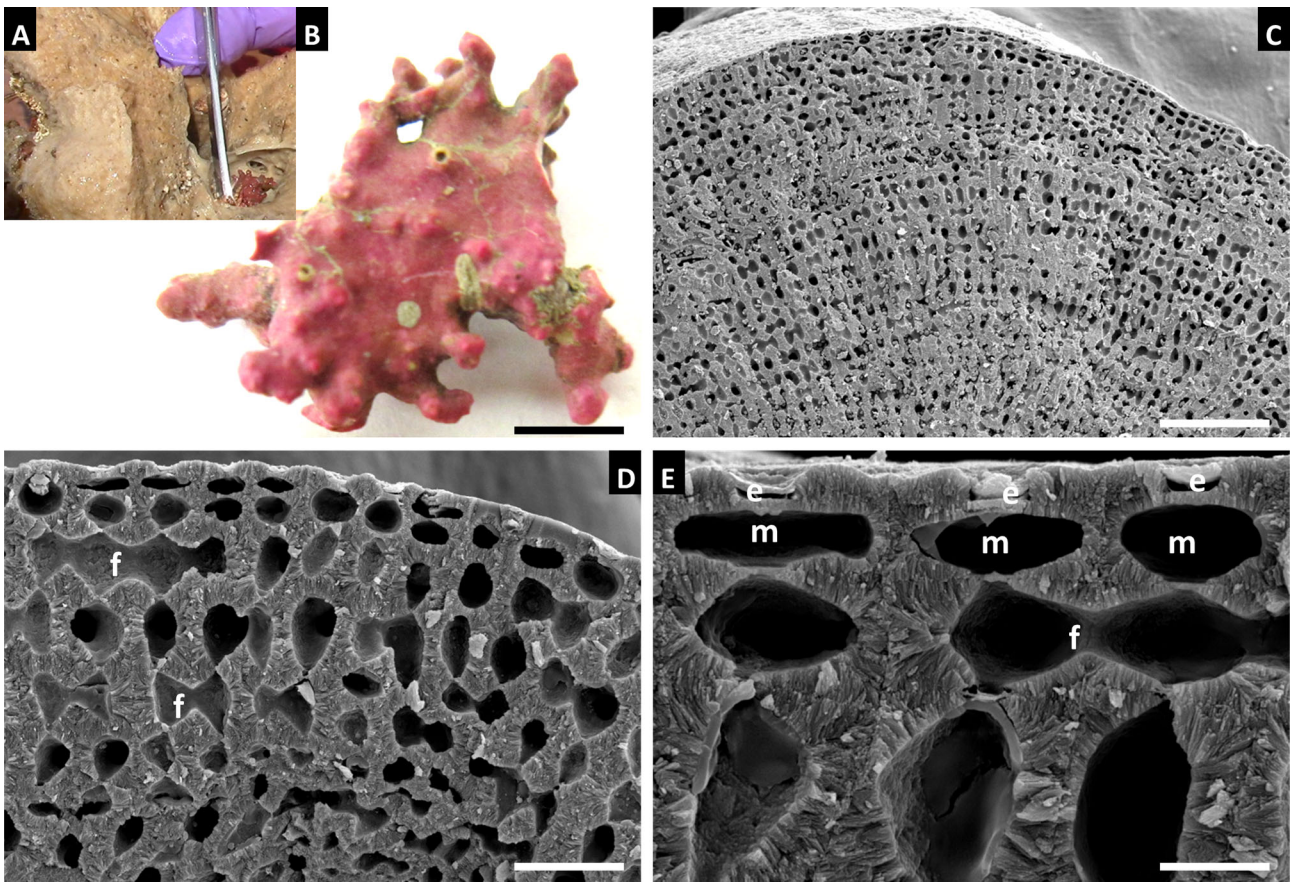

FIGURE 6 | *Sporolithon sinusmexicanum*, voucher no. LAF 7255 (A-E). **(A)** Thallus habit *in situ* growing inside of a marine sponge. **(B)** Thallus habit. Scale bar = 0.4 cm. **(C)** Longitudinal section of rhodolith protuberance. Scale bar = 110 µm **(D)** Magnified view of longitudinal section of protuberance showing cell fusions between perithallial cells (f). Scale bar = 25 µm **(E)** Magnified view of epithallial cells (e), some with intact epithallial cell roofs, intercalary meristematic cells (m), and cell fusions between perithallial cells (f) Scale bar = 7 µm.

rosette cells. The rosette cells and pores have a pitted appearance that is characteristic of the genus, which appears to be from a disintegration of surface cells surrounding the pores as previously reported by the genus authorities. See Richards et al. (2016) for images of multiporate conceptacles.

Distribution: Currently known only from Ewing Bank, offshore Louisiana, U.S.A.

Roseolithon occidentaleatlanticum J.L.Richards & Fredericq sp. nov.

Holotype: LAF 6957B (field ID no. 9-7-14-1-3): Sackett Bank, offshore Louisiana, U.S.A. (28° 38.0' N; 89° 33.028' W), Gulf of Mexico, western Atlantic Ocean, 7.ix.2014, depth 65-68 meters, *leg*. J. Richards & S. Fredericq.

Etymology: The specific epithet refers to the western Atlantic Ocean.

Description:

DNA sequences: *psb*A and *rbc*L sequences diagnostic for this species (GB accessions KU557501, ON394007). UPA and LSU sequences are also provided (GB accessions KU514429, ON427748) (**Supplementary Table S1**; see also Richards et al., 2016).

Habit and vegetative anatomy: Vegetative anatomy as for the genus, including non-geniculate thallus habit with monomerous thallus construction, plumose hypothallus growing parallel to substratum, adjacent perithallial cells linked by cell fusions, secondary pit connections and trichocytes absent, and a single layer of armored (ie. flared) epithallial cells. See Richards et al. (2016) for detailed habit and vegetative anatomy description ("as *Lithothamnion* sp. B"), as well as thallus habit image and SEM images.

Reproduction: No reproductive structures were observed in the holotype of this species.

Distribution: Currently known from the Gulf of Mexico and Brazil.

Roseolithon rhodolapidosum J.L.Richards & Fredericq sp. nov.

Holotype: LAF 6820: Ewing Bank, offshore Louisiana, U.S.A. (28° 05.041'N; 91° 01.648'W), Gulf of Mexico, western Atlantic

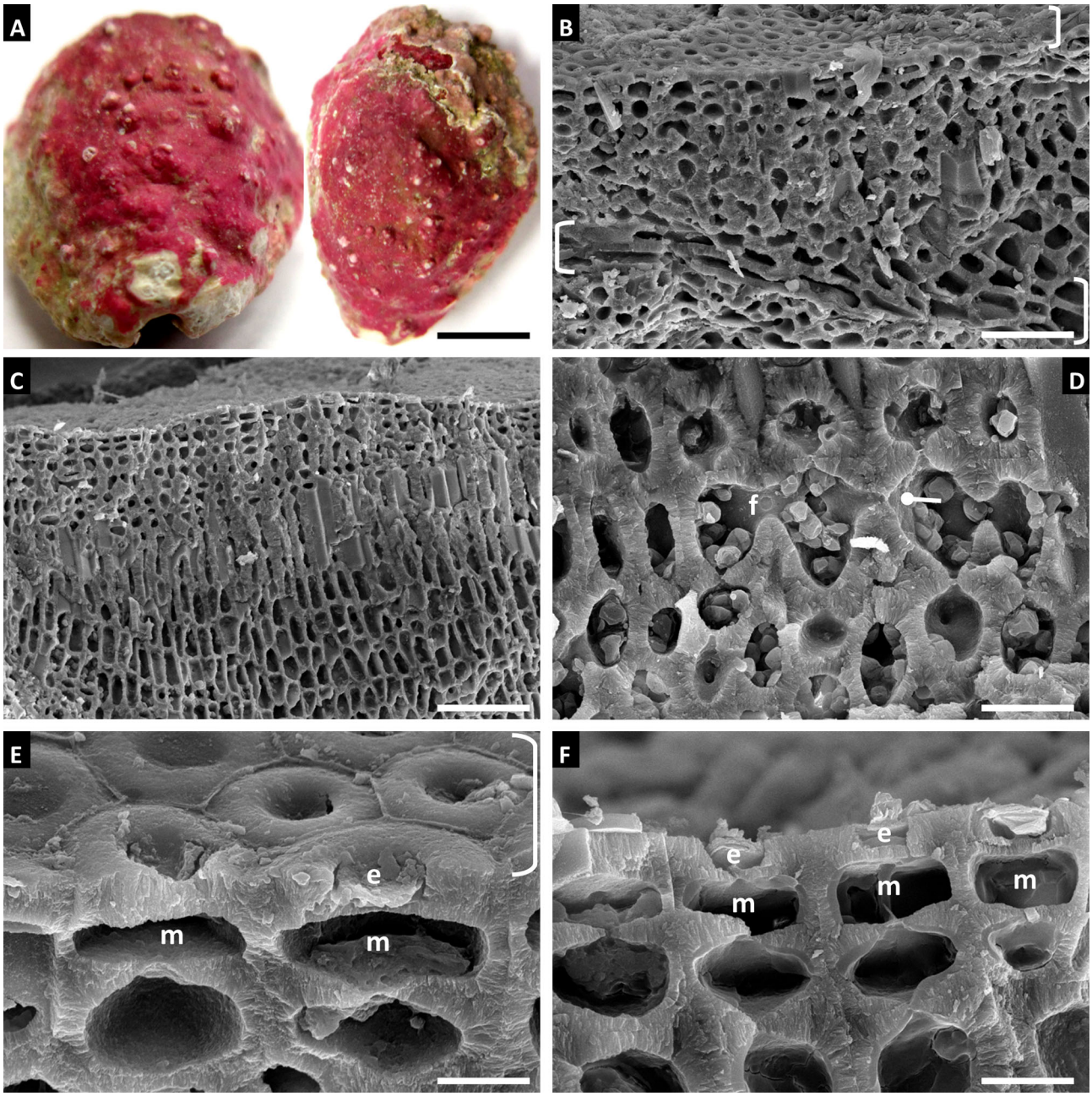

FIGURE 7 | *Sporolithon* sp., voucher no. LAF 6726. **(A)** Thallus habit epizoic upon *Naria acicularis* shell. Scale bar = 0.4 cm. **(B)** Vertical fracture showing incomplete view of hypothallus (lower brackets), perithallus, and partial surface view of epithallus (upper bracket). Scale bar = 30 µm. **(C)** Vertical fracture of thallus showing perithallus. Scale bar = 55 µm. **(D)** Magnified view of perithallus showing cell fusion (f) and secondary pit connection (circle pointer). Scale bar = 11 µm. **(E)** Surface view of epithallus (bracket) and partial section view showing epithallial cells (e) and intercalary meristematic cells (m). Scale bar = 5 µm. **(F)** Vertical fracture showing epithallial cells (e) and intercalary meristematic cells (m). Scale bar = 6 µm.

Ocean, 19.x.2013, depth 70-75 meters, leg. J. Richards & S. Fredericq.

Additional specimen examined: LAF 6956B: Sackett Bank, offshore Louisiana, U.S.A. (28° 38.0'N; 89° 33.028'W), Gulf of Mexico, western Atlantic Ocean, 7.ix.2014, depth 65-68 meters, *leg.* J. Richards & S. Fredericq.

Etymology: The specific epithet refers to the stony rhodolith-forming habit of this species.

Description

DNA sequences: *psb*A and *rbc*L sequences diagnostic for this species (GB accessions for the holotype: *psb*A = KU557498; GB

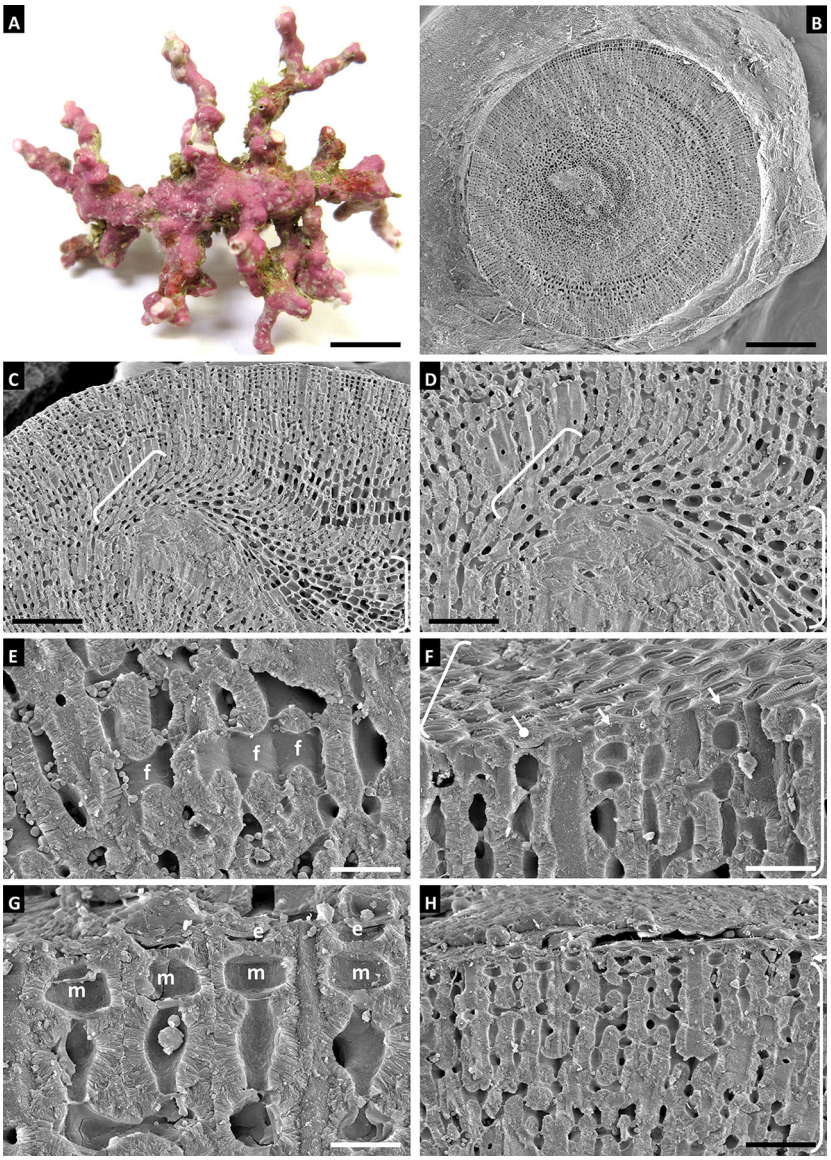

FIGURE 8 | *Roseolithon purii*, voucher no. LAF 7384 (A-H). **(A)** Thallus habit. Scale bar = 0.4 cm. **(B)** Protuberance cross section showing radial construction and partial surface view of thallus at base of protuberance. Scale bar = 260 µm. **(C)** Protuberance section showing location of new growth layer with secondary hypothallus (brackets) over older growth layer. Scale bar = 100 µm. **(D)** Magnified view of secondary hypothallus (brackets). Scale bar = 53 µm. **(E)** Perithallus with cell fusions (f). Scale bar = 18 µm. **(F)** Surface view showing epithallus (upper bracket) and section view showing perithallus (lower bracket), and epithallial cells with roof intact (circle pointer) and roofs missing (arrows). Scale bar = 18 µm. **(G)** Intercalary meristematic cells (m) and epithallial cells in the process of sloughing (e). Scale bar = 10 µm. **(H)** Perithallus (lower bracket), intercalary meristem (arrow), and epithallus in the processing of sloughing off. Scale bar = 35 µm.

accession for the additional specimen examined: *psb*A = KU557499, *rbc*L = ON394006). UPA and LSU sequences are also provided (GB accessions for the holotype: UPA = KU514427, LSU = ON427746; GB accessions for the addition specimen examined: UPA = KU514428, LSU = ON427747) (**Supplementary Table S1**; see also Richards et al., 2016).

Habit and vegetative anatomy: Vegetative anatomy as for the genus, including non-geniculate thallus habit forming free-living biogenic rhodoliths, adjacent perithallial cells linked by cell fusions, secondary pit connections and trichocytes absent, and a single layer of armored (i.e. flared) epithallial cells. See Richards et al. (2016) for detailed habit and vegetative anatomy description ("as *Lithothamnion* sp. C").

Reproduction: This species produces abundant uniporate gametangial conceptacles that become overgrown by new layers of vegetative thallus. It was not determined if these uniporate conceptacles are male or female conceptacles. See Richards et al. (2016) for images of uniporate conceptacles.

Distribution: Currently known only from offshore Louisiana, U.S.A.

DISCUSSION

Our phylogenetic analyses (**Figures 1**, **2**) show at least 17 species of rhodolith-forming coralline algae are present in the northwestern Gulf of Mexico. Minnery (1990) reported 18 species of non-geniculate coralline algae from the Flower Garden Banks in the northwestern Gulf of Mexico, including 13 species currently classified in the Corallinales, four species currently classified in the Hapalidiales, and one species currently classified in the Sporolithales. However, it is difficult to make meaningful direct comparisons to the reports of Minnery (1990) because 1) the taxonomy of these corallines has undergone significant changes since the time that study was conducted, and 2) at the time of the study, Minnery identified corallines based on morpho-anatomy alone. Therefore, it is difficult to parse the names of those taxa reported by Minnery (1990) with the names verified by DNA sequencing that are reported in this current study.

Phylogenetic analyses (**Figures 1**–**3**) and sequence divergence values (**Supplementary Tables S2**, **S3**) show that *Sporolithon gracile* is a distinct species of biogenic rhodolith-forming coralline algae that is sister to *S. sinusmexicanum* and also closely related to *S. mesophoticum* and *S. yoneshigueae*. For context, the *psb*A and *rbc*L sequences of *Sporolithon gracile* were 3.39% and 2.46% diverged, respectively, from *S. sinusmexicanum*. These divergence values are similar to other closely related species of *Sporolithon*, for example, *psb*A and *rbc*L sequences of *S. episporum* and *S. indopacificum* are 3.1%, and 2.7% diverged, respectively (Maneveldt et al., 2017).

Sporolithon sp. LAF 6726 and *Roseolithon* sp. LAF 6555B are represented in this study by the LSU marker alone, thus a marker that is more diagnostic at the species level, such as *psb*A, *rbc*L, or COI, should be generated to confirm their species identity, especially for LAF 6726, which showed a short branch length from its closest sister taxon (**Figure 3**). LAF 6726 may represent a separate species sister to *Sporolithon amadoi*, although this needs to be assessed by sequencing additional markers in a future study. Although previous studies have shown that LSU is more conserved and thus has more limited utility in distinguishing species compared to other markers such as *psb*A, *rbc*L, and COI (Sherwood et al., 2010; Richards et al., 2014; Richards et al., 2017) it is still useful in assessing the diversity of rhodoliths in the northwestern Gulf of Mexico and worldwide. LSU may also amplify easier than other markers for coralline algae (Sherwood et al., 2010), and for some samples in this study it was the only marker that could be amplified as was the case with *Sporolithon* sp. LAF 6726 and *Roseolithon* sp. LAF6555B. LSU rDNA has also recently been used in environmental DNA metabarcoding studies (Bombin et al., 2021). Therefore, sequencing LSU rDNA of preserved algal specimens, as was performed in this study, is also important to link sequences generated from environmental samples to those sequences generated from algal specimens.

Regarding the Hapalidiales, four species of *Roseolithon* are present in the northwestern Gulf of Mexico, including *Roseolithon purii*, *R. louisianaensis* sp. nov., *R. rhodolapidosum* sp. nov. and *R. occidentaleatlanticum* sp. nov. Species delimitation analyses (ABGD and GMYC) of these newly described species was conducted previously in Richards et al. (2016) and the results indicated these taxa are unique species. These *Roseolithon* taxa were also delimited as separate species by Coutinho et al. (2021) using ABGD, GMYC, and bPTP delimitation methods. Additionally, *Mesophyllum erubescens* is also present offshore Louisiana (Richards et al., 2020; **Figures 1**, **2**, present study), as well as three species tentatively identified as "*Lithothamnion* sp. E", "*Lithothamnion* sp. G" and "*Lithothamnion* sp. I". The taxonomy of these three taxa tentatively identified as "*Lithothamnion*" needs to be reassessed in future studies in light of the *Lithothamnion muelleri* sequence data that was provided in Jeong et al. (2021).

Although the morpho-anatomical characters for the genus *Roseolithon* were observed in the *Roseolithon* species described in this study (namely non-geniculate thallus habit with monomerous thallus construction, plumose hypothallus, adjacent perithallial cells linked by cell fusions, secondary pit connections and trichocytes absent, a single layer of armored/flared epithallial cells, and multiporate tetrasporangial conceptacles with rosette cells that have a pitted appearance), this suite of characters overlaps with other genera of Hapalidiales. Moreover, there is considerable overlap in character states between species within *Roseolithon* (Richards et al., 2016; Coutinho et al., 2021; present study). Thus, DNA sequencing is needed to identify species within this genus.

Roseolithon species present in both the Gulf of Mexico and Brazil highlight the presence of this genus in both the northern and southern hemisphere. This distribution is interesting considering the presence of *Roseolithon* in rhodolith beds associated with salt domes (diapirs) rich in petroleum deposits in offshore mesophotic habitats in the Gulf of Mexico and offshore Brazil (Amado-Filho et al., 2012; Coutinho et al., 2021). Other non-geniculate coralline algae, for example *Sporolithon amadoi*, show a similar distribution in both the Gulf of Mexico and Brazil (Richards et al., 2019). Additional sampling and sequencing should be done worldwide to determine the full range of the species described in this study and in Coutinho et al. (2021) and to identify and describe additional species worldwide. Currently, sample sizes are too low to confirm if some species are endemic to the Gulf of Mexico. For example, *R. louisianense* and *R. rhodolapidosum* are each only represented only by two specimens (or possibly three specimens for *R. rhodolapidosum*, see above note about specimen LAF 6555B). Moreover, additional sampling should be conducted in the southeastern, southwestern, and northeastern Gulf of Mexico to determine the full ranges of these species within the Gulf of Mexico.

Regarding the Corallinales, *Lithophyllum* sp. and "*Titanoderma*" spp. that are present offshore the northwestern Gulf of Mexico are different taxa than those *Lithophyllum* spp. found in the Western Atlantic offshore North Carolina (Richards et al., 2014; Richards et al., 2018a; **Figures 1**, **2**, present study). The Lithophylloideae spp. present offshore the northwestern Gulf of Mexico need to be described in future studies.

Likewise, the three species of *Harveylithon*, *H. munitum* (Foslie & M.Howe) A.Rösler, Perfectti, V.Peña & J.C.Braga, *H. saldomum* J.Richards, W.E.Schmidt & Fredericq, and *H. felderii* J.Richards, W.E.Schmidt & Fredericq, that are found offshore the northwestern Gulf of Mexico are different species than the *Harveylithon* species, *H. catarinense* I.O.Costa, P.A.Horta & J.M.C.Nunes, that is found offshore North Carolina (Richards et al., 2021; **Figures 1**, **2**, present study).

CONCLUSION

The northwestern Gulf of Mexico is a hotspot for non-geniculate, rhodolith-forming coralline algae. In total, at least 17 species of rhodolith-forming coralline species are found offshore the northwestern Gulf of Mexico including six species of Corallinales, eight species of Hapalidiales, and three species of Sporolithales. Four species of corallines are newly described in this study and one species is newly reported for the region. Regarding the status of names, 11 species from the northwestern Gulf of Mexico have been assigned names verified by comparative DNA sequence analyses. Continuing to assess the diversity of rhodolith-forming corallines, including naming other new species of Hapalidiales and Corallinales, is of critical importance to conservation efforts in the region.

DATA AVAILABILITY STATEMENT

The datasets presented in this study can be found in online repositories. The names of the repository/repositories and accession number(s) can be found in the article/**Supplementary Material**.

AUTHOR CONTRIBUTIONS

JR, RK, WS, and SF conceived the study. JR, RK, TS, WS, DG, CG and SF collected the samples. JR, WS, and RK conducted the laboratory work. JR, RK, and TS performed the data analyses. JR and SF wrote the manuscript with contributions from RK, WS, TS, DG, and CG. All authors edited the manuscript before submission.

FUNDING

This study was funded by NSF grant DEB–1754504 to SF for rhodolith research in the Gulf of Mexico. NSF grants MRI-1920166 and DEB-0315995 also provided funding. CFDG acknowledges CNPq grant 306304/2019-8 and 437115/2018-6.

ACKNOWLEDGMENTS

We thank the crews of the *R/V Pelican* and *R/V Manta*, as well as Jason White and Eric Glidden from the University of North Carolina-Undersea Vehicle Program (WUNCW-UVP), for help with sampling protocols during rhodolith collection expeditions offshore the Gulf of Mexico. We also thank our close research collaborators Darryl L. Felder, Sherry Krayesky-Self, Paul W. Gabrielson, and Emma Hickerson (FGBNMS). Sincere thanks to Dr. Tom Pesacreta, Mike Purpera, and Lily Ann Hume from the Microscopy Center at UL Lafayette for help and advice while using the SEM and FIB-SEM, and Emilio Garcia for help with Mollusca identification.

SUPPLEMENTARY MATERIAL

The Supplementary Material for this article can be found online at: https://www.frontiersin.org/articles/10.3389/fmars.2022.906679/full#supplementary-material

Supplementary Table 1 | List of taxa names, voucher numbers, localities, GenBank numbers and reference information for newly generated sequences and sequences downloaded from GenBank of taxa included in phylogenetic analyses. Newly generated sequences are shown in bold. N.A. = not available.

Supplementary Table 2 | Divergence values of *psb*A sequences for *Sporolithon* spp.

Supplementary Table 3 | Divergence values of *rbc*L sequences for *Sporolithon* spp.

Supplementary Table 4 | Divergence values of *psb*A sequences for *Roseolithon* spp.

Supplementary Table 5 | Divergence values of *rbc*L sequences (366 bp) for *Roseolithon* spp.

Supplementary Table 6 | Divergence values of *rbc*L sequences (623 bp) for *Roseolithon* spp.

REFERENCES

Amado-Filho, G. M., Moura, R. L., Bastos, A. C., Salgado, L. T., Sumida, P. Y., Guth, A. Z., et al. (2012). Rhodolith Beds are Major $CaCO_3$ Bio-Factories in the Tropical South West Atlantic. *PloS One* 7 (4), e35171. doi: 10.1371/journal.pone.0035171

Bombin, S., Wysor, B., and Lopez-Bautista, J. M. (2021). Assessment of Littoral Algal Diversity From the Northern Gulf of Mexico Using Environmental DNA Metabarcoding. *J. Phycol* 57, 269–278. doi: 10.1111/jpy.13087

Coutinho, L. M., Gomes, F. P., Sissini, M. N., Vieira-Pinto, T., Muller de Oliveira Henriques, M. C., Oliveira, M. C., et al. (2021). Cryptic Diversity in non-Geniculate Coralline Algae: A New Genus *Roseolithon* (Hapalidiales, Rhodophyta) and Seven New Species From the Western Atlantic. *Eur. J. Phycol.* 57, 227–250. doi: 10.1080/09670262.2021.1950839

Fredericq, S., Arakaki, N., Camacho, O., Gabriel, D., Krayesky, D., Self-Krayesky, S., et al. (2014). A Dynamic Approach to the Study of Rhodoliths: A Case Study for the Northwestern Gulf of Mexico. *Cryptogamie Algologie* 35, 77–98. doi: 10.7872/crya.v35.iss1.2014.77

Fredericq, S., Cho, T. O., Earle, S. A., Gurgel, C. F., Krayesky, D. M., Mateo-Cid, L. E., et al. (2009). "Seaweeds of the Gulf of Mexico," in *Gulf of Mexico: Its Origins, Waters, and Biota. I. Biodiversity*. Eds. D. L. Felder and D. K. Camp (College Station, Texas A&M Univ. Press), 187–259.

Fredericq, S., Krayesky-Self, S., Sauvage, T., Richards, J., Kittle, R., Arakaki, N., et al. (2019). The Critical Importance of Rhodoliths in the Life Cycle Completion of Both Macro- and Microalgae, and as Holobionts for the Establishment and Maintenance of Biodiversity. *Front. Mar. Sc.– Mar. Ecosyst. Ecol.* 5. doi: 10.3389/fmars.2018.00502

Jeong, S. Y., Nelson, W. A., Sutherland, J. E., Peña, V., Le Gall, L., Diaz-Pulido, G., et al. (2021). Corallinapetrales and Corallinapetraceae: A New Order and

Family of Coralline Red Algae Including *Corallinapetra Gabrielii* Comb. Nov. *J. Phycol* 57, 849–862. doi: 10.1111/jpy.13115

Joyce, E. A., and Williams, J. (1969). Rationale and Pertinent Data. *Mem. Hourglass Cruises* 1 (1), 11–50.

Krayesky-Self, S., Richards, J. L., Rahmatian, M., and Fredericq, S. (2016). Aragonite Infill in Overgrown Conceptacles of Coralline Lithothamnion Spp. (Hapalidiaceae, Hapalidiales, Rhodophyta): New Insights in Biomineralization and Phylomineralogy. *J. Phycol* 52, 161–173. doi: 10.1111/jpy.12392

Kumar, S., Stecher, G., Li, M., Knyaz, C., and Tamura, K. (2018). MEGA X: Molecular Evolutionary Genetics Analysis Across Computing Platforms. *Mol. Biol. Evol.* 35, 1547–1549. doi: 10.1093/molbev/msy096

Leão, L. A. S., Bahia, R. G., Jesionek, M. B., Adey, W. H., Johnson, G., Salgado, L. T., et al. (2020). *Sporolithon Franciscanum* Sp. Nov. (Sporolithales, Rhodophyta), a New Rhodolith-Forming Species From Northeast Brazil. *Diversity* 12, 199. doi: 10.3390/d12050199

Maneveldt, G. W., Gabrielson, P. W., and Kangwe, J. (2017). *Sporolithon Indopacificum* Sp. Nov. (Sporolithales, Rhodophyta) From Tropical Western Indian and Western Pacific Oceans: First Report, Confirmed by DNA Sequence Data, of a Widely Distributed Species of *Sporolithon*. *Phytotaxa* 326, 115–128. doi: 10.11646/phytotaxa.326.2.3

Miller, M. A., Pfeiffer, W., and Schwartz, T. (2010). "Creating the CIPRES Science Gateway for Inference of Large Phylogenetic Trees," in *Proceedings of the Gateway Computing Environments Workshop (GCE)*, New Orleans, LA, 14 Nov. 2010. 1–8. doi: 10.1109/GCE.2010.5676129

Minnery, G. A. (1990). Crustose Coralline Algae From the Flower Garden Banks, Northwestern Gulf of Mexico; Controls on Distribution and Growth Morphology. *J. Sedim Petrol* 60, 992–1007.

Minnery, G. A., Rezak, R., and Bright, T. J. (1985). ""Chapter 18: Depth Zonation and Growth Form of Crustose Coralline Algae: Flower Garden Banks, Northwestern Gulf of Mexico,"," in *Paleoalgology: Contemporary Research and Applications*. Eds. D. F. Toomey and M. H. Titecki (Berlin; Heidelberg: Springer-Verlag), 238–246. doi: 10.1306/D4267663-2B26-11D7-8648000102C1865D

Nelson, W. A., Neill, K. F., Twist, B. A., and Sutherland, J. E. (2021). A New Genus and Species in the Sporolithales (Corallinophycidae, Rhodophyta) From Northern New Zealand: *Roseapetra Farriae* Sp. Nov. *Phytotaxa* 490, 35–46. doi: 10.11646/phytotaxa.490.1.3

Rezak, R., Bright, T. J., and McGrail, D. W. (1985). *Reefs and Banks of the Northwestern Gulf of Mexico: Their Geological, Biological, and Physical Dynamics* (New York, NY: Wiley), 259.

Richards, J. L., Bahia, R. G., Jesionek, M. B., and Fredericq, S. (2019). *Sporolithon Amadoi* Sp. Nov. (Sporolithales, Rhodophyta), a New Rhodolith-Forming non-Geniculate Coralline Alga From Offshore the Northwestern Gulf of Mexico and Brazil. *Phytotaxa* 423, 49–67. doi: 10.11646/phytotaxa.423.2.1

Richards, J. L., and Fredericq, S. (2018). *Sporolithon Sinusmexicanum* Sp. Nov. (Sporolithales, Rhodophyta): A New Rhodolith-Forming Species From Deepwater Rhodolith Bed in the Gulf of Mexico. *Phytotaxa* 350, 135–146. doi: 10.11646/phytotaxa.350.2.2

Richards, J. L., Gabrielson, P. W., and Fredericq, S. (2014). New Insights Into the Genus *Lithophyllum* (Lithophylloideae, Corallinaceae, Corallinales) From Deepwater Rhodolith Beds Offshore the NW Gulf of Mexico. *Phytotaxa* 190, 162–175. doi: 10.11646/phytotaxa.190.1.11

Richards, J. L., Gabrielson, P. W., Hughey, J. R., and Freshwater, D. W. (2018a). A Re-Evaluation of Subtidal *Lithophyllum* Species (Corallinales, Rhodophyta) From North Carolina, USA, and the Proposal of L. Searlesii Sp. Nov. *Phycologia* 57, 318–330. doi: 10.2216/17-110.1

Richards, J. L., Gabrielson, P. W., and Schneider, C. W. (2018b). Sporolithon Mesophoticum Sp. Nov. (Sporolithales, Rhodophyta) From Plantagenet Bank Off Bermuda at a Depth of 178 M. *Phytotaxa* 385, 67–76. doi: 10.11646/phytotaxa.385.2.2

Richards, J. L., Kittle, R. P.III, Abshire, J. R., Fuselier, D., Schmidt, W. E., Gurgel, C. F., et al. (2020). Range Extension of *Mesophyllum Erubescens* (Foslie) Me. Lemoine (Hapalidiales, Rhodophyta): First Report From Mesophotic Rhodolith Beds in the Northwestern Gulf of Mexico Offshore Louisiana and Texas, Including the Flower Garden Banks National Marine Sanctuary. *Check List* 16, 513–519. doi: 10.15560/16.3.513

Richards, J. L., Sauvage, T., Schmidt, W. E., Fredericq, S., Hughey, J. R., and Gabrielson, P. W. (2017). The Coralline Genera *Sporolithon* and *Heydrichia* (Sporolithales, Rhodophyta) Clarified by Sequencing Type Material of Their Generitypes and Other Species. *J. Phycol* 53, 1044–1059. doi: 10.1111/jpy.12562

Richards, J. L., Schmidt, W. E., Fredericq, S., Sauvage, T., Peña, V., Le Gall, L., et al. (2021). DNA Sequencing of Type Material and Newly Collected Specimens Reveals Two Heterotypic Synonyms for *Harveylithon Munitum* (Metagoniolithoideae, Corallinales, Rhodophyta) and Three New Species. *J. Phycol* 57, 1234–1253. doi: 10.1111/jpy.13161

Richards, J. L., Vieira-Pinto, T., Schmidt, W. E., Sauvage, T., Gabrielson, P. W., Oliveira, M. C., et al. (2016). Molecular and Morphological Diversity of Lithothamnion Spp. (Hapalidiales, Rhodophyta) From Deepwater Rhodolith Beds in the Northwestern Gulf of Mexico. *Phytotaxa* 278, 81–114. doi: 10.11646/phytotaxa.278.2.1

Sherwood, A. R., Sauvage, T., Kurihara, A., Conklin, K. Y., and Presting, G. G. (2010). A Comparative Analysis of COI, LSU and UPA Marker Data for the Hawaiian Florideophyte Rhodophyta: Implications for DNA Barcoding of Red Algae. *Cryptogamie Algologie* 31, 451–465.

Stecher, G., Tamura, K., and Kumar, S. (2020). Molecular Evolutionary Genetics Analysis (MEGA) for macOS. *Mol. Biol. Evol.* doi: 10.1093/molbev/msz312

Tamura, K., and Nei, M. (1993). Estimation of the Number of Nucleotide Substitutions in the Control Region of Mitochondrial DNA in Humans and Chimpanzees. *Mol. Biol. Evol.* 10, 512–526. doi: 10.1093/oxfordjournals.molbev.a040023

Thiers, B. (2022). *Index Herbariorum: A Global Directory of Public Herbaria and Associated Staff* (New York: New York Botanical Garden's Virtual Herbarium). Available at: http://sweetgum.nybg.org/ih.

Conflict of Interest: The authors declare that the research was conducted in the absence of any commercial or financial relationships that could be construed as a potential conflict of interest.

Publisher's Note: All claims expressed in this article are solely those of the authors and do not necessarily represent those of their affiliated organizations, or those of the publisher, the editors and the reviewers. Any product that may be evaluated in this article, or claim that may be made by its manufacturer, is not guaranteed or endorsed by the publisher.

frontiers | Frontiers in Marine Science

TYPE Original Research
PUBLISHED 26 July 2022
DOI 10.3389/fmars.2022.898308

OPEN ACCESS

EDITED BY
Daniela Basso,
University of Milano-Bicocca, Italy

REVIEWED BY
Ricardo Bahia,
Rio de Janeiro Botanical Garden, Brazil
Marina Nasri Sissini,
Fluminense Federal University, Brazil

*CORRESPONDENCE
Matthew S. Mills
Matthew.Mills@research.usc.edu.au

†These authors have contributed equally to this work

SPECIALTY SECTION
This article was submitted to Marine Ecosystem Ecology, a section of the journal Frontiers in Marine Science

RECEIVED 17 March 2022
ACCEPTED 04 July 2022
PUBLISHED 26 July 2022

CITATION
Mills MS, Deinhart ME, Heagy MN and Schils T (2022) Small tropical islands as hotspots of crustose calcifying red algal diversity and endemism. *Front. Mar. Sci.* 9:898308. doi: 10.3389/fmars.2022.898308

Small tropical islands as hotspots of crustose calcifying red algal diversity and endemism

Matthew S. Mills[1,2*†], Mari E. Deinhart[1], Mackenzie N. Heagy[1] and Tom Schils[1†]

[1]Marine Laboratory, University of Guam, Mangilao, GU, United States, [2]School of Science, Technology, and Engineering, University of the Sunshine Coast, Sippy Downs, QLD, Australia

In the tropics, crustose calcifying red algae (Corallinophycidae and Peyssonneliales; CCRA) are dominant and important reef builders that serve a suite of ecological functions affecting reef health. However, CCRA taxa have historically been overlooked in floristic and ecological studies because of their high degrees of phenotypic plasticity and morphological convergence that impede reliable identifications based on morphology. This study provides an update of the CCRA diversity of Guam (Mariana Islands) based on a recent DNA barcoding effort. This account of CCRA taxa is compared to (1) the most current species inventories for Guam based on morphological identifications and (2) similar floristic accounts of CCRA from other regions using DNA barcoding. 492 CCRA specimens were collected from Guam for which two markers, COI-5P and *psb*A, were used for phylogenetic analysis and species delimitation. Phylogenetic relationships were inferred using maximum likelihood. Species richness estimates were obtained through a conservative approach using the Automatic Barcode Gap Discovery method for species delimitation. A total of 154 putative CCRA species were identified, with 106 representatives of the subclass Corallinophycidae and 48 belonging to the order Peyssonneliales. When compared to previous studies based on morphological identification, molecular data suggests that all but one of the CCRA species reported for Guam were incorrectly identified and CCRA species richness is more than six times higher than previously assumed. Species accumulation curves show that CCRA species richness will continue to rise with increased sampling effort and the exploration of new (micro)habitats before reaching a plateau. Guam's true CCRA richness might eventually exceed the currently reported species richness of all marine red algae for the island. Of the 154 putative species documented in this study, only ten closely match (≥ 98% COI-5P sequence similarity)

previously described species, implying that many are probably new species to science. The here-reported CCRA diversity for Guam as a small, remote tropical island in the Western Pacific Ocean is greater than those of well-documented CCRA floras for much larger nearshore ecosystems in Brazil and New Zealand, emphasizing the value of tropical islands as hotspots of marine biodiversity.

KEYWORDS

Corallinophycidae, Peyssonneliales, DNA barcoding, biodiversity, cryptic species, COI-5P, *psb*A

Introduction

In ecology, biodiversity has been the subject of extensive study, and has been shown to affect the stability, health, ecosystem processes, and overall performance of ecosystems (Naeem et al., 1994; Loreau et al., 2002; Tilman et al., 2006). Moreover, the implementation of new technologies (Mora et al., 2011) and the rapid changes that many ecosystems are experiencing (Hughes et al., 2003; Hughes et al., 2007) emphasize the need to further examine biodiversity worldwide, especially in the tropics (Paulay, 2003). Macroalgae are an integral component of tropical reefs and contribute significantly to the biodiversity of tropical reef ecosystems in the Pacific (Vroom, 2011). Of these, crustose calcifying red algae (CCRA) provide major ecological functions for tropical reefs. In this study, CCRA are comprised of the non-geniculate, calcified members of the Corallinophycidae and the Peyssonneliales. CCRA have long been considered as essential components of tropical reefs due to their role as reef builders and cementers (Gordon et al., 1976; Adey, 1998), as well as their significant contribution to the carbonate budget on tropical reefs (Lee and Carpenter, 2001). Some CCRA species can also act as suppressors of potentially harmful nutrient indicator algae (Vermeij et al., 2011; O'Leary et al., 2017), as well as remove nitrogenous compounds, thereby reducing the mortality of reef-building corals (Yuen et al., 2009). Moreover, some CCRA are particularly important in the early stages of colonization of bare reef substrates, as they are the dominant organisms that colonize such habitats and have been shown to serve as the preferred settlement substrates for many invertebrate larvae (Tebben et al., 2015; Vargas-Ángel et al., 2015; Deinhart et al., 2022). Other CCRA taxa, however, can have vastly different ecological roles on reefs. Some members of the order Peyssonneliales, for example, flourish on disturbed reefs, outcompeting and overgrowing entire reef communities (Verlaque et al., 2000; Pueschel and Saunders, 2009; Eckrich et al., 2011; Eckrich and Engel, 2013; Nieder et al., 2019; Williams and García-Sais, 2020).

CCRA are thought to be some of the most sensitive organisms to the effects of climate change, ocean acidification, and global warming (Vásquez-Elizondo and Enríquez, 2016). Since CCRA can be more sensitive to chronic disturbances than scleractinian corals, they could be considered as sentinel taxa of tropical marine ecosystems (Fabricius and De'ath, 2001; Ries, 2011; Yamamoto et al., 2012; Mallela, 2013). This does not apply to all CCRA, however. Recent evidence suggests that some CCRA species, particularly those with shorter generation times, high phenotypic plasticity, or broad thermal tolerance, could be more capable of acclimatizing and adapting to increasing ocean temperatures (Cornwall et al., 2019). Further research demonstrated that the reef-cementing and reef-accreting *Hydrolithon boergesenii* (Foslie) Foslie gained tolerance to ocean acidification over six generations of exposure, suggesting that some CCRA species could maintain their ecological roles in the face of ocean acidification (Cornwall et al., 2020). It is unclear, however, if such findings can be extended to other CCRA species and how this response is influenced by other environmental factors (Cornwall et al., 2020).

Historically, CCRA have often been overlooked by phycologists and ecologists, despite their abundance and ecological importance on reefs. This can largely be attributed to their phenotypic plasticity and convergent morphologies that complicate identifications based on morphology, even at family or genus level (Steneck, 1986; Hernández-Kantún et al., 2014). Molecular phylogenies of CCRA have shown that morpho-anatomical features alone often fail to correctly identify CCRA to species and sometimes to genus-level (Sissini et al., 2014; Gabrielson et al., 2018). However, DNA-based identification has proven to be an effective method to identify CCRA species in diversity, biogeographic, and ecological studies (Sherwood et al., 2010; Hernández-Kantún et al., 2014; Hind et al., 2014; Peña et al., 2014; Sissini et al., 2014; Gabrielson et al., 2018; Manghisi et al., 2019; Sherwood et al., 2020).

CCRA are among the most dominant organisms on reefs in the Mariana Islands and throughout the Pacific Islands (Schils et al., 2013), yet little is known about their diversity and the

communities they form. Studies on fossil and living CCRA from Guam date back to 1964 (Johnson, 1964; Gordon, 1975; Gordon et al., 1976; Tsuda, 2003). The first study to provide a floristic account of extant CCRA in Guam was a master's thesis by Gordon (1975) and the resulting publication (Gordon et al., 1976). In the study, CCRA specimens were collected from sites around Guam and 15 CCRA species were identified through detailed morphological and anatomical observations. The most recent inventory of CCRA was part of a checklist and bibliography on the seaweed flora of Guam and the Mariana Islands (Tsuda, 2003) and the resulting publication (Lobban and Tsuda, 2003). As it stands, 24 extant species of CCRA have been reported for Guam. Of those 24 species, two are representatives of the Peyssonneliales, one belongs to the Sporolithales, four belong to the Hapalidiales, and 17 are Corallinales. Since Lobban and Tsuda (2003), four of the reported species have been transferred to another genus, two of the species have been synonymized, and *Peyssonnelia corallis* Tsuda is an erroneously used, invalid name for the brown alga *Lobophora variegata* (J.V.Lamouroux) Womersley ex E.C.Oliveira (Guiry and Guiry, 2022). Most of the previously published CCRA records for Guam relied on thorough morphological and anatomical examination but did not use DNA-based identification. The technical challenges associated with morphological studies of these limestone-encrusted algae, their taxonomic diversity, and their high levels of cryptic diversity warrant a re-examination of Guam's CCRA flora as these algae have played an important role in benthic community changes on Guam's reefs in the last decade. Studies on red seaweeds in other Pacific islands, such as Hawaii and Easter Island, report endemism levels of 14-24% (Santelices and Abbott, 1987; Tsuda, 2014) and suggest that many species have much smaller distribution ranges than previously believed. Many of the 24 reported CCRA species for Guam have type localities in far off regions like the Caribbean Sea, Atlantic Ocean, or Mediterranean Sea, stressing the need for a floristic update. As such, the intent of this study is to provide a much-needed review of the taxonomic diversity of CCRA on Guam, as well as a revision of the CCRA flora as reported by Gordon et al. (1976) based on morphology.

Methods

Study area

The island of Guam (13°28'N, 144°46'E) is an organized, unincorporated territory of the United States of America and it is the southernmost island of the Mariana Archipelago (Figure 1). Guam has a diverse geology and topography, with northern Guam comprised primarily of flat, uplifted limestone and southern Guam consisting of volcanic hills. The island is surrounded by fringing reefs that have developed into a barrier reef at its southern tip (i.e., Cocos Lagoon). Guam's nearshore marine ecosystems also contain patch reefs, seagrass beds, and mangrove stands. Habitats differ distinctly between the east and west coasts, largely due to differences in current, wind, and wave exposure. Prevailing winds and typhoons originate from the east, making eastern reefs more exposed than western reefs (Paulay, 2003). The north equatorial current is thought to split around Guam such that one part sweeps along the east coast, travelling around the southern tip of the island, and flowing up the bottom half of the west coast before joining with the other stream roughly halfway up the coast line (Emery, 1962). Despite the increased exposure, reefs on the east coast have higher rugosity, habitat complexity, live coral cover, and fish diversity and abundance than western reefs (Randall and Holloman, 1974; Randall and Eldredge, 1976; Burdick et al., 2008).

Specimen collection and preservation

492 CCRA specimens were selectively and opportunistically collected from 31 sites around Guam (**Figure 1**; Supplementary Table 1). Sampling was directed toward maximizing the number of different CCRA morphotypes in an attempt to cover a broad range of CCRA taxa. Because the initial study of Guam's CCRA (Gordon et al., 1976) contained detailed collection information of the studied specimens, 12 of the 15 reported species were re-collected based on the habit and gross morphology as described in Gordon et al. (1976). Most species were re-collected from the same locations as reported by Gordon et al. (1976), with only two species that were collected from other sites (Table 1). The specimens were collected by hand or with a hammer and chisel while SCUBA diving or freediving (<25 m depth). Photographs of each specimen were taken *in situ* prior to collection, as well as *ex situ* following the removal of tissue used for DNA extraction. In addition to these photographs, all other appropriate metadata (e.g., herbarium accession number, site information, GPS coordinates, etc.) were recorded for each specimen. Specimens were stored separately upon collection and transferred to holding tanks with running seawater to keep them alive until DNA extraction could be performed. Upon completion of DNA extractions, all samples were added to the herbarium collection of the University of Guam (GUAM; Thiers, 2016) as air-dried, silica-dried, and formalin-preserved specimens and were individually stored in custom-made clear acrylic boxes.

DNA extraction

Each CCRA specimen was carefully examined to find an area visibly free of epiphytes, which was then swabbed using 10% bleach or 95% ethanol to remove potential surface contaminants. CCRA tissue was collected by using a Dremel rotary tool, a pair of tweezers, or a single-edged razor blade (single use) to scrape

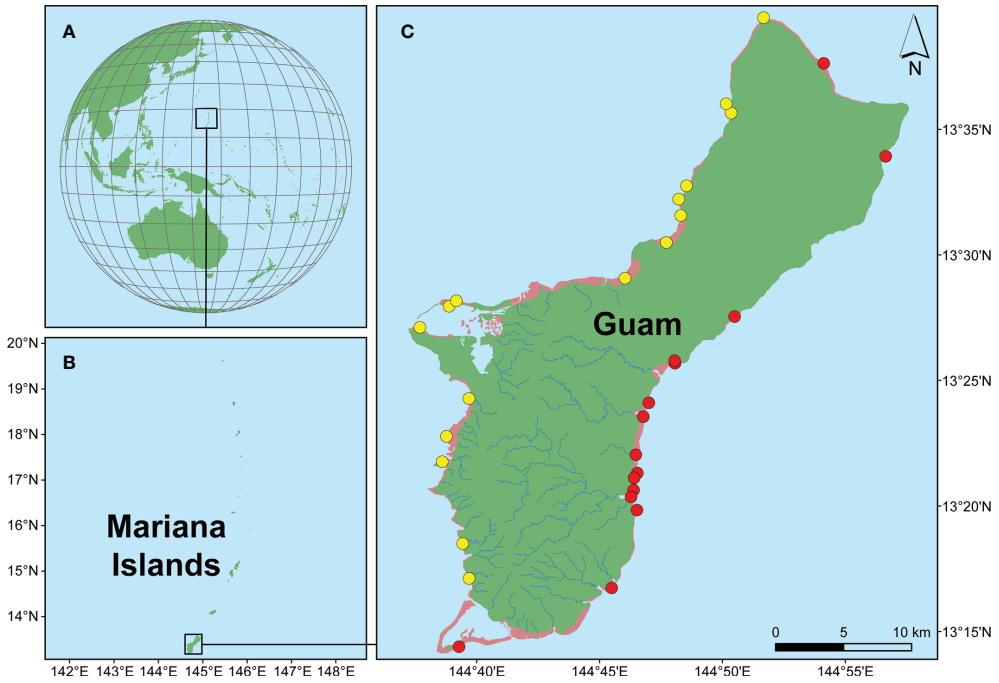

FIGURE 1
Maps indicating the study area and sample collection sites. **(A)** Pacific-centered map showing the location of the Mariana Islands. **(B)** Map of the Mariana Islands with Guam as the largest and southernmost island. **(C)** Map of Guam identifying the 31 sites from which CCRA were collected, separated into eastern sites (red dots) and western sites (yellow dots). Scale bar = 10 km.

off minimal amounts of tissue from specimens. To prevent sample contamination, the Dremel drill bit (or tweezers) were soaked in 10% bleach, 100% ethanol, and burned between each use. Total genomic DNA from CCRA tissue was extracted using either the QIAGEN DNeasy Blood & Tissue Kit (Qiagen Inc., Valencia, CA) or the GenCatch Blood & Tissue Genomic Mini Prep Kit (Epoch Life Science Inc., Missouri City, TX) following the manufacturer's bench protocol. The extracted DNA was stored at 4°C until the polymerase chain reaction (PCR) was successful, after which it was stored at -20°C.

Polymerase chain reaction (PCR)

Two genetic markers were PCR amplified for DNA barcoding (species delimitation and taxon identification). The mitochondrial cytochrome c oxidase subunit 1 DNA barcode region, or COI-5P (roughly 664 bp), was the primary marker used for CCRA barcoding and species delimitation due to its proven accuracy for species identification (Sherwood et al., 2010; Dixon and Saunders, 2013; Hind and Saunders, 2013; Manghisi et al., 2019). COI-5P is the primary marker used in the barcode of life database (BOLD) but can be difficult to amplify for CCRA. Therefore, different primer combinations were tested to amplify COI-5P for every specimen. The primers used include GWSFn and GWSRx, the primers utilized by Saunders and McDevit (2012), as well as TS_COI_F01_10 (Mills and Schils, 2021). COI-5P was amplified following the amplification profile 95°C for 3 minutes; 35 cycles of 94°C for 40 seconds, annealing at 48°C for 40 seconds, extension at 72°C for 1:40 minutes; and a final extension at 72°C for 10 minutes.

The chloroplast photosystem II thylakoid membrane protein D1, or *psb*A (roughly 950 bp) was also used for CCRA barcoding and species delimitation due to its high amplification success. This marker is often used in CCRA barcoding and identification studies (Broom et al., 2008; Carro et al., 2014; Maneveldt et al., 2019). *Psb*A is more conserved than COI-5P and provides additional support for deeper nodes of the CCRA phylogeny. The gene was amplified using the primers psbAF and psbAR2, developed by Yoon et al. (2002) following the amplification profile 95°C for 3 minutes; 35 cycles of 94°C for 40 seconds, annealing at 50°C for 40 seconds, extension at 72°C for 1:40 minutes; a final extension step at 72°C for 10 minutes.

DNA sequencing and sequence analysis

PCR products were sent to Macrogen Inc. (Seoul, Republic of Korea) for DNA sequencing. Consensus sequences were generated from the forward and reverse reads, which were

TABLE 1 Currently accepted names of CCRA species (Guiry and Guiry, 2022) reported for Guam by Gordon et al. (1976).

Gordon et al. (1976)		This Study	
Species ID	**Type Locality**	**Species ID**	**Collection Site**
Dawsoniolithon conicum (E.Y.Dawson) Caragnano, Foetisch, Maneveldt & Payri [*Neogoniolithon conicum* (E.Y.Dawson) G.D.Gordon, Masaki & Akioka]	Mexico	*Dawsoniolithon* sp. 3	Apra Harbor*
Hydrolithon boergesenii (Foslie) Foslie [*Hydrolithon reinboldii* (Weber Bosse & Foslie) Foslie]	U.S. Virgin Islands	*Hydrolithon* sp. 5	Pago Bay
Hydrolithon farinosum (J.V.Lamouroux) Penrose & Y.M.Chamberlain [*Fosliella farinosa* (J.V.Lamouroux) M.Howe]	Mediterranean	N/A	Pago Bay
Lithophyllum kotschyanum Unger	Bahrain	*Lithophyllum* sp. 6	Double Reef
Lithophyllum pygmaeum (Heydrich) Heydrich [*Lithophyllum moluccense* Foslie]	Papua New Guinea	*Lithophyllum* sp. 8	Pago Bay & Tanguisson
Lithoporella melobesoides (Foslie) Foslie	Maldives	*Mastophora* sp. 2	Apra Harbor*
Mastophora pacifica (Heydrich) Foslie [*Lithoporella pacifica* (Heydrich) Foslie]	Hawaii	*Mastophora* sp. 1	Pago Bay
Mesophyllum erubescens (Foslie) Me.Lemoine[#]	Brazil	N/A	N/A
Mesophyllum mesomorphum (Foslie) W.H.Adey	Bermuda	*Rhizolamellia* sp. 1	Pago Bay
Neogoniolithon brassica-florida (Harvey) Setchell & L.R.Mason [*Neogoniolithon frutescens* (Foslie) Setchell & L.R.Mason]	South Africa	*Neogoniolithon* sp. 4	Hagatna Bay
Neogoniolithon fosliei (Heydrich) Setchell & L.R.Mason	Egypt	*Neogoniolithon* sp. 6	Anae Island, Agat
Neogoniolithon megalocystum (Foslie) Setchell & L.R.Mason [*Neogoniolithon pacificum* (Foslie) Setchell & L.R.Mason]	Indonesia	N/A	N/A
Phymatolithopsis repanda (Foslie) S.Y.Jeong, Maneveldt, P.W.Gabrielson, W.A.Nelson & T.O.Cho [*Lithothamnium asperulum* Foslie]	Australia	N/A	N/A
Porolithon onkodes (Heydrich) Foslie	Papua New Guinea	*Porolithon* sp. 1, 2, & 12	Pago Bay
Sporolithon schmidtii (Foslie) G.D.Gordon, Masaki & Akioka	Thailand	*Sporolithon* sp. 3	Pago Bay

[#]The taxonomic or nomenclatural status of this taxa is unresolved in some way.
Synonyms as used by Gordon et al. (1976) are listed in square brackets. The remaining three columns list the type localities of each species, the species ID used in this study, and the site(s) in Guam from which the taxa were re-collected. Taxa denoted with 'N/A' for both Collection Site and Species ID in this study are those which were not successfully collected, and those that list a Collection Site but have 'N/A' in the Species ID are taxa for which sequences were not successfully obtained. Collection sites marked with an asterisk (*) refer to sites that differ from those mentioned by Gordon et al. (1976).

then compared to a database of available CCRA specimens *via* BLAST search or *via* the Barcode of Life Database (BOLD; Ratnasingham and Hebert, 2007). All sequence data were archived and analyzed using the Geneious Pro 11.0.5 computer software (https://www.geneious.com; Kearse et al., 2012).

CCRA specimens belonging to the order Peyssonneliales and the subclass Corallinophycidae were analyzed separately, and alignments for each of the gene regions were created using the MUSCLE plugin (Edgar, 2004) in Geneious Pro 11.0.5. Partitioned maximum likelihood analyses of the concatenated two-locus alignments (COI-5P and *psb*A) of the Corallinophycidae and Peyssonneliales were run in IQ-TREE (Minh et al., 2020). ModelFinder (Kalyaanamoorthy et al., 2017) was used to identify the best-fit substitution model for each locus. Ultrafast bootstrap approximations (UFBoot; 1,000 bootstrap replicates) were calculated to evaluate branch support in a single IQ-TREE run. Two independent single-locus methods were used to assess CCRA diversity and delimitate putative species: distance-based Barcode-Gap analyses (Hebert et al., 2003; Meier et al., 2008) and the tree-based Bayesian implementation of the Poisson Tree Processes (bPTP) model (Zhang et al., 2013). Recent studies investigating cryptic diversity in CCRA, and other red algae have often reported a 2-4% COI-5P barcode-gap between species (Saunders, 2008; Dixon and Saunders, 2013; Hind and Saunders, 2013; Hind et al., 2014). Automatic Barcode Gap Discovery (ABGD; Puillandre et al., 2012) was performed using the default parameters for both COI-5P and *psb*A to help delimitate putative species in this study. Taxa that matched sequences of described species (≥ 98% COI-5P similarity) were identified as those species. All other taxa were identified to the highest possible taxonomic resolution using BOLD, GenBank, and by comparing the sequences generated for this study against those used in recent large-scale taxonomic and phylogenetic investigations of the Corallinophycidae (Peña et al., 2020) and the Peyssonneliales (Pestana et al., 2021) based on the phylogenetic species concept.

Rarefaction and extrapolation curves

Sample-size-based rarefaction-and-extrapolation curves, which depict the relationship between species richness estimates and sample size (number of specimens sequenced), were computed in the statistical software environment R (R Core Team, 2022) using the R package iNEXT (Hsieh et al., 2016). Hill number of order zero (q = 0) were used to interpolate and predict species richness based on the number of specimens sequenced. The function ggiNEXT was used to plot the rarefaction-and-extrapolation curves.

Results

DNA sequences were obtained for 492 CCRA specimens. Of those, 341 specimens belonged to the subclass Corallinophycidae, and 151 specimens belonged to the order Peyssonneliales (**Table 2**). ModelFinder identified GTR+F+I+G4 as the best-fit model for both partitions in the Corallinophycidae alignment. GTR+F+G4 (COI-5P) and GTR+F+I+G4 (*psb*A) was the best-fit partition model for the Peyssonneliales. Both ABGD analyses of COI-5P and *psb*A alignments resolved a total of 122 and 125 distinct species respectively, with a barcode gap of 2-3% interspecific sequence divergence for COI-5P and ~1.5% for *psb*A. Species delimitation based on the bPTP model was largely concordant with the ABGD results but resolved a few more cryptic species for both COI-5P (135 species) and *psb*A (134 species) than the distance-based approach. The species delimitation results of the ABGD and bPTP analyses of COI-5P and *psb*A supported each other, though there were rare disagreements when the bPTP model identified cryptic sister species or species complexes (*Mastophora rosea* (C.Agardh) Setchell and *Hydrolithon* sp. 5) where ABGD identified a single species (Figures 2, 3, in bold type). On the few occasions where the two analyses disagreed, the more conservative ABGD results were used to define species boundaries. Both genes were not successfully sequenced for all specimens, so a combined analysis of both genes resulted in the recognition of 154 putative CCRA species. DNA sequence data suggested that the 341 specimens belonging to the Corallinophycidae comprised 106 putative species (Figure 2), while the 152 Peyssonneliales specimens represented 48 putative species (Figure 3). However, there were a few instances where the ABGD and bPTP analyses of COI-5P resolved a group of closely related taxa as separate sister-species, while the analysis of *psb*A resolved them as a species complex. In the few cases where the two analyses did not agree, COI-5P results were followed because this marker is less conserved than *psb*A and serves as a benchmark for species delimitation in red algae (Sherwood et al., 2010; Dixon and Saunders, 2013; Manghisi et al., 2019). For all trees (Figures 2, 3), bootstrap support values are shown on nodes.

Discussion

Specimens of the same apparent taxa from largely the same locations as in Gordon et al. (1976) were collected to compare morphospecies identifications with molecular species identifications. Of the 15 species, 12 were able to be re-collected, 10 of which were collected from the same locations as in Gordon et al. (1976), and sequence data were obtained for 11 of the 12 species. *Porolithon* onkodes (Heydrich) Foslie, thought to be the one of Guam's most dominant and important CCRA species identified by Gordon et al. (1976), was found to be comprised of three separate cryptic species based on molecular data. In fact, DNA sequence analysis suggested that none of the 11 re-collected and sequenced CCRA species initially identified morphologically by Gordon et al. (1976) matched any of the molecularly-identified species of this DNA barcoding effort (Table 1). DNA sequence analysis validated only one of the 24 CCRA species listed in the most recent checklist of Guam's seaweed flora (Lobban and Tsuda, 2003). This species is *Mastophora rosea* (C.Agardh) Setchell, for which Guam is the type locality. The differences between molecular and morphospecies identification observed further

TABLE 2 Breakdown of the number of CCRA species at ordinal level and the coastline that they were collected from.

	Number of Species			
	Guam	**East and West**	**East**	**West**
Corallinales	87	12	60	39
Hapalidiales	11	0	7	4
Sporolithales	8	2	6	4
Peyssonneliales	48	14	38	24
Total	**154**	**28**	**111**	**71**
Percent of total	**100%**	**18%**	**72% (54%)**	**46% (28%)**

The total number of species per order are listed under the heading "Guam". The following three columns list the number of species that were found on both the East and West Coast and the number of species found on both coasts respectively. The bottom row shows the percent of the total number of species, and the values in parentheses show the percentage of species that were only found along one of both coastlines.

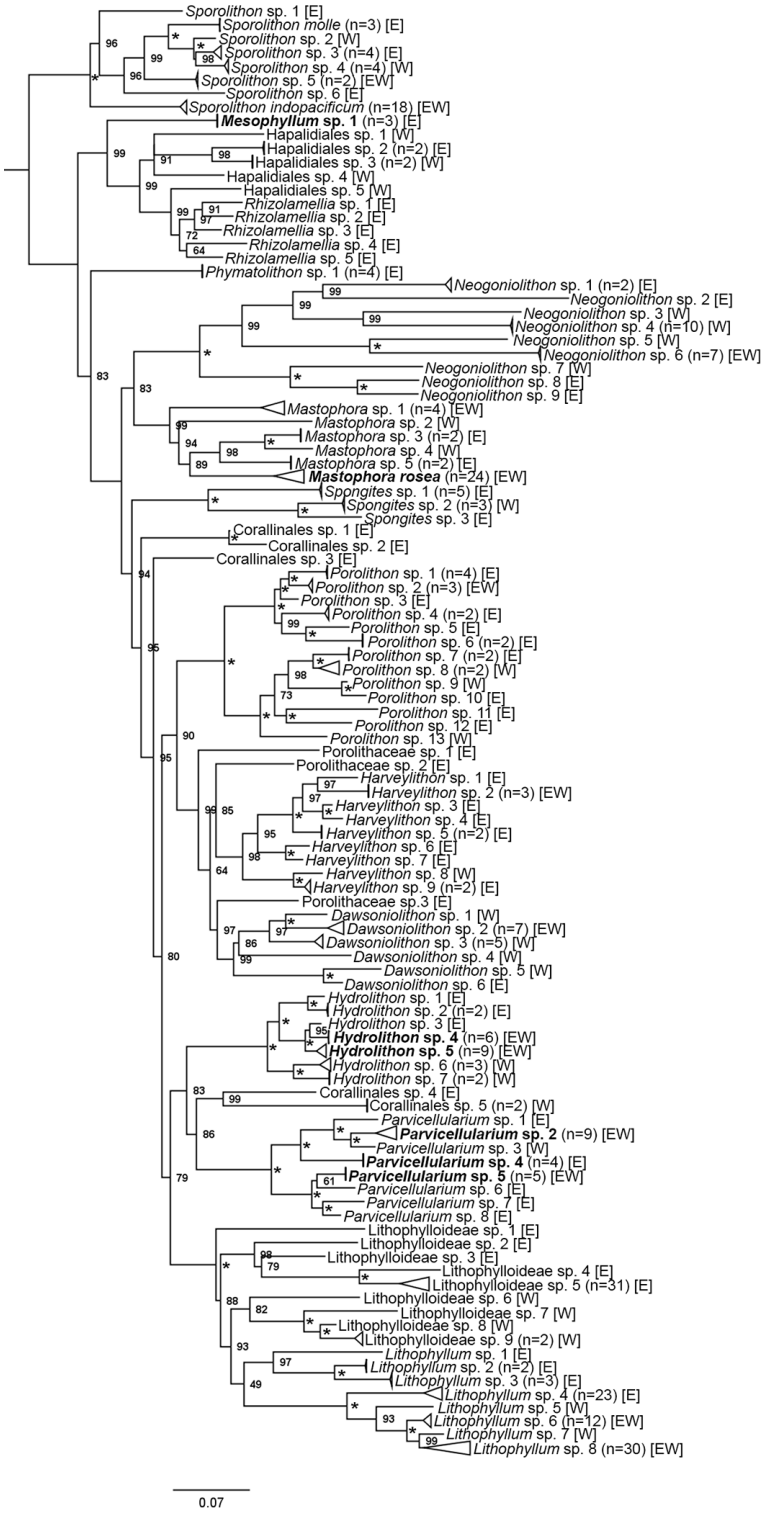

FIGURE 2
Maximum likelihood phylogenetic tree of concatenated COI-5P and *psb*A sequences for all specimens in the subclass Corallinophycidae collected during this study with bootstrap support values located at the nodes. Asterisks (*) denote nodes with full support. The side of the island that each species was found is shown using [E] for east side, [W] for west side, and [EW] for both sides. Tips denote putative species (n=106). Species recognized by ABGD, but split into one or two additional sister species by bPTP species delimitation are in bold type. *Batrachospermum gelatinosum* (Linnaeus) De Candolle was used as the outgroup and pruned from the depicted tree.

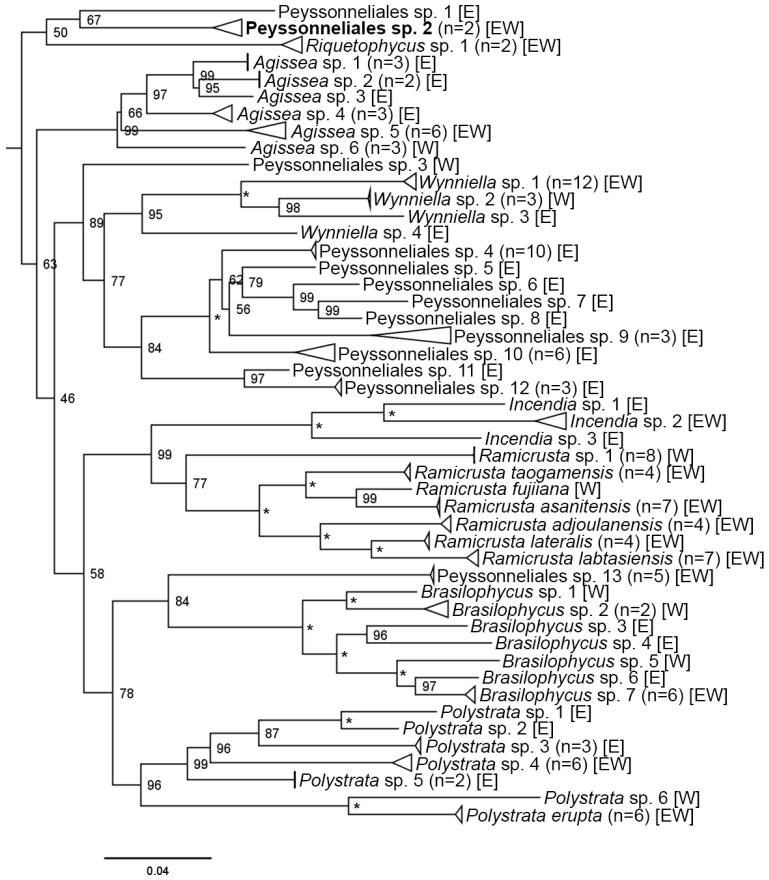

FIGURE 3
Maximum likelihood phylogenetic tree of concatenated COI-5P and *psb*A sequences for all specimens collected during this study belonging to the order Peyssonneliales with bootstrap support values located at the nodes. Asterisks (*) denote nodes with full support. The side of the island that each species was found is shown using [E] for east side, [W] for west side, and [EW] for both sides. Tips denote putative species (n=48). Species recognized by ABGD, but split into one or two additional sister species by bPTP species delimitation are in bold type. *Plocamium cartilagineum* (Linnaeus) P.S.Dixon was used as the outgroup and pruned from the depicted tree.

reiterate the unreliability of morphoanatomical identification and the utility of DNA based identification in revealing cryptic diversity among CCRA (Carro et al., 2014; Sissini et al., 2014; Pezzolesi et al., 2016; Gabrielson et al., 2018; Maneveldt et al., 2019; Peña and Torres, 2021). The 106 Corallinophycidae species detected in this study represent members of the orders Corallinales (87 spp.), Hapaladiales (11 spp.), and Sporolithales (8 spp.). This is more than a quadruple increase of the currently reported 22 species of crustose calcifying representatives of the Corallinophycidae from Guam. In addition, the 48 detected Peyssonneliales species represent a more than 20-fold increase of the previous two species reported for Guam. Overall, the 154 species recognized in this study represent more than a six-fold increase in CCRA species previously listed for Guam. However, the sample-size-based rarefaction-and-extrapolation curves (Figure 4) show that the true CCRA species richness of Guam is probably substantially higher as the gain in CCRA species has not begun to level off with increased sampling effort. If the species richness of Guam's CCRA would approach 300 as predicted by the extrapolation curve, the red algal diversity of Guam (currently at 356 species; Lobban and Tsuda, 2003) would almost double.

Of the 154 species found in this study, only ten of them matched (≥ 98% COI-5P similarity) sequences of described species, four of those were only described from Guam last year (Mills and Schils, 2021), suggesting that many of these CCRA species are possibly new to science. These findings are also consistent with recent studies that revealed extensive degrees of endemism and cryptic diversity within Guam's seaweed flora (Verbruggen and Schils, 2012; Gabriel et al., 2017; Leliaert et al., 2018; Gabriel et al., 2019; Mills and Schils, 2021; Vieira et al., 2022). Additionally, the CCRA diversity reported herein is greater than those of much larger coastal and oceanic ecosystems, including those documented in recent studies in New Zealand and Brazil (Twist et al., 2019; Sissini et al., 2021), in other barcoding blitzes in Hawaii, Taiwan, Tunisia, and

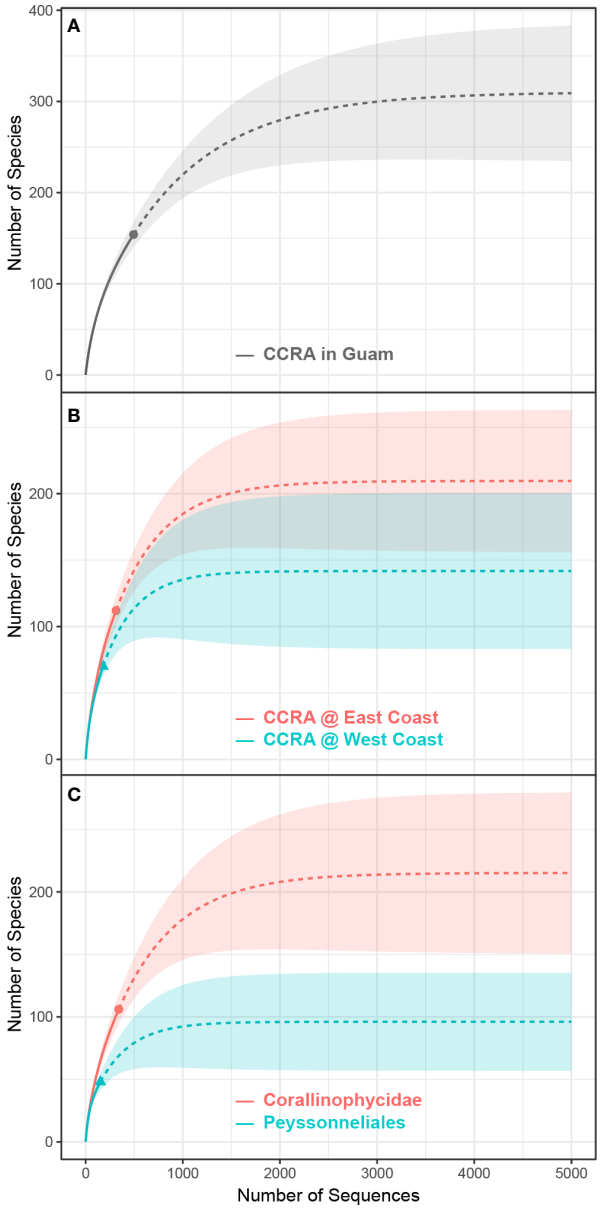

FIGURE 4
Sample-size-based rarefaction (solid line) and extrapolation (dashed line) curves. **(A)** Rarefaction-and-extrapolation curve of the number of sequenced specimens (x-axis) versus CCRA species richness (y-axis) for the whole of Guam. The grey dot indicates the total number of specimens sequenced and the overall species richness. **(B)** Rarefaction-and-extrapolation curve of the number of sequenced specimens (x-axis) versus CCRA species richness (y-axis) for the east and west coast of Guam. The red and green dots indicate the total number of specimens sequenced and the species richness for the east and west coast, respectively. **(C)** Rarefaction-and-extrapolation curve of the number of sequenced specimens (x-axis) versus CCRA species richness (y-axis) of the Corallinophycidae and Peyssonneliales. The red and green dots indicate the total number of specimens sequenced and the species richness of the Corallinophycidae and Peyssonneliales, respectively.

northern Madagascar (Sherwood et al., 2010; Liu et al., 2018; Manghisi et al., 2019; Vieira et al., 2021), and in comprehensive checklists of seaweeds from México and the Philippines (Lastimoso and Santiañez, 2020; Pedroche and Sentíes, 2020). The comparatively higher CCRA diversity for the small, remote western Pacific island of Guam emphasizes the conservation value of tropical islands as hotspots of marine biodiversity. Although based on different taxonomic concepts (phylogeny versus morphology), the high cryptic diversity and the potentially high levels of endemism in CCRA corroborate ecological studies that revealed pronounced differences in (1) the community composition of seaweed assemblages

(Schils et al., 2013) and (2) the floristic diversity (Schils and Guiry, 2016) between islands of different marine ecoregions in the tropical Pacific. Even at a smaller geographical scale, the distribution of CCRA taxa seems to be structured. This structure could be influenced by any number of factors, including habitat diversity and availability, species interactions, environmental factors, macro-ecological forces, and geographic isolation (Schils et al., 2013; Selkoe et al., 2016). Despite being similar in length (~70 km as a smoothened contour line), the east (windward) coast of Guam appears to have a higher CCRA species richness than the west (leeward) coast, possibly due to a higher (micro)habitat diversity along the east coast (Randall and Holloman, 1974; Randall and Eldredge, 1976; Paulay, 2003; Burdick et al., 2008). In addition, a high number of CCRA species seems to be restricted to either coast (82%, or 126 out of 154 species), with only a small number of shared species that were collected along the east and west coast (18%, or 28 out of 154 species). Further sampling is necessary to validate these hypotheses. Approximately 50% of the 154 species were represented by a single specimen. Similar results have been reported in recent studies of CCRA diversity in New Zealand and Brazil, indicating the need to increase sampling effort to detect more and to better document the distribution of these potentially rare species (Twist et al., 2019; Sissini et al., 2021).

While this study comprised 492 CCRA specimens collected from 31 sites surrounding the rather small island of Guam (549 km^2), it represents a modest sampling effort at best. Because of the opportunistic nature of specimen collection, long stretches of reef were not sampled. Moreover, despite being found as deep as the mesophotic and rariphotic zones (Littler et al., 1985; Richards et al., 2018), all CCRA specimens were collected from reef flats and shallow (<25 m) nearshore reef ecosystems. Species accumulation curves (Figure 4) show that Guam's CCRA species richness will continue to grow with increased sampling effort and the exploration of new (micro)habitats. However, it is expected that more complete sampling of Guam's shallow reefs and expanding sampling to greater depths will result in even higher CCRA species richness than currently predicted in the species extrapolation curves. On a global scale, the discovery of 154 CCRA species corresponds to 27% of all currently described and accepted non-geniculate members of the Corallinophycidae (449 spp.) and Peyssonneliales (134 spp.; Guiry and Guiry, 2022). Based on the current data, the species discovery curve is expected to rise to about 300 species for Guam. Guam is a rather small island with a total shoreline length of 244 km. Considering this, the global CCRA species diversity is expected to be orders of magnitude higher than the currently known 538 species, emphasizing the need to further investigate the diversity of this ecologically important group.

The results of this study serve to emphasize just how little is known about the diversity of Guam's CCRA flora, despite their ecological significance and dominant benthic cover on tropical reefs. A better understanding of Guam's CCRA communities could improve the overall understanding of ecosystem processes and community dynamics of tropical reef systems. More accurate estimates of Guam's CCRA diversity can only be reached through increased collection from more collection sites and depth zones to obtain a broader geographical and more complete (micro)habitat representation. This study serves not only as a testament to the utility of DNA-based identification in examining CCRA diversity, but also as an important first step toward better understand this dominant, ecologically important, and often overlooked group of reef builders and cementers.

Data availability statement

The datasets presented in this study can be found in online repositories. The names of the repository/repositories and accession number(s) can be found in the article/ **Supplementary Material**.

Author contributions

Conceptualization: MM and TS. Data curation: MM, TS, MD, and MH. Formal analysis: MM, TS. Funding acquisition: MM and TS. Investigation: MM, TS, MD, and MH. Methodology: MM and TS. Project administration: MM and TS. Resources: MM and TS. Supervision: MM and TS. Validation: MM and TS. Visualization: MM and TS. Writing – original draft: MM and TS. Writing – review and editing: MM, TS, and MD. All authors contributed to the article and approved the submitted version.

Funding

This research is based upon work supported by the National Aeronautics and Space Administration (NASA; nasa.gov) and the National Science Foundation (NSF; nsf.gov) under grant numbers 80NSSC17M0052 and OIA-1946352 awarded to TS and managed through the Guam EPSCoR offices of NASA and NSF. The work for this paper was also partly funded as an award to MM by a cooperative agreement with the National Oceanic and Atmospheric Administration (NOAA; noaa.gov), Project NA14OAR4170116, which is sponsored by the University of Guam Sea Grant from NOAA Office of Sea Grant, Department of Commerce. Any opinions, findings, and conclusions or recommendations expressed in this manuscript are those of the authors and do not necessarily reflect the views of NASA, NSF, NOAA or any of their subagencies. The funders had no role in study design, data collection and analysis, decision to publish, or preparation of the manuscript.

Conflict of interest

The authors declare that the research was conducted in the absence of any commercial or financial relationships that could be construed as a potential conflict of interest.

Publisher's note

All claims expressed in this article are solely those of the authors and do not necessarily represent those of their affiliated organizations, or those of the publisher, the editors and the reviewers. Any product that may be evaluated in this article, or claim that may be made by its manufacturer, is not guaranteed or endorsed by the publisher.

Supplementary material

The Supplementary Material for this article can be found online at: https://www.frontiersin.org/articles/10.3389/fmars.2022.898308/full#supplementary-material

References

Adey, W. H. (1998). Coral reefs: algal structured and mediated ecosystems in shallow, turbulent, alkaline waters. *J. Phycol.* 34, 393–406. doi: 10.1046/j.1529-8817.1998.340393.x

Broom, J. E. S., Hart, D. R., Farr, T. J., Nelson, W. A., Neill, K. F., Harvey, A. S., et al. (2008). Utility of *psb*A and nSSU for phylogenetic reconstruction in the corallinales based on new Zealand taxa. *Mol. Phylogenet. Evol.* 46, 958–973. doi: 10.1016/j.ympev.2007.12.016

Burdick, D., Brown, V., Asher, J., Caballes, C., Gawel, M., Goldman, L., et al. (2008). *Status of the coral reef ecosystems of Guam* (Guam, U.S.A.: Bureau of Statistics and Plans, Guam Coastal Management Program).

Carro, B., Lopez, L., Peña, V., Bárbara, I., and Barreiro, R. (2014). DNA Barcoding allows the accurate assessment of European maerl diversity: a proof-of-Concept study. *Phytotaxa* 190 (1), 176–189. doi: 10.11646/phytotaxa.190.1.12

Cornwall, C. E., Comeau, S., DeCarlo, T. M., Larcombe, E., Moore, B., Giltrow, K., et al. (2020). A coralline alga gains tolerance to ocean acidification over multiple generations of exposure. *Nat. Clim. Change* 10 (2), 143–146. doi: 10.1038/s41558-019-0681-8

Cornwall, C. E., Diaz-Pulido, G., and Comeau, S. (2019). Impacts of ocean warming on coralline algal calcification: meta-analysis, knowledge gaps, and key recommendations for future research. *Front. Mar. Sci.* 6, 186. doi: 10.3389/fmars.2019.00186

Deinhart, M. E., Mills, M. S., and Schils, T. (2022). Community assessment of crustose calcifying red algae as coral recruitment substrates. *PLoS One*, in press.

Dixon, K. R., and Saunders, G. W. (2013). DNA Barcoding and phylogenetics of *Ramicrusta* and *Incendia* gen. nov., two early diverging lineages of the peyssonneliaceae (Rhodophyta). *Phycologia* 52, 82–108. doi: 10.2216/12-62.1

Eckrich, C. E., and Engel, M. S. (2013). Coral overgrowth by an encrusting red alga (*Ramicrusta* sp.) overgrowing scleractinian corals, gorgonians, a hydrocoral, sponges, and other algae in lac bay, bonaire, Dutch Caribbean. *Coral Reefs* 32, 81–84. doi: 10.1007/s00338-012-0961-5

Eckrich, C. E., Engel, M. S., and Peachey, R. B. J. (2011). Crustose, calcareous algal bloom (*Ramicrusta* sp.) overgrowing scleractinian corals, gorgonians, a hydrocoral, sponges, and other algae in lac bay, bonaire, Dutch Caribbean. *Coral Reefs* 30, 131. doi: 10.1007/s00338-010-0683-5

Edgar, R. C. (2004). MUSCLE: multiple sequence alignment with high accuracy and high throughput. *Nucleic Acids Res.* 32 (5), 1792–1797. doi: 10.1093/nar/gkh340

Emery, K. O. (1962). Marine geology of Guam. *Geol. Surv. Prof. Pap.* 403-B, B1–B76. doi: 10.3133/pp403B

Fabricius, K., and De'ath, G. (2001). Environmental factors associated with the spatial distribution of crustose coralline algae on the great barrier reef. *Coral Reefs* 19, 303–309. doi: 10.1007/s003380000120

Gabriel, D., Draisma, S. G. A., Schils, T., Schmidt, W. E., Sauvage, T., Harris, D. J., et al. (2019). Quite an oddity: new worldwide records of *Renouxia* (Rhodogorgonales, rhodophyta), including r. marerubra sp. nov. *Eur. J. Phycol.* 55 (2), 197–206. doi: 10.1080/09670262.2019.1670362

Gabriel, D., Draisma, S. G. A., Schmidt, W. E., Schils, T., Sauvage, T., Maridakis, C., et al. (2017). Beneath the hairy look: the hidden reproductive diversity of the *Gibsmithia hawaiiensis* complex (Dumontiaceae, rhodophyta). *J. Phycol.* 53 (6), 1171–1192. doi: 10.1111/jpy.12593

Gabrielson, P. W., Hughey, J. R., and Diaz-Pulido, G. (2018). Genomics reveals abundant speciation in the coral reef building alga *Porolithon onkodes* (Corallinales, rhodophyta). *J. Phycol.* 54 (4), 429–434. doi: 10.1111/jpy.12761

Gordon, G. D. (1975). *Floristic and distributional account of the common crustose coralline algae of Guam.* [master's thesis]. [Mangilao (GU)]: University of Guam.

Gordon, G. D., Masaki, T., and Akioka, H. (1976). Floristic and distributional account of the common crustose coralline algae on Guam. *Micronesica* 12 (2), 247–277.

Guiry, M. D., and Guiry, G. M. (2022) *AlgaeBase* (Galway: World-wide electronic publication, National University of Ireland). Available at: https://www.algaebase.org (Accessed June 4, 2022).

Hebert, P. D. N., Cywinska, A., Ball, S. L., and deWaard, J. R. (2003). Biological identifications through DNA barcodes. *Proc. R. Soc B* 270, 313–321. doi: 10.1098/rspb.2002.2218

Hernández-Kantún, J. J., Riosmena-Rodriguez, R., Adey, W. H., and Rindi, F. (2014). Analysis of the cox2-3 spacer region for population diversity and taxonomic implications in rhodolith-forming species (Rhodophyta: Corallinales). *Phytotaxa* 190 (1), 331–354. doi: 10.11646/phytotaxa.190.1.20

Hind, K. R., Gabrielson, P. W., and Saunders, G. W. (2014). Molecular-assisted alpha taxonomy reveals pseudocryptic diversity among species of *Bossiella* (Corallinales, rhodophyta) in the eastern pacific ocean. *Phycologia* 53 (5), 443–456. doi: 10.2216/13-239.1

Hind, K. R., and Saunders, G. W. (2013). A molecular phylogenetic study of the tribe corallineae (Corallinales, rhodophyta) with an assessment of genus-level taxonomic features and descriptions of novel genera. *J. Phycol.* 49, 103–114. doi: 10.1111/jpy.12019

Hsieh, T. C., Ma, K. H., and Chao, A. (2016). iNEXT: an r package for rarefaction and extrapolation of species diversity (Hill numbers). *Methods Ecol. Evol.* 7 (12), 1451–1456. doi: 10.1111/2041-210X.12613

Hughes, T. P., Baird, A. H., Bellwood, D. R., Card, M., Connolly, S. R., Folke, C., et al. (2003). Climate change, human impacts, and the resilience of coral reefs. *Science* 301, 929–933. doi: 10.1126/science.1085046

Hughes, T. P., Rodrigues, M. J., Bellwood, D. R., Ceccarelli, D., Hoegh-Guldberg, O., McCook, L., et al. (2007). Phase shifts, herbivory, and the resilience of coral reefs to climate change. *Curr. Biol.* 17 (4), 360–365. doi: 10.1016/j.cub.2006.12.049

Johnson, J. H. (1964). "Fossil and recent calcareous algae from Guam," in *Geol. surv. Prof. pap*, 403–40G. Washington, DC, U.S.A.; United States Geological Survey (USGS).

Kalyaanamoorthy, S., Minh, B. Q., Wong, T. K. F., von Haeseler, A., and Jermiin, L. S. (2017). ModelFinder: fast model selection for accurate phylogenetic estimates. *Nat. Methods* 14, 587–589. doi: 10.1038/nmeth.4285

Kearse, M., Moir, R., Wilson, A., Stones-Havas, S., Cheung, M., Sturrock, S., et al (2012). Geneious Basic: an integrated and extendable desktop software platform for the organization and analysis of sequence data. *Bioinformatics* 28 (12) 1647–1649. doi: 10.1093/bioinformatics/bts199

Lastimoso, J. M. L., and Santiañez, W. J. E. (2020). Updated checklist of the benthic marine macroalgae of the Philippines. *Phillipp. J. Sci.* 150 (S1), 29–92.

Lee, D., and Carpenter, S. J. (2001). Isotopic disequilibrium in marine calcareous algae. *Chem. Geol.* 172 (3–4), 307–329. doi: 10.1016/S0009-2541(00)00258-8

Leliaert, F., Payo, D. A., Gurgel, C. F. D., Schils, T., Draisma, S. G. A., Saunders, G. W., et al. (2018). Patterns and drivers of species diversity in the indo-pacific red seaweed *Portieria*. *J. Biogeogr.* 45 (10), 2299–2313. doi: 10.1111/jbi.13410

Littler, M. M., Littler, D. S., Blair, S. M., and Norris, J. N. (1985). Deepest known plant life discovered on an uncharted seamount. *Science* 227, 57–59. doi: 10.1126/science.227.4682.57

Liu, L.-C., Lin, S.-M., Caragnano, A., and Payri, C. (2018). Species diversity and molecular phylogeny of non-geniculate coralline algae (Corallinophycidae, rhodophyta) from taoyuan algal reefs in northern Taiwan, including *Crustaphytum* gen. nov. and three new species. *J. Appl. Phycol.* 30, 3455–3469. doi: 10.1007/s10811-018-1620-1

Lobban, C. S., and Tsuda, R. T. (2003). Revised checklist of benthic marine macroalgae and seagrasses of Guam and Micronesia. *Micronesica* 35, 54–99.

Loreau, M., Naeem, S., and Inchausti, P. (2002). *Biodiversity and ecosystem functioning: synthesis and perspectives* (Oxford, UK: Oxford University Press).

Mallela, J. (2013). Calcification by reef-building sclerobionts. *PloS One* 8, e60010. doi: 10.1371/journal.pone.0060010

Maneveldt, G. W., Gabrielson, P. W., Townsend, R. A., and Kangwe, J. (2019). *Lithophyllum longense* (Corallinales, rhodophyta): a species with a widespread Indian ocean distribution. *Phytotaxa* 49 (2), 149–168. doi: 10.11646/phytotaxa.419.2.2

Manghisi, A., Miladi, R., Armeli Minicante, S., Genovese, G., Le Gall, L., Abdelkafi, S., et al. (2019). DNA Barcoding sheds light on novel records in the Tunisian red algal flora. *Cryptogam. Algol.* 40 (3), 5–27. doi: 10.5252/cryptogamie-algologie2019v40a3

Meier, R., Zhang, G., and Ali, F. (2008). The use of mean instead of smallest interspecific distances exaggerates the size of the "Barcoding gap" and leads to misidentification. *Syst. Biol.* 57 (5), 809–813. doi: 10.1080/10635150802406343

Mills, M. S., and Schils, T. (2021). The habitat-modifying red alga *Ramicrusta* on pacific reefs: a new generic record for the tropical northwestern pacific and the description of four new species from Guam. *PloS One* 16 (11), e0259336. doi: 10.1371/journal.pone.0259336

Minh, B. Q., Schmidt, H. A., Chernomor, O., Schrempf, D., Woodhams, M. D., von Haeseler, A., et al. (2020). IQ-TREE 2: new models and efficient methods for phylogenetic inference in the genomic era. *Mol. Biol. Evol.* 37 (5), 1530–1534. doi: 10.1093/molbev/msaa015

Mora, C., Tittensor, D. P., Adl, S., Simpson, A. G. B., and Worm, B. (2011). How many species are there on earth and in the ocean? *PloS Biol.* 9 (8), e1001127. doi: 10.1371/journal.pbio.1001127

Naeem, S., Thompson, L. J., Lawler, S. P., Lawton, J. H., and Woodfin, R. M. (1994). Declining biodiversity can alter the performance of ecosystems. *Nature* 368, 734–737. doi: 10.1038/368734a0

Nieder, C., Chen, P.-C., Chen, C. A., and Liu, S.-L. (2019). New record of the encrusting alga *Ramicrusta textilis* overgrowing corals in the lagoon of dongsha atoll, south China Sea. *Bull. Mar. Sci.* 95 (3), 459–462. doi: 10.5343/bms.2019.0010

O'Leary, J. K., Barry, J. P., Gabrielson, P. W., Rogers-Bennett, L., Potts, D. C. , Palumbi, S. R., et al. (2017). Calcifying algae maintain settlement cues to larval abalone following algal exposure to extreme ocean acidification. *Sci. Rep.* 7, 5774. doi: 10.1038/s41598-017-05502-x

Paulay, G. (2003). Marine biodiversity of Guam and the Marianas: overview. *Micronesica* 35-36, 3–25.

Pedroche, F. F., and Sentíes, A. (2020). Diversidad de macroalgas marinas en méxico. una actualización florística y nomenclatural. *Cymbella* 6 (1), 4–55.

Peña, V., Rousseau, F., De Reviers, B., and Le Gall, L. (2014). First assessment of the diversity of coralline species forming maerl and rhodoliths in Guadeloupe, Caribbean using an integrative systematic approach. *Phytotaxa* 190 (1), 190–215. doi: 10.11646/phytotaxa.190.1.13

Peña, V., and Torres, T. G. (2021). *Lithophyllum artabricum* V.Peña, sp. nov. (Corallinales, rhodophyta): a cryptic species in the Atlantic Iberian peninsula hitherto assigned to *Lithophyllum stictiforme* (Areschoug) hauck. *Cryptogam. Algol.* 42 (11), 153–172. doi: 10.5252/cryptogamie-algologie2021v42a11

Peña, V., Vieira, C., Braga, J. C., Aguirre, J., Rösler, A., Baele, G., et al. (2020). Radiation of the coralline red algae (Corallinophycidae, rhodophyta) crown group as inferred from a multilocus time-calibrated phylogeny. *Mol. Phylogenet. Evol.* 150, 106845. doi: 10.1016/j.ympev.2020.106845

Pestana, E. M. D. S., Nunes, J., Cassano, V., and Lyra, G. (2021). Taxonomic revision of the peyssonneliales (Rhodophyta): circumscribing the authentic *Peyssonnelia* clade and proposing four new genera and seven new species. *J. Phycol.* 57, 1749–1767. doi: 10.1111/jpy.13207

Pezzolesi, L., Falace, A., Kaleb, S., Hernández-Kantún, J. J., Cerrano, C., and Rindi, F. (2016). Genetic and morphological variation in an ecosystem engineer, *Lithophyllum byssoides* (Corallinales, rhodophyta). *J. Phycol.* 53 (1), 146–160. doi: 10.1111/jpy.12488

Pueschel, C. M., and Saunders, G. W. (2009). *Ramicrusta textilis* sp. nov. (Peyssonneliaceae, rhodophyta), an anatomically complex Caribbean alga that overgrows corals. *Phycologia* 48 (6), 3–25. doi: 10.2216/09-04.1

Puillandre, N., Lambert, A., Brouillet, S., and Achaz, G. (2012). ABGD, automatic barcode gap discovery for primary species delimitation. *Mol. Ecol.* 21, 1864–1877. doi: 10.1111/j.1365-294X.2011.05239.x

Randall, R. H., and Eldredge, L. G. (1976). *Atlas of the reefs and beaches of Guam* (Mangilao (GU: University of Guam Marine Laboratory).

Randall, R. H., and Holloman, J. (1974). *Coastal survey of Guam* (Mangilao (GU: University of Guam Marine Laboratory).

Ratnasingham, S., and Hebert, P. D. N. (2007). BOLD: The barcode of life data system (www.barcodinglife.org). *Mol. Ecol. Notes* 7, 355–364. doi: 10.1111/j.1471-8286.2006.01678.x

R Core Team (2022). *R: a language and environment for statistical computing* (Vienna, Austria: R Foundation for Statistical Computing). Available at: https://www.R-project.org/.

Richards, J. L., Gabrielson, P. W., and Schneider, C. W. (2018). *Sporolithon mesophoticum* sp. *nov.* (Sporolithales, rhodophyta) from plantagenet bank off Bermuda at a depth of 178 m. *Phytotaxa* 385 (2), 67–76. doi: 10.11646/phytotaxa.385.2.2

Ries, J. B. (2011). Skeletal mineralogy in a high-CO2 world. *J. Exp. Mar. Bio.Ecol.* 403, 54–64. doi: 10.1016/j.jembe.2011.04.006

Santelices, B., and Abbott, I. A. (1987). Geographic and marine isolation: an assessment of the marine algae of Easter island. *Pac. Sci.* 41 (1), 1–20.

Saunders, G. W. (2008). A DNA barcode examination of the red algal family dumontiaceae in Canadian waters reveals substantial cryptic species diversity. 1. the foliose *Dilsea-Neodilsea* complex and *Weeksia*. *Botany* 86, 773–789. doi: 10.1139/B08-001

Saunders, G. W., and McDevit, D. C. (2012). Methods for DNA barcoding photosynthetic protists emphasizing the macroalgae and diatoms. *Methods Mol. Biol.* 858, 207–222. doi: 10.1007/978-1-61779-591-6_10

Schils, T., and Guiry, M. D. (2016). Donor-recipient relationships of non-indigenous marine macroalgae between tropical pacific islands. *Cryptogam. Algol.* 37 (3), 1–14. doi: 10.7872/crya/v37.iss3.2016.199

Schils, T., Vroom, P. S., and Tribollet, A. D. (2013). Geographical partitioning of marine macrophyte assemblages in the tropical pacific: a result of local and regional diversity processes. *J. Biogeogr.* 40, 1266–1277. doi: 10.1111/jbi.12083

Selkoe, K. A., Gaggiotti, O. E., Treml, E. A., Wren, J. L. K., Donovan, M. K., Connectivity Consortium, H. R., et al. (2016). The DNA of coral reef biodiversity: predicting and protecting genetic diversity of reef assemblages. *Proc. R. Soc B* 283, 20160354. doi: 10.1098/rspb.2016.0354

Sherwood, A. R., Kurihara, A., Conklin, K. Y., Sauvage, T., and Presting, G. G. (2010). The Hawaiian rhodophyta biodiversity survey (2006-2010): a summary of principal findings. *BMC Plant Biol.* 10, 1–29. doi: 10.1186/1471-2229-10-258

Sherwood, A. R., Paiano, M. O., Spalding, H. L., and Kosaki, R. K. (2020). Biodiversity of Hawaiian peyssonneliales (Rhodophyta): Sonderophycus copusii sp. nov., a new species from the northwestern Hawaiian islands. *Algae* 35 (2), 145–155. doi: 10.4490/algae.2020.35.5.20

Sissini, M. N., Koerich, G., de Barros-Barreto, M. B., Coutinho, L. M., Gomes, F. P., Oliveira, W., et al. (2021). Diversity, distribution, and environmental drivers of coralline red algae: the major reef builders in the southwestern Atlantic. *Coral Reefs* 41, 711–725. doi: 10.1007/s00338-021-02171-1

Sissini, M. N., Oliveira, M. C., Gabrielson, P. W., Robinson, N. M., Okolodkov, Y. B., Riosmena-Rodríguez, R., et al. (2014). *Mesophyllum erubescens* (Corallinales, rhodophyta)–so many species in one epithet. *Phytotaxa* 190 (1), 299–319. doi: 10.11646/phytotaxa.190.1.18

Steneck, R. S. (1986). The ecology of coralline algal crusts: convergent patterns and adaptative strategies. *Annu. Rev. Ecol. Syst.* 17, 273–303. doi: 10.1146/annurev.es.17.110186.001421

Tebben, J., Motti, C. A., Siboni, N., Tapiolas, D. M., Negri, A. P., Schupp, P. J., et al. (2015). Chemical mediation of coral larval settlement by crustose coralline algae. *Sci. Rep.* 5, 10803. doi: 10.1038/srep10803

Thiers, B. (2016) *Index herbariorum: a global directory of public herbaria and associated staff. new York botanical garden's virtual herbarium*. Available at: http://sweetgum.nybg.org/science/ih/.

Tilman, D., Reich, P. B., and Knops, J. M. H. (2006). Biodiversity and ecosystem stability in a decade-long grassland experiment. *Nature* 441 (6), 629–632. doi: 10.1038/nature04742

Tsuda, R. (2003). *Checklist and bibliography of the marine benthic algae from the Mariana islands (Guam and CNMI)* (Mangilao (GU: University of Guam Marine Laboratory).

Tsuda, R. (2014). Endemism of marine algae in the Hawaiian islands. *Bishop Mus. Occas. Pap.* 115, 23–27.

Twist, B. A., Neill, K. F., Bilewitch, J., Jeong, S. Y., Sutherland, J. E., and Nelson, W. A. (2019). High diversity of coralline algae in new Zealand revealed: Knowledge gaps and implications for future research. *PloS One* 14 (12), e0225645. doi: 10.1371/journal.pone.0225645

Vargas-Ángel, B., Richards, C. L., Vroom, P. S., Price, N. N., Schils, T., Young, C. W., et al. (2015). Baseline assessment of net calcium carbonate accretion rates on U.S. pacific reefs. *PloS One* 10 (12), 1–25. doi: 10.1371/journal.pone.0142196

Vásquez-Elizondo, R. M., and Enríquez, S. (2016). Coralline algal physiology is more adversely affected by elevated temperature than reduced pH. *Sci. Rep.* 6 (1), 1–14. doi: 10.1038/srep19030

Verbruggen, H., and Schils, T. (2012). *Rhipilia coppejansii*, a new coral reef-associated species from Guam (Bryopsidales, chlorophyta). *J. Phycol.* 48 (5), 1090–1098. doi: 10.1111/j.1529-8817.2012.01199.x

Verlaque, M., Ballesteros, E., and Antonius, A. (2000). *Metapeyssonnelia corallepida* sp. nov. (Peyssonneliaceae, rhodophyta), an Atlantic encrusting red alga overgrowing corals. *Botanica Marina* 43, 191–200. doi: 10.1515/BOT.2000.020

Vermeij, M. J. A., Dailer, M. L., and Smith, C. M. (2011). Crustose coralline algae can suppress macroalgal growth and recruitment on Hawaiian coral reefs. *Mar. Ecol. Prog. Ser.* 422, 1–7. doi: 10.3354/meps08964

Vieira, C., N'Yeurt, A. D. R., Rasomanendrika, F. A., D'Hondt, S., Tran, L. A. T., den Spiegel, D. V., et al. (2021). Marine macroalgal biodiversity of northern Madagascar: morpho-genetic systematics and implications of anthropic impacts for conservation. *Biodivers. Conserv.* 30, 1501–1546. doi: 10.1007/s10531-021-02156-0

Vieira, C., Schils, T., Kawai, H., D'hondt, S., Paiano, M. O., Sherwood, A. R., et al. (2022). Phylogenetic position of *Newhousia* (Dictyotales, phaeophyceae) and the description of *N. sumayensis* sp. nov. from Guam. *Phycologia*. 61 (3), 255–264. doi: 10.1080/00318884.2022.2034364

Vroom, P. S. (2011). "Coral dominance": a dangerous ecosystem misnomer? *J. Mar. Biol.* 2011, 164127. doi: 10.1155/2011/164127

Williams, S. M., and García-Sais, J. R. (2020). A potential new threat on the coral reefs of Puerto Rico: The recent emergence of *Ramicrusta* spp. *Mar. Ecol.* 41 (4), e12592. doi: 10.1111/maec.12592

Yamamoto, S., Kayanne, H., Terai, M., Watanabe, A., Kato, K., Negishi, A., et al. (2012). Threshold of carbonate saturation state determined by CO2 control experiment. *Biogeosciences* 9, 1441–1450. doi: 10.5194/bg-9-1441-2012

Yoon, H. S., Hackett, J. D., and Bhattacharya, D. (2002). A single origin of the peridinin- and fucoxanthin-containing plastids in dinoflagellates through tertiary endosymbiosis. *Proc. Natl. Acad. Sci. U.S.A.* 99 (18), 11724–11729. doi: 10.1073/pnas.172234799

Yuen, Y. S., Yamazaki, S. S., Nakamura, T., Tokuda, G., and Yamasaki, H. (2009). Effects of live rock on the reef-building coral *Acropora digitifera* cultured with high levels of nitrogenous compounds. *Aquac. Eng.* 41, 35–43. doi: 10.1016/j.aquaeng.2009.06.004

Zhang, J., Kapli, P., Pavlidis, P., and Stamatakis, A. (2013). A general species delimitation method with applications to phylogenetic placements. *Bioinformatics* 29 (22), 2869–2876. doi: 10.1093/bioinformatics/btt499

frontiers | Frontiers in Earth Science

TYPE Original Research
PUBLISHED 26 August 2022
DOI 10.3389/feart.2022.958148

OPEN ACCESS

EDITED BY
Sebastian Teichert,
Friedrich-Alexander Universität Erlangen-Nürnberg, Germany

REVIEWED BY
Marco Brandano,
Sapienza University of Rome, Italy
Guilherme Henrique Pereira-Filho,
Universidade Federal de São Paulo, Brazil

*CORRESPONDENCE
Julio Aguirre,
jaguirre@ugr.es

SPECIALTY SECTION
This article was submitted to Paleontology, a section of the journal Frontiers in Earth Science

RECEIVED 31 May 2022
ACCEPTED 30 June 2022
PUBLISHED 26 August 2022

CITATION
Aguirre J and Braga JC (2022), Middle Miocene (Serravallian) rhodoliths and coralline algal debris in carbonate ramps (Betic Cordillera, S Spain).
Front. Earth Sci. 10:958148.
doi: 10.3389/feart.2022.958148

Middle Miocene (Serravallian) rhodoliths and coralline algal debris in carbonate ramps (Betic Cordillera, S Spain)

Julio Aguirre* and Juan C. Braga

Departamento de Estratigrafía y Paleontología, Facultad de Ciencias, Universidad de Granada, Granada, Spain

Serravallian (middle Miocene) coralline algal assemblages at the southern margin of the Guadalquivir Basin (southern Spain) occur as rhodoliths preserved *in situ* or very close to their growth habitats (autochthonous–parautochthonous assemblages) and also as reworked remains (allochthonous assemblages). The former assemblages consist of spherical rhodoliths built up by encrusting to warty plants and also of large fragments of branches, whereas the latter are mostly unrecognizable small fragments occurring in channeled packstone–grainstone beds. In both cases, the most abundant components are members of the order Hapalidiales (*Mesophyllum roveretoi*, *Mesophyllum* sp., *Lithothamnion ramosissimum*, and less frequently *Phymatolithon* group *calcareum* and *Lithothamnion* group *corallioides*). Laminar growths of *Lithoporella minus* and branches of *Spongites* group *fruticulosus* and *Sporolithon* sp. occur very rarely. There are also anecdotal records of *Subterraniphyllum thomasii*, extending its upper stratigraphic range up to the Serravallian in the western Tethys. The autochthonous–parautochthonous coralline algal assemblages formed in a middle ramp, at several tens of meters of water depth, as suggested by the dominance of Hapalidiales. The allochthonous assemblages represent fragments of coralline algae derived from the middle ramp and redeposited in deeper settings, most likely the outer ramp, due to storm-generated currents.

KEYWORDS

rhodolith beds, autochthonous-allochthonous assemblages, carbonate ramps, Guadalquivir Basin, Jimena, Jódar, Betic Cordillera.

Introduction

The Serravallian (middle Miocene) is a time interval of global temperature decline following the middle Miocene climatic transition. Superimposed to the climatic trend, deep paleogeographic transformations affected the Mediterranean during the middle Miocene, mostly due to tectonism associated with the relative movements of the African, Arabian, and Eurasian Plates: 1) restriction of the Paratethys to become a megalake during the late Miocene (Rögl, 1998; Meulenkamp and Sissingh, 2003; Palcu et al., 2011), 2) disconnection of the Mediterranean from the Indian Ocean (Rögl, 1998; Cornacchia et al.,

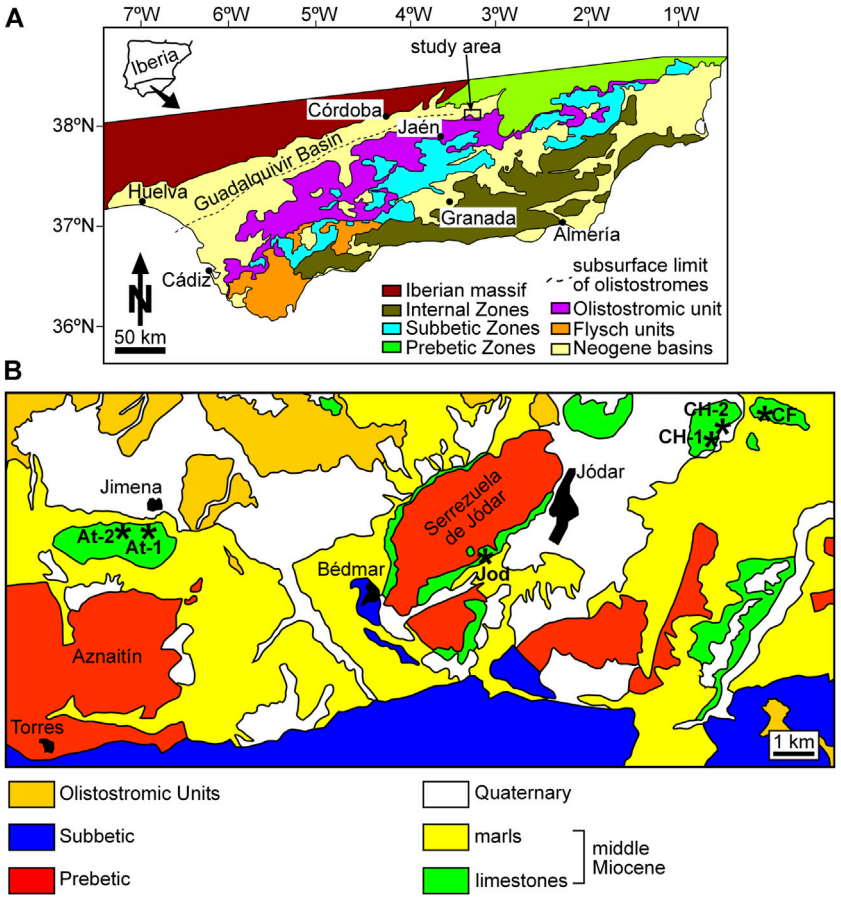

FIGURE 1
(A) geological map of the Betic Cordillera with indication of the study area NE Jaén. **(B)** geological map of the study area. Asterisks indicate the location of the stratigraphic columns.

2021), and 3) folding and thrusting at the western Mediterranean that led to the uplifting of the Betic-Rif mountain belt (Galindo-Zaldívar et al., 2000; Pedrera et al., 2012; Ruiz-Costán et al., 2012). The interplay of the climatic evolution, tectonic–paleogeographic changes, and sea-level fluctuations during the middle Miocene had critical effects on the paleoceanography of the Mediterranean, which, in turn, controlled carbonate production (Cornacchia et al., 2021).

In the Betic Cordillera, several carbonate ramps with varying siliciclastic supplies developed associated with the newly emerging reliefs during the Serravallian. These carbonate deposits, although widespread in the region, are poorly known, except for the Serravallian carbonate ramp located at the western end of the North-Betic strait (Braga et al., 2010a), which connected the Mediterranean Basin with the Atlantic Ocean at the front of the uplifting Betic orogen (Martín et al., 2009). Further west–southwest, coeval Serravallian carbonates occur at the southern margin of the Guadalquivir Basin, the foreland basin of the Betic Cordillera. They are heterozoan carbonates dominated by coralline algae, larger benthic foraminifera (LBF), echinoderms, bryozoans, serpulids, and mollusks.

In this study, we investigated the coralline algae in Serravallian limestones at the southern margin of the Guadalquivir Basin that crop out in the vicinity of Jimena, Bedmar, and Jódar (Jaén Province, SE Spain). The coralline algae are major biotic components in these carbonates, occurring in densely packed rhodolith beds and as dispersed fragments together with other bioclasts. Rhodolith coralline algal composition, shape, and size are valuable tools to infer the paleoenvironmental contexts in which they grew (e.g., Aguirre et al., 2017). In a regional context, the paleogeography and tectonic scenario at the southern margin of the Guadalquivir Basin during the middle Miocene played an important role in controlling carbonate deposition and the main biotic carbonate producers. At last, rhodolith-dominated deposits were widespread in the Mediterranean during the middle Miocene (Braga, 2017; Cornacchia et al., 2021). Therefore, the study of the

Serravallian coralline algae and rhodolith beds, together with the analysis of their lithofacies and stratal geometry, is key to understanding the significance of this type of deposit in carbonate production within the western Mediterranean.

Geographic location and geological settings

The Serravallian carbonates were studied in three areas of the Jaén Province (SE Spain): 1) Cerro de la Atalaya, a hill immediately south of Jimena, 2) southeast of Serrezuela de Jódar, and 3) Cerro Hernando–Cerro de Fontanar, east of Jódar (Figure 1).

These areas are located at the southern margin of the Guadalquivir Basin, the foreland basin of the Betic Cordillera (Figure 1A). This is a mountain belt in the western Mediterranean Alpine orogen that can be divided into three main tectonic domains: 1) the Internal Zones, mostly made up of metamorphic rocks; 2) the External Zones, consisting of the thrusted and folded sediments accumulated at the southern margin of the Iberian Plate; and 3) the Campo de Gibraltar or Flysch units, formed in deep-water fan systems in areas between the two former domains (García-Hernández et al., 1980) (Figure 1A). The External Zones can be divided, in turn, into the Prebetic Zones, the paleogeographic area closest to the continent, and the Subbetic Zones, corresponding to more distal settings further to the south.

During the formation of the Betic Cordillera, the overgrowth of the orogenic wedge led to the flexure of the crust underneath, originating the Guadalquivir foreland Basin between the passive margin to the north and the active margin of the orogen to the south (Perconing, 1960-62; García-Castellanos et al., 2002). Large amounts of allochthonous deposits derived from the orogen frontal wedge, the Olistostrome unit (Figure 1A), were transported into the Guadalquivir Basin (Perconing, 1960-62; Roldán, 1995, 2008; Berasátegui et al., 1998; Rodríguez-Fernández et al., 2012, 2013). The study limestones unconformably overlies chaotic deposits of the Olistostrome unit and Mesozoic carbonates of the Prebetic Zones. They are folded and faulted due to the northward thrusting of the Betic front units (García-Tortosa et al., 2008; Sanz de Galdeano et al., 2013). Marls in the lower part of the study sections contain rich planktonic foraminifer assemblages of the late Serravallian, attributable to biozone M9 of Wade et al. (2011), including *Fohsella fohsi*, *Sphaeroidinellopsis* spp., *Paragloborotalia siakensis*, *Globorotalia praemenardii*, and *Globigerina bulloides*.

Materials and methods

Six sections were logged in the three study areas (Figure 1B). One hundred and five limestone samples were collected from the distinguished lithofacies intervals throughout sections. One rock sample was collected in each of these intervals, except in the rhodolith beds, where several samples were taken in the selected sampling sites. Ultrathin sections were prepared from all collected samples to analyze their microfacies and coralline algal assemblages. Relative abundance of bioclastic and terrigenous components was estimated using the comparison charts of Baccelle and Bosellini (1956). Coralline algae were identified at the lowest taxonomic level possible. Taxonomic identification of fragments was difficult because, in most cases, there were insufficient diagnostic characters preserved. The relative species abundance in lithified rhodolith beds is difficult to estimate as any quantification of component proportions had to be performed in thin sections under the microscope. The collection of rock samples and thin-section preparation is conditioned by several factors that prevent a simple random or systematic sampling and, therefore, bias the results. Taxonomic subdivisions follow the most recent molecular phylogenetic schemes (Peña et al., 2020; Jeong et al., 2021). The cementation of the study rocks precluded the extraction of isolated rhodoliths; therefore, the rhodolith shape has been analyzed in 2D sections at the outcrops. Rhodolith description (external shapes, algal growth forms, inner arrangement, etc.) and rhodolith bed characterization follow the terminology reviewed by Aguirre et al. (2017).

FIGURE 2
(A) panoramic view of the stratigraphic section corresponding to the CH-2 section: Cerro Hernando–Cerro Fontanar area. Note the whitish marls in the lower part of the section and the carbonates on top of the marls. **(B)** panoramic view of the Serravallian carbonates unconformably overlying Cretaceous limestones in the Serrezuela de Jódar area.

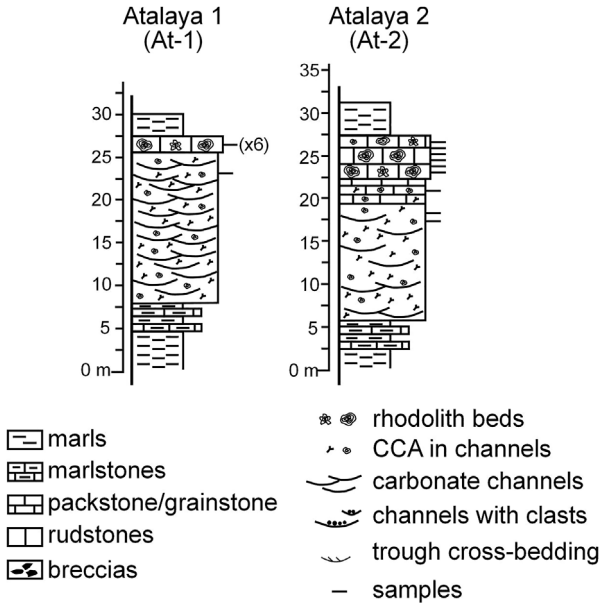

FIGURE 3
Stratigraphic sections in the Cerro de la Atalaya area, S of Jimena.

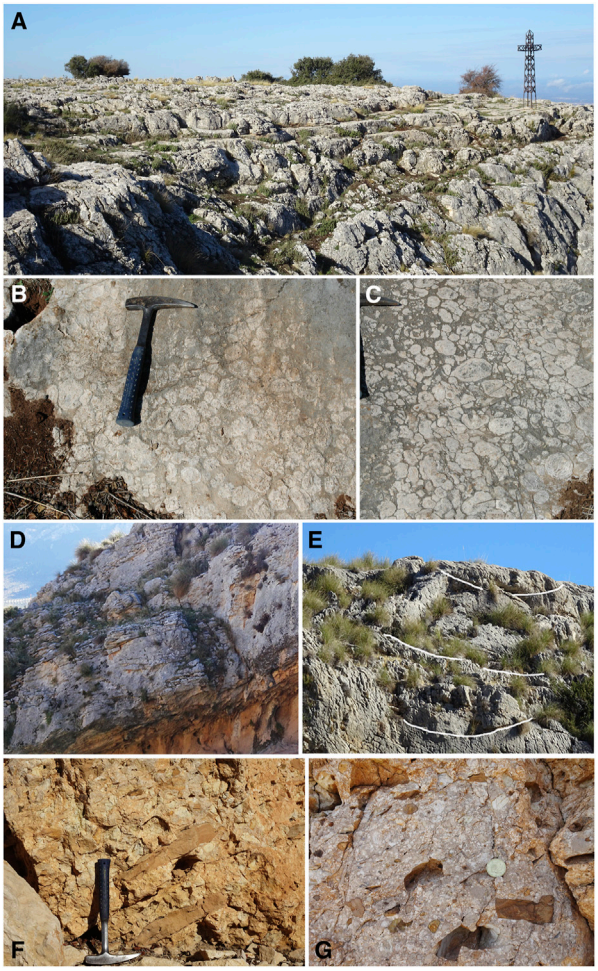

FIGURE 4
(A) plane-parallel densely packed rhodolith beds from the La Atalaya area: At-2 section. **(B,C)** massive rhodolith beds in the La Atalaya area: At-1 section. **(D)** trough crossbedding at the lower part of the Serravallian carbonates in the Jódar section. **(E)** channeled beds in the Jódar section. **(F)** Breccia including large angular boulders and cobbles in the CF section (Cerro Hernando–Cerro Fontanar area). **(G)** same breccia bed as in F but including numerous rhodoliths and coralline algal debris (whitish spots).

Stratigraphic sections

Both in the Cerro de la Atalaya and in the Cerro Hernando–Cerro Fontanar areas, Serravallian successions show similar stratigraphic patterns, consisting of marls at the base that change upwards to limestones and, finally, to silts and marls (Figure 2A). In the Serrezuela de Jódar area, Serravallian sediments unconformably overlie Cretaceous limestones (Figure 2B).

Cerro de la Atalaya

The Serravallian deposits in Cerro de la Atalaya form a northward-verging anticline north of Sierra del Aznaitín, which is made up of Cretaceous limestones of the Prebetic Zones (García-Tortosa et al., 2008; Sanz de Galdeano et al., 2013) (Figure 1B). The lower part of the sections consists of marls rich in planktonic foraminifers. In the transition to the carbonate above, thin planktonic foraminifera-rich packstone beds intercalate with the marls (Figure 3). They change upwards to channeled fine- to coarse-grained packstones, rarely rudstones (Figure 3). The beds are decimeters up to a meter in thickness. The major components are benthic foraminifera (LBF and small forms), bryozoans, coralline algae, echinoderms, and bivalves, with varying proportions of planktonic foraminifera. Siliciclastic content, consisting of fine angular quartz grains, ranges from 10 to 50%. Above the channeled deposits, the coralline algal content substantially increases. In a lower interval, they occur in rudstone beds, 20–50-cm thick, as branch fragments and small rhodoliths (1–2 cm in diameter). This facies changes upwards to densely packed rhodolith beds (rudstones with rhodoliths embedded in a packstone matrix), up to 2-m thick (Figure 4A). The algal nodules reach up to 17 cm in the longest diameter (Figures 4B and C). The matrix includes LBF, bryozoans, echinoderms, bivalves, *Ditrupa* worm tubes and other encrusting serpulids, and scarce barnacles. On occasions, planktonic foraminifera are significant. Above the rhodolith beds, the Serravallian sections end with marls rich in planktonic foraminifers (Figure 3).

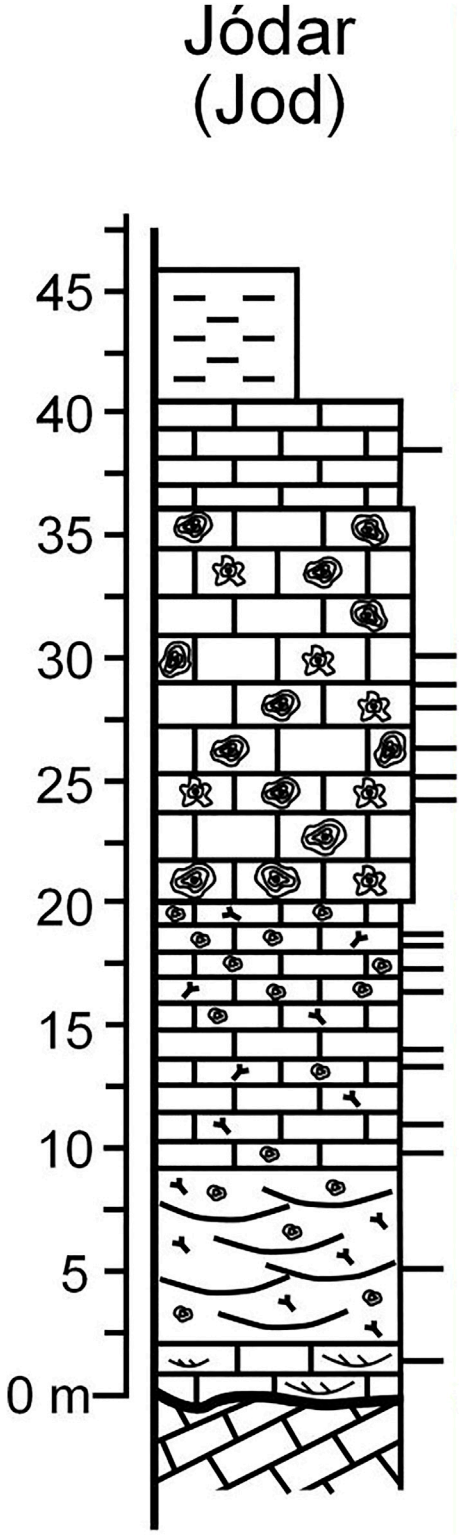

FIGURE 5
Stratigraphic section in the Jódar area (symbols as in Figure 3).

Serrezuela de Jódar

The Serravallian limestones crop out in a belt surrounding Serrezuela de Jódar and Serrezuela de Bédmar (also called Sierra de Bédmar–Jódar), a series of hills made up of Prebetic Cretaceous limestones (García-Tortosa et al., 2008; Sanz de Galdeano et al., 2013) (Figures 1B and 2B). One stratigraphic section, about 3 km south of Jódar, was logged (Figure 5). The lower part of the limestones consists of centimeter–decimeter-thick packstone–grainstone beds displaying rough trough cross-bedding (Figure 4D). The major components are LBF, bryozoans, echinoderms, bivalves, fragments of coralline algae, and scattered barnacles and serpulids (including *Ditrupa*). The terrigenous content (angular, fine-grained particles of quartz), although scarce, reaches up to 10%. Higher up in the section, decimeter-thick channeled beds of packstones occur (Figure 4E). They are rich in LBF, echinoderms, and bryozoans. The coralline algal content progressively increases upwards, and rhodoliths become the main components, originating densely packed rhodolith rudstone beds up to several meters in thickness (Figure 5) with a packstone matrix dominated by LBF, bryozoans, echinoderms, and, less frequently, serpulids and bivalves (pectinids and oysters). Above the rhodolith beds, the grain size decreases passing to centimeter–decimeter-thick packstone beds rich in planktonic foraminifera. Silts and marls end the Serravallian succession (Figure 5).

Cerro Hernando–Cerro Fontanar

The Serravallian deposits form the hills named Cerro Hernando and Cerro Fontanar, ENE of Jódar, and unconformably overlie chaotic materials of the Olistostrome unit (Figure 1B). The study carbonates form a homoclinal sequence dipping ~15° to the NNW in Cerro Hernando and to the E in Cerro Fontanar. The study sections can be divided into two parts: the lower part made up of planktonic foraminifera-bearing marls and the upper part consisting of bioclastic limestones (Figures 2A and 6). The transition between both is gradual, characterized by fine-grained packstone beds, centimeter to decimeter in thickness, intercalated in the marls. The packstone beds are made up of planktonic foraminifer ooze and show a rough parallel lamination. Higher up in the section, marls pass to decimeter-thick plane-parallel bedded packstone rich in planktonic foraminifera with abundant benthic foraminifera as well as fragments of coralline algae, echinoderms, bryozoans, bivalves, and serpulids. Limestones change upward to decimeter–meter-thick channeled beds formed by alternating finer-grained (packstone) and coarser-grained (rudstone) beds up to the top of the Serravallian

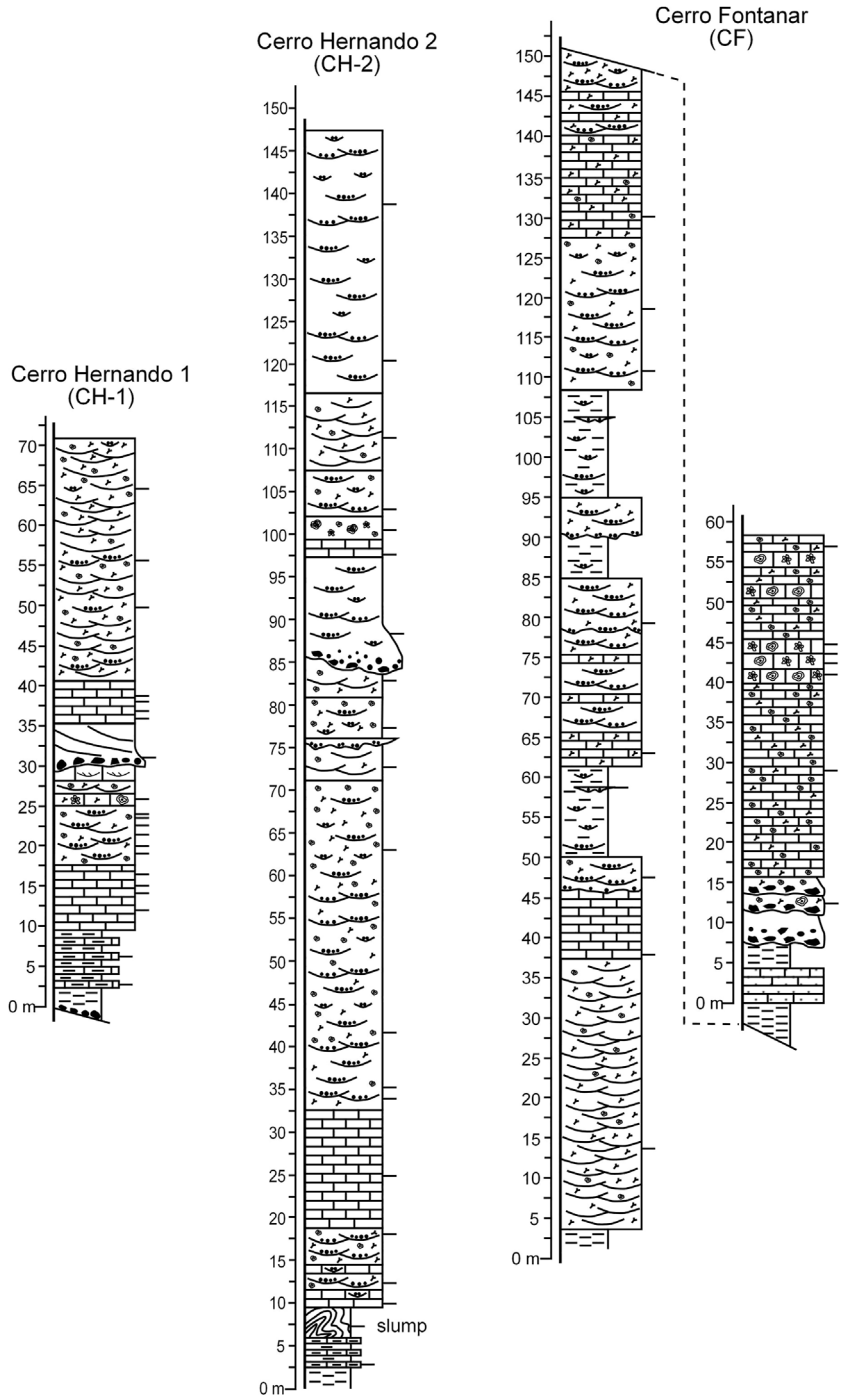

FIGURE 6
Stratigraphic sections in the Cerro Hernando–Cerro Fontanar area (symbols as in Figure 3).

succession. Some beds show incomplete Bouma sequences, preserving layers A and B and, occasionally, layer C. The proportion of the terrigenous components can reach up to 5% of the rock volume. They are quartz sand grains and angular pebbles to boulders of Mesozoic limestone and sandstone. In the Cerro Fontanar, a 3-m-thick breccia containing cobbles and boulders (up to 1.2 m in diameter) is observed (Figures 4F and G). This breccia contains rhodoliths and abundant coralline algal debris, LBF, and bryozoans with varying amounts of echinoderms, bivalves, serpulids (including *Ditrupa*), and rare barnacles.

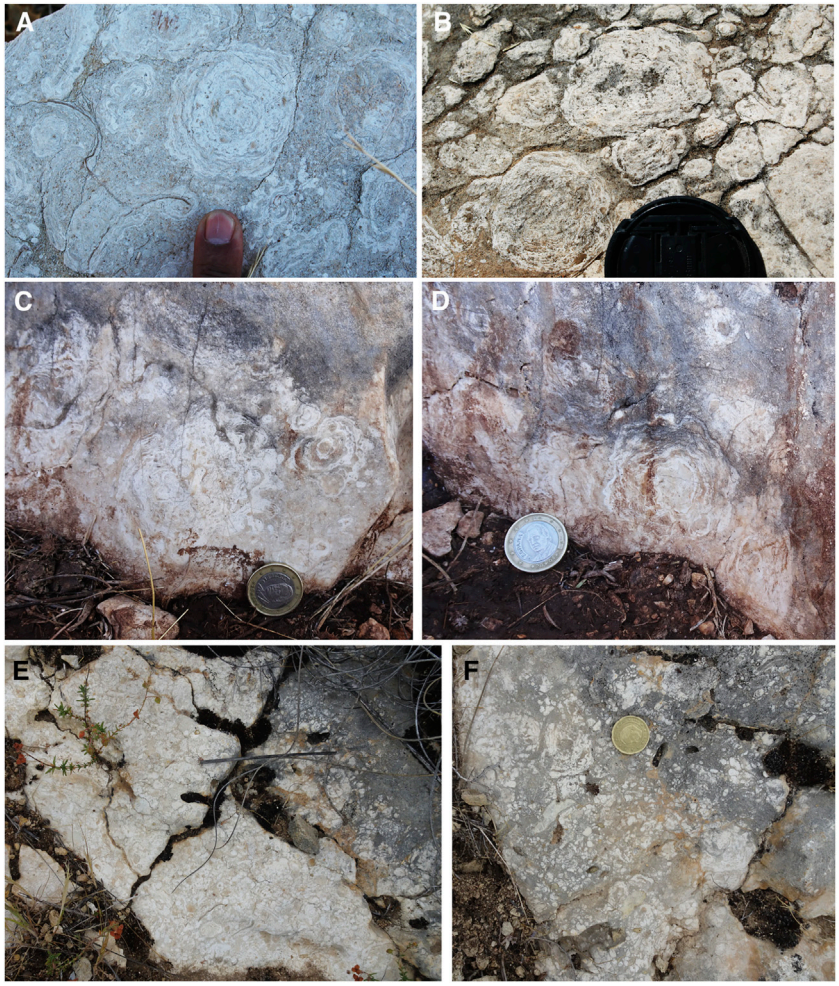

FIGURE 7
(A,B) rhodolith concentrations in the At-2 section (Cerro de la Atalaya area). Rhodoliths are spheroidal in shape, and some of them show an ellipsoidal morphology. Inner algal arrangement is characterized by concentric laminar-encrusting algal thalli. Rarely, i.e., right of the finger in **(A)**, rhodoliths are made up of warty–fruticose algal plants. **(C,D)** rhodolith rudstones in the Jódar section (Serrezuela de Jódar area). As in Cerro de la Atalaya, rhodoliths are mostly spheroidal in shape and made up of laminar-encrusting algal thalli. **(E,F)** small rhodoliths and coralline algal fragments observed in the channeled facies of the Cerro Hernando–Cerro Fontanar area. Note that the size of the rhodoliths is smaller than the size of those present in Serrezuela de Jódar and Cerro de la Atalaya.

In the upper half of the Serravallian succession, some channeled beds, 25–50-cm thick, contain rhodoliths and fragments of coralline algal branches as the main components, together with angular lithoclasts derived from the basement (Figure 6).

Coralline algal occurrence and taxonomic composition

In the Cerro de la Atalaya and Serrezuela de Jódar areas, rhodoliths occur in loosely to densely packed massive rudstone beds (Figures 7A–D), as well as in channeled facies. In the Cerro Hernando–Cerro Fontanar, rhodoliths are only found in channeled beds (Figures 7E and F). In all cases, rhodoliths are mostly spheroidal in shape with some ellipsoidal nodules. On average, the ratio between the shorter and larger axes is ca. 0.75, indicating the dominance of spheroidal nodules (Figure 8).

In the massive rhodolith rudstone beds, rhodoliths attain similar mean sizes both in Cerro de la Atalaya (5.2 × 3.8 cm) and Serrezuela de Jódar (4.5 × 3.5 cm), although the size range of the largest dimension is higher in Cerro de la Atalaya (from 1.3 to 17.4 cm) than in Serrezuela de Jódar (1.4–8.8 cm) (Figure 8).

Rhodoliths show nearly concentric inner arrangements with dominantly encrusting and warty coralline algal growth forms, less frequently fruticose, and small proportions of constructional

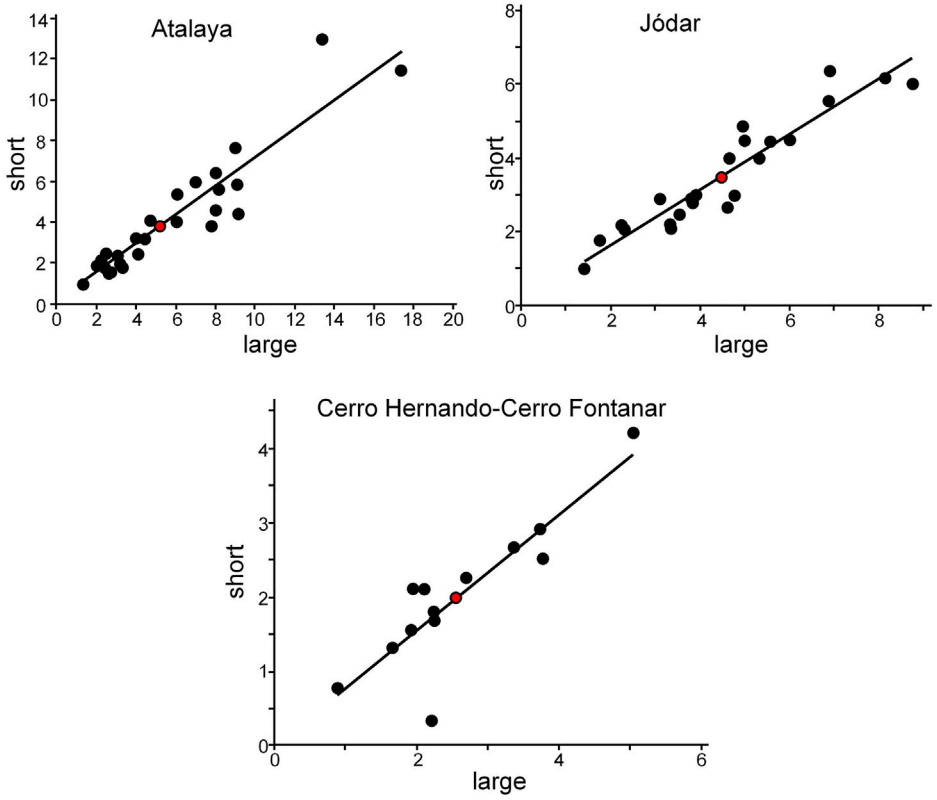

FIGURE 8
Size of the rhodoliths in the three study areas represented as the relationship between large and short axes. Red dots denote the average rhodolith sizes. Note the good adjustment of the size values to a straight line, indicating the dominance of spheroidal morphology. Number of measured rhodoliths: Atalaya, *n* = 25; Jódar, *n* = 23; Cerro Hernando–Cerro Fontanar, *n* = 13.

voids (Figures 7A–D). Rhodoliths are built up by complex intergrowths of corallines with other encrusting organisms, such as benthic foraminifera, bryozoans, serpulids, and, occasionally, barnacles (Figure 9). In a very few cases, encrusting benthic foraminifera are more abundant than coralline algae, forming the so-called for-algaliths (Prager and Gingsburg, 1989) or macroids (Hottinger, 1983; Bassi et al., 2012). The nuclei of rhodoliths are bioclasts, mainly bivalves, bryozoans, coralline algae, and LBF, or lithoclasts.

Sixteen species of coralline algae have been identified, with representatives of the three calcified orders Sporolithales, Corallinales, and Hapalidiales (Table 1). However, in terms of taxonomic composition, rhodoliths are generally monospecific or paucispecific, with two to three species. Hapalidiales is the dominant group, with *Mesophyllum roveretoi*, *Mesophyllum* sp., and *Lithothamnion ramosissimum* being the most abundant, followed by *Lithothamnion* group *corallioides* and *Phymatolithon* group *calcareum*, (Figure 10). Additional Hapalidiales are anecdotal: *Lithothamnion* sp. 1 and *Melobesia* sp. (Figures 11A and B). The order Corallinales is scarcely represented, with *Spongites* group *fruticulosus* and *Lithoporella minus* standing out as the most frequent species (Figures 11C and D), with occasional records of *Spongites* spp., *Hydrolithon lemoinei*, and very rare fragments of calcified intergenicula of unidentifiable geniculates. It is also worth highlighting the scarce occurrence of *Subterraniphyllum thomasii* fragments in the lower part of the Cerro Fontanar (Figures 11E–G). At last, Sporolithales are only anecdotally present as branch fragments of *Sporolithon* sp. (Figure 11H).

Coralline algae in the packstone channeled lithofacies are mostly abraded fragments of branches and crusts. They occur in highly varying proportions, from 3% up to 50% of the rock volume. Small rhodoliths, from 0.9 to 5 cm in the largest diameter (mean, 2.6 cm) (Figure 8), and broken rhodoliths also occur. They show an inner concentric arrangement of thin encrusting and warty algal growth forms, with very rare fruticose plants. In some cases, the sediment filling up the internal voids of these rhodoliths is different (wackestone) from the sediment surrounding them (packstone), indicating that they are displaced from their growth places.

Most fragments do not show enough taxonomic features to be identified at any taxonomic level. Among the identifiable ones,

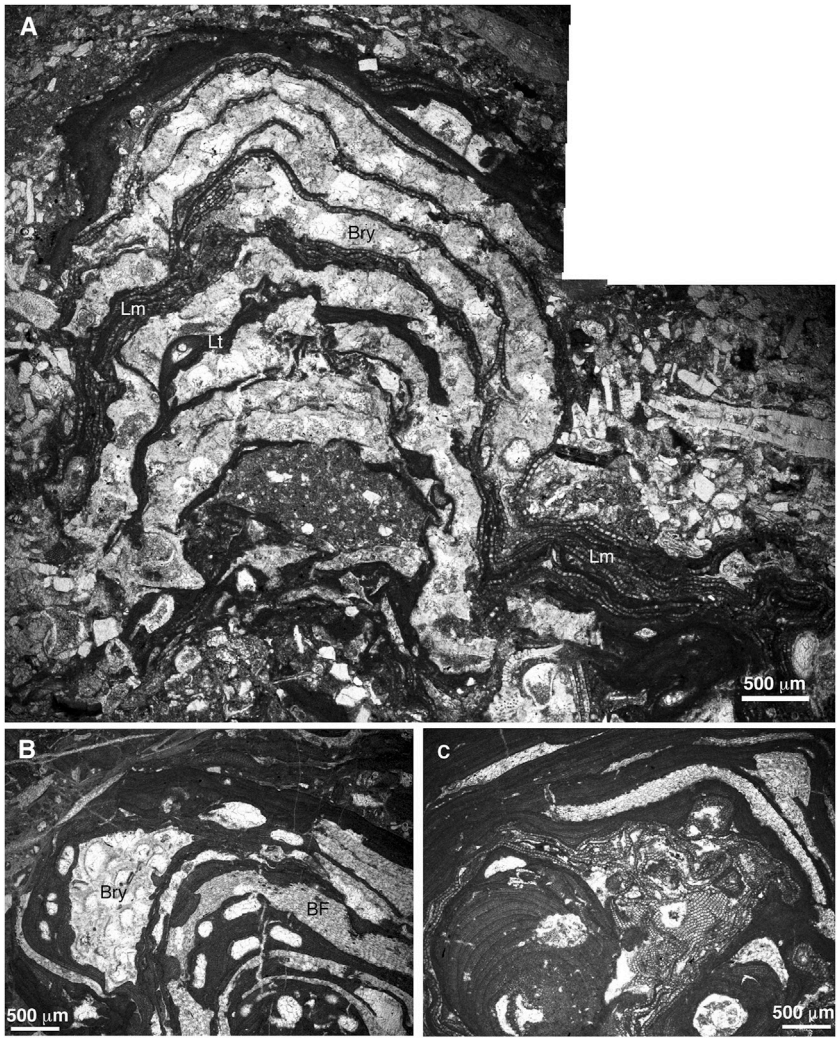

FIGURE 9
Intergrowth of different organisms building up the rhodoliths. **(A)** laminar-encrusting *Lithoporella minus* (Lm) and *Lithothamnion* sp. 1. (Lh) intergrowing with bryozoans (Bry). Sample JOD-5 (Serrezuela de Jódar section). **(B)** *Lithothamnion* sp. 1 growing with bryozoan (Bry) and benthic foraminifera (BF). Sample JOD-8ii (Serrezuela de Jódar section). **(C)** intergrowth of different coralline algal species and BF. Sample JOD-9ii (Serrezuela de Jódar section).

the most abundant are branch fragments of *L. ramosissimum*, as well as crusts of *M. roveretoi* and *Mesophyllum* sp. On occasions, there are fragments of *P.* group *calcareum*, *S.* group *fruticulosus*, and *Sporolithon* sp.

Discussion

Paleoenvironmental interpretation and sedimentary model

In Cerro de la Atalaya and Cerro Hernando–Cerro Fontanar, Serravallian carbonates rest conformably on top of planktonic foraminifera-rich marls and marlstones, which were deposited in basinal settings. The sediments at the transition between the marls and the carbonates represent a gradual facies change, characterized by sediment gravity flow deposits intercalated in the marls.

The overlying channeled packstones are interpreted as sediments reworked during storm events and redeposited offshore in low-relief channels formed by storm rip currents (see below). Similar storm-related deposits were described in Oligocene–Miocene carbonate ramps from southern Italy and Malta (Pedley, 1998). In Cerro Hernando–Cerro Fontanar, channeled beds dominate the Serravallian carbonate successions. Some of them contain abundant rhodoliths and

TABLE 1 Distribution of the coralline algal species identified in the study areas.

	Cerro de la Atalaya	Serrezuela de Jódar	Cerro Hernando-Cerro Fontanar
Mesophyllum roveretoi	X	X	X
Mesophyllum sp	X	X	X
Lithothamnion ramosissimum	X	X	X
Lithothamnion group *corallioides*	X	X	X
Lithothamnion sp. 1	X		X
Lithothamnion sp. 2			X
Phymatolithon group *calcareum*	X		X
Melobesia sp		X	
Spongites group *fruticulosus*	X	X	X
Spongites sp. 1	X		
Spongites sp. 2	X	X	
Spongites sp. 3	X		
Hydrolithon lemoinei	X	X	X
Lithoporella minus	X	X	X
Subterraniphyllum thomasii			X
Sporolithon sp	X	X	X
Unidentifiable geniculate			X

angular lithoclasts, indicating that they were reworked from shallower parts of the ramp.

In the Cerro de la Atalaya and Serrezuela de Jódar areas, densely and loosely packed rhodolith beds overlie the channeled facies. The external algal covers of the rhodoliths are well preserved. In the case of fruticose algal growth forms, they show well-preserved slender branches. In addition, they do not show significant inner erosive surfaces, indicating that rhodoliths grew nearly continuously, without substantial interruptions due to episodic reworking and/or temporal burial that hindered algal growth. These features suggest that rhodoliths formed autochthonous–parautochthonous accumulations (factory facies) in low-energy conditions in the middle ramp. In parallel, in the Mediterranean Sea, present-day rhodolith beds extend from 9 to 150 m of water depth, but they preferentially occur at 30–75-m depth on average (Bressan and Babbini, 2003; Aguilar et al., 2009; Basso et al., 2017; Rendina et al., 2020; Del Río et al., 2022).

The most abundant rhodolith-forming species belong to the order Hapalidiales, *Mesophyllum roveretoi*, *Mesophyllum* sp., and *Lithothamnion ramosissimum*, with accompanying *Phymatolithon* group *calcareum* and *Lithothamnion* group *corallioides*. In the present-day Mediterranean, the genera *Lithothamnion* and *Phymatolithon* preferentially live at tens of meters of water depth, mainly below 30–40-m depth (Basso, 1995, 1998; Peña et al., 2015; Basso et al., 2017; Bracchi et al., 2019; Rendina et al., 2020). Recent *Mesophyllum* species in the Mediterranean have a wide depth range, from a few meters down to 80–100 m (e.g., Fravega and Vannucci, 1989; Athanasiadis 1999; Athanasiadis and Neto, 2010), but they show the highest abundance at 30–50 m (Hamel and Lemoine, 1952; Basso, 1995). Therefore, the dominant coralline algal association indicates that rhodolith beds formed in middle-ramp settings, most likely at about 40–50 m of water depth. The presence of the serpulid *Ditrupa*, a calcified worm typically inhabiting in deep-water settings of shelves (Le Loc'h et al., 2008; Aguirre et al., 2015), is consistent with this paleobathymetric interpretation.

As observed in present-day settings, the movement of rhodoliths in deep-water, low-energy settings could be produced either by the action of vagile organisms (Prager and Gingsburg, 1989; Marrack, 1999; Pereira-Filho et al., 2015; Millar and Gagnon, 2018; O'Connell et al., 2020) or by exceptionally intense storm events (Basso and Tomaselli, 1994; Joshi et al., 2017). Some of these high-energy events would rework sediment from shallow settings, including siliciclastic particles of variable sizes and fragments of different organisms. In our study case, storm events transported particles to deeper settings forming the channeled facies. The abraded fragments of coralline algal branches and other organisms, together with the presence of angular terrigenous granules to pebbles, account for the allochthonous nature of the algae. Therefore, the channeled packstone beds represent more distal deposits formed offshore the rhodolith beds and fed by biogenic components produced in the middle ramp. The homoclinal strata geometry observed in the Cerro Hernando–Cerro Fontanar area can be interpreted as the most distal parts of the middle-ramp or upper outer-ramp growth due to the accumulation of these storm-dominated deposits. In the recent Bay of Naples, Toscano et al. (2006) documented a

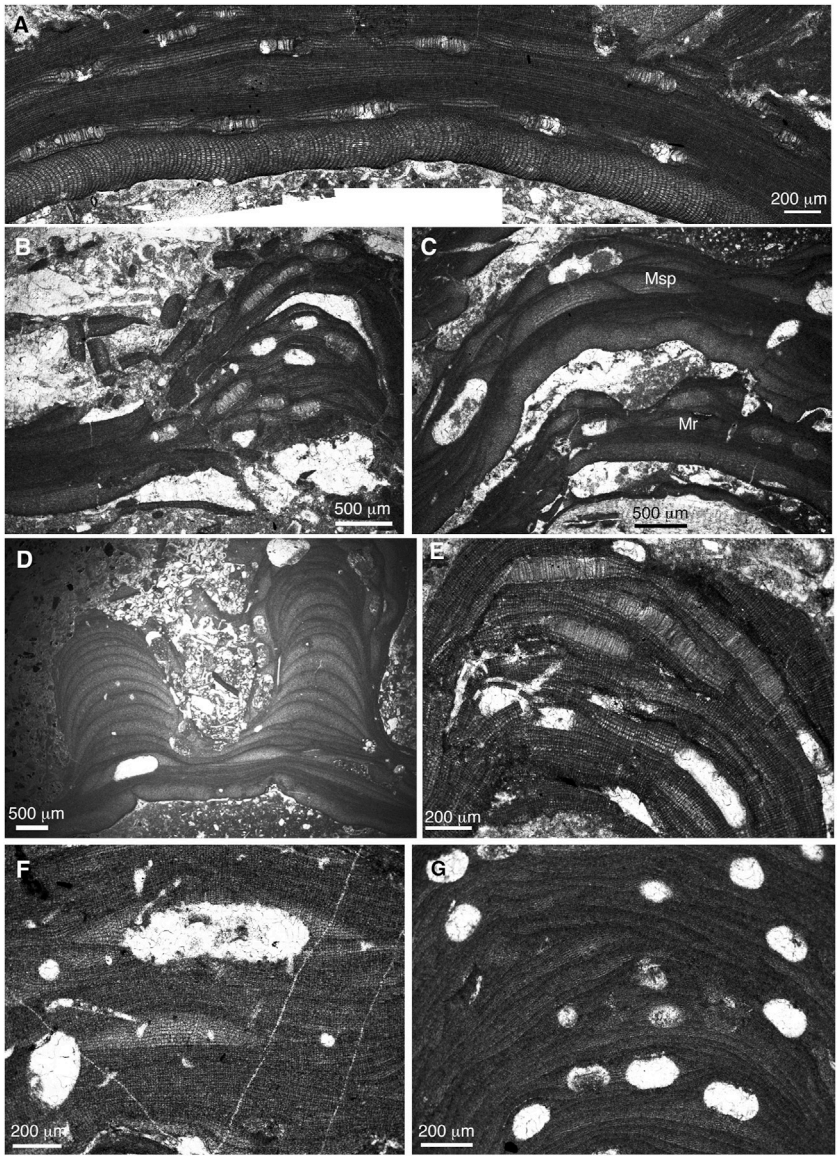

FIGURE 10
(A) encrusting plant of *Mesophyllum roveretoi*. Sample JIM-CR-3 (Cerro de la Atalaya-2 section). **(B)** encrusting–warty thallus of *M. roveretoi*. Sample JOD-7 (Serrezuela de Jódar section). **(C)** superposition of encrusting thalli of *M. roveretoi* (Mr) and *Mesophyllum* sp. (Msp). Sample JIM-CR-4 (Cerro de la Atalaya-2 section). **(D)** fruticose plant of *Mesophyllum* sp. Sample JIM-CR-4 (Cerro de la Atalaya-2 section). **(E)** *Lithothamnion ramosissimum*. Sample JOD-7i (Serrezuela de Jódar section). **(F)** *Lithothamnion* group *corallioides*. Sample JIM-CR-5i (Cerro de la Atalaya-2 section). **(G)** *Phymatolithon* group *calcareum*. Sample JIM-CR-3 (Cerro de la Atalaya-2 section).

similar rhodalgal facies system, characterized by production areas (rhodolith factories) in shallow ramps connected with offshore-transported rhodoliths in channeled facies.

Rhodoliths in the channeled beds are smaller and better sorted (smaller variance in size) than those present in massive rhodolith beds in Cerro de la Atalaya and Serrezuela de Jódar. These differences in rhodolith size among areas represent a sorting of particles in a proximal–distal transect along the ramp. That is, storm events swept rhodoliths from shallower areas on the ramp, and the smaller ones were able to travel longer distances offshore.

Rhodolith beds in the context of the middle Miocene Mediterranean Sea

During the early–middle Miocene, rhodolith-dominated deposits were globally widespread (Halfar and Mutti, 2005).

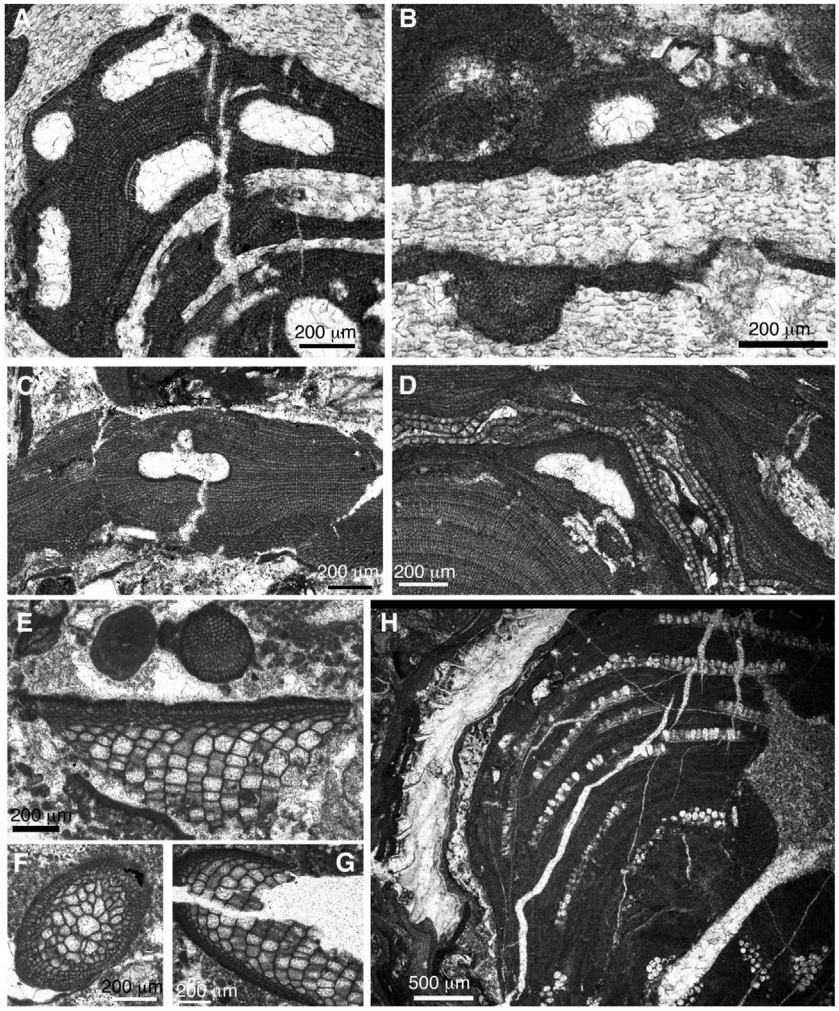

FIGURE 11
(A) *Lithothamnion* sp. 1. Sample JOD-8ii (Serrezuela de Jódar section). **(B)** *Melobesia* sp. Sample JOD-9ii (Serrezuela de Jódar section). **(C)** *Spongites* group *fruticulosus*. Sample CH-1.7 (Cerro Hernando-1 section). **(D)** *Lithoporella minus*. Sample JOD-9ii (Serrezuela de Jódar section). **(E–G)** *Subterraniphyllum thomasii*. Sample CH-3–1 (Cerro Hernando-1 section). **(H)** *Sporolithon* sp. Sample JOD-8 (Serrezuela de Jódar section).

In the Mediterranean, rhodalgal lithofacies peaked during the Langhian, coinciding with the Miocene climatic optimum and the subsequent mid-Miocene climatic transition, up to the Tortonian, when they started to decline (Braga, 2017). The final closure of the Eastern Mediterranean and Indian Ocean connections during the middle Miocene led to significant paleoceanographic changes and a major shift in carbonate producers in the Mediterranean, with coralline algae being one of the major carbonate producers in carbonate platforms (Pedley, 1998; Cornacchia et al., 2021). In addition, tectonics in the Mediterranean generated shallow carbonate platforms with reduced or no terrigenous supply that promoted widespread development of rhodalgal facies (Braga, 2017).

The autochthonous–parautochthonous rhodolith beds in the study area formed in ramps located at the southeastern margin of the Guadalquivir foreland Basin, in a wide passage connecting the Atlantic and the Mediterranean. Coeval deposits occur further to the northeast, in the Prebetic Zone (Braga et al., 2010a). Here, rhodoliths and loose algal branches, dominated by *Lithothamnion*, *Mesophyllum*, and *Sporolithon* species, as well as bryozoan colonies, formed at several tens of meters of water depth in the middle ramp (Braga et al., 2010a). All these Serravallian ramps formed surrounding newly emerged reliefs as a consequence of the Betic Cordillera uplift.

In parallel, during the middle Miocene, major development of rhodolith beds throughout the entire Mediterranean occurred overall in the middle–outer ramps, from 30 to 80 m of water depth (Studenki, 1979, 1988; Scott and Govean, 1985; Bucur and Filipescu, 1994, 2011; Randazzo et al., 1999; BouDagher-Fadel and Clark, 2006; Ruchonnet and Kindler, 2010; Brandano et al.,

2017; Cornacchia et al., 2021). The rhodoliths in these rhodalgal facies are mostly accompanied by large and small benthic foraminifera, mollusks, echinoids, serpulids, and bryozoans (Halfar and Mutti, 2005). On occasions, scattered coral patch-reefs also occur associated with these rhodolith-dominated facies (Pedley, 1979; Bosence and Pedley, 1982; Scott and Govean, 1985; Studencki, 1988; Bucur and Nigorici, 1992; Buchbinder et al., 1993).

Offshore-transported rhodoliths, together with coralline algal debris, have been described in lower–middle Miocene deposits from the Piedmont Basin (NW Italy) (Vannucci, 1980; Fravega and Vannucci, 1982; Fravega et al., 1984, 1993; Basso et al., 2012), southern Apennines (SW Italy) (Checconi et al., 2010; Bassi et al., 2010, 2017), and Sardinia (Murru et al., 2015). In all these cases, reworked rhodoliths are mostly spheroidal in shape and built up by encrusting–laminar and warty plants concentrically arranged. Inferred basinward transport mechanisms are sediment gravity flows (Bassi et al., 2010, 2017; Basso et al., 2012; Murru et al., 2015) and, occasionally, storm currents (Checconi et al., 2010; Bassi et al., 2017). As aforementioned in the study of Serravallian deposits, allochthonous rhodoliths concentrate in wide and shallow channels piled up in continuous carbonate successions formed in the distal middle ramp or upper outer ramp due to storm events. Just in one particular case, in the Cerro Fontanar section, rhodoliths are embedded in a breccia with angular pebbles to cobbles (sometimes boulders). In this case rhodoliths were redeposited due to a high-density mass transport.

In terms of taxonomic composition and species abundance, it is difficult to compare our results with those previously published in other Mediterranean areas due to discrepancies in taxonomic practices and lack of chronologic precision (Braga et al., 2010b). For instance, middle Miocene Paratethys coralline algal assemblages from different areas in Poland are represented by up to 62 species (Studencki, 1979, 1988). Other studies, however, show more conservative figures, indicating approximately 20 coralline algal species from different Mediterranean areas (Vannucci, 1980; Fravega and Vannucci, 1982; Fravega et al., 1984, 1993; Bucur and Filipescu, 1994, 2011; Basso et al., 2012; Hrabovsky, 2019), a species richness similar to that identified in the Betic Serravallian coralline algal assemblages (16 species).

At last, it is worth highlighting the presence of *Subterraniphyllum thomasii* in the Cerro Hernando–Cerro Fontanar area (Figures 11E–G). This species was originally described by Elliott (1957) to refer to a geniculate coralline alga with a "distinctive vey coarse and irregular cell-mesh of the medullary tissue" (Elliott, 1957; p.73). Despite disagreements concerning its thallus organization, either geniculate (Elliott, 1957; Vannucci et al., 2000) or nongeniculate (Bassi et al., 2000), *S. thomasii* has been traditionally cited in upper Eocene–lowermost Miocene (Aquitanian) deposits, with its highest abundance and largest expansion during the Oligocene (Elliott, 1957; Bassi et al., 2000; Vannucci et al., 2000). Nonetheless, this species has been recently cited in middle Eocene deposits of the Betic Cordillera (S Spain), extending its lower stratigraphic range (Aguirre et al., 2020). In this study, we recorded *S. thomasii* in Serravallian carbonate deposits from SE Spain; thus, also widening the stratigraphic range of the species.

Conclusion

The coralline algae of Serravallian (middle Miocene) carbonate deposits cropping out in Jimena and in the vicinity of Jódar (Jaén Province, S Spain) have been studied. They occur forming rhodoliths and as coralline algal debris in two different paleoenvironmental contexts. Autochthonous–parautochthonous rhodolith beds, up to 2-m thick, were originated by the *in situ* production of the algal nodules in the middle ramp, at several tens of meters of water depth. The rhodoliths, averaging 4.5–5 cm in size, are spheroidal in shape and are built up by the intergrowth of laminar-encrusting coralline algae, less frequently warty and fruticose plants, with other encrusting organisms, such as benthic foraminifera, bryozoans, serpulids and, rarely, barnacles. Rhodolith-forming algal species are dominated by Hapalidiales: *Mesophyllum roveretoi*, *Mesophyllum* sp., *Lithothamnion ramosissimum*, and, less frequently, *Lithothamnion* group *corallioides* and *Phymatolithon* group *calcareum*. Accompanying species are *Lithothamnion* sp. 1, *Spongites* group *fruticulosus*, *Spongites* spp., *Lithoporella minus*, *Hydrolithon lemoinei*, and *Sporolithon* sp. It is worth mentioning the presence of a few fragments of *Subterraniphyllum thomasii*, a species previously considered extinct in the early Miocene.

Coralline algae also occur as rhodoliths and algal fragments in channeled beds characterized by rudstone containing angular cobbles to pebbles. Large and small benthic foraminifera, echinoderms, bryozoans, bivalves, serpulids (including *Ditrupa*), and barnacles occur with the algae. Rhodoliths are smaller than those formed in the middle ramp, averaging 2.6 cm in the largest diameter, spherical in shape, and formed by laminar-encrusting algal plants. These rhodoliths are composed of the same species as those described above. The rhodoliths and algal debris in the channeled facies are interpreted as elements formed in the middle ramp and transported offshore by storm currents. These mechanisms of transport produced segregation by rhodolith size; thus, the smaller ones traveled longer distances downslope.

Data availability statement

The original contributions presented in the study are included in the article/supplementary material; further inquiries can be directed to the corresponding author.

Author contributions

All authors listed have made a substantial, direct, and intellectual contribution to the work and approved it for publication.

Funding

We acknowledge the reviewers Brandano and Pereira-Filho for their valuable comments and suggestions that have improved the quality of the article. This study was funded by the research project PGC2018-099391-B-100 of the Spanish Ministerio de Ciencia e Innovación and by the research group RNM-190 of the Junta de Andalucía.

Conflict of interest

The authors declare that the research was conducted in the absence of any commercial or financial relationships that could be construed as a potential conflict of interest.

Publisher's note

All claims expressed in this article are solely those of the authors and do not necessarily represent those of their affiliated organizations, or those of the publisher, the editors, and the reviewers. Any product that may be evaluated in this article, or claim that may be made by its manufacturer, is not guaranteed or endorsed by the publisher.

References

Aguilar, R., Pastor, X., Torriente, A., and García, S. (2009). "Deep-sea coralligenous beds observed with rov on four seamounts in the Western Mediterranean," in *UNEP – MAP – RAC/SPA Proc. 1st Mediterranean symp. on the conservation of the coralligenous and other calcareous bio-concretions*. Editors C. Pergent-Martini and T. Brichet (Tabarka, Tunisia: UNEP - MAP - RAC/SPA, 148–150.

Aguirre, J., Braga, J. C., and Bassi, D. (2017). "Rhodoliths and rhodolith beds in the rock record," in *Rhodolith/maërl beds: A global perspective*. Editors R. Riosmena-Rodríguez, W. Nelson, and J. Aguirre (Basel, Switzerland): Springer Intern. Publ.), 105–138.

Aguirre, J., Braga, J. C., Pujalte, V., Orue-Etxebarria, X., Salazar-Ortiz, E., Rincón-Martínez, D., et al. (2020). Middle Eocene rhodoliths from tropical and mid-latitude regions. *Diversity* 12, 117. doi:10.3390/d12030117

Aguirre, M., J., Braga, J. C., Martín, J. M., Puga-Bernabéu, Á., Pérez-Asensio, J. N., Sánchez-Almazo, I. M., et al. (2015). An enigmatic kilometer-scale concentration of small mytilids (Late Miocene, Guadalquivir Basin, S Spain). *Palaeogeogr. Palaeoclimatol. Palaeoecol.* 436, 199–213. doi:10.1016/j.palaeo.2015.07.015

Athanasiadis, A. (1999). *Mesophyllum macedonis*, nov. sp. (Rhodophyta, Corallinales), a putative Tethyan relic in the north Aegean Sea. *Eur. J. Phycol.* 34, S0967026299002103–S0967026299002252. doi:10.1017/s0967026299002103

Athanasiadis, A., and Neto, A. I. (2010). On the occurrence of *Mesophyllum expansum* (Philippi) Cabioch et Mendoza (Melobesioideae, Corallinales, Rhodophyta) in the Mediterranean Sea, the Canary Isles and the Azores. *Bot. Mar.* 53, 333–341. doi:10.1515/bot.2010.042

Baccelle, L., and Bosellini, A. (1956). Diagrammi per la stima visiva della composizione percentuale nelle rocche sedimentary. *Ann. Univ. Ferrara (Nuova Ser.), Sez. 9, Sc. Geol. Paleontol.* 1, 59–62.

Bassi, D., Carannante, G., Checconi, A., Simone, L., and Vigorito, M. (2010). Sedimentological and palaeoecological integrated analysis of a Miocene channelized carbonate margin, Matese Mountains, Southern Apennines, Italy. *Sediment. Geol.* 230, 105–122. doi:10.1016/j.sedgeo.2010.07.002

Bassi, D., Iryu, Y., Humblet, M., Matsuda, H., Machiyama, H., Sasaki, K., et al. (2012). Recent macroids on the Kikai-jima shelf, Central Ryukyu Islands, Japan. *Sedimentology* 59, 2024–2041. doi:10.1111/j.1365-3091.2012.01333.x

Bassi, D., Simone, L., and Nebelsik, J. H. (2017). "Re-sedimented rhodliths in channelized depositional systems," in *Rhodolith/maërl beds: A global perspective*. Editors R. Riosmena-Rodríguez, W. Nelson, and J. Aguirre (Basel, Switzerland): Springer Intern. Publ.), 139–167.

Bassi, D., Woelkerling, W. J., and Nabelsik, J. H. (2000). Taxonomic and biostratigraphical re-assessments of *Subterraniphyllum* Elliott (Corallinales, Rhodophyta). *Palaeontology* 43, 405–425. doi:10.1111/j.0031-0239.2000.00133.x

Basso, D., Babbini, L., Ramos-Esplá, A. A., and Salomidi, M. (2017). "Mediterranean rhodolith beds," in *Rhodolith/maërl beds: A global perspective*. Editors R. Riosmena-Rodríguez, W. Nelson, and J. Aguirre (Basel, Switzerland): Springer Intern. Publ.), 281–298.

Basso, D. (1998). Deep rhodolith distribution in the Pontian Islands, Italy: A model for the paleoecology of a temperate sea. *Palaeogeogr. Palaeoclimatol. Palaeoecol.* 137, 173–187. doi:10.1016/s0031-0182(97)00099-0

Basso, D., Quaranta, F., Vannucci, G., and Piazza, M. (2012). Quantification of the coralline carbonate from a Serravallian rhodolith bed of the Tertiary Piedmont Basin (Stazzano, Alessandria, NW Italy). *Geodiversitas* 34, 137–149. doi:10.5252/g2012n1a8

Basso, D. (1995). Study of living calcareous algae by a paleontological approach: The non-geniculate corallinaceae (Rhodophyta) of the soft bottoms of the Tyrrhenian Sea (Western Mediterranean). The genera *Phymatolithon* Foslie and *Mesophyllum* Lemoine. *Riv. It. Paleontol. Strat.* 100, 575–596.

Basso, D., and Tomaselli, V. (1994). "Palaeoecological potentiality of rhodoliths: A Mediterranean case history, in studies on ecology and paleoecology of benthic communities,"*Boll. Soc. Paleontol. Ital. Spec*. Editors L. Matteucci, M. G. Carboni, and J. S. Pignatti (Mucchi, Modena: Boll. Soc. Paleontol. Ital.), 2, 17–27.

Berasátegui, X., Banks, C. J., Puig, C., Taberner, C., Waltham, D., and Fernàndez, M. (1998). "Lateral diapiric emplacement of Triassic evaporites at the southern margin of the Guadalquivir Basin, Spain," in *Cenozoic foreland basins of western europe*. Editors A. Mascle, C. Puigdefàbregas, H. P. Luterbacher, and M. Fernàndez, Geol. Soc. London (London: Sp. Publ.), 134, 49–68.

Bosence, D. W. J., and Pedley, H. M. (1982). Sedimentology and palaeoecology of a Miocene coralline algal biostrome from the Maltese Islands. *Palaeogeogr. Palaeoclimatol. Palaeoecol.* 38, 9–43. doi:10.1016/0031-0182(82)90062-1

BouDagher-Fadel, M., and Clark, G. N. (2006). Stratigraphy, paleoenvironment and paleogeography of maritime Lebanon: A key to Eastern Mediterranean Cenozoic history. *Stratigraphy* 3, 1–38.

Bracchi, V. A., Angeletti, L., Marchese, F., Taviani, M., Cardone, F., Hajdas, I., et al. (2019). A resilient deep-water rhodolith bed off the Egadi archipelago (Mediterranean Sea) and its actuopaleontological significance. *Alp. Medit. Quater.* 32, 131–150. doi:10.26382/AMQ.2019.09

Braga, J. C., Bassi, D., and Piller, W. E. (2010b). "Paleoenvironmental significance of Oligocene-Miocene coralline red algae – A review," in *Carbonate systems during the Oligocene-Miocene climatic transition*. Editors M. Mutti, W. E. Piller, and C. Betzler (IAS Spec. Publ.), 42, 165–182.

Braga, J. C., Martín, J. M., Aguirre, J., Baird, C. D., Grunnaleite, I., Jensen, N. B., et al. (2010a). Middle-Miocene (Serravallian) temperate carbonates in a seaway connecting the Atlantic Ocean and the Mediterranean Sea (north Betic Strait, S Spain). *Sediment. Geol.* 225, 19–33. doi:10.1016/j.sedgeo.2010.01.003

Braga, J. C. (2017). "Neogene rhodoliths in the Mediterranean basins," in *Rhodolith/maërl beds: A global perspective*. Editors R. Riosmena-Rodríguez, W. Nelson, and J. Aguirre (Basel, Switzerland: Springer Intern. Publ.), 169–193.

Brandano, M., Cornacchia, I., and Tomassetti, L. (2017). Global versus regional influence on the carbonate factories of Oligo-Miocene carbonate platforms in the Mediterranean area. *Mar. Pet. Geol.* 87, 188–202. doi:10.1016/j.marpetgeo.2017.03.001

Bressan, G., and Babbini, L. (2003). Corallinales del Mar Mediterraneo: Guida Alla Determinazione. *Biol. Mar. Medit.* 10 (Suppl. 2), 1–237.

Buchbinder, B., Martinotti, G. M., Siman-Tov, R., and Zilberman, E. (1993). Temporal and spatial relationships in Miocene reef carbonates in Israel. *Palaeogeogr. Palaeoclimatol. Palaeoecol.* 101, 97–116. doi:10.1016/0031-0182(93)90154-b

Bucur, I. I., and Filipescu, S. (2011). "Middle Miocene red algae from Lopadea Veche (western border of the Transylvanian Basin)," in *Calcareous algae from Romanian Carpathians*. Editors I. I. Bucur, and E. Sasaran (Cluj-Napoca, Romania: Press University Clujeana), 115–122.

Bucur, I. I., and Filipescu, S. (1994). Middle Miocene red algae from the Transylvanian Basin (Romania). *Beitr. Paläont.* 19, 39–47.

Bucur, I. I., and Nigorici, E. (1992). Calcareous algae from the Sarmatian deposits in the Smileu Basin (Romania). *Stud. Univ. Babes-Bolyai, Geol.* 37, 3–7.

Checconi, A., Bassi, D., Monaco, P., and Carannante, G. (2010). Re-deposited rhodoliths in the middle Miocene hemipelagic deposits of Vitulano (southern Apennines, Italy): Coralline assemblage characterization and related trace fossils. *Sediment. Geol.* 225, 50–66. doi:10.1016/j.sedgeo.2010.01.001

Cornacchia, I., Brandano, M., and Agostini, S. (2021). Miocene paleoceanographic evolution of the Mediterranean area and carbonate production changes: A review. *Earth. Sci. Rev.* 221, 103785. doi:10.1016/j.earscirev.2021.103785

De Río, J., Angelo Ramos, D., Sánchez-Tocino, L., Peñas, J., and Braga, J. C. (2022). The Punta de la Mona rhodolith bed: Shallow-water Mediterranean rhodoliths (Almuñecar, Granada, southern Spain). *Front. Earth Sci.* 10, 884685. doi:10.3389/feart.2022.884685

Elliott, G. F. (1957). *Subterraniphyllum*, a new Tertiary calcareous alga. *Palaeontology* 1, 73–75.

Fravega, P., Giammarino, S., and Vannucci, G. (1984). Episodi ad «algal balls» e loro significato al passaggio arenarie di Serravalle-Marne di S. Agata fossili a nord di Gavi (bacino Terziario del Piemonte). *Atti Soc. Tosc. Sci. Nat. Ser. A* 91, 1–20.

Fravega, P., Piazza, M., and Vannucci, G. (1993). "Importance and significance of the rhodolithic bodies in the miocenic sequences of Tertiary Piedmont Basin," in *Studies on fossil benthic algae*. Editors F. Barattolo, P. De Castro, and M. Parente (Ital., Sp.: Boll. Soc. Paleontol), 1, 197–210.

Fravega, P., and Vannucci, G. (1989). Rhodophycee calcaree nelle biocenosi del Golfo di Calvi (Corsica). *Atti 3° Simp. Ecol. Paleoecol. Com. Bent.*, 711–727.

Fravega, P., and Vannucci, G. (1982). Significato e caratteristiche degli episodi e rhodoliti al «top» del Serravalliano tipo. *Geol. Romana* 21, 705–715.

Galindo-Zaldívar, J., Ruano, P., Jabaloy, A., and López-Chinaco, M. (2000). Kinematics of faults between subbetic units during the Miocene (central sector of the Betic Cordillera). *Comptes Rendus de l'Academie. des Sci. - Ser. IIA - Earth Planet. Sci.* 331, 811–816. doi:10.1016/s1251-8050(00)01484-1

García-Castellanos, D., Fernàndez, M., and Torné, M. (2002). Modeling the evolution of the Guadalquivir foreland basin (southern Spain). *Tectonics* 21, 9-1–9-17. doi:10.1029/2001TC001339

García-Hernández, M., López-Garrido, A. C., Rivas, P., Sanz de Galdeano, C., and Vera, J. A. (1980). Mesozoic palaeogeographic evolution of the External Zones of the Betic Cordillera. *Geol. Mijnbou* 59, 155–168.

García-Tortosoa, F. J., Sanz de Galdeano, C., Sánchez-Gómez, M., and Alfaro, P. (2008). Tectónica reciente en el frente de cabalgamiento bético. Las deformaciones de Jimena y Bedmar (Jaén). *Geogaceta* 44, 59–62.

Halfar, J., and Mutti, M. (2005). Global dominance of coralline red-algal facies: A response to Miocene oceanographic events. *Geol.* 33, 481. doi:10.1130/g21462.1

Hamel, G., and Lemoine, M. P. (1952). Corallinacées de France et d'Afrique du Nord. *Arch. Mus. Hist. Nat. Paris Sér.* 7, 15–136.

Hottinger, L. (1983). "Neritic macroid genesis, an ecological approach," in *Coated grains*. Editor T. M. Peryt (Berlin: Springer-Verlag), 38–55.

Hrabovsky, J. (2019). Reproductive phases of Miocene algae from central Paratethys and their bearing on systematics. *Acta Palaeontol. Pol.* 64, 417–439. doi:10.4202/app.00579.2018

Jeong, S. Y., Nelson, W. A., Sutherland, J. E., Peña, V., Le Gall, L., Diaz-Pulido, G., et al. (2021). Corallinapetrales and Corallinapetraceae: A new order and new family of coralline red algae including *Corallinapetra gabriellii* comb. nov. *J. Phycol.* doi:10.1111/jpy.13115-20-107

Joshi, S., Duffy, G. P., and Brown, C. (2017). Mobility of maerl-siliciclastic mixtures: Impact of waves, currents and storm events. *Estuar. Coast. Shelf Sci.* 189, 173–188. doi:10.1016/j.ecss.2017.03.018

Le Loc'h, F., Hily, C., and Grall, J. (2008). Benthic community and food web structure on the continental shelf of the Bay of Biscay (North Eastern Atlantic) revealed by stable isotopes analysis. *J. Mar. Syst.* 72, 17–34. doi:10.1016/j.jmarsys.2007.05.011

Marrack, E. (1999). The relationship between water motion and living rhodolith beds in the southwestern Gulf of California, Mexico. *Palaios* 14, 159. doi:10.2307/3515371

Martín, J. M., Braga, J. C., Aguirre, J., and Puga-Bernabéu, Á. (2009). History and evolution of the North-Betic Strait (Prebetic Zone, Betic Cordillera): A narrow, early Tortonian, tidal-dominated, Atlantic–Mediterranean marine passage. *Sediment. Geol.* 216, 80–90. doi:10.1016/j.sedgeo.2009.01.005

Meulenkamp, J. E., and Sissingh, W. (2003). Tertiary palaeogeography and tectonostratigraphic evolution of the Northern and Southern Peri-Tethys platforms and the intermediate domains of the African–Eurasian convergent plate boundary zone. *Palaeogeogr. Palaeoclimatol. Palaeoecol.* 196, 209–228. doi:10.1016/s0031-0182(03)00319-5

Millar, K. R., and Gagnon, P. (2018). Mechanisms of stability of rhodolith beds: Sedimentological aspects. *Mar. Ecol. Prog. Ser.* 594, 65–83. doi:10.3354/meps12501

Murru, M., Bassi, D., and Simone, L. (2015). Displaced/re-worked rhodolith deposits infilling parts of a complex Miocene multistorey submarine channel: A case history from the Sassari area (Sardinia, Italy). *Sediment. Geol.* 326, 94–108. doi:10.1016/j.sedgeo.2015.07.001

O'Connell, L. G., James, N. P., Harvey, A. S., Luick, J., Bone, Y., Shepherd, S. A., et al. (2020). Reevaluation of the inferred relationship between living rhodolith morphologies, their movements, and water energy: Implications for interpreting paleoceanographic conditions. *Palaios* 35, 543–556.

Palcu, D. V., Patina, I. S., Şandric, I., Lazarev, S., Vasiliev, I., Stoica, M., et al. (2011). Late Miocene megalake regressions in Eurasia. *Sci. Rep.* 11, 11471. doi:10.1038/s41598-021-91001-z

Pedley, H. M. (1998). "A review of sediment distributions and processes in Oligo-Miocene ramps of southern Italy and Malta (Mediterranean divide),". Editors V. P. Wright, and T. P. Burchette. *Carbonate ramps* (London, United Kingdom: Geol. Soc. London, Sp. Publ.), 149, 163–179.

Pedley, H. M. (1979). Miocene bioherms and associated structures in the upper coralline limestone of the Maltese islands: Their lithification and palaeoenvironment. *Sedimentology* 26, 577–591. doi:10.1111/j.1365-3091.1979.tb00930.x

Pedrera, A., Marín-Lechado, C., Martos-Rosillo, S., and Roldán, F. J. (2012). Curved fold-and-thrust accretion during the extrusion of a synorogenic viscous allochthonous sheet: The Estepa Range (External Zones, western Betic Cordillera, Spain). *Tectonics* 31, TC4013. doi:10.1029/2012TC003119

Peña, V., Pardo, C., López, L., Carro, B., Hernández-Kantun, J., Adey, W. H., et al. (2015). *Phymatolithon lusitanicum* sp. nov. (Hapalidiales, Rhodophyta): The third most abundant maerl-forming species in the Atlantic Iberian peninsula. *Cryptogam. Algol.* 36, 429–459. doi:10.7872/crya/v36.iss4.2015.429

Peña, V., Vieira, C., Braga, J. C., Aguirre, J., Rösler, A., Baele, G., et al. (2020). Radiation of the coralline red algae (Corallinophycidae, Rhodophyta) crown group as inferred from a multilocus time-calibrated phylogeny. *Mol. Phylogenet. Evol.* 150, 106845. doi:10.1016/j.ympev.2020.106845

Perconing, E. (1960-62). "Sur la constitution géologique de L'Andalousie occidentale en particuler du bassin du Guadalquivir (Espagne méridionale),". *Livre a la Mémorie du Professeur Paul Fallot* Editor M. Durand Delga. (Tome: Soc. Géol. Fr.), 1, 229–256.

Pereira-Filho, G. H., Veras, P. C., Francini-Filho, R. B., de Moura, R. L., Pinheiro, H. T., Gibran, F. Z., et al. (2015). Effects of the sand tilefish *Malacanthus plumieri* on the structure and dynamics of a rhodolith bed in the Fernando de Noronha Archipelago, tropical West Atlantic. *Mar. Ecol. Prog. Ser.* 541, 65–73.

Prager, E. J., and Gingsburg, R. N. (1989). Carbonate nodule growth on Florida's outer shelf and its implications for fossil interpretations. *Palaios* 4, 310. doi:10.2307/3514555

Randazzo, A. F., Müller, P., Lelkes, G., Juhász, E., and Hámor, T. (1999). Cool-water limestones of the Pannonian basinal system, middle Miocene, Hungary. *J. Sediment. Res.* 69, 283–293. doi:10.2110/jsr.69.283

Rendina, F., Kaleb, S., Caragnano, A., Ferrigno, F., Appollino, L., Donnarumma, L., et al. (2020). Distribution and characterization of deep rhodolith beds off the Campania coast (SW Italy, Mediterranean Sea). *Plants* 9, 985. doi:10.3390/plants9080985

Rodríguez-Fernández, J., Azor, A., and Azañón, J. M. (2012). "The Betic intramontane basins (SE Spain): Stratigraphy, subsidence, and tectonic history," in *Tectonics of sedimentary basins: Recent advances*. Editors C. Busby, and A. Azor (Blackwell Publishing Ltd.), Hoboken, New Jersey, United States, 461–479.

Rodríguez-Fernández, J., Roldán, F. J., Azañón, J. M., and García-Cortés, A. (2013). El colapso gravitacional del frente orogénico alpino en el Dominio Subbético

durante el Mioceno medio-superior: El complejo extensional Subbético. *Bol. Geol. Min. Esp.* 124, 477–504.

Rögl, F. (1998). Palaeogeographic considerations for Mediterranean and Paratethys seaways (Oligocene to Miocene). *Ann. Natur. Mus. Wien* 99, 279–310.

Roldán, F. J. (1995). *Evolución neógena de la Cuenca del Guadalquivir*. Spain: Univ. Granada. Ph.D. Thesis.

Roldán, F. J. (2008). "Las unidades olistostrómicas del antepaís Bético," in *Contextos geológicos españoles. Una aproximación al patrimonio geológico español de relevancia internacional*. Editor A. García-Cortés (Madrid): IGME), 124–132.

Ruchonnet, C., and Kindler, P. (2010). "Facies models and geometries of the Ragusa platform (SE Sicily, Italy) near the Serravallian–Tortonian boundary,"*Carbonate systems during the Oligocene-Miocene climatic transition*. Editors M. Mutti, W. E. Piller, and C. Betzler (IAS Spec. Publ.), 42, 71–88.

Ruiz-Constán, A., Pedrera, A., Galindo-Zaldívar, J., Pous, J., Arzate, J., Roldán-Garcia, F. J., et al. (2012). Constraints on the frontal crustal structure of a continental collision from an integrated geophysical research: The central-western Betic Cordillera (SW Spain). *Geochem., Geophys., Geosyst.* 13, Q08012. doi:10.1029/2012GC004153

Sanz de Galdeano, C., García-Tortosa, F. J., and Peláez, J. A. (2013). Estructura del Prebético de Jaén (sector de Bedmar). Su relación con el avance del Subbético y con fallas en el basamento. *Rev. Soc. Geol. Esp.* 26, 55–68.

Scott, R. W., and Govean, F. M. (1985). Early depositional history of a rift basin: Miocene in Western Sinai. *Palaeogeogr. Palaeoclimatol. Palaeoecol.* 52, 143–158. doi:10.1016/0031-0182(85)90035-5

Studencki, W. (1988). Facies and sedimentary environment of the Pinczow limestones (middle Miocene; Holy Cross Mountains, Central Poland). *Facies* 18, 1–25. doi:10.1007/bf02536793

Studencki, W. (1979). Sedimentation of algal limestones from Busko-Spa environs (middle Miocene, Central Poland). *Palaeogeogr. Palaeoclimatol. Palaeoecol.* 27, 155–165. doi:10.1016/0031-0182(79)90098-1

Toscano, F., Vigliotti, M., and Simone, L. (2006). "Variety of coralline algal deposits (rhodalgal facies) from the Bays of Naples and Pozzuoli (northern Tyrrhenian Sea, Italy)," *Cool-water carbonates: Depositional systems and palaeoenvironmental controls*. Editors H. M. Pedley and G. Carannante (London, United Kingdom: Geol. Soc., London, Sp. Publ.), 255, 85–94.

Vannucci, G., Basso, D., and Fravega, P. (2000). New observations on the anatomy of the fossil calcareous alga *Subterraniphyllum* Elliott. *Riv. It. Paleotol. Strat.* 106, 237–246.

Vannucci, G. (1980). Prime indagini sulle rhodoliti del "Serravalliano" della Valle Scrivia. *Quater. Ist. Geol. Univ. Genova* 1, 59–64.

Wade, B. S., Pearson, P. N., Berggren, W. A., and Pälike, H. (2011). Review and revision of Cenozoic tropical planktonic foraminiferal biostratigraphy and calibration to the geomagnetic polarity and astronomical time scale. *Earth. Sci. Rev.* 104, 111–142. doi:10.1016/j.earscirev.2010.09.003

frontiers | Frontiers in Earth Science

TYPE Original Research
PUBLISHED 30 August 2022
DOI 10.3389/feart.2022.961632

OPEN ACCESS

EDITED BY
Olev Vinn,
University of Tartu, Estonia

REVIEWED BY
Ergun Taskin,
Celal Bayar University, Turkey
Rodrigo Carvalho,
Rio de Janeiro Botanical Garden, Brazil

*CORRESPONDENCE
Daniela Basso,
daniela.basso@unimib.it

SPECIALTY SECTION
This article was submitted to Quaternary Science, Geomorphology and Paleoenvironment, a section of the journal Frontiers in Earth Science

RECEIVED 05 June 2022
ACCEPTED 22 July 2022
PUBLISHED 30 August 2022

CITATION
Basso D, Bracchi VA, Bazzicalupo P, Martini M, Maspero F and Bavestrello G (2022), Living coralligenous as geo-historical structure built by coralline algae.
Front. Earth Sci. 10:961632.
doi: 10.3389/feart.2022.961632

Living coralligenous as geo-historical structure built by coralline algae

Daniela Basso[1,2]*, Valentina Alice Bracchi[1,2], Pietro Bazzicalupo[1], Marco Martini[3], Francesco Maspero[3] and Giorgio Bavestrello[4]

[1]Department of Earth and Environmental Sciences, University of Milano-Bicocca, Milano, Italy, [2]Conisma Local Research Unit, University of Milano-Bicocca, Milano, Italy, [3]Department of Materials Science, University of Milano-Bicocca, Milano, Italy, [4]DiSTAV, Università di Genova, Genova, Italy

The most important reef of the Mediterranean is the Coralligène (Coralligenous = C), including several types of calcareous algal-invertebrate build-ups growing in normal open marine conditions. We analyzed and compared two C samples from the Ligurian Sea developed in different environmental settings: 1) off Portofino on a rocky cliff, at a depth of about 40 m and 2) in front of Bogliasco, on a sub-horizontal substrate at a depth of 10 m. The maximum AMS radiocarbon dating provided an older age for Bogliasco (about 5 ka BP) than for Portofino (about 3.6 ka BP), and the mean accumulation rate of the Portofino build-up (about 80 μm y^{-1}) was found to be higher than the one in Bogliasco (about 65 μm y^{-1}). The different sides of each build-up showed a remarkable heterogeneity in the dominant cover by living organisms, and the comparison between the two build-ups highlighted an evident diversity in their taxonomic composition and structure, although crustose coralline algae (CCA) are the dominant framework builder and major autogenic ecosystem engineers at both localities, in the present as in the past millennia. Other major components of the structure are bryozoans and serpulids, and an important role is played by sediment filling. In Bogliasco, extreme climate events and major peaks of fine matrix and terrigenous grains are observed, lithologically related to the drainage basin of the Poggio creek and associated with charophyte occurrence and reduced CCA abundance. The occurrence of the rare *Sporolithon ptychoides* was observed both in Portofino at about 750 BCE and in Bogliasco. These *Sporolithon* phases are likely related to warm and humid spells punctuating the Holocene climate fluctuations in the Ligurian Sea. Because coralline algae are confirmed to be the most important habitat engineer of the Mediterranean reefs, they deserve more attention in the framework of any monitoring initiative aimed at C management and conservation.

KEYWORDS

coralligenous, algal reef, coralline algae, *Sporolithon*, Ligurian Sea, extreme climate events, Holocene

1 Introduction

Coralline algae are autogenic habitat engineers responsible for the formation of intertidal algal rims, subtidal rhodoliths, and algal reefs known in the Mediterranean as Coralligène (Coralligenous = C). Coralligenous is known in the Mediterranean as a hard biogenic substrate mainly produced by the superposition of several generations of calcareous red algae, living in dim light conditions. In the framework of marine benthic bionomics, C is identified as the ecological climax stage for the Mediterranean circalittoral zone (Pérès, 1982), although further studies recognized also C in dim-light infralittoral settings (Ballesteros, 2006; Bracchi et al., 2016).

The C bio-constructions grew at a water depth of 20–140 m (Laborel 1961, 1987) by *in situ* superposition of carbonate skeletal material, produced during the last Holocene sea level rise (Sartoretto et al., 1996). Coralligenous is a heterogeneous habitat (Sartoretto, 2017) and a prominent biogeological system of the Mediterranean seascape (Ballesteros, 2006; Casas-Guell et al., 2016; Bracchi et al., 2017; Pierdomenico et al., 2021), a unique hot spot of marine biodiversity (Laubier, 1966; Ballesteros, 2006; Di Iorio et al., 2021; Piazzi et al., 2021), a major carbonate factory and storage (Canals and Ballesteros, 1997; Cebrian et al., 2000; Marchese et al., 2020), and a target of EU environmental protection, due to the ecosystem services that it provides and its sensitivity to direct and indirect human impacts, including the ongoing climate change (among others: Balata et al., 2005; Martin and Gattuso, 2009; Piazzi et al., 2011; Gatti et al., 2015; Montefalcone et al., 2017; Costanzo et al., 2021).

C includes several types of open marine algal-invertebrate reefs, a few centimeters to several meters in thickness, which can be described in terms of benthic zonation, build-up morphology, type of basal substrate, style of development, and components (Pérès 1982; Laborel 1987; Bracchi et al., 2017; Bracchi et al., 2019). Several species of calcareous red algae Corallinophycidae (crustose coralline algae, CCA) and some calcareous Peyssonneliales are characteristic habitat-engineers (Laubier 1966; Pérès 1982; Ballesteros, 2006; Rosso and Sanfilippo 2009; Ponti et al., 2011; Boudouresque et al., 2016; De Jode et al., 2019) and the volumetrically most important fossil framework builders in C (Basso et al., 2007; Titschack et al., 2008; Bracchi et al., 2014, 2016, 2022). Other important builders are bryozoans, polychaetes, and cnidarians (Ballesteros 2006; Bellan-Santini et al., 2007; Corriero et al., 2019), and bryozoans producing large, long-lived, habitat-forming colonies may be primary builders (Cocito, 2004; Di Geronimo et al., 2002; Novosel et al., 2004; Rosso and Sanfilippo 2009). The coralligenous habitat has been defined as an eco-ethological crossroads and an assemblage of several communities rather than a unique community (Sartoretto, 2017), and several different associations and facies have been described under the term "coralligenous" (Ballesteros, 2006; Casas-Güell et al., 2016; Sartoretto, 2017; Corriero et al., 2019). The most obvious and coarse distinction is between C developing on rocky walls and C developing from subhorizontal substrates (sedimentary or rocky) (Pérès 1982; Bracchi et al., 2017; Sartoretto, 2017; Piazzi et al., 2009; Piazzi et al., 2022). The interplay of biotic and abiotic factors (mainly light exposure, availability of trophic resources, substrate exposure, sedimentation rate, freshwater influence, and biotic interactions) controls the several facies of C, unevenly distributed along geographical and depth gradients (among others: Gili and Ros 1985; Sartoretto, 1994; Garrabou et al., 2002; Di Geronimo et al., 2001; Virgilio et al., 2006; Casellato and Stefanon, 2008; Ponti et al., 2011; Falace et al., 2015; Çinar et al., 2020).

Our knowledge about C accumulation rate and age, although very fragmentary (Sartoretto et al., 1996; Bertolino et al., 2017a; Sartoretto, 2017), suggests that present-day conspicuous algal build-ups required thousands of years to form, depending on favorable combinations of biologically mediated carbonate precipitation by algal engineers, persistence of compatible oceanographic conditions, and sedimentation rate, in turn controlled by the overarching geological setting. Radiocarbon dating has revealed that the accumulation rate of the C build-ups is very low (0.006–0.83 mm y^{-1}). It has been suggested that after 6,000 years BP, the accretion rate of deep C, below a depth of 60 m, could have been very low to nil, possibly because of the increasingly unfavorable environmental conditions during Holocene sea level rise (Sartoretto et al., 1996) or the human pressures which strongly affected the species living on the surface of the biogenic build-ups (Montefalcone et al., 2017; Zunino et al., 2019; Gómez-Gras et al., 2021). For example, the increase in turbidity, burial, and sediment deposition represents threats to coralligenous assemblages, leading to a shift in the community structure and influencing its spatial and temporal variability (Bourcier, 1986; Balata et al., 2005).

Increasing atmospheric CO_2 concentration is leading to global warming, marine pH decrease, and lower carbonate saturation state (Sarmiento et al., 1998; IPCC 2022). High-Mg calcite CCA and aragonite skeletal remains of invertebrates are the most soluble carbonates to respond to ocean acidification (Hall-Spencer et al., 2008; Kuffner et al., 2008; Rodolfo-Metalpa et al., 2010; Basso, 2012), and in the meantime, both chemical and biogenic erosion of marine carbonates will be enhanced by marine acidification (Wisshak et al., 2014). Predictions of future habitat evolution require knowledge of former climates and can be modeled on the basis of long time-series and information recorded in the recent geological past (Alverson and Kull 2003; Luterbacher et al., 2012). The coralline-engineered habitats identified as C are structured by a range of physical forces and geobiological processes over geological times and are complex paleoenvironmental archives (Nalin et al., 2006; Titschack et al., 2008; Bracchi et al., 2014, 2016). The aim of this study is to assess the contribution of calcareous autogenic engineers to the present-day Ligurian C growing on rocky wall vs.

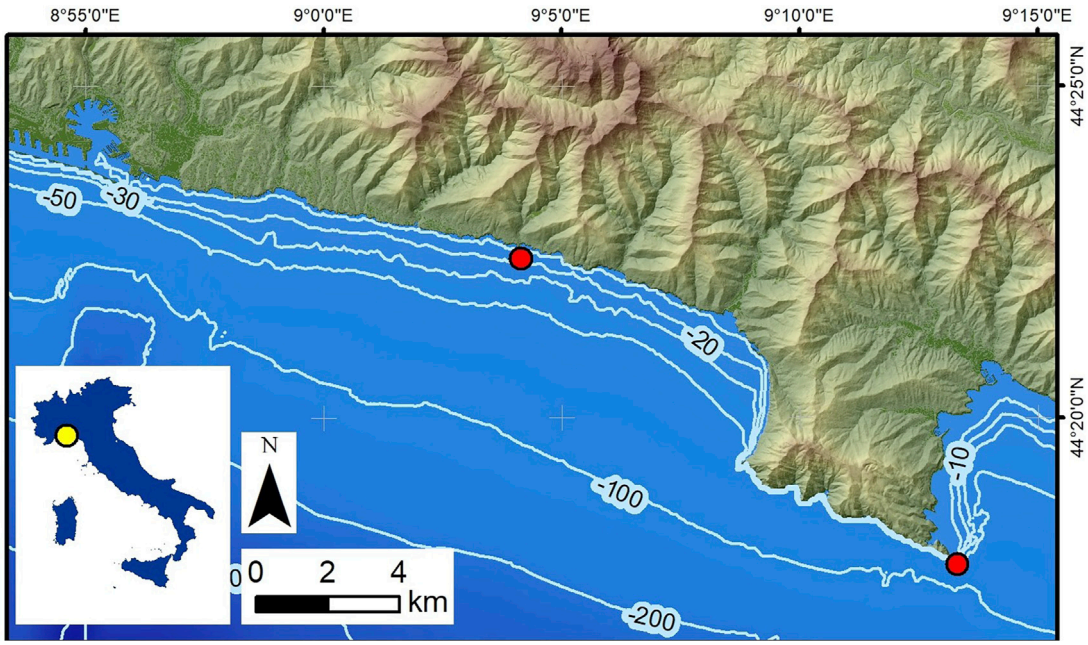

FIGURE 1
Locations of the two sampled sites (red circles). Portofino is bottom right, and Bogliasco is in the centre.

sub-horizontal substrate, to define its age and mean accumulation rate, and to explore the response of C structural composition and major calcareous bio-engineers to climate and oceanographic Holocene changes potentially recorded in the build-ups.

2 Materials and methods

Coralligenous build-ups were sampled by SCUBA diving from two localities along the Ligurian coast (NW Italy) (Figure 1; Bertolino et al., 2014). One was collected using a hammer and chisel from the base of a submerged vertical cliff in Portofino (P), at a water depth (wd) of 40 m in front of Punta del Faro (Figures 1, 2A; Cánovas Molina et al., 2016, Figure 4). The other one was recovered 150 m off Bogliasco (B) at a water depth (wd) of 10 m (Figures 1, 2B), where it lay on a sub-horizontal seafloor among the *Posidonia* meadow (Bertolino et al., 2017b, Figure 1).

2.1 Build-up surface cover

The external surface of each build-up was studied in terms of cover and coverage of 12 major categories, based on their visual distinctivity and potential role in bioconstruction: FilF_A, filamentous algae and algal turf <2 cm high (Connell et al., 2014); ErF_A, erect fleshy macroalgae, including *Halimeda, Flabellia,* and *Padina* sp.; Pey, other weakly calcified or fleshy laminar algae, mainly *Peyssonnelia* spp.; CCA_CCPey, non-geniculate Corallinophycidae and completely calcified *Peyssonnelia* spp; FORAM, encrusting foraminifera; SPNG, sponges; Encr_ ANTH, encrusting corals; Er_ANTH, erect corals; MOL, mollusks; ANN, tube-dwelling annelids; Encr_BRY, encrusting bryozoans; and Er_BRY, erect bryozoans. The acronym CCA to indicate crustose coralline algae is widely used in the scientific literature, although the term crustose is not correct within the accepted nomenclature for coralline growth forms (Woelkerling et al., 1993). For the sake of simplicity, we use the term CCA to indicate the non-geniculate Corallinophycidae, with no implication about their growth-form.

We indicate as *cover* the percentage of surface occupied by live organisms vs. dead skeletal remains (based on preservation of soft tissues and delicate structures, original sheen, and color). Because the build-up is biogenic, the live + dead covers give 100%. We indicate as *coverage* the sum of the percentage of surface covered by each category. Because of possible superposition of different organisms, the sum of *coverages* may exceed 100%. We approximated each build-up to a hexahedron and named the six sides from A to F. Each side was sampled with 15 × 15 cm frames, in order to map the surface and to calculate the percentage cover and the total coverage for each category. Manual mapping of each component has been performed using ImageJ Image Analysis

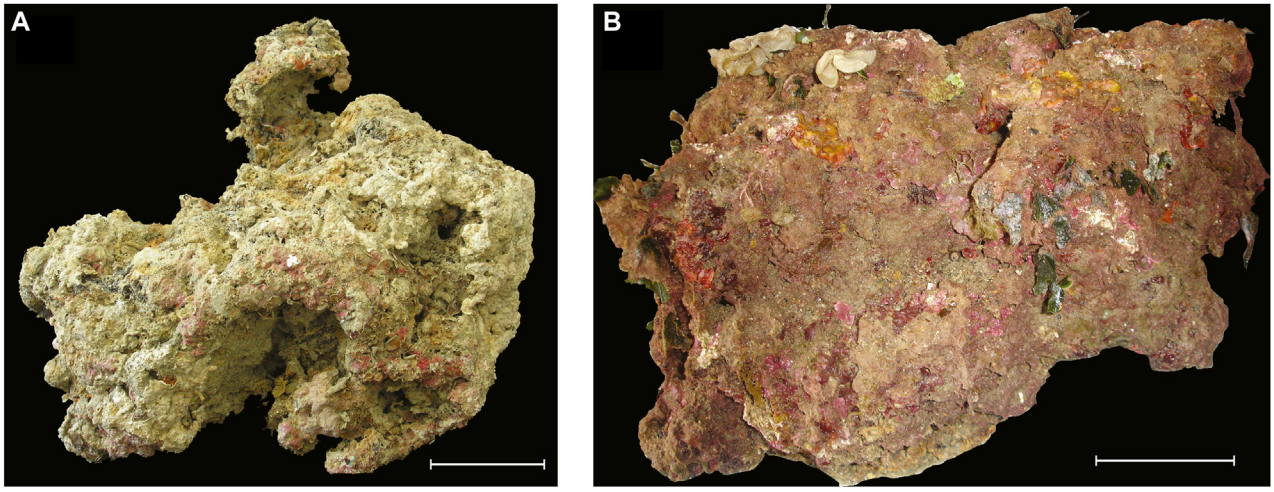

FIGURE 2
Two build-ups before slicing/coring. **(A)** Portofino side A. **(B)** Bogliasco side E. Scale is 10 cm.

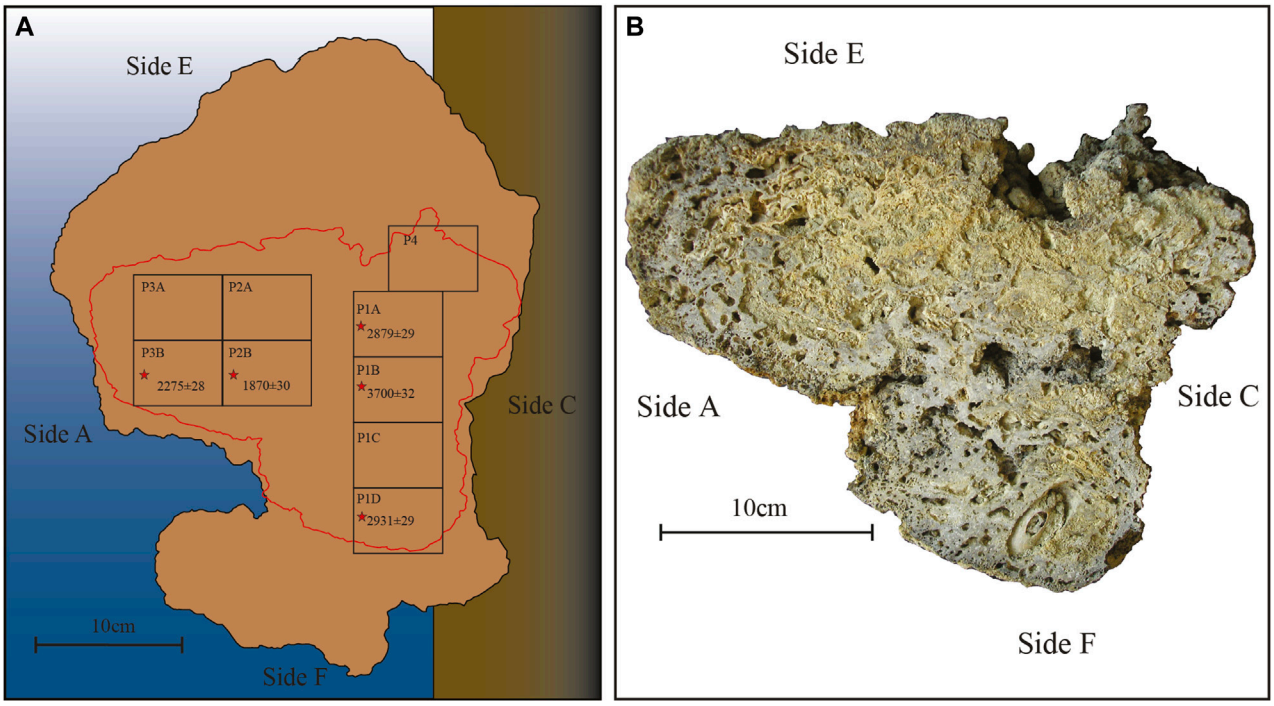

FIGURE 3
Portofino build-up. **(A)** Reconstruction of the original position with the indication of the different sides indicated by letters. The red line indicates the position of the slice from which the panoramic thin sections (= numbered rectangles) have been obtained. The asterisks indicate the dated thin sections along with their tRC age (BP) (Table 4). **(B)** The slice before cutting for thin sections, oriented on the base of the build-up sides. Note the large embedded *Lithophaga* shell close to side F.

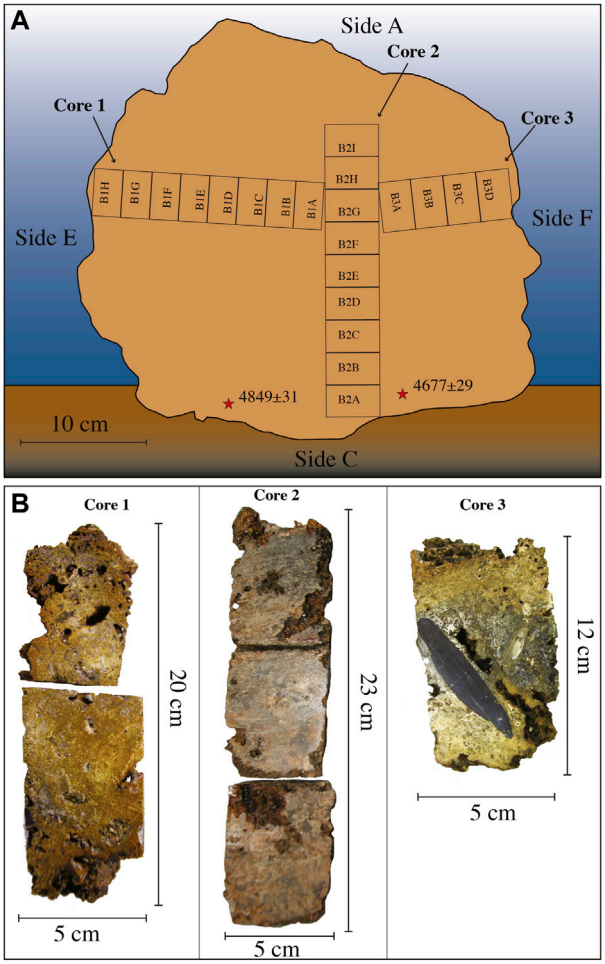

FIGURE 4
Bogliasco build-up. **(A)** Reconstruction of the original position with the indication of the different sides indicated by letters. The numbered rectangles indicate the position of the thin sections and the asterisks indicate the position of the dated fragments. **(B)** The Bogliasco cores. In core 3, note the dark layer rich in matrix and terrigenous grains, with a large cobble.

Software (Rasband, 1997). Voucher specimens were detached from the build-up surface for identification at the lowest possible taxonomic level, under an optical microscope and/or a scanning electron microscope (SEM) (soft-bodied and calcareous algae, mollusks, bryozoans, corals, and annelids). Live crustose coralline algae were identified under an SEM following the morphoanatomical keys provided by Irvine and Chamberlain, (1994), Bressan and Babbini (2003) and more recent updates (among others: Basso and Rodondi, 2006; Athanasiadis and Ballantine, 2014; Pezzolesi et al., 2019). *Lithophyllum stictiforme* is a common species of C encompassing a group of molecularly defined cryptic species (Pezzolesi et al., 2019). For this reason, in absence of molecular data and with the aim to keep a uniform taxonomic framework both for the living and the dead/fossil corallines, this species is indicated here as *Lithophyllum* group *stictiforme*. Algal taxonomy follows AlgaeBase (Guiry and Guiry, 2022), and invertebrate taxonomy follows WoRMS (WoRMS Editorial Board, 2019).

2.2 Multivariate statistics

The percentage values of the categories identified in the external cover of the two build-ups were considered separately for each of the 12 surfaces of the build-ups (6 for Portofino and 6 for Bogliasco) and statistically treated using the software Past (Hammer et al., 2001). A Q-mode clustering of the surfaces based on percentage data was performed by Euclidean distance with no preliminary transformation. The same similarity data were used for the ordination of the surfaces by 2D Multidimensional Scaling and Correspondence Analysis.

TABLE 1 Percentage values of total superficial cover (live vs. dead) and categories' coverage on the surface of the Portofino build-up.

Code	Portofino	Side A	Side B	Side C	Side D	Side E	Side F
	Total surface cm²	**1,092**	**962.5**	**1,452.5**	**827**	**1,014**	**905**
	Living cover %	92	69	32	42	89	43
	Dead cover %	8	31	68	58	11	57
FilF_A	Algal turf	22	19	2	0	13	13
Pey	Fleshy Peyssonneliales	16	8	2	0	13	0
CCA_CCPey	CCA & calc. Peyssonneliales	49	45	17	3	50	2
FORAM	Encrusting Foraminifera	0	0.1	0.1	0	0	0.1
SPNG	Sponges	4	0	1	3	1	3
Encr_ANTH	Encrusting Anthozoa	0	0	1	7	0	6
Er_ANTH	Erect Anthozoa	3	0.1	0.5	4	1	2
MOL	Mollusca	0	0.1	0.1	1	1	1
ANN	Annelida	12	2	6	7	4	10
Encr_BRY	Encrusting Bryozoa	9	8	7	21	8	17
Er_BRY	Erect Bryozoa	2	0	1	1	1	1
	Total coverage %	117	82	38	47	92	55

Coverage can exceed 100% due to superposition.

TABLE 2 Percentage values of total superficial cover (live vs. dead) and categories' coverage on the surface of the Bogliasco build-up.

Code	Bogliasco	Side A	Side B	Side C	Side D	Side E	Side F
	Total surface cm²	**1770**	**1,307**	**2,845**	**973**	**1,431**	**1,457**
	Living cover %	99	71	23	60	84	57
	Dead cover %	1	29	77	40	16	43
FilF_A	Algal turf	69	36	0	22	49	22
ErF_A	Erect fleshy algae	10	5	0,3	5	6	12
Pey	Peyssonneliales	9	6	0	2	4	4
CCA_CCPey	CCA & calc. Peyssonneliales	22	21	4	12	19	13
FORAM	Encrusting Foraminifera	0.1	0.2	0.3	0.6	0.5	0.3
SPNG	Sponges	1	0.2	1	0	7	0
MOL	Mollusca	0.1	0.3	0.5	0.1	2	0.5
ANN	Annelida	0.1	4	11	9	6	8
Encr_BRY	Encrusting Bryozoa	0.1	3	8	14	4	5
Er_BRY	Erect Bryozoa	0	2	0.3	0	0.3	0.5
	Total coverage %	111.4	83.7	25.4	65.7	94.8	66.3

Coverage can exceed 100% due to superposition.

2.3 Carbonate framework builders

In order to study the internal structure of build-ups, the Portofino sample has been sliced along the apparent growth direction, normal to side A. Nine panoramic thin sections (60 × 45 mm) were prepared from the slice (Figure 3).

The sample of Bogliasco has been cored (Figure 4). Three cores with a diameter of 50 mm and different lengths have been obtained. Core 1 (cm 20) was sampled from side E toward side F, and core 3 (cm 12) joined core 1 from side F. Cores 1 and 3 were more or less perpendicular to core 2. Core 2 had a recovery of 23 cm, from side C toward side A, stopping at 9 cm below the surface of side A. Thus, a total sample thickness of 32 cm (23 cm cored +9 cm not cored) was measured from side C to side A. Cores have been hardened by embedding in resin, in order to avoid fragmentation, and sliced in half. Twenty-one standard petrographic thin sections (48 × 28 mm) have been obtained from the Bogliasco cores (Figure 4).

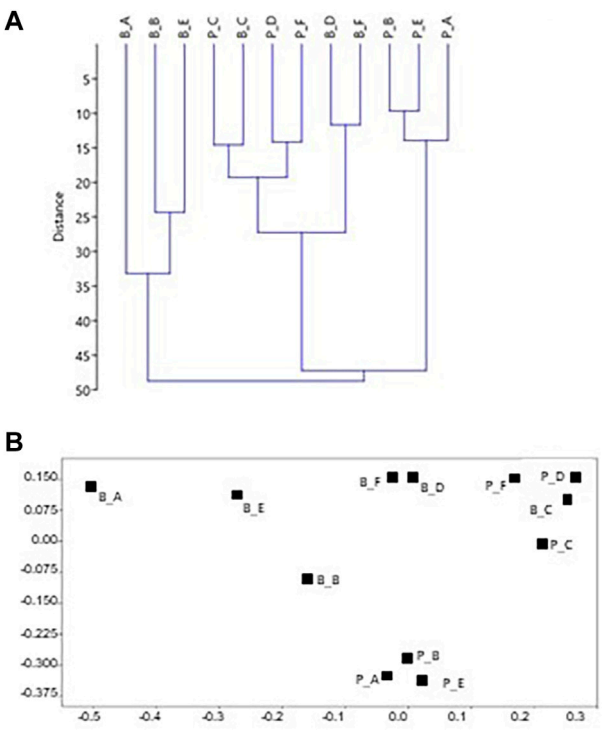

FIGURE 5
Plots of the statistical treatment based on surface coverage data from the two build-ups. Each side is labeled with a first letter indicating the build-up (P=Portofino and B=Bogliasco) with another letter indicating the side. For example, P_A is side A of Portofino build-up. Euclidean distance, no transformation. **(A)** Dendrogram **(B)** 2D plot of the ordination by multidimensional scaling. In **(B)** the bottom and darker sides are plotted together on the top right. Top left is the shallow well-lit side, while the well-lit deep sides are plotted at the bottom center.

Observation and identification of the build-up components in petrographic thin sections were performed under transmitted-light optical microscopes (an Olympus BH-2 and a Leica Leitz-Laborlux-S) in the facilities of the Milano-Bicocca University. The biological literature has been integrated with paleontological contributions for the identification of fossil algae (Braga and Bassi, 2007; Basso et al., 2009; Hrabovský et al., 2016).

Point counting was performed on a total of 30 thin sections to quantify the contribution of the major coralligenous builders (Flügel, 2010). We analyzed a grid of 100 points for each of the 21 standard petrographic thin sections obtained from the Bogliasco cores and 200 points each for the 9 panoramic thin sections from the Portofino slice. Identified categories in the thin section were as follows: porosity, CCA, geniculate coralline algae, Peyssonneliales, unidentified encrusting algae; Charophyceae; bryozoans; annelids; mollusks; foraminifera; muddy matrix; terrigenous grains. Points corresponding to voids within the buildup framework, such as spaces between different skeletal particles, have been considered and counted as indicative of structural porosity of the build-up, whilst microcavities inside individual skeletal elements, like the interior of conceptacles or annelid tubes, were not considered. We counted as terrigenous grains those extrabasinal elements corresponding to sand grains or larger (>63 μm), while the finer fraction (<63 μm) was attributed to the matrix category, with no distinction about its composition.

2.4 Radiocarbon dating

Radiocarbon dating was performed by the Milano-Bicocca University Centre for Dating and Archaeometry (CUDAM) on selected fragments of CCA from both build-ups, after ascertaining the absence of diagenetic overprints and recrystallization. Five samples for radiocarbon dating were collected from the Portofino slice, numbered RC300, 301, 302, 303, and 304 moving from side F to side E (Figure 3), and 2 samples from the Bogliasco build-up, just internally to the C surface, named RC305 and 306 (Figure 4). The net accumulation rate was assumed as constant and calculated upon the vertical distance between the dated samples (calibrated ages) and the top living surface. We use the term accumulation rate to indicate the net accretion of the build-up that results from the interplay of the original growth rate of the builders, the accumulation of sediment, and the erosion. For the Bogliasco build-up, assuming a more or less constant accumulation rate along the vertical direction, we associated an approximate age to each thin section of the vertical core 2.

3 Results

3.1 Build-up surface cover

3.1.1 Portofino

The build-up sample was a 45 × 37 × 41 cm block, irregularly shaped, with a protuberance toward side F (Figure 2A).

Side C was partially attached to the sub-vertical substrate and had only 32% of living cover. Sides D and F showed a low percentage of living cover, 42% and 43% respectively (Figure 3), whereas sides A, B, and E had the most abundant cover of living organisms, up to 92% (Figure 3; Table 1).

Coverage showed the highest percentages on sides A, B, and E (up to 117%, Table 1).

The most abundant organisms were calcareous algae (up to 50%), with the exception of sides D and F where encrusting bryozoan colonies dominated. Filamentous algae were also abundant (up to 22%), while erect fleshy algae were not observed. Bryozoans and, among them, encrusting colonies were abundant. Tube-dwelling annelids reached considerable percentage cover on sides A and F (13 and 10%, respectively) (Supplementary Table S2).

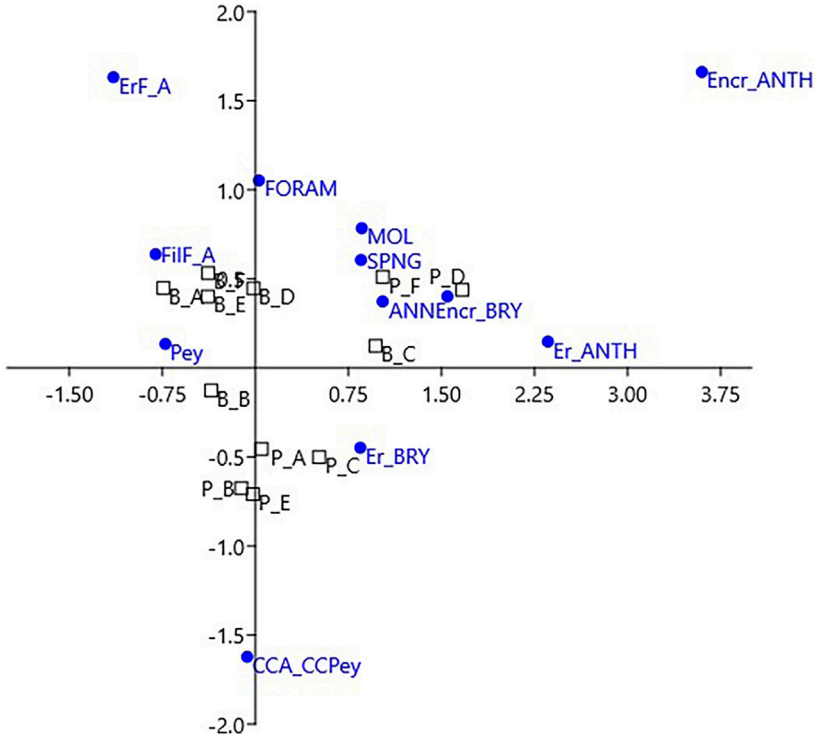

FIGURE 6
Correspondence analysis for the coverage data of the two build-ups. Labels of sides as in Figure 5. Labels of categories as in Tables 1, 2.

3.1.2 Bogliasco

The build-up sample was a 50 × 40 × 40 cm block, showing a porous surface with cm- to mm-sized irregular cavities (Figure 2B). The block clearly showed a more densely populated portion with a high living cover, corresponding to the sides originally exposed to light (sides A, B, and E, Figure 4), contrasting with the very low living cover of side C, which was partially in contact with the seafloor, and almost devoid of algae. Sides A, B, and E were dominated by filamentous (up to 69%) and subordinate calcareous algae (up to 22%, Table 2). Erect fleshy algae are reported for all sides but were most abundant on sides A (10%) and F (12%). Bryozoans were abundant on side D (14%), whereas annelids are dominant on side C (11%) (Table 2). Anthozoa were not observed (Supplementary Table S2).

3.2 Multivariate statistics

The percentages of the identified categories for each side of the two build-ups (Tables 1, 2) were plotted in the dendrogram (Figure 5A). At the Euclidean distance of 35%, three clusters of similar sides are identified (1–3), based on their cover components. Cluster 1 exclusively contains the well-lit sides of Bogliasco, while cluster 3 is composed of the Portofino sides with the highest cover of calcareous algae. The same clusters were recognized in the 2D MDS (Euclidean distance, no transformation, Figure 5B). Cluster 2 contains the remaining sides, highlighting a similarity (only 15% distance) between the "dark" sides C of both build-ups.

The correspondence analysis (CA) of the same data showed the plot of the build-up sides in a space with 3 opposite vertices (Figure 6). The upper left corresponds to erect fleshy algae, calcareous algae are plotted below, and encrusting corals on the upper right, respectively. All of the fleshy algae (turf and filamentous, erect, and laminar *Peyssonnelia*) fell in the upper left quadrant, while the upper right quadrant is animal-dominated. In the lower half of the CA plot, calcareous algae drive the position of the Portofino sides belonging to cluster 3 (Figures 5B, 6).

3.3 The build-up framework builders

3.3.1 Radiocarbon dating and accumulation rates

Radiocarbon dating of the Portofino build-up provided a calibrated age ranging between 1720 and 1620 BCE (3700 ± 32 years BP, RC301) in the proximity of side F and between

TABLE 3 Point counting results for the 9 thin sections of the Portofino build-up.

Components	P1C	P1B	P1D	P1A	P3B	P2B	P2A	P3A	P4
Porosity	15.3	13.9	16.8	21.3	19.8	20.6	12.1	13.7	16.1
CCA	46.8	41.5	35.6	53.2	27.9	56.2	51.7	46.6	42.4
S. ptychoides	0.0	0.0	11.4	0.0	0.0	0.0	0.0	0.0	0.0
T. pustulatum	8.1	3.1	2.7	8.5	5.4	5.5	3.5	11.0	12.7
S. fruticolosus	10.8	16.9	0.0	4.3	1.8	16.4	15.5	0.0	0.0
L. stictiforme	0.0	0.0	0.0	0.0	0.0	0.0	0.0	0.0	12.7
L. sonderi	0.0	1.5	0.0	0.0	0.0	1.4	0.0	0.0	0.0
P. cf. *lenormandii*	0.0	0.0	0.0	0.0	0.0	2.7	0.0	0.0	0.0
M. cf. *philippii*	3.6	7.7	0.0	0.0	0.0	5.5	0.0	2.7	0.0
CCA ind.	24.3	12.3	21.5	40.4	20.7	24.7	32.8	32.9	17.0
Genic. corallines	0	0	0	0	0	0	0	0	0
Peyssonneliales	5.4	1.5	2.0	4.3	0	4.1	5.2	4.1	2.5
Bryozoans	0	6.2	1.3	8.5	0.9	0	0	1.4	0.9
Annelids	0.9	1.5	0.7	6.4	3.6	4.1	3.5	2.7	3.4
Foraminifers	0.9	0	0	0	0.9	0	0	0	0
Mollusks	0	3.1	2.0	0	3.6	0	1.7	8.2	0.9
Matrix	30.6	32.3	41.6	6.4	43.2	15.1	25.9	23.3	33.9
Terrigenous	0	0	0	0	0	0	0	0	0

The abundance of the identified components is shown as a percentage.

485 and 585 CE (1870 ± 30 years BP, RC303) in the proximity of side E (Supplementary Table S1). The oldest material was recovered from the side of the build-up that was in close proximity of the substrate from which the build-up developed, whereas the youngest portion was located near the photophilous side of the coralligenous block. The mean calculated accumulation rate is 80 μm y^{-1}.

Two separate CCA fragments at the base of the Bogliasco sample (side C, bottom) were dated at 3290–3130 BCE (4849 ± 31 years BP, RC305) and 2985–2895 BCE (4677 ± 29 years BP, RC306). The mean calculated accumulation rate corresponds to 65 μm y^{-1}.

3.3.2 Portofino

Dating the internal structure of the Portofino build-up revealed a complex pattern of growth direction. For this reason, thin sections have been reorganized on the basis of the results of radiocarbon dating, from the oldest one (P1B) to the most recent (P4), the latter obtained next to side E (Figure 3). The inner structure was macroscopically porous but hard and lithified, with cm-thick compact areas. Crustose coralline algae were the dominant component in most sections, ranging from 28% (P3B) to 56% (P2B) (Table 3, Figures 7, 8). In sections P1D and P3B, the most abundant component was matrix (Figure 8), formed by microgranular mud, mainly composed of biogenic fragments. Matrix typically filled the intraskeletal porosity or the interskeletal porosity between adjacent algal crusts.

Among the other biogenic components, bryozoans were abundant in sections P1B (6.15%) and P1A (8.51%), annelids had a significant cover in section P1A (6.38%), and mollusks were relatively abundant in section P3A (8.22%) (Table 3, Figure 8). Peyssonneliales and encrusting foraminifera, although present, were never abundant. Porosity was more or less constant, ranging from 13.70% to 21.28% (Table 3, Figure 8).

The most abundant species of coralline algae were *Spongites fruticulosus* Kützing (up to 16.92% in P1B), *Titanoderma pustulatum* (J.V.Lamouroux) Nägeli (up to 12.71% in P4), and *Mesophyllum* cf. *philippi* (Foslie) Adey (7.68% in P1B) (Table 3). *Lithophyllum* group *stictiforme* (12.71%) was identified only in thin section P4, whereas *Phymatolithon* cf. *lenormandii* (Areschoug) W.H.Adey (2.74%) was identified only in thin section P2B. Thin section P1D also contained *Sporolithon ptychoides* Heydrich (11.41%) (Table 3).

3.3.3 Bogliasco

Core 2 was sampled from side C (bottom) to side A (top), almost crossing the whole build-up along its mainly vertical growth direction (Figure 4). The 9 thin sections, named from B2A (bottom) upward to B2I, showed a poor preservation of the calcareous skeletal components, hindering the identification of calcareous algae, which nevertheless remained the dominant biogenic component with up to 57% in thin section B2E (Table 4, Figure 9). Among the identified species, the most common were *T. pustulatum* and *L.* gr. *stictiforme*. *S. fruticulosus* was identified in thin section B2G, whereas the uncommon *S. ptychoides* was detected in B2H, associated with *T. pustulatum* and a significant contribution by bryozoans, annelids, and foraminifera. Uncommon

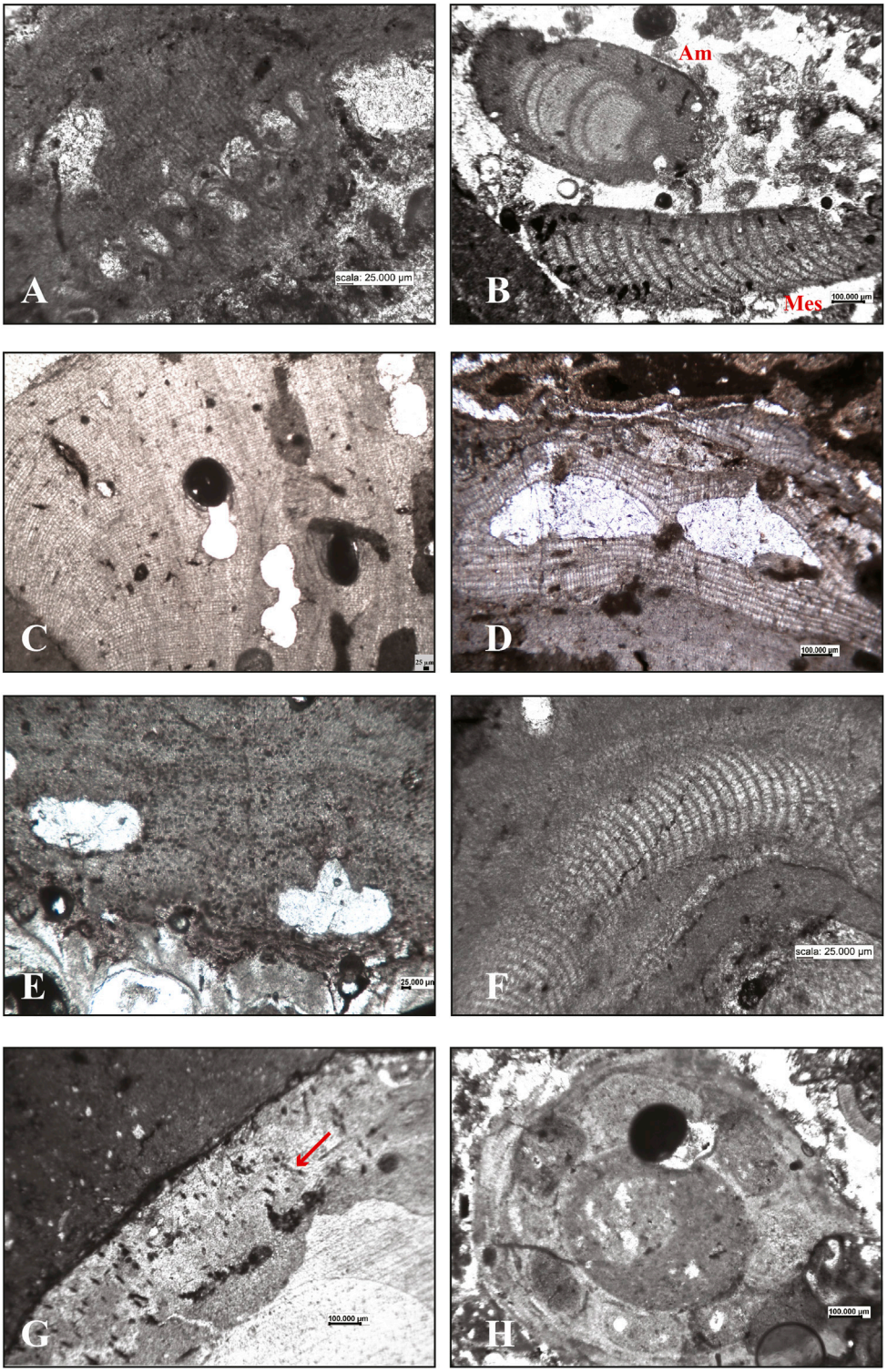

FIGURE 7
Calcareous algae in the internal structure of the studied build-ups. Corallinophycidae: **(A)** oblique section of solitary sporangia of *Sporolithon ptychoides;* **(B)** longitudinal section of *Amphiroa* intergeniculum (Am) and a fragment of a *Mesophyllum* sp. hypothallus (Mes); **(C)** longitudinal section of *Lithophyllum* gr. *stictiforme*; **(D)** longitudinal section of *Titanoderma pustulatum* showing the distinctive palisade cells and two uniporate conceptacles; **(E)** *Spongites fruticulosus* growing on a bryozoan colony; **(F)** the hypothallus of a *Mesophyllum* sp. Peyssonneliales: **(G)** *Peyssonnelia* sp, hypobasal aragonite calcification showing traces of rhizoids (arrow). Charophyta: **(H)** unidentified charophyte remains.

10.3389/feart.2022.961632

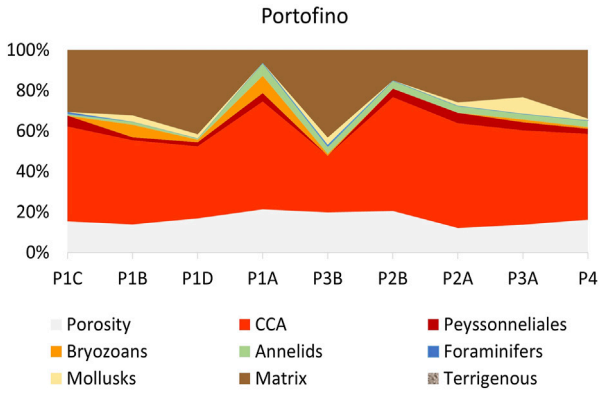

FIGURE 8
Portofino C: internal dominance from thin section point counting of the categories as in Table 3. The label of the studied thin sections is reported on the horizontal axis.

intergenicula of articulated coralline algae occurred randomly (B2E and B2G) (Table 4).

Bryozoans were co-dominant with CCA in thin sections B2F (35.7%) and common elsewhere, with the exception of the CCA-dominated section B2E, where bryozoans were missing. Annelids were abundant in thin section B2G (18.7%), whereas foraminifera were abundant on thin sections B2F (14.3%) and B2H (14.7%) and mollusks on thin sections B2D (39.39%) and B2F (14.3%).

Matrix and terrigenous were variable through the core, absent from section B2F and up to 42.5% in B2B. Section B2G records about 34% of the sedimentary infill associated with the maximum abundance of annelids and the occurrence of charophytes. Porosity varied cyclically along the core (Table 4, Figure 9).

Cores 1 and 3, perpendicular to core 2, have been considered as representative of the presumed lateral development of the build-up (Figure 4). The inner structure was found to be lithified and locally highly compact, although pluricentimetric irregular cavities were observed.

In the thin sections obtained from Core 1, from B1A (internal) to B1H (toward side E) (Figure 4), the most abundant biogenic component was CCA (up to 61.11% in B1A) (Table 5). Among them *L.* gr. *stictiforme*, which was always present, and *T. pustulatum* were the most abundant species (Table 5). The species *S. fruticulosus* was uncommon, identified only in thin section B1G (Table 5).

Bryozoans were ubiquitous and particularly abundant in thin sections B1D (20%) and B1F, where they overcome CCA abundance (Table 5). Annelids were also common and abundant in thin section B1E, where they equaled CCA (18.2%) and where foraminifers also reached an important percentage. Mollusks were remarkably common in thin section B1C (14.3%), associated with the occurrence of charophytes and abundant sedimentary infill (matrix + terrigenous = 42.8%), while both bryozoans and annelids were missing (Table 5).

Matrix, as microgranular mud mostly of biogenic origin, was very abundant in thin sections B1D (50%), B1C (37.1%), and B1F (35.3%) (Table 5). Terrigenous grains were dominant in thin sections B1G (41.2%) where, adding to matrix, the sum of these two categories reached the maximum value, exceeding 55% (Table 5).

The thin sections of Core 3 (B3A internal, to B3H, close to side F, Figure 4) showed CCA as the most abundant biogenic component, although percentages did not exceed 31.8% (B3A) (Table 5). Bryozoans, annelids, and mollusks remarkably overtook where CCA were absent (B3D). The identified CCA species were *L.* gr. *stictiforme* and *T. pustulatum*.

TABLE 4 Point counting results for Bogliasco core 2.

Components	B2A	B2B	B2C	B2D	B2E	B2F	B2G	B2H	B2I
Porosity	14.6	0	5.5	6.1	7.1	0	0	14.7	7.4
CCA total	33.3	30	5.7	6.1	57	35.7	21	26.5	29.7
S. ptychoides	0	0	0	0	0	0	0	16.3	0
T. pustulatum	16.1	10	5.7	0	0	5.7	12	10.2	10.4
L. gr. *stictiforme*	17.2	20	0	0	2	0	0	0	0
S. fruticulosus	0	0	0	0	0	0	1	0	0
CCA ind.	0	0	11	6.1	55	30	8	0	19.3
Genic. cor.	0	0	0	0	0.1	0	0.9	0	0
Charophyceae	0	0	0	0	0	0	9.4	0	0
Bryozoa	8.3	12.5	11.1	3.0	0.0	35.7	12.5	8.8	18.5
Annelida	0.0	7.5	0.0	0.0	0.0	0.0	18.7	5.9	0.0
Foraminifera	4.2	2.5	5.6	9.1	2.4	14.3	3.1	14.7	11.1
Mollusca	2.1	5.0	11.1	39.4	2.4	14.3	0.0	2.9	11.1
Matrix	18.8	42.5	33.3	24.2	26.2	0.0	25.0	14.7	14.8
Terrigenous	18.7	0.0	16.7	12.1	4.8	0.0	9.4	11.8	7.4

The abundance of the identified components is shown as a percentage.

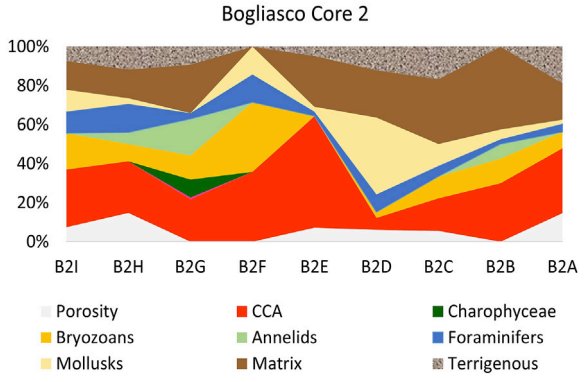

FIGURE 9
Bogliasco C, core 2: internal dominance from thin section point counting of the categories as in Table 4. The label of the studied thin sections is reported on the horizontal axis.

Matrix was ubiquitous and abundant, and together with terrigenous grains, these two abiogenic components became dominant in thin sections B3A and B3B (Table 5), coarsely corresponding to a gray layer where terrigenous grains up to 6 cm long occurred (Figure 4). The largest fragments showed an elongated shape with well-rounded margins and were composed of calcareous shale.

4 Discussion

4.1 External components

The quantitative analysis of surface cover and coverage of both coralligenous build-ups easily allows us to identify the photophilic and sciaphilic sides, highlighting an important variability in C surface associations, depending on substrate orientation. The Portofino C, overhanging on a rocky wall at a depth of about 40 m, shows the most abundant living cover and coverage on its best-lit sides A and E, with calcareous algae as the dominant category. Filamentous algae, although present, are never dominant, as expected on the basis of the water depth of the sample close to the lower limit of the infralittoral zone in the Mediterranean. An important reduction of the live cover is observed on the other sides, with Bryozoa and tube-dwelling Annelida becoming dominant on the westward side D and on the lower and darkest side F. Both octocorals and Scleractinia are also more common on the dim-lit sides, although with low total dominance.

The Bogliasco C is presently growing within the infralittoral *Posidonia* meadow, with its upper, best-lit side dominated by filamentous and fleshy algae, with subordinate Peyssonneliales and CCA. Bryozoans are also important contributors, especially on sides D and F, together with annelids, confirming their preference for the shadowed and protected substrates (Rosso and Sanfilippo, 2009; Sanfilippo et al., 2011), including the lower surface of calcareous laminar algae.

The comparison between the overhanging and deeper Portofino C and the shallower Bogliasco build-up highlights the abundant fleshy algal cover and the absence of corals as the most distinctive traits of Bogliasco C, likely due to its shallow position. The distinctive green algae *Halimeda tuna* and *Flabellia petiolata* are scattered over the Bogliasco C surface, as commonly reported in other shallow coralligenous algal assemblages (Ballesteros, 2006; Piazzi et al., 2022), while they were not observed in the Portofino sample. Calcareous algae in Bogliasco exhibit about half of the cover in Portofino, confirming their basically sciaphilic nature and the negative effect of space competition with the faster-growing fleshy algae.

TABLE 5 Point counting results for Bogliasco cores 1 and 3.

Components	B1H	B1G	B1F	B1E	B1D	B1C	B1B	B1A	B3A	B3B	B3C	B3D
Porosity	15.8	0.0	11.8	18.2	0.0	8.6	22.7	5.6	13.6	7.4	17.9	0
CCA total	52.0	35.3	8.8	18.2	15.0	36.4	18.2	61.1	31.8	25.9	20	0
T. pustulatum	31.0	18.3	6.5	0	0	21.0	0	6	22.8	10.4	0	0
L. gr. *stictiforme*	19.0	8.5	2.3	18.2	15.0	15.4	18.2	55.1	9	15.5	20.0	0
S. fruticulosus	0	8.5	0	0	0	0	0	0	0	0	0	0
M. cf. *philippii*	2	0	0	0	0	0	0	0	0	0	0	0
Genic. cor.	0	0	0	0	0	0	0	0	0	0	0	0
Peyssonneliales	0.6	0	0	0	0	0	0	0	0	0	1.4	0
Charophyceae	0	0	0	0	0	2.9	0	0	0	0	0	0
Bryozoa	5.3	5.9	14.7	0.0	20.0	0	13.6	11.1	9.1	3.7	17.9	38.9
Annelida	0	2.9	2.9	18.2	5.0	0	0.0	5.6	0	3.7	3.6	22.2
Foraminifera	5.3	0	2.9	9.1	5.0	0	0.0	5.6	4.6	11.1	7.1	5.6
Mollusca	0	0	8.8	0	5.0	14.3	4.5	0	0	0	7.1	16.7
Matrix	10.5	14.7	35.3	18.2	50.0	37.1	27.3	5.6	22.7	22.2	25.0	16.7
Terrigenous	10.5	41.2	14.7	18.2	0	5.7	13.6	5.6	18.2	25.9	0	0

Thin sections are ordered from side E (B1H) to side F (B3D), as in Figure 4. The abundance of the identified components is shown as a percentage.

The surface of C pillars in Sicily (Di Geronimo et al., 2001) presents a similar pattern of algal dominance, confirming the early reports of shallow-water corallines becoming hidden under a canopy of *H. tuna* and *F. petiolata* (Laborel, 1987).

Coralligenous was indicated as the climax biocenosis of the circalittoral zone (Pérès, 1982; Ballesteros, 2006; Cánovas Molina et al., 2016), although C habitats are considered as heterogeneous systems, showing high spatial, morphological, and biological variability (Ferdeghini et al., 2000; Casas-Güell et al., 2015; Cánovas Molina et al., 2016; Sartoretto, 2017; Piazzi et al., 2022). Light exerts a major control on the depth extent of the infralittoral and circalittoral zones and certainly also on the depth distribution of the various coralligenous facies (Pérès, 1982; Ballesteros, 2006; Cánovas Molina et al., 2016). C is reported to develop between 0.05% and 3% of the surface irradiance (Ballesteros, 2006). Irradiance values >3% correspond to the shallowest coralligenous, once defined as "precoralligenous" (Pérès, 1982) because they typically hosted a higher diversity of fleshy algae, among which were *Flabellia petiolata* and *Halimeda tuna*.

Coralligenous is known in the circalittoral zone mainly 1) on rocky cliffs, 2) on sedimentary seafloors, and 3) as an enclave of circalittoral, in the shadow of the canopy of leaves at the base of the infralittoral *Posidonia* meadows (Sartoretto 2017). Portofino C clearly corresponds to the first type, while Bogliasco C is not completely included in category 2) nor 3) above, being developed among *Posidonia* plants and reaching a considerable height in the middle of the meadow that, by definition, characterizes the infralittoral zone. A similar infralittoral coralligenous, apparently a paradox of benthic bionomics, was reconstructed in the Quaternary marine terrace of Le Castella (MIS 3, Bracchi et al., 2016; Nalin et al., 2020).

4.2 Framework builders and Holocene oceanographic fluctuations

Crustose coralline algae showed a roughly antithetical pattern with matrix, alternating as the dominant components of the C internal structure. Although present and locally abundant, the other biogenic components played a secondary role as framework builders (Figures 8, 9).

4.2.1 Portofino

The interior structure of the Portofino build-up was very compact, with a rather constant percent porosity, never exceeding 21.28%. Among CCA, the most common species belong to the genus *Mesophyllum*. Contrarily to previous reports indicating *M. alternans* (junior synonym of *M. philippii* (Athanasiadis and Ballantine, 2014) as a shallow component (Sartoretto et al., 1996; Ballesteros, 2006), this coralline species was remarkably abundant in the relatively deep Portofino C (40 m).

T. pustulatum was ubiquitous. This species is widespread in the Mediterranean (Babbini and Bressan, 1997) and has already been indicated as an important framework builder in C (Sartoretto et al., 1996). This suggestion was confirmed in the Pleistocene C examples outcropping in the Cutro terraces (Nalin et al., 2006; Basso et al., 2007).

S. fruticulosus is also widespread in the Mediterranean Sea (Babbini and Bressan, 1997; Basso and Rodondi, 2006), where it occurs as rhodoliths on soft bottoms (Basso and Rodondi, 2006; Barberá et al., 2012; Joher et al., 2015), and was rarely reported as a component of the coralligenous build-ups, down to a water depth of 75 m (Basso and Rodondi, 2006; Catra et al., 2007). *S. fruticulosus* occurred cyclically in the Portofino build-up, around 3700 BP (P1B), 2879 BP (P1A), and 1870 BP (P2B), always together with low matrix abundance. Therefore, it can be associated with periods with low sedimentation rate and consequently interpreted as a species with a low tolerance for disturbance by sediment deposition, and likely associated turbidity.

In the Portofino inner structure, up to 40.43% CCA did not show or preserve sufficient diagnostic features for taxonomic identification. Nevertheless, merging the two components (identified + non-identified coralline algae) highlights CCA as the most important framework builder in late Holocene coralligenous build-up, as already reported for the Ligurian Sea (Sartoretto et al., 1996; Cerrano et al., 2001; Bertolino et al., 2017a; Bertolino et al., 2017b). All the other calcareous organisms showed negligible contributions and rather invariant quantitative distribution in the inner structure. Across the build-up, high CCA abundance was accompanied by a minor matrix, filling the sub-millimeter cavities between crusts. On the contrary, local dominant matrix was observed filling not only the cavities between crusts but also cm-size voids, apparently corresponding to a phase of slow growth of the primary builders. In correspondence of high-matrix content, the most abundant CCA species was *T. pustulatum* for thin sections P1D and P3B and *S. ptychoides* for thin section P1D.

Thin section P1D corresponded to a calibrated age of 790–745 BCE which is known as a phase of increasing temperature in the Alboran Sea (Martrat et al., 2014; Bazzicalupo et al., 2020) and increased humidity and terrestrial runoff in the Southern Alps and in the Gulf of Lyon (Wirth et al., 2013; Jalali et al., 2016), associated with negative North Atlantic Oscillation (NAO) index (Faust et al., 2016) (Figures 8, 10). During this time interval, warm summers and dry winters characterized the south-western Mediterranean (Zielhofer et al., 2019). The genus *Sporolithon* is considered a warm-water taxon (Bressan and Babbini, 2003; Braga and Bassi, 2007; Basso et al., 2009). In particular, the species *S. ptychoides* is common at tropical latitudes (Adey and Macintyre, 1973; Johansen, 1981), overgrowing coral on shallow fringing reefs and reef flats 1–1.5 m deep (Richards et al., 2017), or in relatively deep water and cryptic sites (Adey, 1979, 1986). *S. ptychoides* is

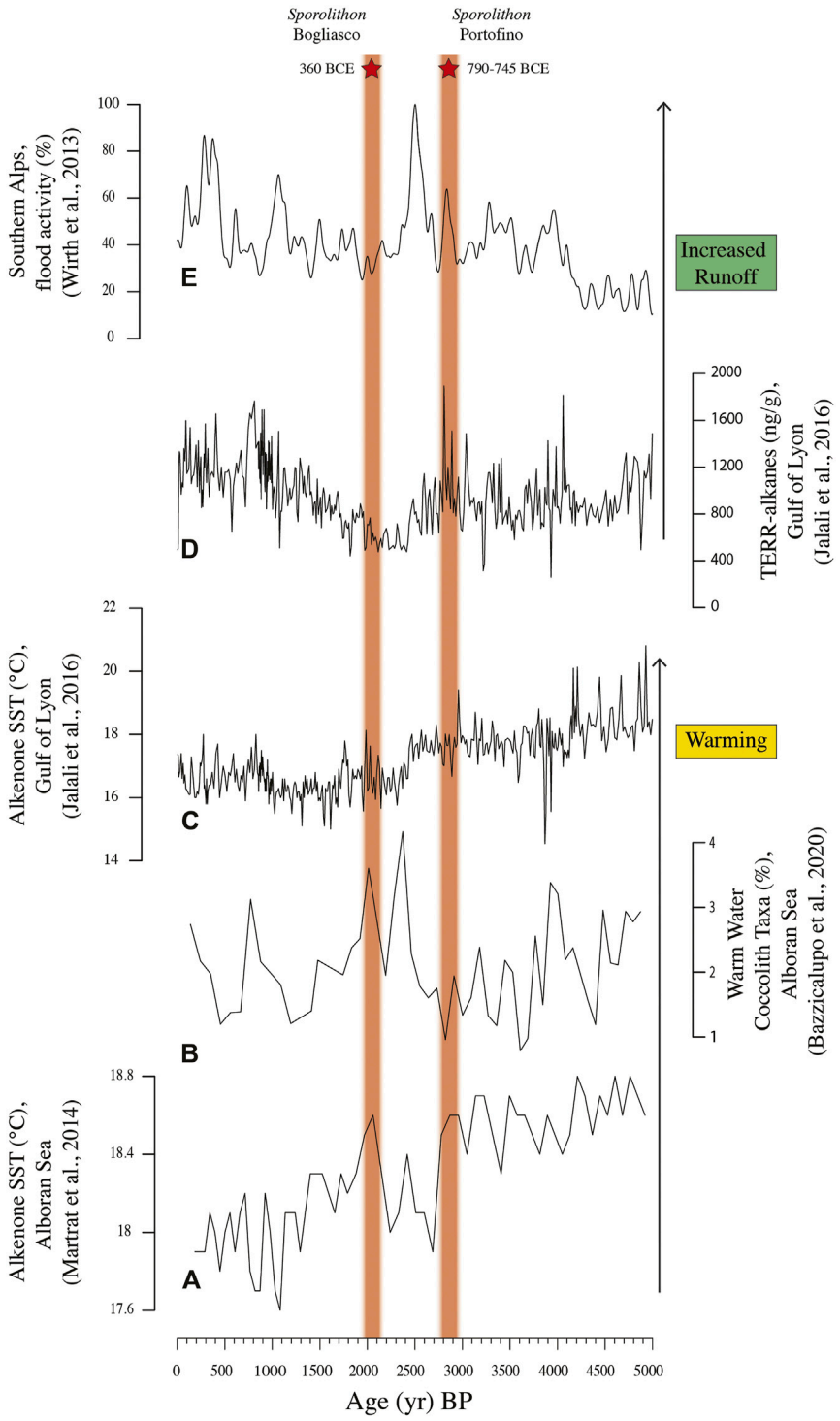

FIGURE 10
Late Holocene climate fluctuations and the stratigraphic position of the *Sporolithon* occurrences recorded in the Portofino and Bogliasco build-ups.

rarely reported in the Mediterranean; it is mainly reported in the central and southern Tyrrhenian Sea and in the Ionian Sea (Alongi et al., 1996; Babbini and Bressan, 1997; Di Geronimo et al., 2002). The occurrence of *S. ptychoides* in the Portofino build-up is therefore a possible index of a milder climate than today. The matrix-dominated thin section P3B corresponded to a calibrated age of 85–175 CE, which falls within the early Roman Climate Optimum. Also, this period is reported in literature as warm and humid, supporting terrestrial run off and sediment deposition at coastal sites (Bini et al., 2020).

The calculated accumulation rate of 0.08 mm y^{-1} for the Portofino C is compatible with previous results from the north-western Mediterranean (Sartoretto et al., 1996).

4.2.2 Bogliasco

The inner structure of the Bogliasco build-up appeared compact, with porosity never exceeding 22.73%. A major contribution of both matrix and terrigenous clasts was reported (up to 42.50% in thin section B2B, Figure 9), as already observed in other shallow coralligenous build-up on horizontal substrate (Cocito et al., 2002). Among CCA, *L.* gr. *stictiforme* was the commonest species. The basal side C was consistently dated at 3,290–3130 BCE (RC305) and 2,985–2895 BCE (RC306); thus, the inception of the Bogliasco build-up occurred during the warm Copper Age, about 5 ka BP. At this time, the sea-level was at least 3 m below the present one along the Ligurian coast (Lambeck et al., 2004); therefore, the build-up started to grow at a water depth of about 7 m, in a very shallow infralittoral environment. Although the abundant matrix and terrigenous grains recorded at the base of the build-up are not surprising in this shallow coastal setting (Figure 9), it should be considered that a coincident phase of wet winters has been reported for the southwestern Mediterranean (Zielhofer et al., 2019), probably favoring the development of sedentary heterotrophs such as annelids and boring mollusks, through the increased food supply from continental weathering. Interestingly, the terrigenous and matrix components showed a decrease toward the core top, although the trend is broken in correspondence to thin section B2F, when these sedimentary components abruptly disappear. This seems to correspond to the end of the Late Bronze Age, ca. 1000 BCE. B2F shows the equal contribution by CCA and bryozoans, accompanied by mollusks and foraminifera. This association might have developed during an arid period, recorded in the western Mediterranean by dry winters and warm summers (Jalut et al., 2000; Bond et al., 2001; Zielhofer et al., 2019; Figure 10).

Successively, a wetter climate fostered the freshwater input from the continent and sedimentation in shallow settings. This was testified in the Bogliasco build-up by an increase in annelids and the occurrence of charophyte remains in thin section B2G, at about 400 BCE (Figure 9). Freshwater and sedimentation are not favorable to CCA, which reduced in abundance. The Roman Period (about 250 BCE-400 CE) brought a warmer phase, probably recorded in the overlying thin section B2H, as testified by the occurrence of the warm-water taxon *S. ptychoides* (Figures 7, 9, 10).

Cores 1 and 3 have been collected more or less normal to core 2. Core 1 crossed core 2 approximately at the level of thin section B2F, thus covering approximately the last 3,000 years, which is compatible with the calculated mean accumulation rate for the Bogliasco build-up.

As already observed in core 2, core 1 also recorded the passage from the drier Late Bronze Age, when CCA were abundant (thin section B1A) to the warm and wetter Roman Period, when sedimentation was favored. This is supported by the abundance of matrix and terrigenous grains in thin sections B1B to B1F, accompanied by the occurrence of charophyte remains (B1C). CCA increased toward the surface of side E in thin sections B1G and B1H.

Core 3 was shorter and recorded a striking and extreme event of sedimentation, likely induced by a flood, with the accumulation of coarse terrigenous clasts up to cobble size (thin sections B3A and B3B). The largest clasts had a rounded shape, supporting the hypothesis of a long transport from the provenance site. The calcareous shale recognized in the largest clasts is compatible with the lithologies of the drainage basin of the Poggio creek, where the Monte Antola Formation outcrops. This Formation is a turbiditic limestone with levels of shales, Upper Cretaceous-Medium Eocene in age (Abbate and Sagri, 1967; Scholle, 1971). The calculated ages of these thin sections were related to the Roman Period.

4.2.3 Build-ups comparison

The inner structure of the build-ups revealed that matrix or biogenic/terrigenous sediments have filled the originally vacuolar framework, resulting in an inner compact structure in both Portofino and Bogliasco build-ups. The overhanging Portofino build-up revealed a complex pattern of growth direction, while the Bogliasco build-up had a more regular vertical accretion. Both build-ups revealed that the most important contributors to the structural development of the rigid framework are CCA. The conservation of calcareous algae was generally poor, despite their very young geological age, and they did not often show the diagnostic features that are required for species identification. This observation opens further questions about the relationship between age and taphonomic signatures in calcareous frameworks. In both build-ups, the genus *Titanoderma* plays an important role among CCA, although its highly distinctive vegetative anatomy may result in an overestimation of its abundance, in comparison to other corallines. The most common species in the shallow Bogliasco C was *L.* gr. *stictiforme,* while the genus *Mesophyllum* was found to be more common in the deeper Portofino C. A very shallow distribution of *L.* gr. *stictiforme* is in agreement with previous observations for the Apulian C (unpublished); however, the observed depth distribution of

the two genera show an opposite pattern with respect to other published records for the NW Mediterranean (Sartoretto et al., 1996). In the C from Banyuls (France), distributed from 20 to 40 m in depth, *Mesophyllum philippi* (as *Mesophyllum lichenoides*) was reported as the most abundant framework builder, with *Lithophyllum stictiforme* (as *Pseudolithophyllum expansum*) also being abundant (Bosence, 1985). However, the paucity of quantitative data suggests caution, and further investigations are required to clarify the matter.

Di Geronimo et al. (2002) reported the occurrence of *S. ptychoides* inside the Sicilian bio-constructed pillars, although they did not provide any temporal frame for the growth of the bioconstruction. In our samples, *S. ptychoides* is reported for thin section P1D in Portofino, dated at 790–745 BCE, and for thin section B2H in Bogliasco, indirectly attributed to the Roman Period. Based on literature data, both intervals correspond to phases of warm and rather humid climate in the western Mediterranean. However, the two occurrences of *Sporolithon* are separated by a few centuries (Figure 10), and the B2H date was calculated on the basis of a presumed constant accumulation rate. Therefore, we cannot exclude the possibility that only one warm "*Sporolithon* event" occurred in the Ligurian build-ups at about 2.7 ka BP. This age corresponds to a negative NAO Index (Faust et al., 2016), but it should be considered that the Portofino and Bogliasco build-ups grew on the Ligurian continental shelf during the Late Holocene, when the teleconnection between the Western Mediterranean winter rains and the NAO index show an opposite pattern (Jalali et al., 2018; Zielhofer et al., 2019; Figure 10).

The main factors influencing structure, biomass, and metabolism of marine benthic organisms such as CCA are sedimentation-related mechanisms, namely, burial or changes in the quantity/quality of suspended matter and water transparency (Balata et al., 2005), which in turn influence light penetration and may alternatively favor the photoautotrophs or the suspension feeders (Laborel, 1961).

Sedimentation in littoral systems is linked to terrestrial sources and can be affected by natural processes and human activities that have historically altered the coastal erosion/deposition profiles and the transport of suspended particles (Owens, 2020).

Marine sedimentation affects the horizontal rather than the vertical surfaces more easily (Cocito et al., 2002), and shallow-water settings are expected to be more frequently affected by terrigenous input than the deeper settings. In the case of the studied build-ups, differences in the sedimentary regime can be traced between the build-up on the vertical cliff in Portofino and the one from the sub-horizontal substrate in Bogliasco. Most of the Portofino build-up had a contribution higher than 40% by calcareous algae, both on its surfaces and in the inner structure, and minor phases of dominance by annelids and bryozoans, as already reported for build-ups on vertical substrate (Balata et al., 2005).

Portofino build-up contained matrix, as microcrystalline mud with abundant biogenic grains, but no larger terrigenous grains were observed, indicating a minor influence of transport from land.

On the contrary, as expected, the sediment contribution was more abundant in the Bogliasco build-up, both as matrix and as terrigenous fragments, partially inhibiting the surficial coralline algal development, which never exceeds 30.67%. The vicinity of the Bogliasco build-up to the coast also allowed the reconstruction of a past extreme event of flood, recorded inside the bioconstruction as an interval of abundant and large terrigenous clasts lithologically related to the drainage basin of the Poggio creek.

In both build-ups, the identification of levels with abundant calcareous skeletal components alternating with levels of matrix/terrigenous suggests the occurrence of a cyclicity in the formation of the framework.

As already indicated, the reconstruction of C build-up development is not trivial. This is related to the alternation of favorable phases of deposition of carbonate and, in particular, calcareous algae as a major framework builder, and disruption linked to high sedimentation transport that results in shifts of abundance among major components, as already observed for sponge diversity (Bertolino et al., 2017a).

According to many authors (Antonioli et al., 2001; Antonioli et al., 2002; Lambeck et al., 2004; Taricco et al., 2009), the Mediterranean sea level rose from −10 m to −4 m about 6.5 ka BP. The studied area is considered as tectonically stable and the estimated sea-level rise is 0.3 mm y^{-1} with slight deceleration during the last 1,500 years and stabilization near the present datum from about 500 years BP (Laborel et al., 1994; Pirazzoli, 2005). Therefore, the Portofino build-up did not undergo any significant depth variation, while the Bogliasco one developed at a depth changing from about 7 m, 5 ka BP, to the present water depth of 10 m.

Sartoretto et al. (1996) reported that after 5 ka BP, the accumulation rate of C should be insignificant below 60 m wd. We did not deal with the C growth below 60 m; however, both the studied Ligurian build-ups are younger than 5 ka BP and are slowly but actively growing, as demonstrated by the occurrence of live habitat formers at their surfaces and by their growth rates, which are compatible with published data for other relatively shallow C build-ups (Sartoretto et al., 1996; Bertolino et al., 2017b).

5 Conclusion

Coralligenous build-ups are among the most important biogenic frameworks of the Mediterranean shelf (Ingrosso et al., 2018), characterized by slow but continuous growth on both vertical and horizontal substrates.

The quantitative analyses of the major components at the surface of the two studied samples of C, collected in the Ligurian

Sea, show an important variability depending on orientation and exposure (Figures 5, 6). The abundant fleshy algal cover and the absence of corals are the most distinctive traits of Bogliasco C when compared with Portofino (Figures 5, 6). Calcareous algae in Bogliasco exhibit about half of the cover in Portofino, confirming their basically sciaphilic nature and the negative effect of higher sedimentation and space competition with the faster-growing fleshy algae, resulting in a lower accumulation rate of the Bogliasco build-up. Surface and internal components indicate that coralline algae and completely calcified Peyssonneliales represent the most important framework builders, with the genus *Lithophyllum* apparently more common in the shallow Bogliasco C, while *Mesophyllum* plays a major role in the deeper Portofino C. Bryozoans are the second most significant contributor to the C framework, locally showing an opposite trend of abundance with respect to coralline algae.

The studied build-ups developed during the Late Holocene, recording its numerous climate fluctuations. Matrix and terrigenous fragments are negatively correlated with calcareous algae, due to the detrimental effect of a high sedimentation rate on the growth of these photosynthetic organisms. Therefore, we recognize a cyclicity in the inner structure of both build-ups, with the framework composition shifting from calcareous algae-dominated to matrix-dominated. These shifts correspond to Late Holocene climate fluctuations, and in particular, matrix-dominated intervals are correlated with wetter periods, under which sediment transport from the continent is favored, whereas calcareous algae-dominated intervals correspond to drier spells. Coralligenous build-ups are special recorders, able to catch extreme events of flooding and the occurrence of warm "*Sporolithon* events."

While the internal structure of the Bogliasco build-up is completely coherent with the definition of Coralligenous, its present-day shallow distribution, growing amid *Posidonia*, documents an important exception to the rule. In fact, this supports the concept that C is not only the climax of the circalittoral zone, also occurring in the *enclave* at the base of *Posidonia* leaves, but it may also develop and gain significant vertical accretion within the infralittoral zone (Ballesteros, 2006; Bracchi et al., 2016). A mosaic of benthic biocoenoses is expected to occur across ecological boundaries, and further investigations are required to clarify the controls of this spatial pattern.

The occurrence of live calcifiers at the surface of the studied build-ups and their accumulation rates of 0.080 mm y^{-1} for Portofino and 0.065 mm y^{-1} for Bogliasco demonstrate that the Ligurian C is slowly but actively growing.

Physical forces and geological and biological processes controlling the build-ups act at variable temporal and spatial scales, which explains the disparate disciplinary and technical approaches displayed for their exploration. The consequence, however, is an insufficient interdisciplinary communication leading to a fragmented and incomplete understanding of the phenomenon of bioconstruction, an inadequate short-term vision, and poor management of these important habitats. Brief, local investigations, and those monitoring methods based exclusively on visual census of the mega-epibenthos presently dwelling on the algal substrate, appear largely insufficient for describing the diverse expressions of the coralline-engineered habitats as historical structures, and should be integrated in the framework of a geobiological approach. Adding the correct temporal and spatial frame has important implications for our understanding of the history and fate of marine temperate/cold biogenic habitats under the ongoing human impacts, ocean warming, and acidification and for improving their management.

Data availability statement

The original contributions presented in the study are included in the article/Supplementary Material; further inquiries can be directed to the corresponding author.

Author contributions

Conceptualization, DB; methodology, DB, VB, and FM; formal analysis, DB and VB; investigation, DB, VB, FM, and GB; data curation, VB, DB, FM, and PB; writing—original draft preparation, DB and VB; writing—review and editing, DB, VB, PB, and GB; supervision, DB; project administration, DB; funding acquisition, DB. All authors have read and agreed to the published version of the manuscript.

Funding

Project "CRESCIBLUREEF—Grown in the blue: new technologies for knowledge and conservation of Mediterranean reefs," funded by the Italian Ministry of Research and University—Fondo Integrativo Speciale per la Ricerca (FISR), project number: FISR_04543.

Acknowledgments

The authors wish to thank Riccardo Broggini, Erika Cantoro, and Elena Grimoldi for their contributions to material preparation and data collection in the framework of their theses in Marine Geology.

Conflict of interest

The authors declare that the research was conducted in the absence of any commercial or financial

relationships that could be construed as a potential conflict of interest.

Publisher's note

All claims expressed in this article are solely those of the authors and do not necessarily represent those of their affiliated organizations, or those of the publisher, the editors, and the reviewers. Any product that may be evaluated in this article, or claim that may be made by its manufacturer, is not guaranteed or endorsed by the publisher.

Supplementary material

The Supplementary Material for this article can be found online at: https://www.frontiersin.org/articles/10.3389/feart.2022.961632/full#supplementary-material.

References

Abbate, E., and Sagri, M. (1967). Suddivisioni litostratigrafiche nei calcare ad elmintoidi Auctt, della placca dell' Ebro-Antola e correlazioni con terreni simili affioranti tra Voghera e Castelnovo de' Monti (Appennino Settentrionale). *Soc. Geol. Ital. Mem.* 6, 23–65.

Adey, W. H. (1986). "Coralline algae as indicators of sea-level", in *sea-level research*. Editor O. van de Plassche (Dordrecht: Springer), 229–280. doi:10.1007/978-94-009-4215-8_9

Adey, W. H. (1979). "Crustose coralline algae as microenvironmental indicators for the Tertiary", in *Historical biogeography, plate tectonics, and the changing environment*. Editors J. Gray and A. J. Boucot (Oregon State University Press), 459–464.

Adey, W. H., and Macintyre, I. G. (1973). Crustose coralline algae: A re-evaluation in the geological sciences. *Geol. Soc. Am. Bull.* 84, 883–904. doi:10.1130/0016-7606(1973)84<883:ccaari>2.0.co;2

Alongi, G., Cormaci, M., and Furnari, G. (1996). On the occurrence of *Sporolithon ptychoides* Heydrich (corallinales, sporolithaceae, rhodophyta) in the Mediterranean sea. *Cryptogam. Algol.* 17, 131–137.

Alverson, K., and Kull, C. (2003). Understanding future climate change using paleorecords, in *Global Climate*. Editors X. Rodó and F. A. Comín (Berlin, Heidelberg: Springer), 153–185. doi:10.1007/978-3-662-05285-3_9

Antonioli, F., Silenzi, S., and Frisia, S. (2001). Tyrrhenian Holocene palaeoclimate trends from spelean serpulids. *Quaternary Science Reviews* 20 (15), 1661–1670. doi:10.1016/S0277-3791(01)00012-9

Antonioli, F., Cremona, G., Immordino, F., Puglisi, C., Romagnoli, C., Silenzi, S., Valpreda, E., and Verrubbi, V. (2002). New data on the Holocenic sea-level rise in NW Sicily (Central Mediterranean Sea). *Global and Planetary Change* 34, 1-2, 121–140, doi:10.1016/s0921-8181(02)00109-1

Athanasiadis, A., and Ballantine, D. L. (2014). The genera *Melyvonnea* gen. nov. and *Mesophyllum* s.s. (Melobesioideae, Corallinales, Rhodophyta) particularly from the central Atlantic Ocean. *Nordic J. Bot.* 32, 385–436. doi:10.1111/njb.00265

Babbini, L., and Bressan, G. (1997). Recensement de Corallinacées de la Mer Méditerranée et considérations phytogéographiques. *Bibl. Phycol.* 103, 1–421.

Balata, D., Piazzi, L., Cecchi, E., and Cinelli, F. (2005). Variability of Mediterranean coralligenous assemblages subject to local variation in sediment deposition. *Mar. Environ. Res.* 60, 403–421. doi:10.1016/j.marenvres.2004.12.005

Ballesteros, E. (2006). Mediterranean coralligenous assemblages. *Oceanogr. Mar. Biol.* 44, 123–195. doi:10.1201/9781420006391.ch4

Barberá, C., Moranta, J., Ordines, F., Ramón, M., De Mesa, A., Díaz-Valdés, M., et al. (2012). Biodiversity and habitat mapping of Menorca channel (Western Mediterranean): Implications for conservation. *Biodivers. Conserv.* 21, 701–728. doi:10.1007/s10531-011-0210-1

Basso, D. (2012). Carbonate production by calcareous red algae and global change. *Geodiversitas* 34(1), 13–33. doi:10.5252/g2012n1a2

Basso, D., Nalin, R., and Massari, F. (2007). Genesis and composition of the Pleistocene Coralligène de plateau of the Cutro Terrace (Calabria, Southern Italy). *N. Jb. Geol.Paläont.* 244/2, 73–182. doi:10.1127/0077-7749/2007/0244-0173

Basso, D., Nalin, R., and Nelson, C. S. (2009). Shallow-water *Sporolithon* rhodoliths from North Island (New Zealand). *Palaios* 24, 92–103. doi:10.2110/palo.2008.p08-048r

Basso, D., and Rodondi, G. (2006). A Mediterranean population of *Spongites fruticulosus* (Rhodophyta, Corallinales), the type species of *Spongites*, and the taxonomic status of *S. stalactitica* and *S. racemosa*. *Phycologia* 45, 403–416. doi:10.2216/04-93.1

Bazzicalupo, P., Maiorano, P., Girone, A., Marino, M., Combourieu-Nebout, N., Pelosi, N., et al. (2020). Holocene climate variability of the Western Mediterranean: Surface water dynamics inferred from calcareous plankton assemblages. *Holocene* 30, 691–708. doi:10.1177/0959683619895580

Bellan-Santini, D., Bellan, G., Bitar, G., Harmelin, J.-G., and Pergent, G. (2007). *Handbook for interpreting types of marine habitat for the selection of sites to be included in the national inventories of natural sites of conservation interest*. Tunis: UNEP-MAP-RAC/SPA.

Bertolino, M., Calcinai, B., Cattaneo-Vietti, R., Cerrano, C., Lafratta, A., Pansini, M., et al. (2014). Stability of the sponge assemblage of Mediterranean coralligenous concretions along a millennial time span. *Mar. Ecol.* 35, 149–158. doi:10.1111/maec.12063

Bertolino, M., Cattaneo-Vietti, R., Costa, G., Pansini, M., Fraschetti, S., and Bavestrello, G. (2017a). Have climate changes driven the diversity of a Mediterranean coralligenous sponge assemblage on a millennial timescale? *Palaeogeogr. Palaeoclimatol. Palaeoecol.* 487, 355–363. doi:10.1016/j.palaeo.2017.09.020

Bertolino, M., Costa, G., Carella, M., Cattaneo-Vietti, R., Cerrano, C., Pansini, M., et al. (2017b). The dynamics of a Mediterranean coralligenous sponge assemblage at decennial and millennial temporal scales. *PLoS ONE* 12, e0177945. doi:10.1371/journal.pone.0177945

Bini, M., Zanchetta, G., Regattieri, E., Isola, I., Drysdale, R. N., Fabiani, F., et al. (2020). Hydrological changes during the Roman Climatic Optimum in northern Tuscany (Central Italy) as evidenced by speleothem records and archaeological data. *J. Quat. Sci.* 35, 791–802. doi:10.1002/jqs.3224

Bond, G., Kromer, B., Beer, J., Muscheler, R., Evans, M. N., Showers, W., et al. (2001). Persistent solar influence on North Atlantic climate during the Holocene. *Science* 294, 2130–2136. doi:10.1126/science.1065680

Bosence, D. W. J. (1985). "The "coralligène" of the mediterranean - a recent analog for Tertiary Coralline Algal Limestones", in *Paleoalgology: Contemporary research and applications*. Editors D. F. Toomey and M. H. Nitecki (Berlin, Heidelberg: Springer), 216–225. doi:10.1007/978-3-642-70355-3_16

Boudouresque, C. F., Blanfuné, A., Harmelin-Vivien, M., Personnic, S., Ruitton, S., Thibaut, T., et al. (2017). "Where seaweed forests meet animal forests: The examples of macroalgae in coral reefs and the mediterranean coralligenous ecosystem", in *Marine animal forests*. Editors S. Rossi, L. Bramanti, A. Gori, and C. Orejas (Cham: Springer), 369–396. doi:10.1007/978-3-319-21012-4_48

Bourcier, M. (1986). "Évolution, en cinq années, des herbiers à *Posidonia oceanica* et du macrobenthos circalittoral action conjuguée des activités humaines et des modifications climatiques", in *Change, over five years, of a* Posidonia oceanica *bed and circalittoral macrobenthos the combined effect of human activity and climatic conditions* (Banyuls s/mer, France: Vie et Milieu), 1–8. Avaliable at: https://hal.sorbonne-universite.fr/hal-03023741.

Bracchi, V. A., Basso, D., Marchese, F., Corselli, C., and Savini, A. (2017). Coralligenous morphotypes on subhorizontal substrate: A new categorization. *Cont. Shelf Res.* 144, 10–20. doi:10.1016/j.csr.2017.06.005

Bracchi, V. A., Basso, D., Savini, A., and Corselli, C. (2019). Algal reefs (Coralligenous) from glacial stages: Origin and nature of a submerged tabular relief (Hyblean Plateau, Italy). *Mar. Geol.* 411, 119–132. doi:10.1016/j.margeo.2019.02.008

Bracchi, V.A., Bazzicalupo, P., Fallati, L., Varzi, A.G., Savini, A., Negri, M.P., et al. (2022). The main builders of Mediterranean Coralligenous: 2D and 3D quantitative approaches for its identification. *Front. Earth Sci. (Lausanne).* 10. doi:10.3389/feart.2022.910522

Bracchi, V. A., Nalin, R., and Basso, D. (2016). Morpho-structural heterogeneity of shallow-water coralligenous in a Pleistocene marine terrace (Le Castella, Italy). *Palaeogeogr. Palaeoclimatol. Palaeoecol.* 454, 101–112. doi:10.1016/j.palaeo.2016.04.014

Bracchi, V. A., Nalin, R., and Basso, D. (2014). Paleoecology and dynamics of coralline dominated facies during a Pleistocene transgressive-regressive cycle (Capo

Colonna marine terrace, Southern Italy). *Palaeogeogr. Palaeoclimatol. Palaeoecol.* 414, 296–309. doi:10.1016/j.palaeo.2014.09.016

Braga, J. C., and Bassi, D. (2007). Neogene history of *Sporolithon* Heydrich (Corallinales, Rhodophyta) in the Mediterranean region. *Palaeogeogr. Palaeoclimatol. Palaeoecol.* 243, 189–203. doi:10.1016/j.palaeo.2006.07.014

Bressan, G., and Babbini, L. (2003). Biodiversità marina delle coste italiane: Corallinales del Mar Mediterraneo: Guida alla determinazione. *Giulio Relini* 10, 1123–4245.

Canals, M., and Ballesteros, E. (1997). Production of carbonate particles by phytobenthic communities on the Mallorca-Menorca shelf, northwestern Mediterranean Sea. *Deep Sea Res. Part II Top. Stud. Oceanogr.* 44, 611–629. doi:10.1016/s0967-0645(96)00095-1

Cánovas Molina, A., Montefalcone, M., Vassallo, P., Morri, C., Nike Bianchi, C., and Bavestrello, G. (2016). Combining literature review, acoustic mapping and *in situ* observations: An overview of coralligenous assemblages in Liguria (NW Mediterranean sea). *Sci. Mar.* 80, 7–16. doi:10.3989/scimar.04235.23A

Casas-Güell, E., Cebrian, E., Garrabou, J., Ledoux, J.-B., Linares, C., and Teixidó, N. (2016). Structure and biodiversity of coralligenous assemblages dominated by the precious red coral *Corallium rubrum* over broad spatial scales. *Sci. Rep.* 6, 36535. doi:10.1038/srep36535

Casas-Güell, E., Teixidó, N., Garrabou, J., and Cebrian, E. (2015). Structure and biodiversity of coralligenous assemblages over broad spatial and temporal scales. *Mar. Biol.* 162, 901–912. doi:10.1007/s00227-015-2635-7

Casellato, S., and Stefanon, A. (2008). Coralligenous habitat in the northern Adriatic Sea: An overview. *Mar. Ecol.* 29, 321–341. doi:10.1111/j.1439-0485.2008.00236.x

Catra, M., Giardina, S., Giaccone, T., Basso, D., and Giaccone, G. (2007). Coralligenous assemblages of Sicchitello (Ustica - Palermo). *Biol. Mar. Mediterr.* 14, 174–175.

Cebrián, E., Ballesteros, E., and Canals, M. (2000). Shallow rocky bottom benthic assemblages as calcium carbonate producers in the Alboran Sea (Southwestern Mediterranean). *Oceanol. Acta* 23, 311–322. doi:10.1016/s0399-1784(00)00131-6

Cerrano, C., Bavestrello, G., Bianchi, C. N., Calcinai, B., Cattaneo-Vietti, R., Morri, C., et al. (2001). "The role of sponge bioerosion in Mediterranean coralligenous accretion," in *The role of sponge bioerosion in the Mediterranean coralligenous accretion" in Mediterranean ecosystems: Structure and processes*. Editors F. M. Faranda, L. Guglielmo, and G. Spezie (Verlag, Italy: Springer), 235–240. doi:10.1007/978-88-470-2105-1_30

Çinar, M. E., Féral, J. P., Arvanitidis, C., David, R., Taşkin, E., Sini, M., et al. (2020). Coralligenous assemblages along their geographical distribution: Testing of concepts and implications for management. *Aquat. Conserv. Mar. Freshw. Ecosyst.* 30, 1578–1594. doi:10.1002/aqc.3365

Cocito, S., Bedulli, D., and Sgorbini, S. (2002). Distribution patterns of the sublittoral epibenthic assemblages on a rocky shoal in the Ligurian Sea (NW Mediterranean). *Sci. Mar.* 66, 175–181. doi:10.3989/scimar.2002.66n2175

Cocito, S. (2004). Bioconstruction and biodiversity: Their mutual influence. *Sci. Mar.* 68, 137–144. doi:10.3989/scimar.2004.68s1137

Connell, S. D., Foster, M. S., and Airoldi, L. (2014). What are algal turfs? Towards a better description of turfs. *Mar. Ecol. Prog. Ser.* 495, 299–307.

Corriero, G., Pierri, C., Mercurio, M., Nonnis Marzano, C., Onen Tarantini, S. O., Gravina, M. F., et al. (2019). A Mediterranean mesophotic coral reef built by non-symbiotic scleractinians. *Sci. Rep.* 9, 1–17. doi:10.1038/s41598-019-40284-4

Costanzo, L. G., Marletta, G., and Alongi, G. (2021). Non-indigenous macroalgal species in coralligenous habitats of the marine protected area Isole Ciclopi (Sicily, Italy). *Ital. Bot.* 11, 31–44. doi:10.3897/italianbotanist.11.60474

De Jode, A., David, R., Haguenauer, A., Cahill, A. E., Erga, Z., Guillemain, D., et al. (2019). From seascape ecology to population genomics and back. Spatial and ecological differentiation among cryptic species of the red algae *Lithophyllum stictiforme/L. cabiochiae*, main bioconstructors of coralligenous habitats. *Mol. Phylogenetics Evol.* 137, 104–113. doi:10.1016/j.ympev.2019.04.005

Di Geronimo, I., Di Geronimo, R., Improta, S., Rosso, A., and Sanfilippo, R. (2001). Preliminary observations on a columnar coralline build-up from off SE Sicily. *Biol. Mar. Medit.* 8, 229–237.

Di Geronimo, I., Di Geronimo, R., Rosso, A., and Sanfilippo, R. (2002). Structural and taphonomic analysis of a columnar coralline algal build-up from SE Sicily. *Geobios* 35 (35), 86–95. doi:10.1016/s0016-6995(02)00050-5

Di Iorio, L., Audax, M., Deter, J., Holon, F., Lossent, J., Gervaise, C., et al. (2021). Biogeography of acoustic biodiversity of NW Mediterranean coralligenous reefs. *Sci. Rep.* 11, 16991 doi:10.1038/s41598-021-96378-5

Falace, A., Kaleb, S., Curiel, D., Miotti, C., Galli, G., Querin, S., et al. (2015). Calcareous bio-concretions in the northern Adriatic Sea: Habitat types, environmental factors that influence habitat distributions, and predictive modeling. *PLoS ONE* 10, e0140931. doi:10.1371/journal.pone.0140931

Faust, J. C., Fabian, K., Milzer, G., Giraudeau, J., and Knies, J. (2016). Norwegian fjord sediments reveal NAO related winter temperature and precipitation changes of the past 2800 years. *Earth Planet. Sci. Lett.* 435, 84–93. doi:10.1016/j.epsl.2015.12.003

Ferdeghini, F., Acunto, S., Cocito, S., and Cinelli, F. (2000). Variability at different spatial scales of a coralligenous assemblage at Giannutri Island (Tuscan Archipelago, northwest Mediterranean). *Hydrobiologia* 440, 27–36. doi:10.1007/978-94-017-1982-7_3

Flügel, E. (2010). *Microfacies of carbonate rocks: Analysis, interpretation and application*. Berlin: Springer-Verlag.

Garrabou, J., Ballesteros, E., and Zabala, M. (2002). Structure and dynamics of north-western Mediterranean rocky benthic communities along a depth gradient. *Estuar. Coast. Shelf Sci.* 55, 493–508. doi:10.1006/ecss.2001.0920

Gatti, G., Bianchi, C. N., Morri, C., Montefalcone, M., and Sartoretto, S. (2015). Coralligenous reefs state along anthropized coasts: Application and validation of the COARSE index, based on a rapid visual assessment (RVA) approach. *Ecol. Indic.* 52, 567–576. doi:10.1016/j.ecolind.2014.12.026

Gili, J. M., and Ros, J. D. (1985). Study and cartography of the benthic communities of Medes Islands (NE Spain). *Mar. Ecol.* 6, 219–238. doi:10.1111/j.1439-0485.1985.tb00323.x

Gómez-Gras, D., Linares, C., Dornelas, M., Madin, J. S., Brambilla, V., Ledoux, J. B., et al. (2021). Climate change transforms the functional identity of Mediterranean coralligenous assemblages. *Ecol. Lett.* 24, 1038–1051. doi:10.1111/ele.13718

Guiry, M. D., and Guiry, G. M. (2022). "AlgaeBase", in *World-wide electronic publication* (Galway: National University of Ireland). AvaliableAt: https://www.algaebase.org.

Hall-Spencer, J. M., Rodolfo-Metalpa, R., Martin, S., Ransome, E., Fine, M., Turner, S. M., et al. (2008). Volcanic carbon dioxide vents show ecosystem effects of ocean acidification. *Nature* 454(7200), 96–99. doi:10.1038/nature07051

Hammer, Ø., Harper, D. A. T., and Ryan, P. D. (2001). Past: Paleontological statistics software package for education and data analysis. *Palaeontol. Electron.* 4, 9.

Hrabovský, J., Basso, D., and Doláková, N. (2016). Diagnostic characters in fossil coralline algae (Corallinophycidae: Rhodophyta) from the miocene of southern moravia (carpathian foredeep, Czech republic). *J. Syst. Palaeontol.* 14, 499–525. doi:10.1080/14772019.2015.1071501

Ingrosso, G., Abbiati, M., Badalamenti, F., Bavestrello, G., Belmonte, G., Cannas, R., et al. (2018). Mediterranean bioconstructions along the Italian coast. *Adv. Mar. Biol.* 79, 61–136. doi:10.1016/bs.amb.2018.05.001

IPCC (2022). *Climate change 2022: Impacts, adaptation, and vulnerability. Contribution of working group II to the sixth assessment report of the intergovernmental panel on climate change*. Editors H. O Pörtner, D. C. Roberts, M. Tignor, E. S. Poloczanska, K. Mintenbeck, A. Alegria, et al. (Cambridge, United Kingdom and New York, NY, USA: Cambridge University Press).

Irvine, L. M., and Chamberlain, Y. M. (1994). "Seaweeds of the British isles," in *Rhodophyta. Part 2B. Corallinales, hildenbrandiales* (London: HMSO).

Jalali, B., Sicre, M. A., Bassetti, M. A., and Kallel, N. (2016). Holocene climate variability in the north-western Mediterranean sea (Gulf of Lyon). *Clim. Past.* 12, 91–101. doi:10.5194/cp-12-91-2016

Jalali, B., Sicre, M. A., Klein, V., Schmidt, S., Maselli, V., Lirer, F., et al. (2018). Deltaic and coastal sediments as recorders of Mediterranean regional climate and human impact over the past three millennia. *Paleoceanogr. Paleoclimatology* 33, 579–593. doi:10.1029/2017pa003298

Jalut, G., Esteban Amat, A. E., Bonnet, L., Gauquelin, T., and Fontugne, M. (2000). Holocene climatic changes in the Western Mediterranean, from south-east France to south-east Spain. *Palaeogeogr. Palaeoclimatol. Palaeoecol.* 160, 255–290. doi:10.1016/s0031-0182(00)00075-4

Johansen, H. W. (1981). *Coralline algae, a first synthesis*. Boca Raton, FL: CRC Press.

Joher, S., Ballesteros, E., and Rodrigues-prieto, C. (2015). Contribution to the study of deep coastal detritic bottoms: The algal communities of the continental shelf off the Balearic Islands, western Mediterranean. *Medit. Mar. Sci.* 16, 573–590. doi:10.12681/mms.1249

Kuffner, I. B., Andersson, A. J., Jokiel, P. L., Rodgers, K. U. S., and Mackenzie, F. T. (2008). Decreased abundance of crustose coralline algae due to ocean acidification. *Nat. Geosci.*. 1(2), 114–117. doi:10.1038/ngeo100

Laborel, J. (1961). Le concrétionnement algal 'coralligène' et son importance géomorphologique en Méditerranée. *Rec. Trav. St. Mar. Endoume* 23, 37–60.

Laborel, J. (1987). Marine biogenic constructions in the Mediterranean, a review. *Sci. Rep. Port. Cros Natl. Park* 13, 97–126.

Laborel, J., Morhange, C., Lafont, R., Le Campion, J., Laborel-Deguen, F., and Sartoretto, S. (1994). Biological evidence of sea-level rise during the last 4500 years on the rocky coasts of continental southwestern France and Corsica. *Mar. Geol.* 120, 203–223. doi:10.1016/0025-3227(94)90059-0

Lambeck, K., Antonioli, F., Purcell, A., and Silenzi, S. (2004). Sea-level change along the Italian coast for the past 10,000yr. *Quat. Sci. Rev.* 23, 1567–1598. doi:10.1016/j.quascirev.2004.02.009

Laubier, L. (1966). Le coralligène des albères : Monographie biocénotique. *Ann. l'Institut Océanogr.* 43, 139–316.

Marchese, F., Bracchi, V. A., Lisi, G., Basso, D., Corselli, C., and Savini, A. (2020). Assessing fine-scale distribution and volume of Mediterranean algal reefs through terrain analysis of multibeam bathymetric data. A case study in the southern Adriatic continental shelf. *Water* 12, 157. doi:10.3390/w12010157

Luterbacher, J., García-Herrera, R., Akcer-On, S., Allan, R., Alvarez-Castro, M. C., Benito, G., et al. (2012). A review of 2000 years of paleoclimatic evidence in the Mediterranean in *The climate of the Mediterranean region: from the past to the future*. Editor P. Lionello (Elsevier), 87–185. doi:10.1016/B978-0-12-416042-2.00002-1

Martin, S., and Gattuso, J.-P. (2009). Response of Mediterranean coralline algae to ocean acidification and elevated temperature. *Glob. Change Biol.* 15, 2089–2100. doi:10.1111/j.1365-2486.2009.01874.x

Martrat, B., Jimenez-Amat, P., Zahn, R., and Grimalt, J. O. (2014). Similarities and dissimilarities between the last two deglaciations and interglaciations in the North Atlantic region. *Quat. Sci. Rev.* 99, 122–134. doi:10.1016/j.quascirev.2014.06.016

Montefalcone, M., Morri, C., Bianchi, C. N., Bavestrello, G., and Piazzi, L. (2017). The two facets of species sensitivity: Stress and disturbance on coralligenous assemblages in space and time. *Mar. Pollut. Bull.* 117, 229–238. doi:10.1016/j.marpolbul.2017.01.072

Nalin, R., Basso, D., and Massari, F. (2006). "Pleistocene coralline algal build-ups (coralligène de plateau) and associated bioclastic deposits in the sedimentary cover of Cutro marine terrace (Calabria, southern Italy)", in *Cool–water carbonates: Depositional systems and palaeoenvironmental controls*. Editors H. M. Pedley and G. Carannante (London, UK: Geol. Soc. Spec. Publ.), 255, 11–22. doi:10.1144/GSL.SP.2006.255.01.02

Nalin, R., Lamothe, M., Auclair, M., and Massari, F. (2020). Chronology of the marine terraces of the Crotone Peninsula (Calabria, southern Italy) by means of infrared-stimulated luminescence (IRSL). *Mar. Petroleum Geol.* 122, 104645. doi:10.1016/j.marpetgeo.2020.104645

Novosel, M., Pozar-Domac, A., and Pasaric, M. (2004). Diversity and distribution of the Bryozoa along underwater cliffs in the Adriatic Sea with special reference to thermal regime. *Mar. Ecol.* 25, 155–170. doi:10.1111/j.1439-0485.2004.00022.x

Owens, P. N. (2020). Soil erosion and sediment dynamics in the Anthropocene: A review of human impacts during a period of rapid global environmental change. *J. Soils Sediments* 20, 4115–4143. doi:10.1007/s11368-020-02815-9

Pérès, J. M. (1982). "Major benthic assemblages", in *Marine ecology*. Editor O. Kinne (Hoboken, NJ: Wiley and Sons), 373–521.

Pezzolesi, L., Peña, V., Le Gall, L., Gabrielson, P., Kaleb, S., Hughey, J., et al. (2019). Mediterranean *Lithophyllum stictiforme* (Corallinales, Rhodophyta) is a genetically diverse species complex: implications for species circumscription, biogeography and conservation of coralligenous habitats. *J. Phycol.* 55, 473–492. doi:10.1111/jpy.12837

Piazzi, L., Balata, D., Cecchi, E., Cinelli, F., and Sartoni, G. (2009). Species composition and patterns of diversity of macroalgal coralligenous assemblages in the north-western Mediterranean Sea. *J. Nat. Hist.* 44, 1–22. doi:10.1080/00222930903377547

Piazzi, L., Cinti, M. F., Guala, I., Grech, D., La Manna, G., Pansini, A., et al. (2021). Variations in coralligenous assemblages from local to biogeographic spatial scale. *Mar. Environ. Res.* 169, 105375. doi:10.1016/j.marenvres.2021.105375

Piazzi, L., Ferrigno, F., Guala, I., Cinti, M. F., Conforti, A., De Falco, G., et al. (2022). Inconsistency in community structure and ecological quality between platform and cliff coralligenous assemblages. *Ecol. Indic.* 136, 108657. doi:10.1016/j.ecolind.2022.108657

Piazzi, L., Gennaro, P., and Balata, D. (2011). Effects of nutrient enrichment on macroalgal coralligenous assemblages. *Mar. Pollut. Bull.* 62, 1830–1835. doi:10.1016/j.marpolbul.2011.05.004

Pierdomenico, M., Bonifazi, A., Argenti, L., Ingrassia, M., Casalbore, D., Aguzzi, L., Viaggiu, E., Le Foche, M., and Chiocci, F.L. (2021). Geomorphological characterization, spatial distribution and environmental status assessment of coralligenous reefs along the Latium continental shelf. *Ecol. Indic.* 131. 108219, doi:10.1016/j.ecolind.2021.108219

Pirazzoli, P. A. (2005). A review of possible eustatic, isostatic and tectonic contributions in eight late-Holocene relative sea-level histories from the Mediterranean area. *Quat. Sci. Rev.* 24, 1989–2001. doi:10.1016/j.quascirev.2004.06.026

Ponti, M., Fava, F., and Abbiati, M. (2011). Spatial-temporal variability of epibenthic assemblages on subtidal biogenic reefs in the northern Adriatic Sea. *Mar. Biol.* 158, 1447–1459. doi:10.1007/s00227-011-1661-3

Rasband, W. S. (1997). ImageJ. Bethesda, Maryland, USA: U. S. National Institutes of Health. AvaliableAt: https://imagej.nih.gov/ij/.

Richards, J. L., Sauvage, T., Schmidt, W. E., Fredericq, S., Hughey, J. R., and Gabrielson, P. W. (2017). The coralline genera *Sporolithon* and *Heydrichia* (Sporolithales, Rhodophyta) clarified by sequencing type material of their generitypes and other species. *J. Phycol.* 53, 1044–1059. doi:10.1111/jpy.12562

Rodolfo-Metalpa, R., Martin, S., Ferrier-Pagès, C., and Gattuso, J.-P. (2010). Response of the temperate coral *Cladocora caespitosa* to mid- and long-term exposure to pCO2 and temperature levels projected for the year 2100 AD, *Biogeosciences*, 7, 289–300, doi:10.5194/bg-7-289-2010

Rosso, A., and Sanfilippo, R. (2009). The contribution of bryozoans and serpuloideans to coralligenous concretions from SE Sicily in UNEP-MAP-RAC/SPA, Proceedings of the First Symposium on the Coralligenous and Other Calcareous Bio-Concretions of the Mediterranean Sea, *Tabarka, January* 15–16, 123–128.

Sanfilippo, R., Rosso, A., Basso, D., Violanti, D., Di Geronimo, I., Di Geronimo, R., Benzoni, F., and Robba, E. (2011). Cobbles colonization pattern from a tsunami-affected coastal area (SW Thailand, Andaman Sea). *Facies* 57, 1–13. doi:10.1007/s10347-010-0226-0

Sarmiento, J. L., Hughes, T., Stouffer, R. J., and Manabe, S. (1998). Simulated response of the ocean carbon cycle to anthropogenic climate warming. *Nature* 393(6682), 245–249. doi:10.1038/30455

Sartoretto, S. (2017). "IV.3.1 Biocénose coralligène," in *Fiches descriptives des biocénoses benthiques de Méditerranée*. Editor L. Riviere (Paris, France: Paris UMS PatriNat OFB-CNRS-MNHN), 497–502.

Sartoretto, S. (1994). Structure et dynamique d'un nouveau type de bioconstruction à *Mesophyllum lichenoides* (Ellis) Lemoine (Corallinales, Rhodophyta). *Acad. Sci., Série 3, Sci. vie* 317, 156–160.

Sartoretto, S., Verlaque, M., and Laborel, J. (1996). Age of settlement and accumulation rate of submarine "coralligène" (−10 to −60 m) of the northwestern Mediterranean Sea; relation to Holocene rise in sea level. *Mar. Geol.* 130, 317–331. doi:10.1016/0025-3227(95)00175-1

Scholle, P. A. (1971). Diagenesis of deep-water carbonate turbidites, upper cretaceous Monte Antola flysch, northern apennines, Italy. *J. Sediment. Pet.* 4, 233–250.

Taricco, C., Ghil, M., Alessio, S., and Vivaldo, G. (2009). Two millennia of climate variability in the Central Mediterranean. *Clim. Past.* 5, 171–181. doi:10.5194/cp-5-171-2009

Titschack, J., Nelson, C. S., Beck, T., Freiwald, A., and Radtke, U. (2008). Sedimentary evolution of a late Pleistocene temperate red algal reef (coralligène) on rhodes, Greece: Correlation with global sea-level fluctuations. *Sedimentology* 55, 1747–1776. doi:10.1111/j.1365-3091.2008.00966.x

Virgilio, M., Airoldi, L., and Abbiati, M. (2006). Spatial and temporal variations of assemblages in a Mediterranean coralligenous reef and relationships with surface orientation. *Coral reefs*. 25, 265–272. doi:10.1007/s00338-006-0100-2

Wirth, S. B., Glur, L., Gilli, A., and Anselmetti, F. S. (2013). Holocene flood frequency across the Central Alps - solar forcing and evidence for variations in North Atlantic atmospheric circulation. *Quat. Sci. Rev.* 80, 112–128. doi:10.1016/j.quascirev.2013.09.002

Wisshak, M., Schönberg, C. H., Form, A., and Freiwald, A. (2014). Sponge bioerosion accelerated by ocean acidification across species and latitudes? *Helgol. Mar. Res.* 68, 253–262. doi:10.1007/s10152-014-0385-4

Woelkerling, W. J., Irvine, L. M., and Harvey, A. S. (1993). Growth-forms in non-geniculate coralline red algae (Coralliinales, Rhodophyta). *Aust. Syst. Bot.* 6, 277–293. doi:10.1071/sb9930277

WoRMS Editorial Board (2019). World register of marine species. Avaliable at: http://www.marinespecies.org.

Zielhofer, C., Köhler, A., Mischke, S., Benkaddour, A., Mikdad, A., and Fletcher, W. J. (2019). Western Mediterranean hydro-climatic consequences of Holocene ice-rafted debris (Bond) events. *Clim. Past.* 15, 463–475. doi:10.5194/cp-15-463-2019

Zunino, S., Canu, D. M., Zupo, V., and Solidoro, C. (2019). Direct and indirect impacts of marine acidification on the ecosystem services provided by coralligenous reefs and seagrass systems. *Glob. Ecol. Conservation* 18, e00625. doi:10.1016/j.gecco.2019.e00625

frontiers | Frontiers in Earth Science

TYPE Original Research
PUBLISHED 02 September 2022
DOI 10.3389/feart.2022.957780

OPEN ACCESS

EDITED BY
Daniela Basso,
University of Milano-Bicocca, Italy

REVIEWED BY
Marco Brandano,
Sapienza University of Rome, Italy
Werner E. Piller,
University of Graz, Austria
Andrej Ernst,
University of Hamburg, Germany

*CORRESPONDENCE
Juan C. Braga,
jbraga@ugr.es

SPECIALTY SECTION
This article was submitted to Paleontology, a section of the journal Frontiers in Earth Science

RECEIVED 31 May 2022
ACCEPTED 22 July 2022
PUBLISHED 02 September 2022

CITATION
Braga JC and Aguirre J (2022), Trough cross-bedded rhodolith limestones in the Atlantic-linked Ronda Basin (Messinian, Southern Spain). *Front. Earth Sci.* 10:957780. doi: 10.3389/feart.2022.957780

Trough cross-bedded rhodolith limestones in the Atlantic-linked Ronda Basin (Messinian, Southern Spain)

Juan C. Braga* and Julio Aguirre

Dpto Estratigrafía y Paleontología, Facultad de Ciencias, Fuentenueva s/n, Universidad de Granada, Granada, Spain

Rhodolith limestones occur in the upper part of the Miocene infill of the Ronda Basin in southern Spain. This basin was an embayment at the southern margin of the Atlantic-linked Guadalquivir Basin, the foreland basin of the Betic Cordillera. Messinian rhodolith limestones crop out in the mesa of the Roman settlement Acinipo. They mostly consist of trough cross-bedded rhodolith rudstones, which change basinward to large-scale planar cross-bedded rhodolith rudstones, which in turn pass laterally to planar cross-bedded and flat-bedded bryozoan rudstones. Rhodoliths in rudstones are generally broken, exhibiting several phases of breakage and restarted growth of coralline algae. Many rhodoliths also show asymmetrical growth. The rudstone matrix is a packstone with fragments of coralline algae, bryozoans, calcitic bivalves, echinoids, and foraminifers. Large lithoclasts from the basement, heavily bored by bivalves, are common in the rhodolith rudstone, especially in the most massive type. Rhodolith characteristics and sedimentary structures suggest that trough cross-bedded rhodolith rudstones accumulated in submarine dunes moved by storm surges in a littoral wedge at the western side of a small bay (the Ruinas de Acinipo bay) in the Ronda Basin. Large-scale planar cross-bedded coralline algal and bryozoan rudstones formed in the foresets of the wedge progradation below the storm-wave base. The dominance of Lithophyllaceae and Hapalidiales, with scarce representatives of Corallinaceae in the coralline algal assemblages, reflects that Ronda and Guadalquivir basins opened to the Atlantic Ocean.

KEYWORDS

fossil coralline algae, storm deposits, littoral wedge, paleobiogeography, late, Miocene

1 Introduction

Fossil rhodolith concentrations formed on gently dipping ramps and rimmed shelves usually are massive or roughly bedded deposits of decimeters to several meters thickness (Pisera and Studencki, 1989; Aguirre et al., 1993, 2012, 2017; Nalin et al., 2008; Brandano et al., 2009; Bassi and Nebelsick, 2010; Brandano and Piller, 2010; Cornée et al., 2012; Brandano and Ronca, 2014; Brandano, 2017; Sola et al., 2022). This reflects

autochthonous to parautochthonous accumulation of rhodoliths growing under low to moderate hydrodynamic conditions and low sediment supply for prolonged times (Aguirre et al., 2017 and references therein; Millar and Gagnon, 2018). Rhodolith concentrations also occur in large-scale cross beds or clinoforms on the slope of platforms, such as in the early Miocene of Sardinia (Benisek et al., 2009, 2010) or on the steeply inclined distal part of ramps, such as in the Late Miocene ramp in Menorca (Obrador et al., 1992; Pomar, 2001; Pomar et al., 2002; Brandano et al., 2005) and in the foresets of a littoral wedge in the Miocene of Corsica (Brandano and Ronca, 2014). The clinoforms reflect a steep depositional profile on which *in situ* rhodolith growth was as important as downslope displacement of coralline nodules from shallower areas. In contrast, trough cross-bedded dense rhodolith accumulations have only been described in short intervals in rhodolith limestones mainly displaying massive to crude bedding or channelized beds (Miocene of Malta, Bosence and Pedley, 1982; Oligocene of Malta and southern Italy, Pedley, 1998; Pliocene of Guadeloupe, Cornée, et al., 2012). The trough cross-bedded intervals probably represent the shallowest facies of middle-ramp rhodolith concentrations (Pedley, 1998; Cornée et al., 2012).

At first sight, trough-cross bedding generated in submarine dunes seems incompatible with *in situ* rhodolith growth, which is usually favored by low to moderate turbulence. However, despite the rarity of reported cases in the geological record, rhodoliths might grow on submarine dunes and be incorporated into them if the frequency of dune reactivation is low enough to allow the slow-growing coralline algae to develop on nodule surfaces between events of dune movement (Testa and Bosence, 1998, 1999).

Here, we describe a cross-bedded rhodolith limestone, up to 20 m thick, which forms a mesa on which the Roman town of Acinipo was settled. This limestone is part of the infill of the Ronda Basin, a Neogene basin at the southern margin of the Atlantic-linked Guadalquivir Basin in southern Spain. We show that rhodoliths grew on submarine dunes in a sheltered bay episodically affected by storms.

The main objectives of this study were: 1) to characterize the facies comprising the rhodolith limestone in Acinipo; 2) to identify the size, shape, internal structure, and components of the rhodoliths; 3) to develop a paleoenvironmental model for rhodolith growth and facies development; and 4) to compare the coralline algal assemblages in the Ronda Basin with coeval assemblages in the western Mediterranean.

2 Geological setting

The rhodolith limestone occurs in the upper part of the Miocene sedimentary infill of the Ronda Basin, which was a marginal basin at the southern margin of the Guadalquivir Basin, the foreland basin of the Betic Cordillera (Figure 1A). This cordillera is the westernmost segment of the Alpine peri-Mediterranean orogenic belt. The Guadalquivir Basin is an elongated foreland basin (Figure 1A), which developed during the late Miocene in response to flexural subsidence of the southern Iberian margin. The subsidence was caused by the stacking of thrust units at the front of the Betic Cordillera during the latest stages of its building (Fernàndez et al., 1998; García-Gastellanos et al., 2002; Iribarren et al., 2009; Vergés and Fernàndez, 2012; Barnolas et al., 2019). The successive closure of the Betic straits from the early Tortonian to the early Messinian due to the uplift of the Betic mountains isolated the Guadalquivir Basin from the Mediterranean Sea (Martín et al., 2001, 2009, 2014; Betzler et al., 2006; Puga-Bernabeu et al., 2022). Since the early Messinian, the basin was only open to the Atlantic Ocean (Martín et al., 2014).

Like other small basins at the active southern margin of the Guadalquivir Basin, the Ronda Basin evolved as a depocenter surrounded by actively uplifting uplands, which fed the basin deposits with terrigenous sediments. The stratigraphic models for the Miocene infill of the basin proposed by various authors differ in several aspects (Bourgois, 1978; Serrano, 1979; Rodríguez-Fernández, 1982; Gläser and Betzler, 2002; Ruiz-Constán et al., 2009). However, they agree on the occurrence of lower Tortonian conglomerates, sands, and silts, which lie unconformably over the basement and change laterally to terrigenous packstones and marls. These deposits are overlain by upper Tortonian terrigenous packstones, and Messinian terrigenous packstones to rudstones, both grading basinward into marls and silty marls. The thickness of the marine sedimentary infill in this basin is irregular and may attain 300 m (Ruiz-Constán et al., 2009). Gläser and Betzler, (2002) suggest facies partitioning due to the irregular relief of the basin, conditioned by folds active at least since the Late Miocene (Balanyá et al., 2007; Galindo-Zaldívar et al., 2019). Embayments in the complex paleogeography were protected from the terrigenous influx and favored carbonate deposition. The Acinipo rhodolith concentration formed in one of these carbonate bays in the northwestern part of the basin (Gläser and Betzler, 2002).

3 Methods

Eight sections (ACI 1–8) were logged along the western and northern sides of the Acinipo outcrop (Figure 1B), and additional observations were made at exposed points at the generally covered eastern side (Figure 2). Another section was logged at the ACI 9 outcrop located 1.8 km to the southeast (Figure 1B). Lithofacies characterization and component identification in the field were completed with optical microscopy analysis of 38 thin sections cut from selected rock samples.

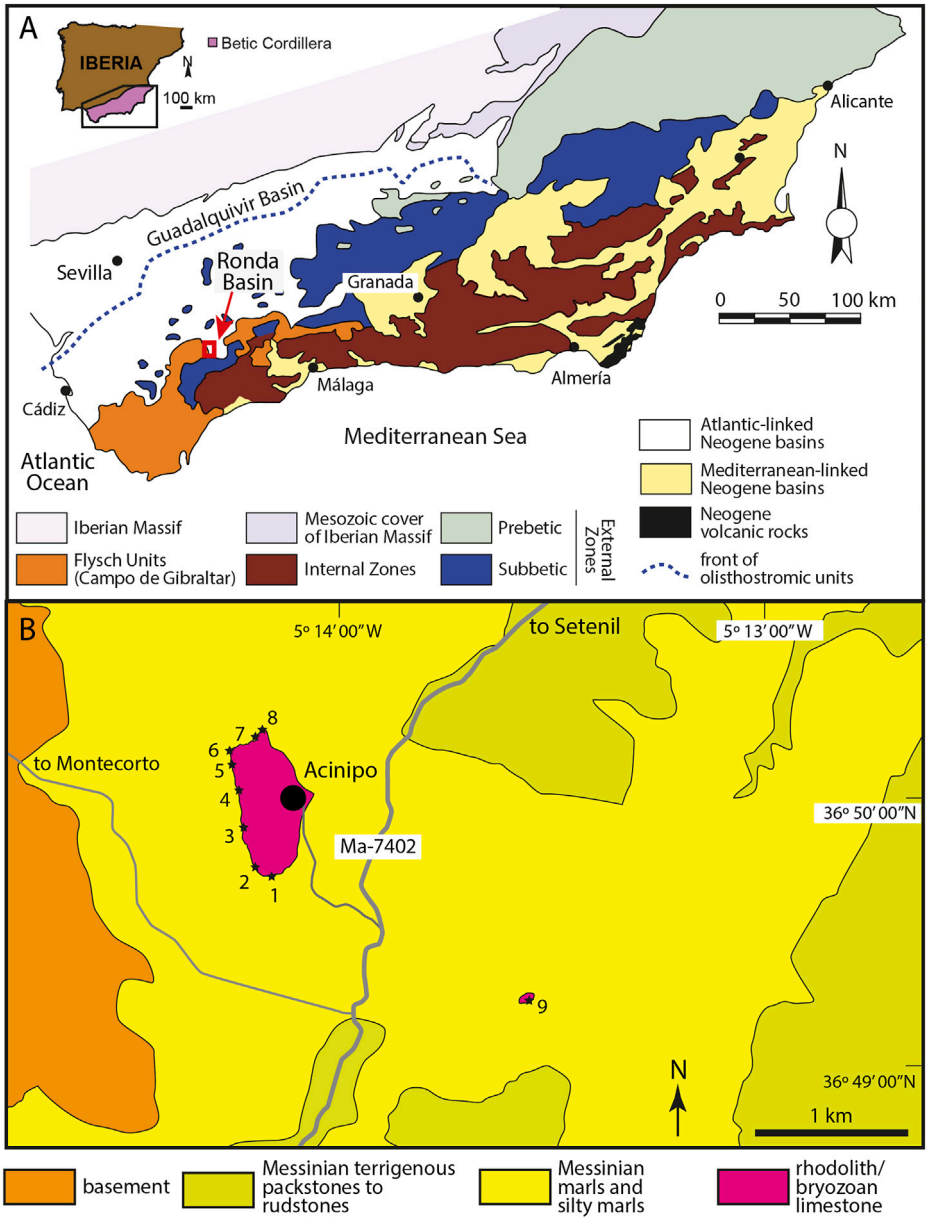

FIGURE 1
(A) Location of the Ronda Basin at the southern margin of the Guadalquivir Basin, the foreland basin of the Betic Cordillera in southern Spain. Red rectangle indicates the location of **(B)**. **(B)** Access roads and lithological map of the Acinipo area with the location of study sections (black stars 1–9).

The size and shape of rhodoliths were examined in 2D sections at the outcrops, as the extraction of isolated rhodoliths was impossible due to limestone cementation. The internal arrangement, algal growth form, and algal composition of rhodoliths were analyzed both at the outcrop and in thin sections. We use the terminology proposed by Woelkerling et al. (1993), as well as the recent terminology updated by Aguirre et al. (2017). Coralline algae were identified at the most precise taxonomic level possible, in most cases identifying the (morpho)species group, i.e., identifying the living or fossil species whose morpho-anatomical diagnostic characters can be observed in the fossil specimens. When identified species could not be confidently assigned to a previously described one, an open specific nomenclature was applied. The taxonomic

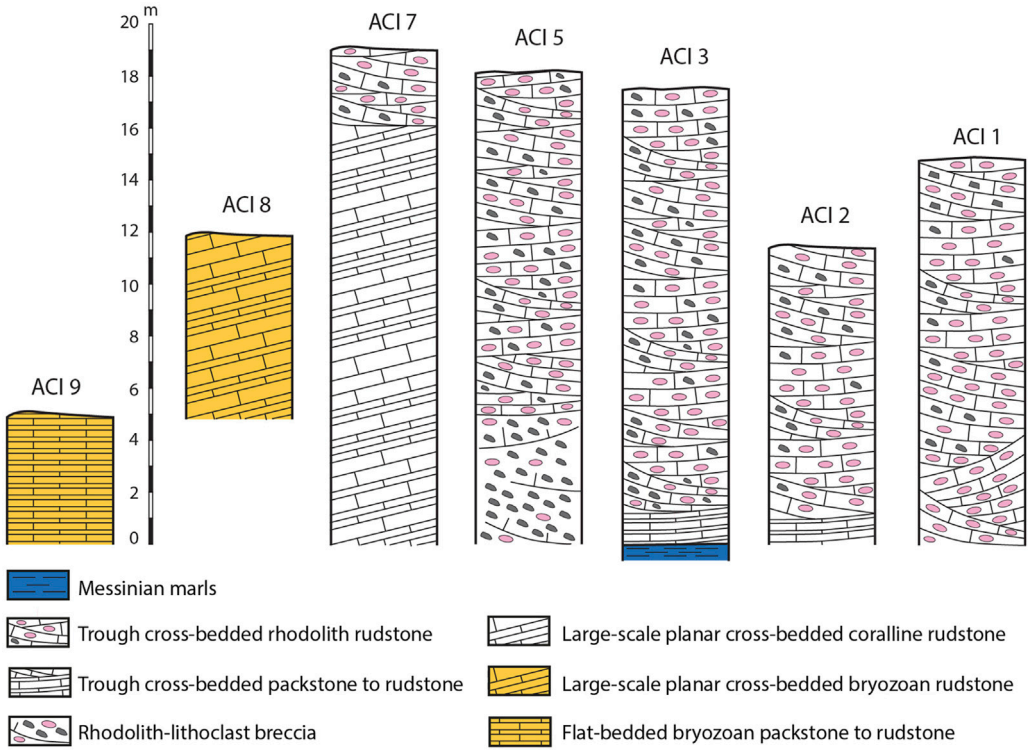

FIGURE 2
Representative columns of study sections (see Figure 1B for location).

scheme of orders, families, subfamilies, and genera follows recent molecular phylogenies (Peña et al., 2020; Jeong et al., 2021).

The age of marls underlying the rhodolith limestone was defined by analyzing planktonic foraminifer and calcareous nannoplankton assemblages. To extract planktonic foraminifers, two marl samples were washed using meshes, and the residue in the 0.125 mm fraction was examined. For calcareous nannoplankton, two smeared slides of sediment were prepared and examined looking for the biostratigraphically significant species.

4 Results

4.1 Age

The Acinipo rhodolith limestone unconformably overlies marls attributable to the early Messinian based on the dominance of the *Globorotalia miotumida* group (Sierro, 1985; Lirer et al., 2019) in the planktonic foraminifer assemblages and the presence of *Amaurolithus amplificus*, a calcareous nannoplankton species first occurring in the early Messinian (Martini, 1971; Okada and Bukry, 1980; Young et al., 1994; Raffi and Flores, 1995).

4.2 Lithofacies

The following lithofacies were distinguished based on field observations and microscopic analysis of thin sections (Figures 3–6).

4.2.1 Trough cross-bedded rhodolith rudstone

The rudstone consists of rhodoliths, most of them broken, and coralline algal debris (Figures 3A–C), fragments of bryozoans, echinoids, bivalves (oysters and pectinids), serpulids, benthic (larger and small) and planktonic foraminifers, and terrigenous grains (quartz and carbonates). Rhodoliths are either randomly oriented or locally at the base of beds, with their long axes parallel to bedding. The identifiable benthic foraminifers belong to *Amphistegina*, *Elphidium*, and *Sphaerogypsina*. Large lithoclasts (centimeters to a few decimeters in size) of marl and marly limestone occur dispersed in the rudstone in varying proportions. Nearly all lithoclasts are bored by bivalves; the boring traces (*Gastrochaenolites*) are differentially preserved and stand out in the voids left by erosion of the marly lithoclasts (Figure 3D). Rhodoliths and other skeletal components are also bored by bivalves, sponges (*Entobia*), and polychaetes (*Trypanites*). The intergranular spaces are partially filled by a wackestone to

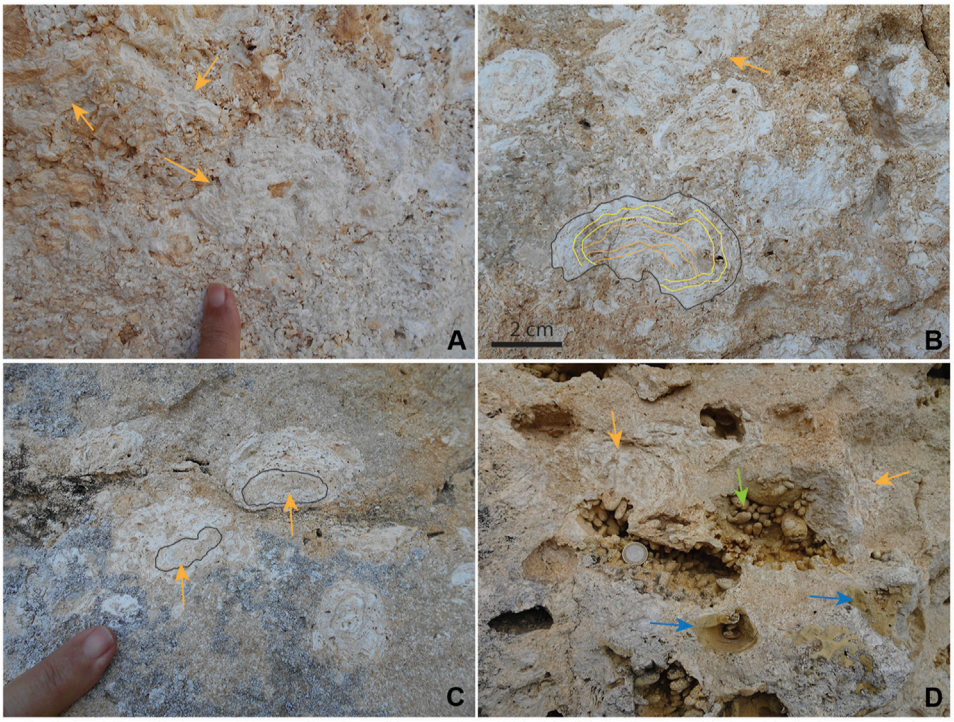

FIGURE 3
Field pictures of rhodoliths and lithoclasts in the Acinipo limestone. **(A)** Broken rhodoliths (arrows) in the trough cross-bedded rhodolith rudstone. Maximum finger width is 2 cm. **(B)** Broken rhodolith (arrow) and rhodolith with three phases of growth and fragmentation outlined in the trough cross-bedded rhodolith rudstone. **(C)** Asymmetrical rhodoliths with an initial growth phase outlined (arrows) in the trough cross-bedded rhodolith rudstone. Maximum finger width is 2 cm. **(D)** Broken rhodoliths (orange arrows) and lithoclasts in the massive rhodolith–lithoclast rudstone. Some lithoclasts partly preserve the original marly limestone composition (blue arrows). In most cases, the original marly limestone is leached/eroded, and only *Gastrochaenolites* borings filled with rudstone/packstone are preserved (green arrow). The coin diameter is 2.3 cm.

packstone matrix, whose distribution is irregular. The remaining space among bioclasts and terrigenous grains and intraskeletal voids are partially to totally filled by sparry calcite cement. The rudstone beds are roughly defined, centimeters to decimeters thick, arranged in troughs of decimeters to several meters (up to 5 m) high and several tens of meters long (Figure 4). Only three trough axes were observed, indicating a northward direction of migration (N5-12E). Most of the bed sets also indicate northward migration, but others dip eastward and southward.

4.2.2 Trough cross-bedded packstone to rudstone

The components of this facies are fragments of coralline algae, bryozoans, echinoids, bivalves (oysters and pectinids), serpulids, benthic (larger and small) and planktonic foraminifers, and terrigenous grains, mainly quartz (Figure 5A). Broken rhodoliths and marly lithoclasts appear dispersed in the rudstone. The matrix is made of wackestone to mudstone (Figure 5A). Intraskeletal and interskeletal voids are filled by sparry calcite. This facies occurs as thin (3–5 cm) packstone beds alternating with thicker (10–20 cm) beds of rudstone, both in troughs decimeters high and a few tens of meters long.

4.2.3 Massive rhodolith–lithoclast rudstone

This facies consists of a mixture of broken rhodoliths and marly lithoclasts, up to 30 cm in size (Figure 3D), with a matrix of composition like that of trough cross-bedded packstone to rudstone. It occurs in the lower part of the ACI 5 section as a roughly trough cross-bedded, lens-shaped body up to 5 m thick (Figure 2).

4.2.4 Large-scale planar cross-bedded rudstone

This facies occurs at the northern extreme of the Acinipo outcrop (Figures 1B, 2). The rudstone beds, centimeters to a few decimeters thick, are arranged in large-scale, planar cross-beds, dipping 15–20° to the east (N80-90E). The bed sets are decimeters to meters thick (Figure 6). There are two subfacies depending on the main component.

Coralline algal rudstone. This subfacies is composed of bioclasts of coralline algae, bryozoans, echinoids, bivalves

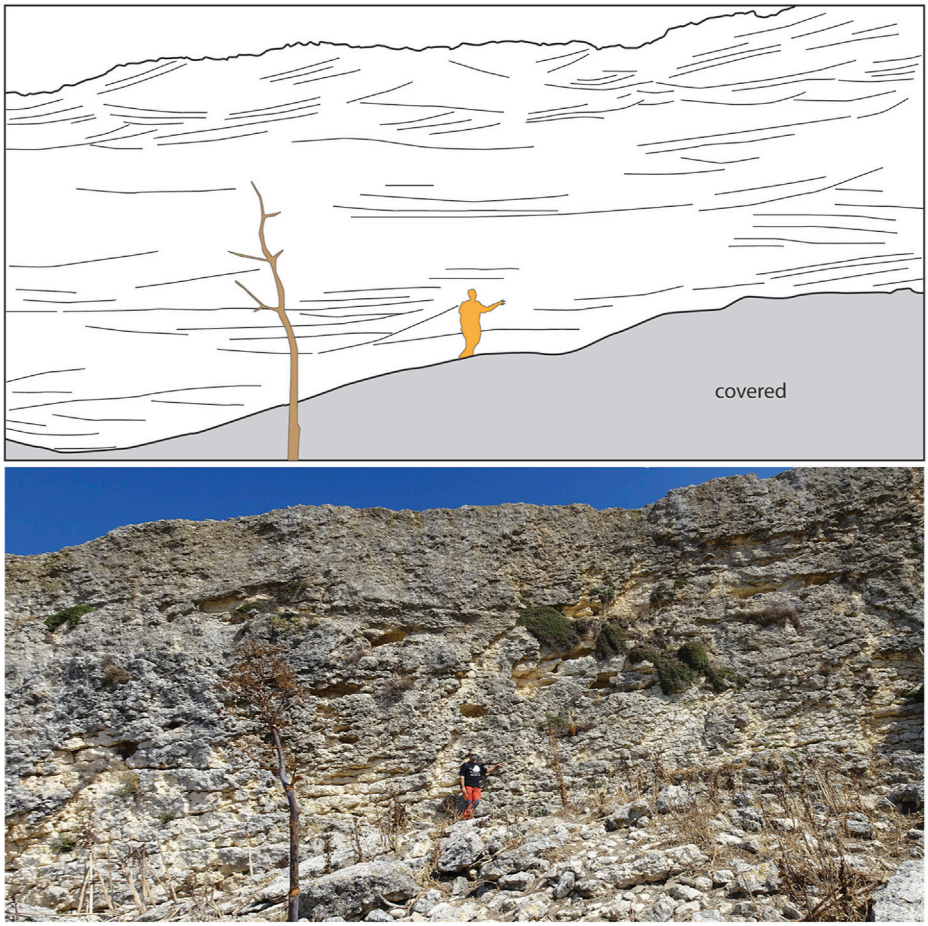

FIGURE 4
View of the trough cross-bedded rhodolith rudstone between Sections 1, 2. The drawing in the upper panel remarks the most outstanding bedding surfaces. Note the poorly defined cross-bedding with most troughs pointing to the north (into the wall and to the left).

(oysters, pectinids, and molds of aragonitic taxa), benthic (larger and small) and planktonic foraminifers, and terrigenous grains, mainly quartz. The matrix is a mudstone to wackestone (Figure 5B). Intraskeletal and interskeletal voids, and molds of aragonitic bivalves are filled by sparry calcite.

Bryozoan rudstone. Bryozoans are the main components in this subfacies with subordinate coralline algae. The rest of the components, matrix, and cement are like those of the coralline algal subfacies, although aragonitic bivalves are scarce (Figure 5C).

4.2.5 Flat-bedded bryozoan packstone to rudstone

Bryozoans are the main components of this facies (Figure 5D) with accessory coralline algae, echinoids, pectinids, serpulids, small benthic and planktonic foraminifers, and quartz grains. The matrix is a mudstone to wackestone. Inter- and intraskeletal voids are filled with sparry calcite.

This facies occurs as alternating thin (a few centimeters) packstone and thicker (up to 20 cm) rudstone beds only in section ACI 9 (Figure 2) separated from the main Acinipo outcrop (Figure 1B). The bedding surfaces show a wavy geometry probably diagenetic in origin.

5 Sections

Trough cross-bedded rhodolith rudstone (Figures 3A–C, 4) is the single or the predominant lithofacies in sections at the southern and western margins of the outcrop (Figures 1B, 2). Trough cross-bedded packstone to rudstone occurs at the base of the southwestern sections, and the rhodolith–lithoclast breccia (Figure 3D) appears at the base in exposures logged in ACI 5. The planar cross-bedded rudstone can only be observed in the northern sections (Figures 1B, 2, 4), overlain at the top of ACI 7 by trough cross-bedded rhodolith rudstones (Figure 2).

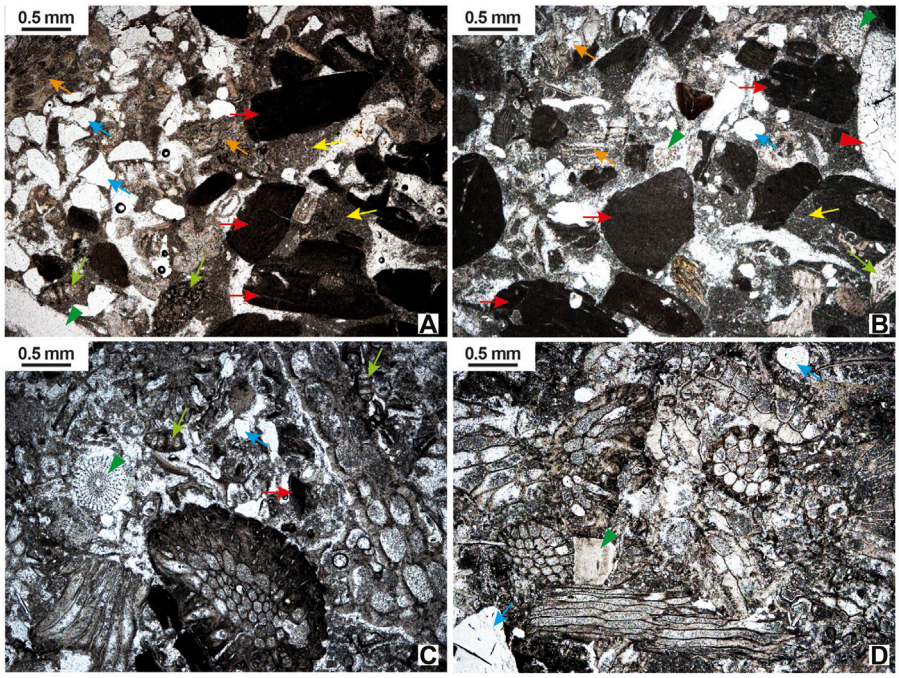

FIGURE 5
Micrographs of selected lithofacies in the Acinipo limestone. **(A)** Trough cross-bedded packstone to rudstone. Coralline algal fragments are the main components, followed by bryozoans (orange arrows). Benthic foraminifers (green arrows) and echinoids (green arrowheads) are secondary components. Quartz grains (blue arrows) are locally abundant. The matrix is commonly mudstone (yellow arrows). **(B)** Large-scale planar cross-bedded coralline rudstone. Coralline algae (red arrows), bryozoans (orange arrows), echinoids (green arrowheads), benthic foraminifers (green arrows), and terrigenous grains, mainly quartz (blue arrows) are the common components. Molds of aragonitic bivalves are filled with sparry calcite (red arrowhead). The matrix is a mudstone to wackestone (yellow arrow). **(C)** Large-scale planar cross-bedded bryozoan rudstone. Bryozoans are the main components with minor coralline algae (red arrows), echinoids (green arrowheads), benthic foraminifers (green arrows), and quartz (blue arrows). **(D)** Flat-bedded bryozoan packstone to rudstone. The rock is made of bryozoan fragments with echinoids (green arrowheads), benthic foraminifers (green arrows), terrigenous grains (blue arrows), and other bioclasts as very minor components.

6 Rhodolith size, morphology, and internal structure

Rhodoliths occur in well-lithified limestones, and they cannot be isolated from the cemented rock. Consequently, only 2D sections can be observed, preventing measuring their three axes. In addition, the length and width observable in sections are minimum values of the true rhodolith dimensions. Taking this into account, rhodoliths in Acinipo are up to 7.7 cm long, with a length median and mode of 4.5 cm (mean 4.6 cm and sd 1.2). The ratio width/length ranges from 0.43 to 0.96 (mean 0.68, median 0.68, and sd 0.12), indicating that they are flat ellipsoidal to spheroidal in shape. The shapes, however, are frequently hemi-ellipsoidal due to asymmetrical growth (see the following).

The rhodoliths are made up of encrusting to warty (very rarely fruticose) coralline algae (Figures 3A–D), intergrown with bryozoans and secondary serpulids, oysters, and encrusting foraminifers. The nuclei are bioclasts (bryozoans, mollusks, and coralline algal fragments) and less commonly lithoclasts. Rhodoliths bigger than 2.5 cm are usually multiphasic (Figure 3B). Coralline algae and other encrusters in the initial phase grew around a nucleus with a concentric arrangement; components of this initial phase were broken and abraded, and new coralline algae and invertebrates built a successive phase, which in turn was broken and overgrown by a third phase. These processes could be repeated several times, resulting in a complex boxwork arrangement, which can be strongly asymmetrical (Figure 3C). In some cases, fragments of two or more separate rhodoliths are bound together in a single nodule by coralline algae overgrowing them. In any phase, rhodoliths were bioeroded by sponges (*Entobia*), bivalves (*Gastrochaenolites*), and worms (*Trypanites*). The constructional and intraskeletal voids of encrusters and bioerosion traces are partially filled by mudstone to wackestone, locally including planktonic foraminifers. The remaining spaces are partially filled by sparry calcite cement.

FIGURE 6
Large-scale planar cross-bedded coralline algal rudstone at Section 7. Beds are dipping to the east.

7 Rhodolith-forming coralline algae

It is difficult to estimate the proportions of the coralline algae forming the rhodoliths in lithified rhodolith beds as any quantification of the relative abundance of components had to be carried out in a thin section under a microscope. The collection of rock samples and cutting of thin sections is conditioned by several factors that prevent a simple, random, or systematic sampling and, therefore, bias the results. In the rhodoliths analyzed in thin sections, *Lithophyllum* is the most common component, followed by Hapalidiales (*Lithothamnion* and *Mesophyllum*) and minor Corallinaceae (*Neogoniolithon* and *Spongites*) and *Sporolithon*.

Lithophyllum is represented by *L.* gr. *incrustans* Philippi 1837 (Figure 7A), *L.* gr. *dentatum* (Kützing) Foslie 1898, *L.* gr. *nitorum* W.H.Adey and P.J.Adey 1973 (Figure 7B), *L.* gr. *orbiculatum* (Foslie) Foslie 1900 (Figure 7C), *L.* gr. *pustulatum* (J.V.Lamouroux) Foslie 1906 (Figure 7F), and a possible specimen of *L.* gr. *hibernicum* Foslie 1906 (see Table 1 for characters separating the identified morphospecies groups).

Lithothamnion ramosissimum (Reuss) Piller 1994 is the most common species of the genus, with additional representatives of *L.* gr. *crispatum* Hauck 1878 (Figure 7D), and an unidentified species with large sporangial conceptacles (*Lithothamnion* sp. 1).

Mesophyllum is represented by one species that can be assigned to *M.* gr. *curtum* Lemoine 1939 (Figure 7E) and another two that cannot be confidently assigned to any described species (*M.* sp. 1 and *M.* sp. 2, see Table 1 for characters separating them).

A species represented by a few specimens can be attributed to *Neogoniolithon* based on the coaxial arrangement of the hypothallus and uniporate sporangial conceptacles with columella. Only one plant can be assigned to *Spongites* gr. *fruticulosus* Kützing 1841, and two other small thalli show the characteristic sporangial compartments of *Sporolithon* (Figure 7F).

8 Depositional model

The extensive occurrence of trough cross-bedded rhodolith rudstones (Figures 2, 4) indicates that submarine dunes with rhodoliths and coralline algal gravel as main particle components covered most of the seafloor on which the Acinipo limestone formed (Figure 8). The dominance of *Lithophyllum* gr. *incrustans* and *Lithophyllum* gr. *dentatum* as components both in the inner and outer layers of rhodoliths from the base to the top of the sections indicates shallow depths of a few tens of meters for rhodolith growth during limestone accumulation. Both species are common in the shallowest 20 m, and their abundance rapidly decreases in deeper settings in the present-day western Mediterranean Sea (Braga et al., 2009; Del Río et al., 2022). *Lithophyllum* gr. *incrustans* is also the main component in the shallowest rhodoliths in the Pliocene of the Atlantic coast of Cádiz (Aguirre et al., 1993). The trough cross-bedded packstone

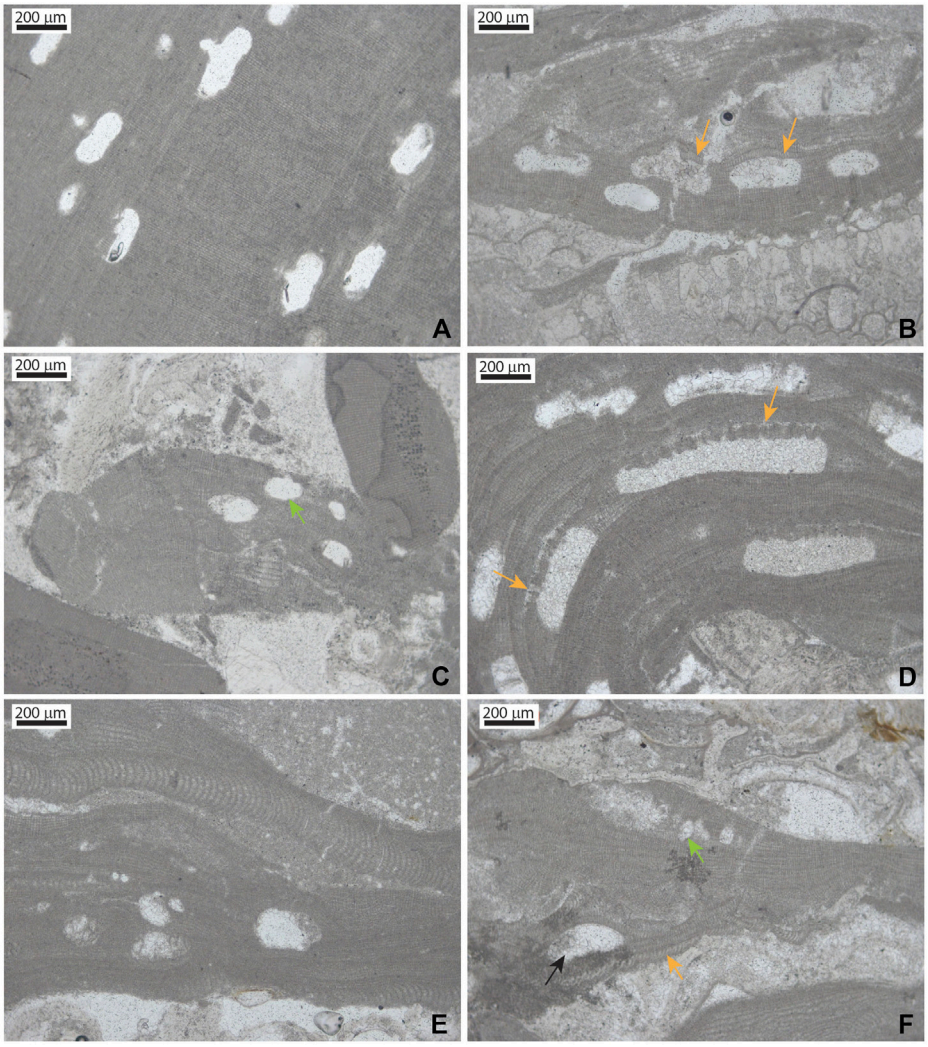

FIGURE 7
Micrographs of selected taxa in the coralline algal assemblages in the Acinipo limestone. **(A)** *Lithophyllum* gr. *incrustans*. Peripheral region with sporangial conceptacles. **(B)** *Lithophyllum* gr. *nitorum* growing on a bryozoan colony. Note the characteristic long cells in the conceptacle roof of the sporangial conceptacles. **(C)** Thallus fragment of *Lithophyllum* gr. *orbiculatum*. Note the small size of sporangial conceptacles (arrow) and the poor lateral alignment of cells of adjacent filaments. **(D)** Section of a short protuberance of *Lithothamnion* gr. *crispatum*. Note the characteristic pits in the sporangial conceptacle roof (arrows). **(E)** Thalli/branches of *Mesophyllum* gr. *curtum* with characteristic small-sized sporangial conceptacles with a hexagonal section. **(F)** *Lithophyllum* gr. *pustulatum* (orange arrow) and *Sporolithon* sp. with a sorus of sporangial compartments (green arrow).

to rudstone was probably a lateral variation of the trough cross-bedded rhodolith rudstones, in which breakage and abrasion of biogenic particles were higher.

The pervasive occurrence of large, angular to subrounded marly limestone clasts with low sphericity in the trough cross-bedded rudstones indicates proximity to the shoreline of the emergent basement. The majority of lithoclasts show *Gastrochaenolites* borings produced by bivalves. Large borings occur densely packed at any side of lithoclasts (Figure 3D), indicating that these remained for long periods on the seafloor by the shoreline before being incorporated into submarine dunes. The lithoclast proportion is higher in the northwestern sections of the outcrop, which probably were closer to the shoreline. The base of section ACI 5 is a massive rudstone of lithoclasts and rhodoliths (Figure 2), which is probably the most proximal lithofacies in the Acinipo limestone. A similar conglomerate of broken, large rhodoliths and lithoclasts was described as a shallow water, nearshore facies in the upper-Tortonian fan-delta deposits in the Almanzora corridor (Braga and Martín, 1988). Although no well-defined sedimentary structures indicating tractive currents were observed in the massive conglomerate, the high degree of rhodolith

TABLE 1 Diagnostic characters separating the taxa recognized in the coralline algal assemblages in the Acinipo limestone. D= conceptacle diameter.

1 sporangial compartment		Sporolithales
1 Multiporate sporangial conceptacles		Hapalidiales
1 Uniporate sporangial conceptacles		Corallinales
Sporolithales		*Sporolithon* sp.
Hapalidiales		
1 Plumose, non-coaxial ventral core		*Lithothamnion*
Lithothamnion	2 Pitted conceptacle roofs	*L.* gr. *crispatum*
	2 Conceptacle roof without pits	3
	3 Conceptacles concentrated in protuberances, D < 450 μm	*L. ramosissimum*
	3 Conceptacles large, D > 600 μm, and thick conceptacle roof (50 μm)	*Lithothamnion* sp. 1
1 Coaxial ventral core		*Mesophyllum*
Mesophyllum	4 Conceptacle section polygonal, D < 400 μm	*M. curtum*
	4 Conceptacle section elliptical, D > 400 μm	5
	5 Conceptacle D < 700 μm	*Mesophyllum* sp. 1
	5 Conceptacles large, D > 700 μm	*Mesophyllum* sp. *2*
Corallinales		
1 Cell fusions		Corallinaceae
	2 Plumose, non-coaxial ventral core	*Spongites* gr. *fruticulosus*
	2 Coaxial ventral core	*Neogoniolithon* sp. 1
1 Secondary pit connections		Lithophyllacea
Lithophyllum	3 Long, palisade cells in hypothallus	*L.* gr. *pustulatum*
	3 Cells in hypothallus like those in perithallus	4
	4 Long, palisade cells in the conceptacle roof	*L.* gr. *nitorum*
	4 Cells in the conceptacle roof like those in perithallus	5
	5 Cells of adjacent filaments well aligned	*L.* gr. *dentatum*
	5 Poorly aligned cells of adjacent filaments	6
	6 Long, cylindrical conceptacle pore	*L.* gr. *hibernicum*
	6 Conical conceptacle pore	7
	7 Conceptacles small, D < 200 μm	*L.* gr. *orbiculatum*
	7 Conceptacle D > 200 μm	*L.* gr. *incrustans*

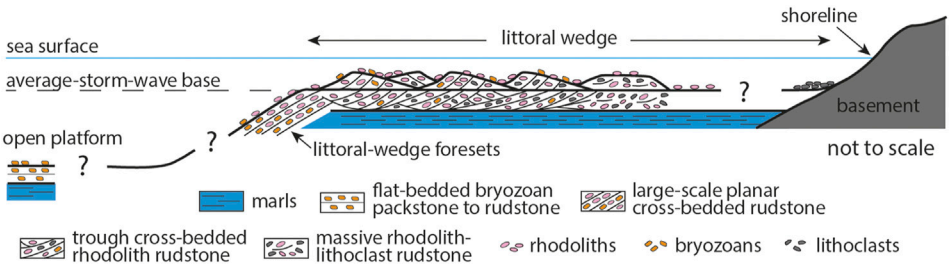

FIGURE 8
Depositional model for the Acinipo limestone. Rhodoliths grew on a littoral wedge at the western side of the Ruinas de Acinipo bay. The wedge was affected by storms that incorporated the rhodoliths, other bioclasts, and lithoclasts from the basement into submarine dunes. Rhodoliths were broken but continued to grow on the dunes. Rhodoliths and bioclastic gravel were swept from the wedge top and accumulated on the foresets of the littoral wedge. Bryozoans dominate bioclasts in the distal portion of the foresets and in the open-platform deposits.

breakage and the large size of lithoclasts indicate reworking under high-energy conditions (Braga and Martín, 1988).

Large-scale planar cross-bedded rudstone in sections ACI 7 (Figure 5) and ACI 8 at the northern end of the Acinipo outcrop denotes deposition of successive beds on a steep slope dipping basinward and located immediately seaward of the submarine dunes. We interpret these beds as foresets of an infralittoral prograding wedge (Hernández-Molina et al., 2000), initially mainly fed by coralline algal gravel and sand-sized particles from the submarine dunes and later with higher proportions of bryozoan skeletons (Figure 8). The flat-bedded bryozoan packstone to rudstone in the isolated outcrop of section ACI 9 is the most distal and deeper deposit (Figure 8), now disconnected from the main outcrop.

Although the exposures do not allow precise measurements of many trough axes, cross-bedded sets indicate migration in several directions with predominant migration toward the north. This, together with the enclosed nature of the depositional setting (Gläser and Betzler, 2002), discards the existence of a persistent current strong enough to generate and move the coarse-grained submarine dunes. They are most probably formed by storm surges, mainly outflowing to N-NE. Storms affected the sediment mostly produced by coralline algae, which accumulated in an infralittoral wedge at the western side of a bay (the Ruinas de Acinipo bay of Gläser and Betzler, 2002). At the seaward front of the infralittoral wedge, bioclasts transported from its top by storm-generated return currents formed foresets below the mean storm wave base (Figure 8).

9 Discussion

9.1 Rhodoliths in storm-related deposits

The internal structure of large rhodoliths, showing several phases of repeated coralline algal growth and fragmentation/erosion (Figure 3B), reflects their growth on a seafloor affected by storms. The edges of coralline thalli were broken and abraded during the removal and transport of rhodoliths by the storm surge. Once the rhodoliths settled on the seafloor, the thalli on the non-buried surface of rhodoliths re-started their growth or the surfaces were colonized by new thalli, during a period of quiescence long enough to allow the development of coralline algae and other encrusters. These processes took place several times in individual rhodoliths (Figure 3B) until their final burial within the dune deposits. Successive phases of fragmentation and re-started growth in multistory rhodoliths in the Middle Miocene carbonates from the Marion Plateau in northeastern Australia were interpreted as reflecting episodic storm reworking (Martín et al., 1993). A two-phase internal structure of Middle Miocene rhodoliths in the southern Apennines (Italy) was also considered by Checconi et al. (2010) as the result of offshore transport of the algal nodules by storm currents.

Rhodolith beds related to storms usually occur as broad, shallow channels filled with rhodoliths in deeper-middle ramp settings, which have been interpreted as storm surge channels. This is the case of the examples in the rhodolith pavement in the Upper Coralline Limestone Formation in Malta (Bosence and Pedley, 1982; Pedley, 1998) and in the Upper Miocene deposits in the Sorbas Basin in SE Spain (Puga-Bernabeu et al., 2007a). In the Malta pavement, however, rhodoliths also occur entrained in large-scale trough cross-bedding formed in submarine dunes. Orientation of foresets and rhodolith long axes indicate two or more current directions suggesting fluctuating energy conditions (Bosence and Pedley, 1982), characteristics of storm processes. According to Pedley (1998), cross-stratified deposits with abraded rhodoliths often occur in the shallowest Oligocene–Miocene rhodolith pavement facies in southern Italy and Malta. Trough cross-bedded intervals in the Pliocene rhodolith beds in Guadeloupe were also interpreted as formed by storms in the shallowest part of a middle ramp (Cornée et al., 2012).

In all these cases, rhodoliths and coralline algal gravel and sand-sized bioclasts are parautochthonous components entrained in submarine dunes on the seafloor. Rhodoliths might even be autochthonous if they grew immediately before the burial of the dune, as suggested by asymmetrical internal arrangements with predominantly upright growth in rhodoliths from the Acinipo limestone. In this limestone, although some siliciclastics and lithoclasts were incorporated into dune sediments, most components were carbonate skeletons produced on the western littoral wedge of the Ruinas de Acinipo bay.

The modern examples of rhodolith concentrations related to submarine dunes are substantially different from the Acinipo trough cross-bedded rhodolith rudstones. On the northeastern Brazilian shelf, rhodoliths grow in troughs of siliciclastic, large-scale submarine dunes and are probably incorporated together with bioclastic gravel in the base of the dunes (Testa and Bosence, 1998, 1999), but they are not their main components. Onshore of the sand-dune zone, rhodoliths grow at the crest and troughs of bioclastic sand ribbons parallel to the current direction. Rhodoliths and coralline gravel are incorporated into small and large wave ripples with crests roughly parallel to ribbon crests. These ripples are generated by waves approaching the coast, which is a flow system different from the one driving sand-ribbon movement (Testa and Bosence, 1999).

Storm deposits with rhodoliths described in the Macaronesian realm are also different from the Acinipo case. In Pleistocene tempestites from Maio (Cape Verde), rhodoliths occur within sand-sized deposits with swaley cross-stratification (Johnson et al., 2017). Hummocky and swaley cross-stratification in rhodolith-bearing packstones are also characteristics of Pleistocene storm deposits in Santiago (Cape Verde) (Johnson et al., 2012) and Miocene–Lower Pliocene tempestites from Santa Maria in the Azores archipelago (Johnson et al., 2017). Other

storm-related rhodolith concentrations in Cape Verde Islands are supratidal deposits resulting from the storm activity that transported the rhodoliths inland from their sites of growth or even from older fossil rhodolith beds (Johnson et al., 2017, 2020).

The large-scale planar cross-bedded coralline algal rudstone at the northern sections of the Acinipo outcrop (Figures 2, 6) is similar to the well-bedded rhodolith rudstone described by Brandano and Ronca, (2014) in the Miocene of northern Corsica. As in the Acinipo case, the dipping beds of the Corsican lithofacies accumulated in the foresets of a littoral wedge with rhodoliths fed from the top surface of the wedge and *in situ* growing coralline algae. The rhodolith floatstone that also occurs in the foresets of the littoral wedge in Corsica is rich in nodular bryozoans (Brandano and Ronca, 2014), which are the dominant components in the distal beds of large-scale planar cross-bedded rudstone in Acinipo. In the Corsican Miocene, however, on the top of the wedge, rhodoliths grew and accumulated in massive beds with only local planar cross-stratification (Brandano et al., 2009), instead of being pervasively incorporated into trough cross-beds.

9.2 Paleobiogeographical traits of the coralline algae

The coralline algal assemblages in the Acinipo rhodolith limestones are dominated by the Lithophyllaceae *Lithophyllum*, and Hapalidiales, with very minor occurrences of the Corallinaceae *Neogoniolithon* and *Spongites*. This composition reflects that the Ronda Basin was a marginal basin of the Guadalquivir Basin, which opened to the Atlantic Ocean. Similar components are reported from the Niebla Fm. in the western end of the Guadalquivir Basin in the only detailed account of Late Miocene coralline algae from this basin (Civis et al., 1994). *Lithophyllum* and Hapalidiales are also the only coralline algae in rhodoliths in the Pliocene of the Cádiz coast (Aguirre et al., 1993, 2017). The predominance of *Lithophyllum* among the Corallinales and the scarcity or absence of thick Corallinaceae is common in modern coralline assemblages in the Atlantic Iberian Peninsula (Lugilde et al., 2016) and in general in the European Atlantic coasts (Irvine and Chamberlain, 1994), and contrasts with a higher abundance of *Neogoniolithon* and *Spongites* in the Mediterranean Sea (Rindi et al., 2019). However, *Neogoniolithon brassica-florida* (Harvey) Setchell and Mason 1943, is locally abundant in *Cymodecea* seagrass meadows in the Bay of Cadiz (Bermejo et al., 2012; Hernández-Kartun et al., 2015). The tendency of thick Corallinaceae to inhabit warmer waters was already recorded in the Late Miocene coralline assemblages in southern Spain. *Neogoniolithon*, *Spongites*, and *Lithoporella* were common during periods of coral reef growth in the Betic Neogene basins, whereas they were scarce or absent during periods of deposition of heterozoan, warm-temperate carbonates (Braga and Aguirre, 2001). In contrast, *Lithophyllum* is common in these heterozoan carbonates, and most species groups found in the Ronda Basin (*L. incrustans*, *L. dentatum*, *L. nitorum*, *L. orbiculatum*, and *L. pustulatum*) were recorded in the Betic Neogene Mediterranean-linked basins (Braga and Aguirre, 1995, 2001; Puga-Bernabeu et al., 2007a; Puga-Bernabeu et al., 2007b).

Data availability statement

The raw data supporting the conclusion of this article will be made available by the authors, without undue reservation.

Author contributions

JB and JA shared the research design, fieldwork, taxonomic identification, and writing the manuscript.

Funding

This research was funded by the Ministerio de Ciencia, Innovación y Universidades, Spain, project PGC 2018-099391-B-I00.

Acknowledgments

The authors are grateful to two reviewers whose suggestions improved this article.

Conflict of interest

The authors declare that the research was conducted in the absence of any commercial or financial relationships that could be construed as a potential conflict of interest.

Publisher's note

References

Adey, W. H., and Adey, P. J. (1973). Studies on the biosystematics and ecology of the epilithic crustose Corallinaceae of the British Isles. *Br. Phycol. J.* 8, 343–407. doi:10.1080/00071617300650381

Aguirre, J., Braga, J. C., and Bassi, D. (2017). "Rhodoliths and rhodolith beds in the rock record," in *Rhodolith/maërl beds: A global perspective*. Editors R. Riosmena-Rodríguez, W. Nelson, and J. Aguirre (Basel: Springer Inter. Publ.), 105–138. doi:10.1007/978-3-319-29315-8_5

Aguirre, J., Braga, J. C., and Martín, J. M. (1993). "Algal nodules in the upper Pliocene deposits at the coast of Cadiz (S Spain)," in *Studies on fossil benthic algae*. Editors F. Barattolo, P. De Castro, and M. Parente (Rome: Boll. Soc. Paleontol. It.), Vol. 1, 1–7.

Aguirre, J., Braga, J. C., Martín, J. M., and Betzler, C. (2012). Palaeoenvironmental and stratigraphic significance of Pliocene rhodolith beds and coralline algal bioconstructions from the Carboneras Basin (SE Spain). *Geodiversitas* 34, 115–136. doi:10.5252/g2012n1a7

Balanyá, J. C., Crespo-Blanc, A., Díaz Azpiroz, M., Expósito, I., and Luján, M. (2007). Structural trend line pattern and strain partitioning around the Gibraltar arc accretionary wedge: Insights as to the mode of orogenic arc building. *Tectonics* 26, TC2005. doi:10.1029/2005TC001932

Barnolas, A., Larrasoaña, J. C., Pujalte, V., Schmitz, B., Sierro, F. J., Mata, M. P., et al. (2019). "Alpine foreland basins," in *The geology of iberia: A geodynamic approach*. Editors C. Quesada, and J. T. Oliveira (Cham: Springer), 7–59. doi:10.1007/978-3-030-11190-8_2

Bassi, D., and Nebelsick, J. H. (2010). Components, facies and ramps: Redefining Upper Oligocene shallow water carbonates using coralline red algae and larger foraminifera (Venetian area, northeast Italy). *Palaeogeogr. Palaeoclimatol. Palaeoecol.* 295, 258–280. doi:10.1016/j.palaeo.2010.06.003

Benisek, M.-F., Betzler, C., Marcano, G., and Mutti, M. (2009). Coralline-algal assemblages of a burdigalian platform slope: Implications for carbonate platform reconstruction (northern Sardinia, Western Mediterranean Sea). *Facies* 55, 375–386. doi:10.1007/s10347-009-0183-7

Benisek, M.-F., Marcano, G., Betzler, C., and Mutti, M. (2010). "Facies and stratigraphic architecture of a Miocene warm-temperate to tropical fault-block carbonate platform, Sardinia (central Mediterranean Sea)," in *Carbonate Syst. Dur. Oligocene-Miocene Clim. Transition*. Editors M. Mutti, W. E. Piller, and C. Betzler (Chichester; Hoboken, NJ: IAS Spec. Publ Wiley-Blackwell), 42, 107–128.

Bermejo, R., Pérez-Llorens, J. L., Vergara, J., and Hernández, I. (2012). Notas corológicas del macrofitobentos marino de Andalucía (España). X. New records for the seaweeds of Andalusia (Spain). X. *Acta Botanica Malacitana* 37, 163–165. doi:10.24310/abm.v37i0.2660

Betzler, C., Braga, J. C., Martín, J. M., Sánchez-Almazo, I. M., and Lindhorst, S. (2006). Closure of a seaway: Stratigraphic record and facies (Guadix basin, southern Spain). *Int. J. Earth Sci. (Geol. Rundschau)* 95, 903–910. doi:10.1007/s00531-006-0073-y

Bosence, D. W. J., and Pedley, H. M. (1982). Sedimentology and palaeoecology of a Miocene coralline algal biostrome from the Maltese Islands. *Palaeogeogr. Palaeoclimatol. Palaeoecol.* 38, 9–43. doi:10.1016/0031-0182(82)90062-1

Bourgois, J. (1978). La transversale de Ronda (cordillères bétiques, espagne). Besançon: University of Besançon. PhD Thesis.

Braga, J. C., and Aguirre, J. (2001). Coralline algal assemblages in upper Neogene reef and temperate carbonates in Southern Spain. *Palaeogeogr. Palaeoclimatol. Palaeoecol.* 175, 27–41. doi:10.1016/S0031-0182(01)00384-4

Braga, J. C., Aguirre, J., and Esteban, J. (2009). Calcareous algae of Cabo de gata-níjar nature park. Field guide, *ACUMED y* consejería *de Medio ambiente*. Madrid: Junta de Andalucía.

Braga, J. C., and Aguirre, J. (1995). Taxonomy of fossil coralline algal species: Neogene Lithophylloideae (Rhodophyta, Corallinaceae) from southern Spain. *Rev. Palaeobot. Palynology* 86, 265–285. doi:10.1016/0034-6667(94)00135-7

Braga, J. C., and Martín, J. M. (1988). Neogene coralline-algal growth-forms and their palaeoenvironments in the Almanzora river valley (almeria, S.E. Spain). *Palaeogeogr. Palaeoclimatol. Palaeoecol.* 67, 285–303. doi:10.1016/0031-0182(88)90157-5

Brandano, M., Frezza, V., Tomassetti, L., Pedley, M., and Matteucci, R. (2009). Facies analysis and palaeoenvironmental interpretation of the late Oligocene attard member (lower coralline Limestone Formation), Malta. *Sedimentology* 56, 1138–1158. doi:10.1111/j.1365-3091.2008.01023.x

Brandano, M. (2017). "Oligocene rhodolith beds in the central Mediterranean area," in *Rhodolith/maërl beds: A global perspective*. Editors R. Riosmena-Rodríguez, W. Nelson, and J. Aguirre (Basel: Springer Inter. Publ), 195–219. doi:10.1007/978-3-319-29315-8_8

Brandano, M., and Piller, W. E. (2010). "Coralline algae, oysters and echinoids – A liaison in rhodolith formation from the burdigalian of the latium-abruzzi platform (Italy)," in *Carbonate systems during the Oligocene-Miocene climatic transition*. Editors M. Mutti, W. E. Piller, and C. Betzler (Chichester; Hoboken, NJ: IAS Spec. Publ. Wiley-Blackwell), 42, 149–164.

Brandano, M., and Ronca, S. (2014). Depositional processes of the mixed carbonate-siliciclastic rhodolith beds of the Miocene Saint-Florent Basin, northern Corsica. *Facies* 60, 73–90. doi:10.1007/s10347-013-036710.1007/s10347-013-0367-z

Brandano, M., Vannucci, G., Pomar, L., and Obrador, A. (2005). Rhodolith assemblages from the lower tortonian carbonate ramp of Menorca (Spain): Environmental and paleoclimatic implications. *Palaeogeogr. Palaeoclimatol. Palaeoecol.* 226, 307–323. doi:10.1016/j.palaeo.2005.04.034

Checconi, A., Bassi, D., Carannante, P., and Monaco, G. (2010). Re-Deposited rhodoliths in the middle Miocene hemipelagic deposits of vitulano (southern Apennines, Italy): Coralline assemblage characterization and related trace fossils. *Sediment. Geol.* 225, 50–66. doi:10.1016/j.sedgeo.2010.01.001

Civis, J., Alonso-Gavilan, G., Gonzalez-Delgado, J. A., and Braga, J. C. (1994). Sédimentation carbonatée transgressive sur la bordure occidentale du couloir nord-bétique pendant le Tortonien supérieur (Fm Calcarenita de Niebla, SW de l'Espagne). *Géol. Méditerr.* 21, 9–18. doi:10.3406/geolm.1994.1493

Cornée, J. J., Léticée, J. L., Münch, P., Quillévéré, F., Lebrun, J. F., Moissette, P., et al. (2012). Sedimentology, palaeoenvironments and biostratigraphy of the Pliocene-Pleistocene carbonate platform of Grande-Terre (Guadeloupe, Lesser Antilles forearc). *Sedimentology* 59, 1426–1451. doi:10.1111/j.1365-3091.2011.01311.x

Del Río, J., Ramos, D. A., Sánchez-Tocino, L., Peñas, J., and Braga, J. C. (2022). The punta de la Mona rhodolith bed: Shallow-water mediterranean rhodoliths (almuñecar, granada, southern Spain). *Front. Earth Sci.* 10, 884685. doi:10.3389/feart.2022.884685

Fernàndez, M., Berástegui, X., Puig, C., Garcia-Castellanos, D., Jurado, M. J., Torné, M., et al. (1998). "Geophysical and geological constraints on the evolution of the Guadalquivir foreland basin, Spain," in *Cenozoic Forel. Basins West. Eur.* Editors A. Mascle, C. Puigdefàbregas, H. P. Luterbacher, and M. Fernàndez (London: Geological Society Special Publication), 134, 29–48.

Foslie, M. (1906). Algologiske notiser II. *Det. K. Nor. Vidensk. Selsk. Skr.* 1906 (2), 1–28.

Foslie, M. (1898). List of species of the lithothamnia. *K. Nor. Vidensk. Selsk. Skr.* 1898 (3), 1–11.

Foslie, M. (1900). Revised systematical survey of the Melobesieae. *K. Nor. Vidensk. Selsk. Skr.* 1900 (5), 1–22.

Galindo-Zaldívar, J., Braga, J. C., Marín-Lechado, C., Ercilla, G., Martín, J. M., Pedrera, A., et al. (2019). "Extension in the western mediterranean," in *The geology of iberia: A geodynamic approach*. Editors C. Quesada, and J. T. Oliveira (Cham: Springer), 61–103. doi:10.1007/978-3-030-11190-8_3

Garcia-Castellanos, D., Fernàndez, M., and Torne, M. (2002). Modeling the evolution of the Guadalquivir foreland basin (southern Spain). *Tectonics* 21, 9–1. doi:10.1029/2001TC001339

Gläser, I., and Betzler, C. (2002). Facies partitioning and sequence stratigraphy of cool-water, mixed carbonate-siliciclastic sediments (Upper Miocene Guadalquivir Domain, southern Spain). *Int. J. Earth Sci. (Geol. Rundschau)* 91, 1041–1053. doi:10.1007/s00531-002-0293-8

Hauck, F. (1878). Beiträge zur Kenntniss der adriatischen Algen. *Osterr. Bot. Z.* 28, 288–295. doi:10.1007/bf01614959

Hernández-Kantún, J., Riosmena-Rodriguez, R., Hall-Spencer, J. M., Peña, V., Maggs, C., and Rindi, F. (2015). Phylogenetic analysis of rhodolith formation in the Corallinales (Rhodophyta). *Eur. J. Phycol.* 50, 46–61. doi:10.1080/09670262.2014.984347

Hernández-Molina, J., Fernández-Salas, L. M., Lobo, F. J., and Somoza, L. (2000). The infralittoral prograding wedge: A new large-scale progradational sedimentary body in shallow marine environments. *Geo-Marine Lett.* 20, 109–117. doi:10.1007./s003670000040

Iribarren, L., Vergés, J., and Fernàndez, M. (2009). Sediment supply from the Betic-Rif orogen to basins through Neogene. *Tectonophysics* 475, 68–84. doi:10.1016/j.tecto.2008.11.029

Irvine, L. M., and Chamberlain, Y. M. (1994). *Seaweeds of the British isles. Volume I. Rhodophyta. Part 2B. Corallinales, Hildebrandiales*. London: The Natural History Museum.

Jeong, S. Y., Nelson, W. A., Sutherland, J. E., Peña, V., Le Gall, L., Diaz-Pulido, G., et al. (2021). Corallinapetrales and corallinapetraceae: A new order and new family

of coralline red algae including *Corallinapetra gabriellii* comb. Nov. *J. Phycol* 57, 849–862. doi:10.1111/jpy.13115-20-107

Johnson, M. E., Baarli, G. B., Cachão, M., da Silva, C. M., Ledesma-Vázquez, J., Mayoral, E. J., et al. (2012). Rhodoliths, uniformitarianism, and Darwin: Pleistocene and Recent carbonate deposits in the Cape Verde and Canary archipelagos. *Palaeogeogr. Palaeoclimatol. Palaeoecol.* 329-330, 83–100. doi:10.1016/j.palaeo.2012.02.019

Johnson, M. E., Ledesma-Vázquez, J., Ramalho, R. S., da Silva, C. M., Rebelo, A., Santos, G. B., et al. (2017). "Taphonomic range and sedimentary dynamics of modern and fossil rhodolith beds: Macaronesian realm (North Atlantic Ocean)," in *Rhodolith/maërl beds: A global perspective*. Editors R. Riosmena-Rodríguez, W. Nelson, and J. Aguirre (Basel: Springer Inter. Publ.), 221–261. doi:10.1007/978-3-319-29315-8_9

Johnson, M. E., Ramalho, R. S., and Marques da Silva, C. M. (2020). Storm-related rhodolith deposits from the upper Pleistocene and recycled coastal holocene on sal island (cabo Verde archipelago). *Geosciences* 10, 419. doi:10.3390/geosciences10110419

Kützing, F. T. (1841). *Über die 'Polypiers calcifères' des Lamouroux*. Nordhausen, F. Thiele, 34.

Lemoine, M. P. (1939). Les algues calcaires fossiles de l'Algérie. *Matériaux Carte Géologique L'Algérie. 1re. Série Paléontologie* 9, 1–128.

Lirer, F., Foresi, L. M., Iaccarino, S. M., Salvatorini, G., Turco, E., Cosentino, C., et al. (2019). Mediterranean Neogene planktonic foraminifer biozonation and biochronology. *Earth-Science Rev.* 196, 102869. doi:10.1016/j.earscirev.2019.05.013

Lugilde, J., Peña, V., and Bárbara, I. (2016). The order Corallinales sensu lato (rhodophyta) in the iberian atlantic: Current state of knowledge. *Anal. Jard. Bot. Madrid* 73, 038. doi:10.3989/ajbm.2424

Martín, J. M., Braga, J. C., Aguirre, J., and Puga-Bernabéu, Á. (2009). History and evolution of the north-Betic strait (prebetic zone, betic cordillera): A narrow, early tortonian, tidal-dominated, atlantic-mediterranean marine passage. *Sediment. Geol.* 216, 80–90. doi:10.1016/j.sedgeo.2009.01.005

Martin, J. M., Braga, J. C., and Betzler, C. (2001). The messinian guadalhorce corridor: The last northern, atlantic-mediterranean gateway. *Terra nova.* 13, 418–424. doi:10.1046/j.1365-3121.2001.00376.x

Martín, J. M., Braga, J. C., Konishi, K., and Pigram, C. J. (1993). A model for the development of rhodoliths on platforms influenced by storms: Middle Miocene carbonates of the Marion Plateau (northeastern Australia). *Proc. Ocean Drill. Program, Sci. Results* 133, 455–460.

Martín, J. M., Puga-Bernabéu, Á., Aguirre, J., and Braga, J. C. (2014). Miocene atlantic-mediterranean seaways in the betic cordillera (southern Spain). *Rev. Soc. Geol. Esp.* 27, 175–186.

Martini, E. (1971). Standard Tertiary and Quaternary calcareous nannoplankton zonation. *Proc. 2nd Int. Conf. Plankton* Vol. 2, 739–785.

Millar, K. R., and Gagnon, P. (2018). Mechanisms of stability of rhodolith beds: Sedimentological aspects. *Mar. Ecol. Prog. Ser.* 594, 65–83. doi:10.3354/meps12501

Nalin, R., Nelson, C. S., Basso, D., and Massari, F. (2008). Rhodolith-bearing limestones as transgressive marker beds: Fossil and modern examples from north island, New Zealand. *Sedimentology* 55, 249–274. doi:10.1111/j.1365-3091.2007.00898.x

Obrador, A., Pomar, L., and Taberner, C. (1992). Late Miocene breccia of Menorca (balearic Islands) a basis for the interpretation of a Neogene ramp deposit. *Sediment. Geol.* 79, 203–223. doi:10.1016/0037-0738(92)90012-G

Okada, H., and Bukry, D. (1980). Supplementary modification and introduction of code numbers to the low-latitude coccolith biostratigraphic zonation (Bukry, 1973; 1975). *Mar. Micropaleontol.* 5, 321–325. doi:10.1016/0377-8398(80)90016-x

Pedley, H. M. (1998). "A review of sediment distributions and processes in Oligo-Miocene ramps of southern Italy and Malta (Mediterranean divide)," in *Carbonate ramps*. Editors V. P. Wrigth, and T. P. Burchette (London: Geol. Soc. London Spec. Publ.), 149, 163–179. doi:10.1144/gsl.sp.1999.149.01.09

Peña, V., Vieira, C., Braga, J. C., Aguirre, J., Rösler, A., Baele, G., et al. (2020). Radiation of the coralline red algae (Corallinophycidae, Rhodophyta) crown group as inferred from a multilocus time-calibrated phylogeny. *Mol. Phylogenetics Evol.* 150, 106845. doi:10.1016/j.ympev.2020.106845

Philippi, R. (1837). Beweiss dass die Nulliporen Pflanzen sind. *Arch. für Naturgeschichte* 3, 387–393.

Piller, W. E. (1994). *Nullipora ramosissima* REUSS, 1847--a rediscovery. *Beitr. Paläontol.* 19, 181–189.

Pisera, A., and Studencki, W. (1989). Middle Miocene rhodoliths from the korytnica basin (southern Poland): Environmental significance and paleontology. *Acta palaeont. Pol.* 34, 179–209.

Pomar, L., Obrador, A., and Westphal, H. (2002). Sub-wavebase cross-bedded grainstones on a distally steepened carbonate ramp, upper Miocene, Menorca, Spain. *Sedimentology* 49, 139–169. doi:10.1046/j.1365-3091.2002.00436.x

Pomar, L. (2001). Types of carbonate platforms: A genetic approach. *Basin Res.* 13, 313–334. doi:10.1046/j.0950-091x.2001.00152.x

Puga-Bernabéu, Á., Braga, J. C., Aguirre, J., and Martín, J. M. (2022). Sedimentary dynamics and topographic controls on the tidal-dominated zagra strait, early tortonian, betic cordillera, Spain. *Geol. Soc. Lond. Spec. Publ.* 523, 85. doi:10.1144/SP523-2021-85

Puga-Bernabéu, Á., Braga, J. C., and Martín, J. M. (2007a). High-frequency cycles in upper-miocene ramp-temperate carbonates (Sorbas Basin, SE Spain). *Facies* 53, 329–345. doi:10.1007/s10347-007-0107-3

Puga-Bernabéu, Á., Martín, J. M., and Braga, J. C. (2007b). Tsunami-related deposits in temperate carbonate ramps, Sorbas basin, southern Spain. *Sediment. Geol.* 199, 107–127. doi:10.1016/j.sedgeo.2007.01.020

Raffi, I., and Flores, J. A. (1995). Pleistocene through Miocene calcareous nannofossils from eastern equatorial pacific ocean (leg 138). *Proc. Ocean Drill. Program, Sci. Results* 138, 233–286. doi:10.2973/odp.proc.sr.138.112.1995

Rindi, F., Braga, J. C., Martin, S., Peña, V., Le Gall, L., Caragnano, A., et al. (2019). Coralline algae in a changing Mediterranean Sea: How can we predict their future, if we do not know their present? *Front. Mar. Sci.* 6, 723. doi:10.3389/fmars.2019.00723

Rodríguez-Fernández, J. (1982). El Mioceno del sector central de las Cordilleras Béticas. Granada: Publ. Univ. Granada, 202. Tesis Doctoral.

Ruiz-Constán, A., Galindo-Zaldívar, J., Pedrera, A., and de Galdeano, C. (2009). Gravity anomalies and orthogonal box fold development on heterogeneous basement in the Neogene Ronda Depression (Western Betic Cordillera). *J. Geodyn.* 47, 210–217. doi:10.1016/j.jog.2008.09.004

Serrano, F. (1979). Los foraminíferos planctónicos del Mioceno superior de la cuenca de Ronda y su comparación con los de otras áreas de la Cordilleras Béticas. Málaga: Univ. Málaga, 272. PhD Thesis.

Setchell, W. A., and Mason, L. R. (1943). Goniolithon and Neogoniolithon. *Proc. Natl. Acad. Sci. U.S.A.* 29, 87–92. doi:10.1073/pnas.29.3-4.87

Sierro, F. J. (1985). The replacement of the"Globorotalia menardii" group by theGloborotalia miotumida group: An aid to recognizing the Tortonian-Messinian boundary in the Mediterranean and adjacent Atlantic. *Mar. Micropaleontol.* 9, 525–535. doi:10.1016/0377-8398(85)90016-7

Sola, F., Braga, J. C., and Sælen, G. (2022). Contradictory coeval vertical facies changes in upper Miocene heterozoan carbonate-terrigenous deposits (Sierra de Gádor, Almería, SE Spain). *J. Sediment. Res.* 92, 257–274. doi:10.2110/jsr.2022.010

Testa, V., and Bosence, D. W. J. (1998). "Carbonate-siliciclastic sedimentation on a high-energy, ocean-facing, tropical ramp, NE Brazil," in *Carbonate ramps*. Editors V. P. Wrigth, and T. P. Burchette (London: Geol. Soc. London Spec. Publ.), 149, 55–71. doi:10.1144/gsl.sp.1999.149.01.05

Testa, V., and Bosence, D. W. J. (1999). Physical and biological controls on the formation of carbonate and siliciclastic bedforms on the north-east Brazilian shelf. *Sedimentology* 46, 279–301. doi:10.1046/j.1365-3091.1999.00213.x

Vergés, J., and Fernàndez, M. (2012). Tethys-Atlantic interaction along the Iberia-Africa plate boundary: The Betic-Rif orogenic system. *Tectonophysics* 579, 144–172. doi:10.1016/j.tecto.2012.08.032

Woelkerling, W. J., Irvine, L. M., and Harvey, A. S. (1993). Growth-forms in non-geniculate coralline red algae (coralliinales, rhodophyta). *Aust. Syst. Bot.* 6, 277–293. doi:10.1071/sb9930277

Young, J. R., Flores, J. A., and Wei, W. (1994). A summary chart of Neogene nannofossil magnetobiostratigraphy. *J. Nannoplankt. Res.* 16, 21–27.

frontiers | Frontiers in Marine Science

TYPE Original Research
PUBLISHED 25 October 2022
DOI 10.3389/fmars.2022.917883

OPEN ACCESS

EDITED BY
Stefano Aliani,
National Research Council (CNR), Italy

REVIEWED BY
Alan Giraldo,
University of Valle, Colombia
Simone Simeone,
National Research Council (CNR), Italy

*CORRESPONDENCE
Ana Cristina Rebelo
acfurtadorebelo@gmail.com

SPECIALTY SECTION
This article was submitted to Marine Ecosystem Ecology, a section of the journal Frontiers in Marine Science

RECEIVED 11 April 2022
ACCEPTED 03 October 2022
PUBLISHED 25 October 2022

CITATION
Rebelo AC, Martín-González E, Melo CS, Johnson ME, González-Rodríguez A, Galindo I, Quartau R, Baptista L, Ávila SP and Rasser MW (2022) Rhodolith beds and their onshore transport in Fuerteventura Island (Canary Archipelago, Spain). *Front. Mar. Sci.* 9:917883. doi: 10.3389/fmars.2022.917883

Rhodolith beds and their onshore transport in Fuerteventura Island (Canary Archipelago, Spain)

Ana Cristina Rebelo[1,2,3,4,5]*, Esther Martín-González[6], Carlos S. Melo[2,3,4,7,8], Markes E. Johnson[9], Alberto González-Rodríguez[10], Inés Galindo[11], Rui Quartau[1,7], Lara Baptista[2,3,4,12], Sérgio P. Ávila[2,3,4] and Michael W. Rasser[5]

[1]Divisão de Geologia Marinha, Instituto Hidrográfico, Lisboa, Portugal, [2]CIBIO-Centro de Investigação em Biodiversidade e Recursos Genéticos, InBio Laboratório Associado, Pólo dos Açores, Portugal, [3]BIOPOLIS Program in Genomics, Biodiversity and Land Planning, CIBIO, Vairão, Portugal, [4]MPB - Marine Palaeontology and Biogeography lab, University of the Azores, Açores, Portugal, [5]SMNS – Staatliches Museum für Naturkunde Stuttgart, Rosenstein 1, Stuttgart, Germany, [6]Museo de Ciencias Naturales de Tenerife, Organismo Autónomo de Museos y Centros, Santa Cruz de Tenerife, Spain, [7]Universidade de Lisboa, Faculdade de Ciências, Departamento de Geologia, Lisboa, Portugal, [8]Universidade de Lisboa, Faculdade de Ciências, Instituto Dom Luiz, Lisboa, Portugal, [9]Department of Geosciences, Williams College, Williamstown, MA, United States, [10]Área de Paleontología, Facultad de Biología, Universidad de La Laguna, San Cristóbal de La Laguna, Spain, [11]Instituto Geológico y Minero de España (IGME-CSIC), Unidad Territorial de Canarias, Las Palmas de Gran Canaria, Spain, [12]Departamento de Biologia, Faculdade de Ciências da Universidade do Porto, Portugal, Faculdade de Ciências da Universidade do Porto, Porto, Portugal

Rhodoliths occur extensively around the shores of Fuerteventura Island in the Canary Archipelago, with *Lithothamnion* cf. *corallioides* being the most prominent species. A large number of rhodoliths end up washed onshore, the debris from which contributes to the formation of sediments constituting modern beaches. In a previous study by one of the co-authors (MEJ), the northern coast of Fuerteventura was shown to comprise various types of rhodolith deposits such as beach, platform overwash, tidal pools, coastal dunes, and others. An extraordinary example of stranded rhodoliths is located near Caleta del Bajo de Mejillones, approximately 3 km west of Corralejo, on the north coast of the island. The deposit forms a supratidal beach 120 m long and 10 m wide that sits above the landward termination of an extensive wave-cut platform eroded in basalt and exposed at low tide to a width of 130 m perpendicular to shore. Here, rhodoliths are very small (<3 cm) resembling popcorn, and the locality is known as the "Popcorn Beach". Other examples are berms up to 150 m long and 9 m wide at Caleta del Bajo de

Mejillones, or an exposed beach at Playa del Hierro with an area of more than 1500 m^2 covered entirely of very coarse rhodolith sand. Extensive living rhodolith beds were found at a water depth of 22 m.

KEYWORDS

coralline algae, modern beaches, taphonomy, marine biodiversity, volcanic islands, Canary Islands

1 Introduction

The North coast of Fuerteventura Island in the Canaries is well known for its beaches of stranded rhodoliths. Here, rhodoliths are very small (<3cm) resembling popcorn and the area is known locally as "Popcorn Beach". Nevertheless, little is still known about which species contribute to the formation of these rhodoliths and which physical and/or biological factors control their occurrence.

Rhodoliths and rhodolith beds (RBs) correspond to unattached nodules of coralline red algae (Rhodophyta) and are essential ecosystem engineers, yielding structurally complex habitats that harbour distinctive high-diversity faunal and floral assemblages, as a consequence of their branching and interlocking nature (Steller et al., 2003; Foster et al., 2007; Teichert, 2014; Riosmena-Rodríguez, 2017; Fredericq et al., 2019). Organisms living on RBs are better protected against predators, and commercially important species (e.g., fish, crustaceans, molluscs) benefit from the existence of such habitats (Teichert, 2014). In this manner, rhodoliths are crucial for the establishment and maintenance of biodiversity and, thus, contribute to major ecosystem functions (Fredericq et al., 2019; Stelzer et al., 2021).

The growth, geographic distribution and sustainability of rhodoliths are controlled by several factors, of which light, temperature, sedimentation, hydrodynamic regime, existence of marine barriers, and abundance of corals are vital (Wilson et al., 2004; Riosmena-Rodríguez, 2017; Rebelo et al., 2021). Depth and correlated wave-induced turbulence and light decrease are also known to directly influence physical processes, as well as salinity (Otero-Ferrer et al., 2020 and references therein). Although rhodoliths are resilient under a variety of environmental disturbances, they can be severely impacted by storms (with onshore transport; cf. Rebelo et al., 2016; Rebelo et al., 2018), harvesting, ocean acidification and global warming (Martin et al., 2014; Sañé et al., 2016). RBs are commonly found at depths where light is sufficient for growth and water motion and bioturbation are sufficient to move the rhodoliths and prevent burial and anoxia from sedimentation (Foster et al., 2013).

Reefless island shelves, such as characteristic in the Canaries, can be particularly dynamic marine environments due to their exposure to strung surf, storms, volcanism, and mass wasting (Stillman, 1999; Acosta et al., 2004; Rodriguez-Martin et al., 2022). These type of shelves are also narrower and steeper than those typically found around continents, a condition that facilitates sediment transport on the entire shelf and contributes significantly to environmental instability (Ávila et al., 2008; Quartau et al., 2012; Ávila et al., 2015a; Rebelo et al., 2016; Johnson et al., 2017a; Ávila et al., 2019; Zhao et al., 2022). RBs are known to occur between 20 to 100 m depth around most of the Canary Islands (Afonso-Carrillo, 2021 and references therein). Shallower RBs develop from ~2m depth detrital bottoms between Fuerteventura, Lanzarote and Lobos, where their nodules can reach up to 20 cm in diameter (Reyes et al., 2005; Afonso-Carrillo, 2021). Nonetheless, studies regarding insular living rhodoliths are so far very few, especially in the northeast Atlantic archipelagos (e.g., Rosas-Alquicira et al., 2009; Rebelo et al., 2018; Otero-Ferrer et al., 2020). It is still relatively unknown how these rhodoliths cope with environmental pressures, and it is hence the focus of this study.

In this work, we report on the distribution of rhodolith-forming species and consider those factors controlling RBs around the shores of Fuerteventura Island, adding to a better understanding of insular rhodolith formation and deposition. We also stress the importance to preserve RBs as biodiversity hotspots and call for a conscientious effort in the protection and maintenance of these valuable biological resources.

2 Geographic and environmental setting

Lanzarote and Fuerteventura are the easternmost islands in the Canary Archipelago (Figure 1). Both constitute the emerged part of the Canary Ridge, an elongated volcanic edifice trending NNE-SSW (Acosta et al., 2004). Coastal erosion and sea level changes commonly generate wide insular shelves (Quartau et al., 2010; Ramalho et al., 2013; Quartau et al., 2016), where channels sometimes develop between two islands, as in the case between Lanzarote and Fuerteventura Islands. Fuerteventura, the oldest of the Canary Islands, dates to 23 Ma together with integrated Jurassic to Cretaceous sea-floor sediments (Steiner et al., 1998;

Stillman, 1999; Acosta et al., 2004; Bogaard, 2013). The shield-building stage on Fuerteventura started about 17–16 Ma and concluded at approximately 9 Ma (Coello et al., 1992). Post-erosional volcanism has occurred sporadically on Fuerteventura over the last 5 Ma. An example is the Bayuyo eruptive fissure that dates 135 ka (Casillas and Torres, 2011; Troll and Carracedo, 2016) with its basaltic lava flows contributing to the Fuerteventura NW coastline. Biogenic sand deposits occur along the coast as the result of currents and wind transport from the shelf to the coast and inland (Roettig et al., 2017; Roettig et al., 2020).

The area under study lies on the north shore of Fuerteventura Island, and is separated from Lanzarote by a 10-14 km wide channel, La Bocaina strait, with an average depth of 40 m. Nowadays, the majority of the waves hitting the Canary Islands come from NE, N and NW (although the NE is predominant), showing mean values of significant wave height of 2 m that may reach 5-7 m during storms (Rusu and Onea, 2016; Gonçalves et al., 2020). The north-easterly trade-winds dominate on the Canary Islands (Azorin-Molina et al., 2017).

The rhodoliths studied, herein, were collected on an intertidal shore platform that extends for approximately 15 km along the north coast of Fuerteventura, from Corralejo in the NE to El Cotillo in the NW part of the island, including L2 - Caleta del Bajo de Mejillones (Figure 1B). This platform was cut by marine erosion, and at low tide presents a width of 130 m, and is exposed to the strong action of the NW, N and NE waves during sea storms. Rhodoliths are found both forming accumulations to organogenic sands of the supratidal beach and in small tide pools.

3 Methods

Field studies were conducted during the 1st Workshop of Marine Palaeontology and Littoral Geology in Canary Islands:

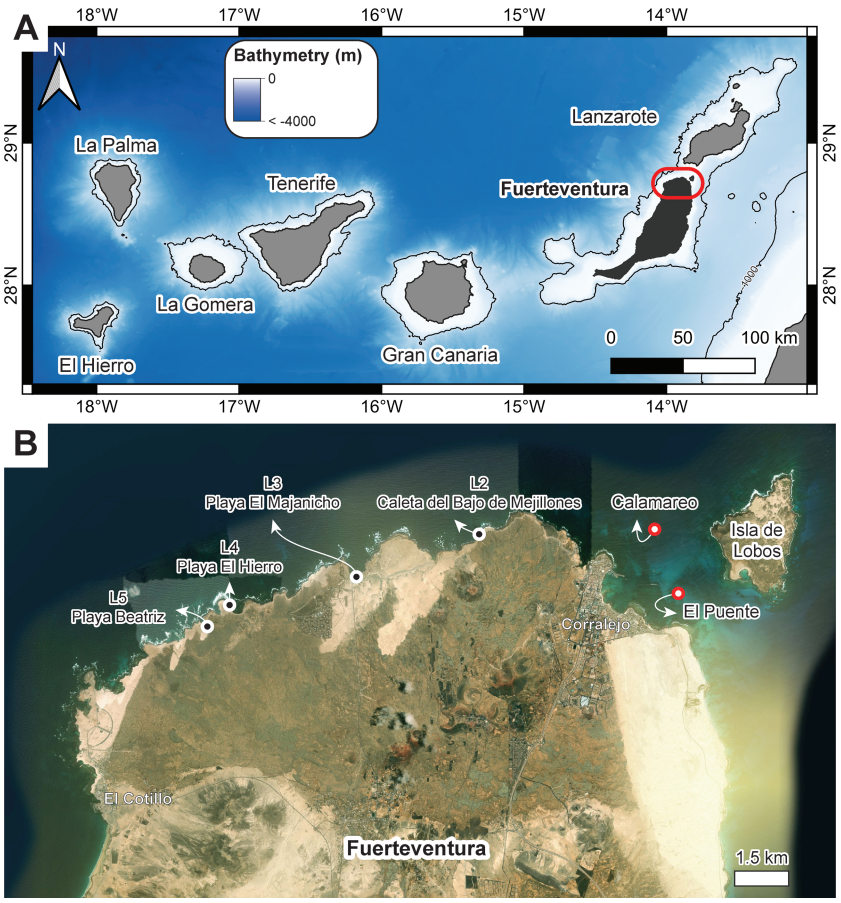

FIGURE 1
(A) Map of islands in the Canaries highlighting the study area in Fuerteventura, **(B)** Aerial view of the north coast of Fuerteventura Island showing the location of study sites between the towns of Corralejo and El Cotillo: L2 – Caleta del Bajo de Mejillones; L3 – Majanicho; L4 – Playa El Hierro; L5 – Caleta de Beatriz; Diving spot Calamareo; Diving spot El Puente, Bathymetry was retrieved from Gobierno de Canarias (https://opendata.sitcan.es/dataset/modelo-digital-de-terreno-mdt-de-25x25-metros). Aerial photo from AppleMap (2022).

Fuerteventura, between 6 and 14 of November of 2021. The north coast of Fuerteventura was canvassed for sites with stranded rhodoliths. A limited number of rhodoliths was collected for taxonomic studies at Caleta del Bajo de Mejillones, Majanicho, Playa El Hierro and Caleta de Beatriz, locations 2, 3, 4 and 5 respectively, indicated by Johnson et al. (2012) (Figure 1). Locality 1 (from Johnson et al., 2012) corresponds to a sandy beach in the eastern part of the island

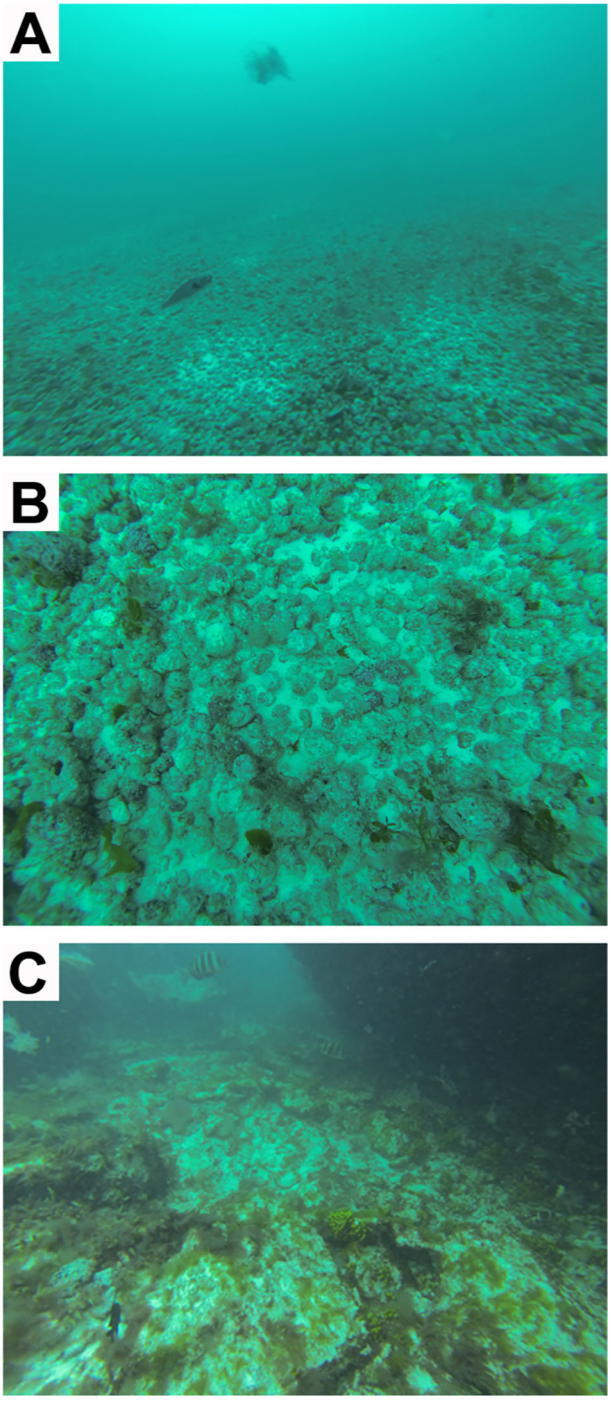

FIGURE 2
Images acquired by scuba diving. **(A)** RB over a sandy sea bottom at Calamareo, **(B)** detail of the RB at Calamareo, **(C)** rocky sea bottom at El Puente without any visible rhodoliths.

and was not here considered. Additionally, scuba diving was performed at Calamareo (Lat: 28.7516, Long: -13.8549) and El Puente (Lat: 28.7347, Long: -13.8471), two diving spots also at the NE coast of Fuerteventura (Figures 1, 2) to report on living rhodoliths and environmental conditions. Sampling of rhodoliths was not possible on this site.

Eleven thin sections (4 of 4.8 x 2.8 cm; 4 of 4.8 x 4.8 cm; 2 of 9.5 x 4.8 cm; and 1 of 9.5 x 7.5 cm) of selected rhodoliths were studied under a compound polarizing microscope (Leica DM750P) equipped with a digital camera (Leica ICC50W). Anatomical and taxonomical terminologies applied to coralline algae follow the works by Braga et al. (1993); Irvine and Chamberlain (1994); Rasser and Piller (1999) and Hrabovský et al. (2016). Growth form terminology conforms to Woelkerling et al. (1993). Morphological classification follows Bosence (1983). Cell and conceptacle dimensions were measured according to Rasser and Piller (1999) using Image J. Mean (M) and standard deviation (SD) were calculated for both cells and conceptacles, whenever the number of measurements allowed (n= 5). All material is stored in the Department of Palaeontology at the State Natural History Museum Stuttgart, Germany.

4 Results

4.1 *In situ* rhodolith bed

At Calamareo, a diving site located less than 2 km north of Corralejo consists of a rocky platform that is 12 m deep, descending vertically to 20-22 m and featuring caves, vaults and passageways (Figure 1B). Here is a sizeable RB at around 22 m depth on a sandy bottom. Rhodoliths vary greatly in shape and size from 2 to 8 cm (n = 18) (Figures 2A, B). The lateral extension of the RB is unknown, but it may reach several hundred square meters, perhaps even square kilometres. The density of rhodoliths varies from closer packing with rhodoliths stacked over each other, to loose rhodoliths lying on sandy substrate. The RBs comprise smaller patches with soft algae; no invertebrates could be observed in the field.

On El Puente, less than 2 km east of Calamareo, and less than 1 km from the coast, abrupt lava formations occur with caves, chimneys, small canyons, cornices and an impressive bridge. The depth in the studied area is 7 to 10 m, and no rhodoliths were observed on the rocky bottom covered with fleshy algae and sponges. Sediment accumulations are restricted to depressions forming sedimentary traps (Figure 2C).

4.2 Stranded rhodolith accumulations

4.2.1 Taphonomic grades

Over a coastal distance of 17 km between the towns of Corralejo in the east and El Cotillo in the west (Figure 1B), the north shore of Fuerteventura offers an extraordinary insight regarding the development and variation in carbonate sediments derived from modern rhodoliths (Figure 1).

Introduced by Brandt (1989), the concept of taphonomic grades was originally applied to fossil assemblages dominated by marine invertebrates with four classes (A to D) representing deterioration in fabric from a starting point (A) of an original community preserved *in situ* with little or no evidence of shell disarticulation, breakage, corrasion, or disruption from original growth position. Maximum depreciation (D), amounts to the formation of what otherwise might be called a shell coquina with more than 75 percent attrition in the categories of fossil breakage, corrasion, and orientation and a possible change in the proportion of matrix to shell content of 50 to 75 percent. The two intermediate grades (B and C) are separated, for example, by the degree of breakage estimated at a level below or above 50 percent. Effectively, the range of taphonomic grades so formulated traces a continuum between a biocenosis, or life assemblage, and a thanatocenosis, i.e., a death assemblage, in the latter case, severely damaged. The application of this classification to modern coralline red algae and by extension to fossilized deposits of rhodoliths, was undertaken in a review paper by Johnson et al. (2017b) covering the Macaronesian region with the best examples derived from Fuerteventura Island.

4.2.2 Rhodolith sites

At L2 - Caleta del Bajo de Mejillones, located about 3 km east Corralejo (Figures 1B, 3A), a massive accumulation of rhodoliths occurs as an overwash deposit in a supratidal setting above the adjacent intertidal rock platform. Because the basalt platform at this location is up to 130 m wide and characteristically clean at low tide, the living rhodoliths that arrived onshore were transported a relatively short distance from offshore. Due to the small size of the rhodoliths, between 1 to 3 cm in diameter, and their lumpy morphology, the locality has been called “Popcorn Beach”. Based on dimensions recorded by Johnson et al. (2012), the beach deposit composed of stranded rhodoliths is 10 m wide and extends for a distance of 120 m parallel to the shore. Using a sample quadrate with an area of 0.25 m^2, the exposed surface layer corresponds to a density of about 5,000 rhodoliths/m^2 (Figure 4). It is estimated that the exposed surface amounts to roughly six million rhodoliths, which is a fraction of the entire assemblage, because an exploratory pit excavated into the beach reveals two layers, each 5 cm thick, separated by a layer of carbonate sand (Johnson et al., 2017b). Overall, only a quarter of the rhodoliths are whole, whereas 65 percent are broken or worn, and at least 10 percent of the surface is strewn by basalt pebbles. According to the scheme proposed by Brandt (1989), a taphonomic grade of C may be applied to the deposit at L2 - Caleta del Bajo de Mejillones.

Farther west near L3 - Majanicho (Figures 1B, 3B–D), another overwash deposit of rhodoliths forms a berm elevated 1.4 m above the adjacent rock platform. This deposit is quite

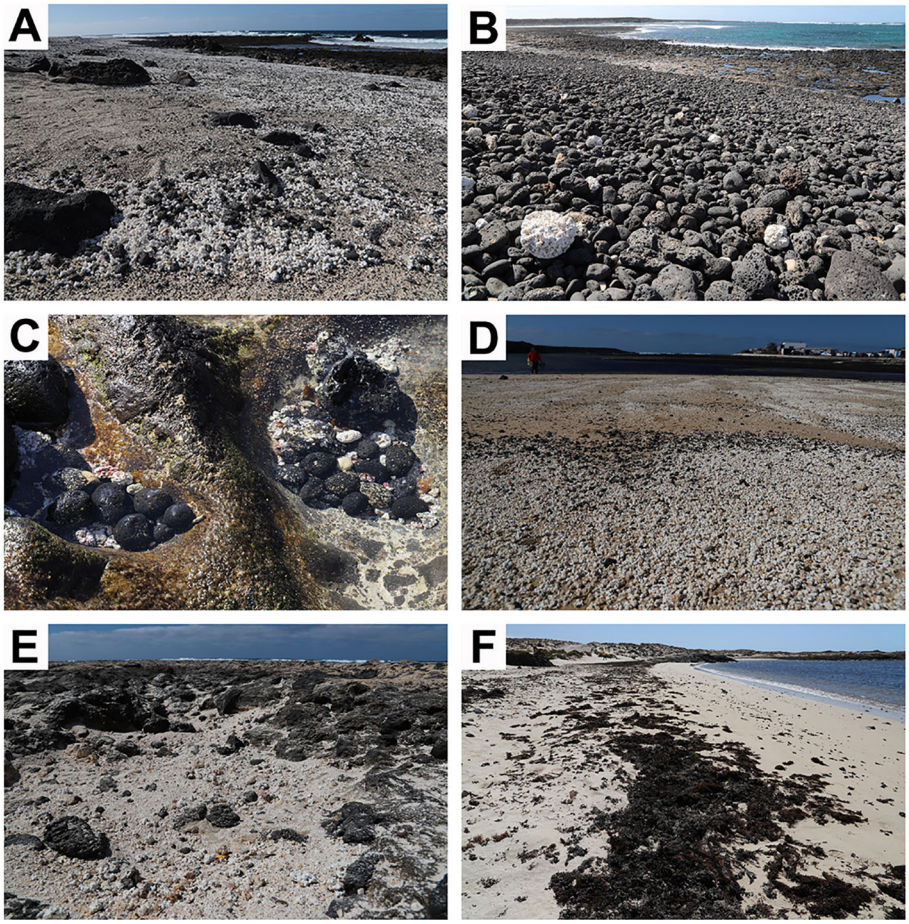

FIGURE 3
Field photos of stranded rhodoliths. **(A)** L2 - Caleta del Bajo de Mejillones, **(B)** L3 - Majanicho berm, **(C)** L3 - Majanicho intertidal pool, **(D)** L3 - Playa El Majanicho, **(E)** L4 - Playa El Hierro, **(F)** L5 - Caleta de Beatriz.

similar to the one at L2 - Caleta del Bajo de Mejillones regarding the average size and the degree of breakage of the rhodoliths. It was therefore classified as a taphonomic grade of C. Notably, when visited in July 2011 (Johnson et al., 2012), some traces of brown algae were found still attached to individual rhodoliths, giving some indication of a more complex algal community *in situ*. This indicates that coralline red algae and foliose brown algae thrived together in shallow, euphotic waters. However, no inclusion of marine invertebrates such as barnacles or small bivalves was observed, either at L2 - Caleta del Bajo de Mejillones or L3 - Majanicho.

At L4 - Playa El Hierro (Figures 1B, 3E), the beach is formed exclusively of very coarse carbonate sand (1 to 2 mm in diameter) derived entirely from the breakdown of rhodoliths. Many of the fragments may be recognized as the somewhat bulbous distal tips of tightly branched rhodoliths (Figure 4B). L5- Caleta de Beatriz (Figures 1B, 3F), shows more evidence of wrack with brown algae mixed with assorted rhodoliths.

In general, the grainsize of carbonate sand decreases progressively over distance to L5 - Caleta de Beatriz where, on a seasonal basis, the wrackline formed by brown algae is even more extensive. Under any consideration, a taphonomic grade of D would be appropriate for these settings. A dune field covering 4 hectares is located inland directly south of the Caleta del Marrajo, near the village of El Cotillo (Figure 1B). Here, the diameter of carbonate sand grains amounts to coarse-to-medium sand (0.25 to 1.0 mm), which reflects blindingly white under the sun. Asymmetrical ripple marks indicate sand migration in a southerly direction, which fits well with an interpretation of fine rhodolith sand lifted from the shore and blown inland. The taphonomic grade for such a dune deposit in the Brandt (1989) scheme merits an extreme D assignment. Carbonate dunes derived exclusively of crushed rhodolith detritus are seldom met in the modern world, but a good example is reported by Sewell et al. (2007) on Isla Coronados in Mexico's Gulf of California. Pleistocene dunes dominated by

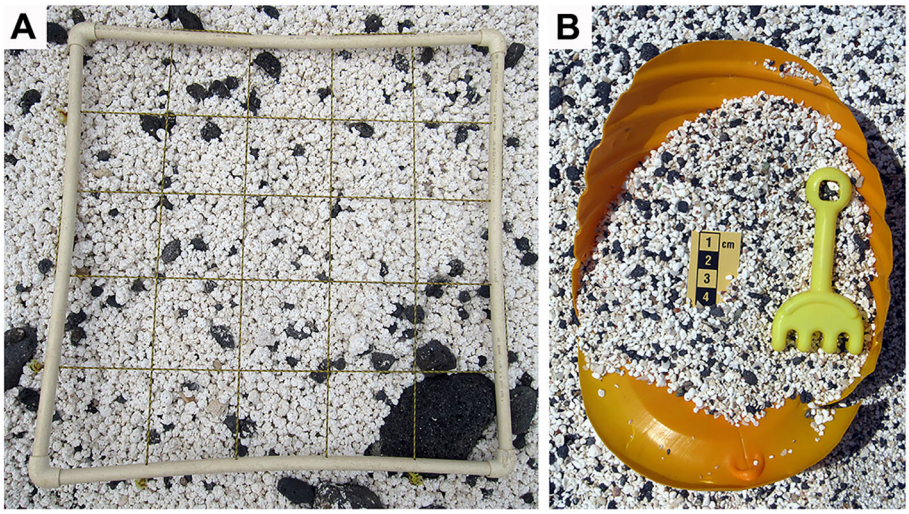

FIGURE 4
(A) Standard sample quadrat (50 x 50 cm) on "popcorn beach" at L2 - Caleta del Bajo de Mejillones on the north shore of Fuerteventura Island. Each square is 10 cm x 10 cm. Approximately 200 rhodoliths may be counted per unit, **(B)** close-up view of finely degraded rhodolith material–from L4 - Playa El Hierro (Figures 2C, 3E).

rhodolith debris also are known to occur on Maio and São Nicolau in the Cabo Verde Archipelago (Johnson et al., 2013).

4.3 Rhodoliths' internal composition

In L2 - Caleta del Bajo de Mejillones rhodoliths are mostly monospecific, with rare borings and encrustations. At L3-Majanicho the rhodoliths living in the intertidal pools have the largest dimensions, reaching up to 8 cm. Rhodoliths here are multispecific and have branching density IV, abundant encrustations, and show small borings on the thallus surface. At L4 - Playa El Hierro rhodoliths are monospecific, and heavily bored with some encrustations. At L5 - Caleta de Beatriz rhodoliths are multispecific and have branching density III; borings are abundant and few encrusters may be found (Table 1; Figure 5).

4.4 Coralline taxonomy

Phylum **Rhodophyta** Wettstein, 1901

Class **Florideophyceae** Cronquist, 1960
Subclass **Corallinophycidae** Le Gall and Saunders, 2007
Order **Hapalidiales** Nelson et al., 2015
Family **Hapalidiaceae** Gray, 1864
Genus ***Lithothamnion*** Heydrich, 1897, nom. et typ. cons.
Lithothamnion* cf. *corallioides (P. Crouan and H. Crouan) Crouan HM and Crouan PL, 1867
(Figure 6A–D)

Studied thin sections: Loc. 2; Loc. 3 Beachway; Loc. 3/1 intertidal; Loc. 3/2 intertidal; Loc. 3/3 intertidal; Loc. 4/1; Loc. 4/2; Loc. 5/2; Loc. 5/3

Description: Growth form encrusting to warty. Thallus monomerous, dorsiventral with non-coaxial core filaments. Protuberances are up to 3 mm in thickness and 2.5 mm in length. Core region is 61-145 µm thick; core cells are 13-19 µm (M = 16; SD = 2) in length and 5-8 µm (M = 7; SD = 1) in diameter. The peripheral region is zoned, formed by 5-11 rows of rectangular cells 5-9 µm (M = 7; SD = 1) in diameter and 9-20 µm (M = 14; SD = 3) in length. Epithallial cells are flat, rounded and flared. Subepithallial cells are as long as or longer than cells subtending them. Cell fusions are present both in the core and

TABLE 1 Localities and selected features from the rhodoliths of the north shore of Fuerteventura Island.

Location number and name	Type of deposit	Rhodolith composition	Borings	Encrusters
L2 - Caleta del Bajo de Mejillones	Platform overwash	Monospecific	Rare	Rare
L3 - Majanicho	Tidal pool; Berm	Multispecific	Recurrent	Abundant
L4 - Playa El Hierro	Outer beach	Monospecific	Abundant	Few
L5 - Caleta de Beatriz	Inner-cove beach	Multispecific	Abundant	Few

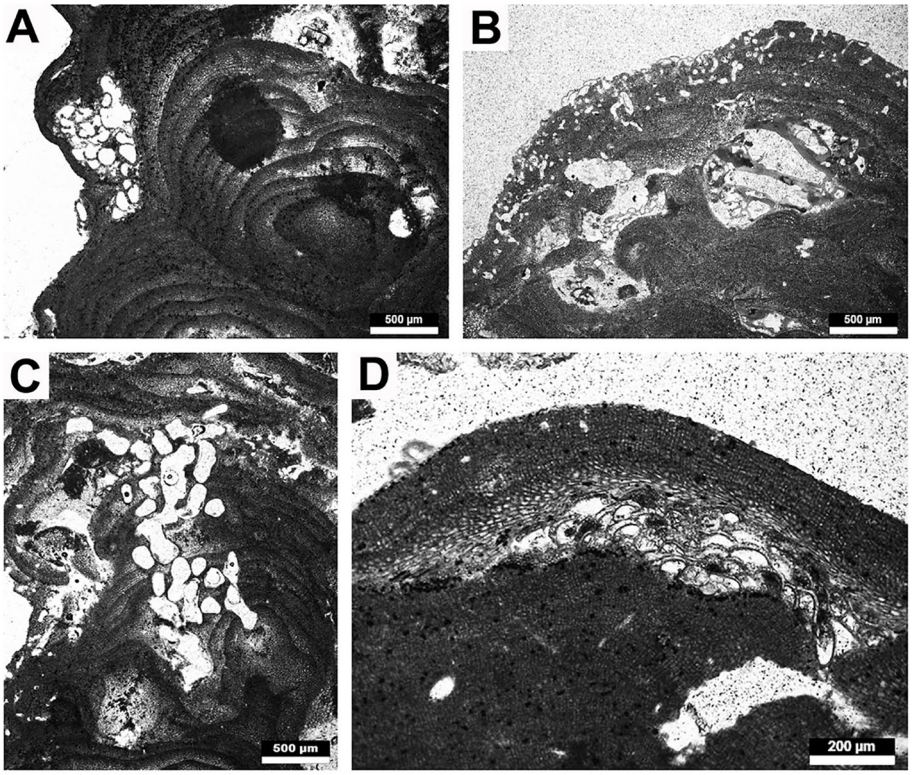

FIGURE 5
Borings and encrusters present on the Fuerteventura rhodoliths. **(A)** Encrusting foraminifer? interspersed in the coralline thalli, **(B)** small-size borings at the coralline thallus extremity and other encrusters, **(C)** medium-size borings throughout a coralline thallus, **(D)** bryozoan? in between the coralline thalli.

peripheral regions. Several multiporate conceptacles throughout the thallus, completely raise above thallus surface. Rectangular to triangular voids above some of the conceptacles' roof. Conceptacles are 427-908 µm (M = 537; SD = 106) in diameter and 191-337 µm (M = 251; SD = 34) in height. The pore canals are 11-37 µm (M = 17; SD = 4) in diameter and 39-83 µm (M = 64; SD = 10) in height; the roofs are flattened, convex, without rim and composed of 4-7 cell layers. Two conceptacles have remaining spores that are zonately divided.

Remarks: The epithallial cells and the long subepithallial cells indicate the genus *Lithothamnion*. The conceptacles shape and rims, and the zonation in the peripheral region seems compatible with those described by Adey and McKibbin (1970); Irvine and Chamberlain (1994), and Mendoza and Cabioch (1998). This species is the most common rhodolith former, being present in all localities from Bajo de Mejillones to Caleta de Beatriz. Because the species was identified on a morpho-anatomical base, and our measurements are slightly different from the ones by Afonso-Carrillo and Gil-Rodríguez (1982) we opted to keep it as *Lithothamnion* cf. *corallioides*.

Geographic distribution: According to Rebelo et al. (2021), *Lithothamnion corallioides* (P. Crouan and H. Crouan) P. Crouan and H. Crouan is reported from the following biogeographic provinces, as defined by Spalding et al. (2007) with modifications from Freitas et al. (2019): Northern European Seas, the Mediterranean Sea and the Lusitania Province, i.e., the South European Atlantic Shelf ecoregion, the Azores Archipelago ecoregion, the Webbnesia ecoregion (which integrates the archipelagos of Madeira, Selvagens and Canary Islands) and the Saharan Upwelling ecoregion.

Order **Corallinales** Silva and Johansen, 1986
Family **Mastophoraceae** Townsend and Huisman, 2018
Subfamily **Mastophoroideae** Setchell, 1943
Genus ***Lithoporella*** (Foslie) Foslie, 1909
***Lithoporella* sp.**
(Figure 6E–F)

Studied thin sections: Loc. 3/2 intertidal, Loc. 3/3 intertidal; Loc. 5/4

Description: Growth form encrusting. Thallus dorsiventral and dimerous; core region unistratose, filaments composed of palisade cells. Thallus 1-3 cells thick. Cells of adjacent filaments joined by cell fusions. Cells 6-16 µm (M = 11; SD = 3) in length and 18-36 µm (M = 25; SD = 6) in diameter. Where conceptacles

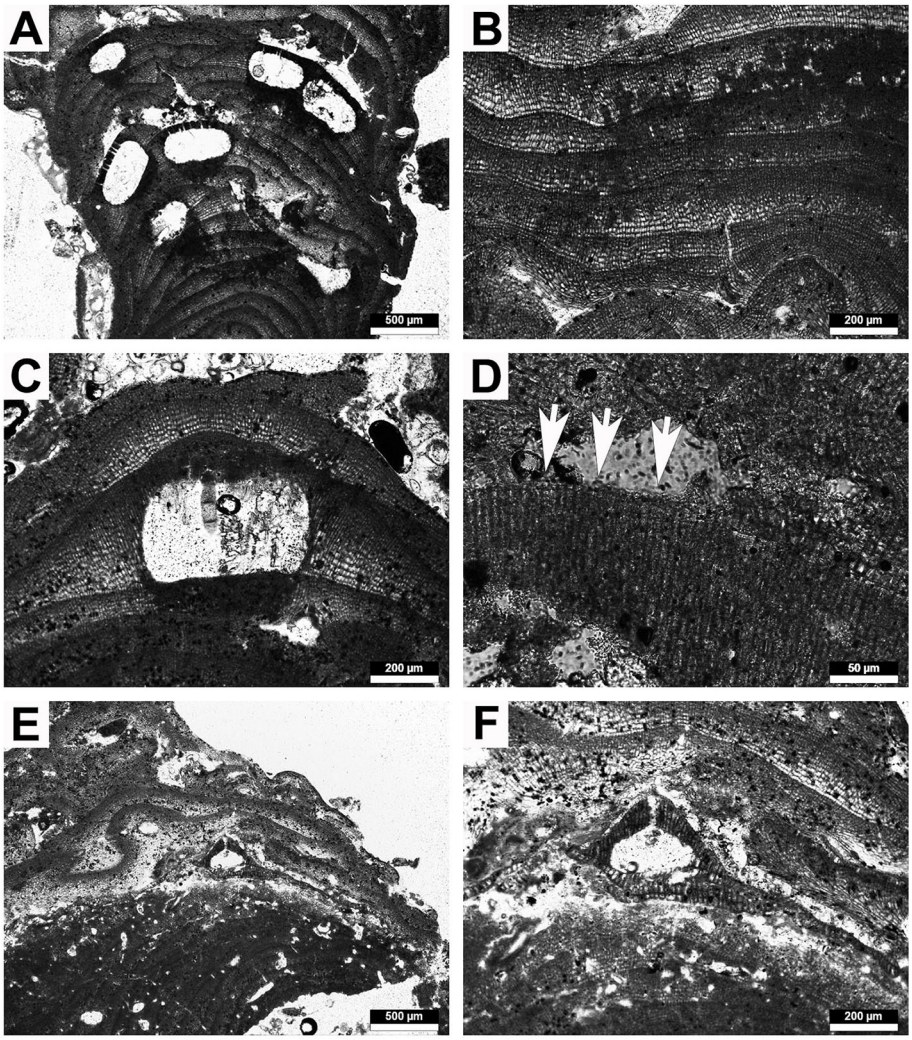

FIGURE 6
Representative rhodolith forming crustose coralline algae. **(A–D)** *Lithothamnion* cf. *corallioides*. **(A)** Portion of thallus with multiporate conceptacles, **(B)** detail of zoned peripheral region, **(C)** multiporate conceptacle with zoned tetraspore, **(D)** detail of epithallial cells (arrows). **(E, F)** *Lithoporella* sp. **(E)** Thallus of *Lithoporella* interspersed between other coralline thalli, **(F)** detail of uniporate conceptacle.

are formed, a small, multi-layered, dorsal region is composed by postigenous filaments, trichocytes not observed. Length of postigenous cells 16-19 µm, diameter 7-12 µm. Tetra/bisporangial conceptacles lacking a columella and completely raised above thallus surface. Cells surrounding the only visible pore canal, perpendicular to the roof surface. Conceptacles 253-297 µm in diameter and 109-121 µm in height. The pore canal is cylindrical in shape and is 38 µm in diameter and 94 µm in height.

Remarks: *Lithoporella* and *Mastophora* are the most closely related genera in the Mastophorioideae, and vegetatively no significant differences are known. However in *Mastophora* a central columella is present (Guiry and Guiry, 2022). Because no columella was found in the studied material, *Lithoporella* is the designated species.

Geographic distribution: A search on AlgaeBase yielded a total of 8 valid, extant species: *Lithoporella atlantica* (Foslie) Foslie, reported from the tropical and subtropical western Atlantic (Wynne, 2017); *Lithoporella bermudensis* (Foslie) W. H. Adey, reported from Bermudas (Taylor, 1960) and from the tropical and subtropical western Atlantic (Wynne, 2017); *Lithoporella indica* (Foslie) Adey, reported from Réunion Island (Silva et al., 1996) and from the Southeast Asia (Silva et al., 1987); *Lithoporella lapidea* (Foslie) Foslie, reported from the Caspian Sea (Foslie, 1909); *Lithoporella melobesioides* (Foslie) Foslie, with a wide geographic range, being reported

from the Mediterranean Sea (Bosence, 1983), eastern Atlantic Ocean (Cabo Verde Archipelago; Prud'homme van Reine et al., 2005), Indian Ocean (Silva et al., 1996) and Pacific Ocean (Womersley and Bailey, 1970); *Lithoporella quadratica* Ishijima, a fossil species described from Japan by Ishijima (1933); *Lithoporella ryukyuensis* W.Ishijima, another fossil species described from the Yukyu Islands by Ishijima (1938); and finally, *Lithoporella sauvageaui* (Foslie) Adey, reported from Canary Islands (Haroun et al., 2002) and from Cabo Verde Archipelago (John et al., 2004). *Lithoporella sauvageaui* (Foslie) Adey is known to occur in Canaries on the islands of Lanzarote, Gran Canaria and Tenerife (Haroun et al., 2002), however no species of *Lithoporella* has been reported, at least to the authors knowledge, at Fuerteventura Island.

Family **Hydrolithaceae** Townsend and Huisman, 2018
Subfamily **Hydrolithoideae** Kato et al., 2011
Genus ***Hydrolithon*** (Foslie) Foslie, 1909
***Hydrolithon* sp.**
(Figure 7A–B)

Studied thin section: Loc. 5/4

Description: Growth form encrusting. Thallus dimerous in construction; core region not a palisade. Thallus is 0.4-1 mm thick. Cells of primigenous filaments are 5-9 µm (M = 7; SD = 1) in diameter and 10-14 µm (M = 12; SD = 13) in lenght. Cells of postigenous filaments are rectangular in shape, show a very well defined alignment and are 7-14 µm (M = 11; SD = 2) in diameter and 14-23 µm (M = 18; SD = 3) in length. Rare cell fusions occur in postigenous filaments. Conceptacles are uniporate with a columella, 186-201 µm in diameter and 72-82 µm in height. The pore canal is cylindrical, 24 µm in diameter and 64 µm in height. Filaments surrounding the pore canal are perpendicular to the conceptacle roof.

Remarks: The thallus dimerous organization, the lack of palisade cells in the primigenous filaments, the presence of cells fusions and the filaments surrounding the pore canal oriented perpendicularly to the conceptacle roof indicates the genus *Hydrolithon*. Because of the absence of further preserved diagnostic characters it was not possible to identify the species.

Geographic distribution: A search on AlgaeBase yielded a total of 22 valid, extant species, of which Rebelo et al. (2021) indicate two as forming rhodoliths: *Hydrolithon boergesenii* Foslie (Foslie) and *Hydrolithon breviclavium* (Foslie) Foslie. Both species have a wide geographic distribution, the former being reported from the Western Central Atlantic (Caribbean and Gulf of Mexico), South America (Brazil), Eastern Atlantic (São Tomé and Príncipe Archipelago), Indian Ocean and Pacific Ocean, whereas *Hydrolithon breviclavium* is reported from the Western Atlantic,

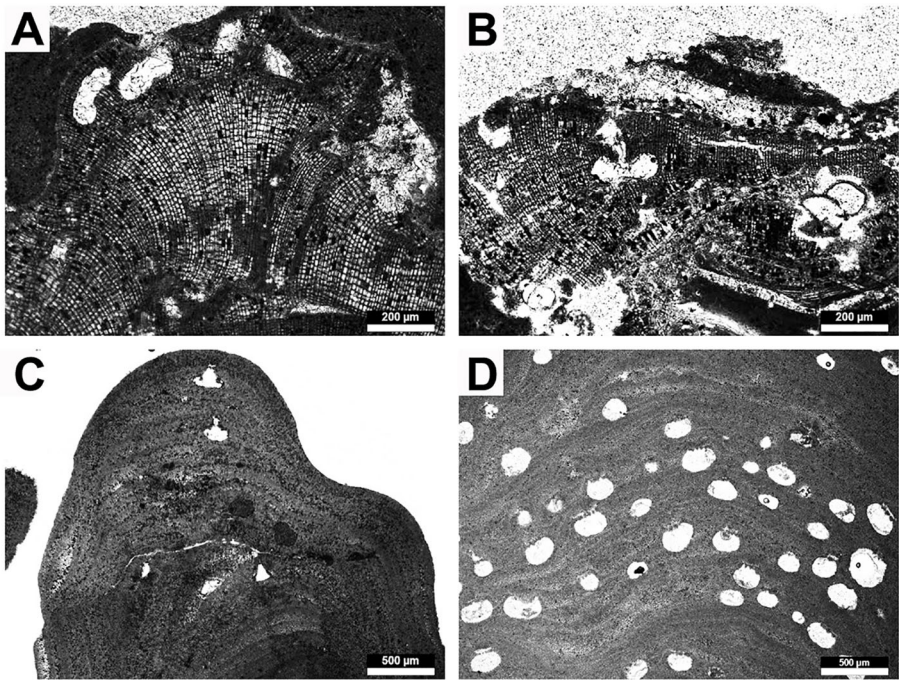

FIGURE 7
Representative rhodolith forming crustose coralline algae. **(A, B)** *Hydrolithon* sp., **(A)** dimerous thallus with uniporate conceptacles, **(B)** detail of uniporate conceptacle, **(C, D)** taxa of uncertain generic placement, **(C)** thallus with uniporate conceptacles, **(D)** several multiporate conceptacles dispersed throughout the thallus.

Indian Ocean (Seychelles) and Pacific Ocean (Guiry and Guiry, 2022). *Hydrolithon boreale* (Foslie) Chamberlain, *H. cruciatum* (Bressam) Chamberlain and *H. farinosum* (Lamouroux) Penrose and Chamberlain and *H. onkodes* (Heydrich) Penrose and Woelkerling are reported for Fuerteventura Island (Haroun et al., 2002).

Taxa of uncertain generic placement

(Figure 7C–D)

Studied thin section: Loc. 2

Unidentified taxon 1: One thallus with two uniporate conceptacles. One conceptacle well rounded, 179 µm in diameter and 92 µm in height. The pore canal is cylindrical, 42 µm in diameter and 73 µm in length. The filaments surrounding the pore canal seem to protrude into the pore. One conceptacle flask shaped, 236 µm in diameter and 72 µm in height. The pore canal is triangular, 100 µm in diameter and 103 µm in length. The poor preservation of the thallus does not allow further identification.

Studied thin section: Loc. 5/1

Unidentified taxon 2: One thallus with several small multiporate conceptacles 230-280 µm (M = 246; SD = 17) in diameter and 112-164 µm (M = 139; SD = 19) in height. The roofs are 32-47 µm thick. The poor preservation of the thallus does not allow further identification.

5 Discussion

5.1 Factors controlling rhodoliths distribution along the northern coast of Fuerteventura

The current knowledge on the extension of the RBs around the Canarian Archipelago is yet incomplete, although efforts are being made in this regard (Otero-Ferrer et al., 2020). Previous studies on rhodoliths from Gran Canaria Island have shown that the local environment has a strong influence on their development, especially as regards water motion and depth (Otero-Ferrer et al., 2020). Dominant wind and wave directions in the Canary Islands are mainly from the NE (Rusu and Onea, 2016; Azorin-Molina et al., 2017). Hence, predominant longshore currents should occur from East to West, although some waves also come from the NW. Rhodolith shape, branching pattern and sphericity are strongly affected by different intensities of water motion (Sciberras et al., 2009 and references therein). All rhodoliths studied show a closely branched morphology suggesting these are formed in a high energy environment. In addition, these were highly eroded rhodoliths showing a degree of breakage of C to D in the Brandt (1989) scheme. This suggests that stormy waves are able to transport and break rhodoliths carried to the nearshore of beaches on the north shores of Fuerteventura. Waves can reach up to 5 m near Fuerteventura (Rusu and Onea, 2016) and are likely able to transport them shoreward towards the beaches as bedload or in suspension aided by the flotation of attached brown algae. This latter effect is not accounted for by the transport mechanisms provided in the review by Masselink et al. (2011). Transport of sediments storm-induced is also a known pattern from the geological past and that appears to be frequent in volcanic oceanic islands [e.g., the Pliocene of Santa Maria Island in the Azores (Meireles et al., 2013; Ávila et al., 2015b; Rebelo et al., 2016; Johnson et al., 2017a)]. Non-algal encrusters, such as foraminifers and bryozoans, are frequently overgrown by the corallines suggesting a temporal disturbance in rhodolith growth that allowed the encrusters to grow only for a short time before the red algae prevailed again. Temporal disturbance also seems to explain why both monospecific and multispecific rhodoliths have borings, many at the extremity of the thallus before their final deposition onshore. We assume that the disturbances were caused by storms that are capable of transporting rhodolith beds into deeper and/or shallower environments, as well as parallel to the shore. It is not known which wave direction is more important for the onshore transport, though waves coming from NW have the longest fetch, hence these are likely to contribute more for this process. This is merely a hypothesis, since the places of rhodolith beds under life conditions has yet to be thoroughly mapped and therefore require future field studies. The Calamareo and El Puente were the only two diving spots we were able to explore during this study and therefore the extension of the rhodolith beds on the north coast of Fuerteventura is still unknown. Calamareo is shown here as a random example of how the rhodolith beds look *in situ*, and we believe that the rhodoliths come from the submarine part of the beaches where they were found. As it can be seen in Figure 8 the shore platform down to -10 m appears to be a smooth rocky platform, the probable place of development of the rhodoliths. Accordingly, a predictive model is here proposed to show the deposition of the rhodoliths on the north coast of Fuerteventura Island (Figure 9).

5.2. Factors promoting rhodolith transport landward the northern coast of Fuerteventura

At L2 - Caleta del Bajo de Mejillones the deposit of rhodoliths being 120 m long and 10 m wide (as described in Johnson et al., 2012) traces out to the west, where the whole rhodoliths vanish. This demonstrates that the bedload with the rhodoliths has petered out. Figure 10A shows the extension of the beach to the west of L2 – Caleta del Bajo de Mejillones with the exposed rock platform in the right side. The dashed lines mark how the mixed basalt and rhodolith sand in successive events terminate to the west, indicating that the source of the material came from the east. The main explanation for this would be a storm event concurrent with the strong NE trade

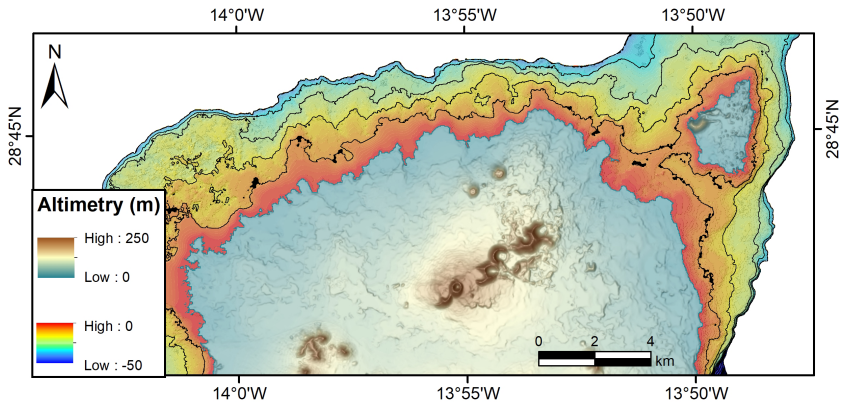

FIGURE 8
Bathymetry of the north coast of Fuerteventura Island screening the possible place of development of the rhodolith beds. Bathymetry lines are every 10 meters.

winds. The way that the rhodolith deposits form excursions onto the rock platform (far right) also indicate that the source of waves is from the east. A small trench made at the beach (Figure 10B) shows that the rhodoliths at the surface represent a single event draped over a pre-existing deposit of beach sand. The overlying rhodolith drift is maximum 5 cm thick while the sand below is no less than 25 cm thick with few rhodoliths mixed. The rhodolith drift on the top represents the most recent event on the beach, since these rhodoliths are positioned well above mean sea level in the supratidal zone.

At L3 - Majanicho stranded rhodoliths also peter out to the west, where they fail to spill into the embayment (Figure 10C). The dashed lines indicate layering represented by stringers of eroded basalt. Figure 10C shows the extent of the distinctive basalt rock platform at extreme low tide. Given the local geography, it is not possible that this deposit came from the west toward the east. Furthermore, individual rhodoliths from L2 - Caleta del Bajo de Mejillones, L3 - Majanicho and L4 - Playa El Hierro still retain an attachment of single strands or blades of brown algae (Figure 10D). This is a well-known phenomenon that in Brazil is called the "arribadas" (Dias and Villaça, 2012), suggesting that the bedload of stranded rhodoliths is quite recent.

Following the definitions of Masselink et al. (2011) regarding the modes of sediment transport, the rhodolith transport on the north coast of Fuerteventura signifies extreme turbulence which the degradation of rhodoliths occurred during saltation. The reason for an interpretation of bedload transport at the highest energy index is that the very wide offshore rock platforms are almost entirely free of sediments except for a few cases where rhodoliths are trapped in small tidal pools. Much stronger currents (eddies) had to have been involved as opposed to the normal traction associated with movement of a bedload. Another

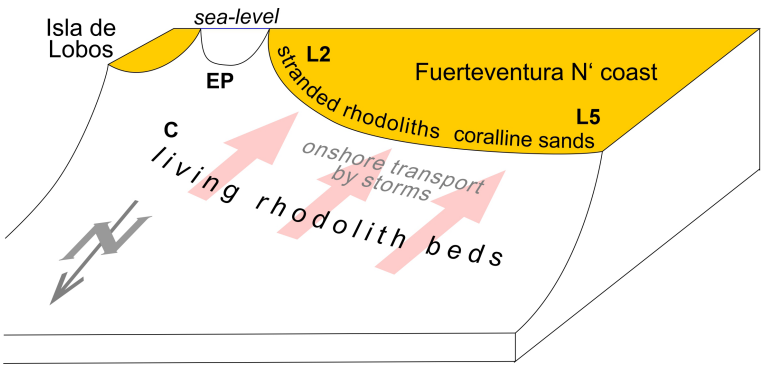

FIGURE 9
Model for the deposition of the rhodoliths on the north coast of Fuerteventura Island. L2 - Caleta del Bajo de Mejillones, L5 - Caleta de Beatriz, C – Calamareo, EP – El Puente.

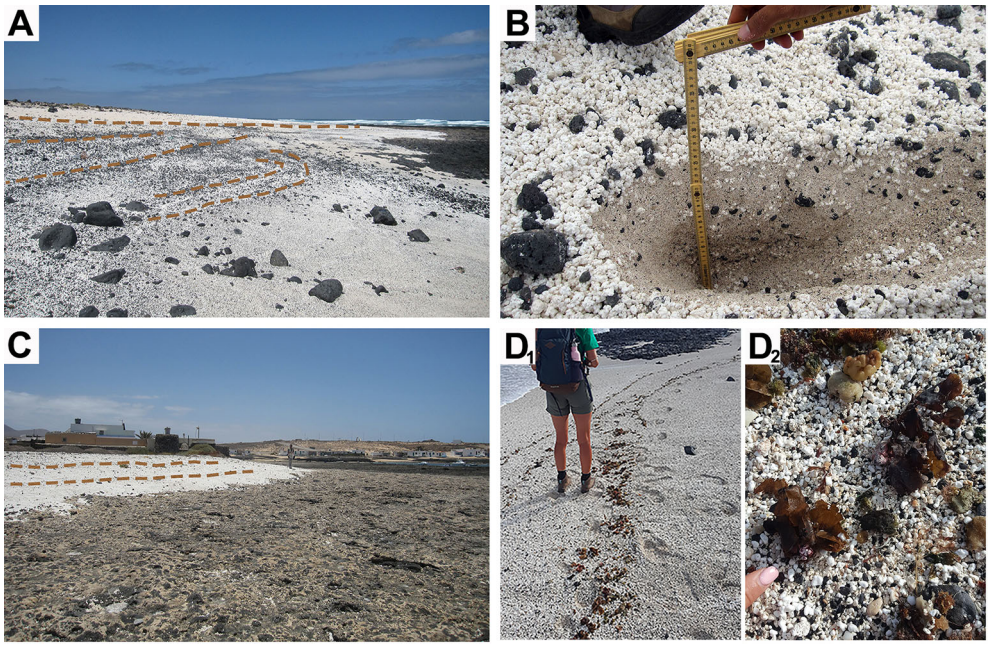

FIGURE 10
(A) Stranded rhodoliths at L2 - Caleta del Bajo de Mejillones. Image is at the far (distal end) of the 120-m long deposit; dashed lines show how the mixed basalt and rhodolith sand in successive events terminate to the west. **(B)** detail of small trench trench made at L2 - Caleta del Bajo de Mejillones evidencing the rhodolith drift overlying the sand. **(C)** Stranded rhodoliths at L3 – Majanicho. Dashed lines show layering indicated by stringers of eroded basalt. **(D1)** Stranded extant rhodoliths attached to brown algae at Playa El Hierro. **(D2)** Detail of stranded rhodoliths attached to brown algae.

reason for this is that mixed among the dominant organic sediments from the rhodoliths, there are larger pebbles and even small cobbles eroded from basalt. It would require stronger wave action to move these heavier clasts in concert with the organic clasts. Thus, the extensive wave cut rock platforms were scoured by strong storm currents, essentially moving along shore from east to west, during which offshore sediments of both rhodoliths and basalt origins were fully swept across the rock platforms to end up in a supratidal setting well above the normal tide line.

5.3 Taphonomic grades

The reduction of rhodolithic shore materials from a grade of C as demonstrated on Popcorn Beach at L2 - Caleta del Bajo de Mejillones to a severely diminished grade of D in the sand dunes near El Cotillo (Figure 1B) reflects the progressive mechanical abrasion of stranded coralline algae under direct influence of onshore wave transport and further beach deflation due to onshore winds. The several pocket beaches between these two areas are dominated by carbonate sand production that shows a clear decrease in average grain size from very coarse grains at L4 - Playa El Hierro (Figure 4B) to finer and finer grains with distance to the west. Overall, the scenario reflects the energy of long-shore currents related to the strong action of wind-driven, moving from east to west across the north coast of Fuerteventura Island and crossing the shore in a diagonal direction. The strongest currents appear at a frequency unrelated to a mere seasonal pattern, although the brisk northeast trade winds are a near constant presence in the region. The exploratory excavation on the beach at L2 - Caleta del Bajo de Mejillones shows that rhodolith deposits are renewed with successive storm events. There exists a general relationship between rhodolith size and the amount of time during which an individual rhodolith continues to grow in diameter by accretion. Mostly less than 3 cm in diameter, the relatively small size of rhodoliths that dominate Popcorn Beach indicates they are harvested during storms that arrive at intervals several years apart. The absence of rhodoliths of an appreciably larger size up to 8 cm in diameter suggests that few if any survive long enough to reach that size in waters directly offshore down to a depth of 25 m along the north coast.

5.4 Coralline algae taxonomic composition

Lithothamnion coralliodes was present at all localities of the present study. *L. coralliodes* is also very common around the

FIGURE 11
(A) Example of a prohibition sign for rhodolith picking at L4 - Playa El Hierro. **(B)** Rhodolith plundering at L2 – Caleta del Bajo de Mejillones. Photo courtesy of Félix de la Rosa.

islands of Cabo Verde and Madeira (Foslie, 1908; Cabioch, 1974; Guiry and Guiry, 2022), and is distributed in all the islands of the Canary Archipelago, with the exception of La Palma and La Gomera (Afonso-Carrillo and Gil-Rodríguez, 1982). *L. corallioides* and *Phymatolithon calcareum* are coralline algae species that are protected by the Habitats Directive (92/43/EEC) as key habitat providers, crucial for the support of numerous other species (Pardo et al., 2014; Hernández-Kantún et al., 2017). The fact that the rhodoliths are composed by species of *Lithothamnion*, *Hydrolithon* and *Lithoporella* which are generally recognized as typical of deep-water (Aguirre et al., 2017 and references therein), could explain the absence of rhodoliths in the shallow diving spot El Puente, not only because of the substrate type but as a result of depth as well. *Lithoporella* is a new record for Fuerteventura (Haroun et al., 2002), which could be due to the incomplete knowledge of the taxonomic inventory of Canary Islands' coralline algae.

5.5 Importance of rhodoliths and conservation implications

We take the opportunity of this study to highlight the negative-impact of rhodolith plundering from the beaches of Fuerteventura Island. Although rhodolith beds have been recognized in various European and international frameworks through the adoption of a collection of protection instruments such as Directives, Regulations and Conventions (Basso et al., 2016), more work in this regard is still needed for the Canary Islands. Each year, substantial amount of rhodoliths is removed from the beaches by tourists and locals which is a threat to these ecosystems, as the debris of dead rhodoliths contributes greatly to the sediments that form the contemporary beaches. Local authorities have been working against this trend and trying to return, whenever possible, all materials back to their place of origin. Large boards are displayed throughout the beaches explaining what these "popcorn" are and how their removal is forbidden, nevertheless the plundering is still very evident (Figure 11). We therefore urge the implementation of more protection and management efforts of the local rhodolith beds, and these should be regarded as ecosystem engineers that generate a complex habitat for a high biodiversity of species. For an effective conservation management, more detailed studies of the distribution, biodiversity and community structure of the Fuerteventura RBs beds are needed.

6 Conclusion

Foremost, this study contributes to the first analysis of species composition of the rhodoliths from the north shore of Fuerteventura Island and contributes to a better understanding of the distribution of taxa in different settings. Our results show that a beach deposit composed of stranded rhodoliths can accumulate up to 5000 rhodoliths/m^2. *Lithothamnion* cf. *corallioides* is the most common species detected in this study. It is also the most representative species from the sea bottom around the Canaries. Although present in the islands of Lanzarote, Gran Canaria and Tenerife the genus *Lithoporella* is a new record for the island of Fuerteventura. We believe that given the size of the rhodoliths (coarse sand) and their high degree of breakage found on the beaches, these were transported shoreward by stormy waves coming from the NW. This work contributes to a more detailed approach on the present knowledge of rhodoliths from Fuerteventura Island and offers a baseline for further investigation, namely on the role of rhodolith beds as key habitat providers in insular settings. Further field studies are necessary, however, to understand the in-place formation of rhodoliths beds and their associated flora and fauna.

Data availability statement

The raw data supporting the conclusions of this article will be made available by the authors, without undue reservation.

Author contributions

ACR and EM-G conceived the idea and conceptualized it. MEJ, MWR, and ACR contributed to sample collecting and processing. All authors contributed to the article and approved the submitted version.

Acknowledgments

This study was endeavoured by the 1st Workshop of Marine Palaeontology and Littoral Geology in Canary Islands: Fuerteventura (1° MPLG-F) led by E. Martín-González. We thank Alejandro de Vera, Sandra Kaiser and Gregor Rasser for help in field work; Scuba diving center Punta Amanay for assistance during the dives; and Christoph Wimmer-Pfeil (Staatlcihes Museum für Naturkunde Stuttgart, Germany) for thin sections preparation. We thank Ministerio de Agricultura, Pesca y Alimentacion (MAPAMA), Dirección General de Sostenibilidad de la Costa y del Mar y al Ministerio para la Transición Ecológica for bathymetry data from "Ecocartografías mapping Project" (https://www.miteco.gob.es/es/costas/temas/proteccion-costa/ecocartografias/default.aspx). ACR was supported by a Post-doctoral grant SFRH/BPD/117810/2016 from the Portuguese Science Foundation (FCT). CSM was supported by a PhD grant M3.1.a/F/100/2015 from The Regional Government of the Azores (FRCT). LB was supported by a PhD grant SFRH/BD/135918/2018 from the Portuguese Science Foundation (FCT). SPA acknowledges his "Investigador FCT" contract (IF/00465/2015), funded by FCT. This work was co-funded by the project NORTE-01-0246-FEDER-000063, supported by Norte Portugal Regional Operational Programme (NORTE2020), under the PORTUGAL 2020 Partnership Agreement, through the European Regional Development Fund (ERDF). The authors also would like to acknowledge research support from National Funds through FCT - Foundation for Science and Technology under the project UIDB/50027/2020 and through DRCT under the project ACORES-01-0145_FEDER-000078 - VRPROTO: Virtual Reality PROTOtype: the geological history of "Pedra-que-pica, and under DRCTM1.1.a/005/ 519 Funcionamento-C-/2016 (CIBIO-A) project.

Conflict of interest

The authors declare that the research was conducted in the absence of any commercial or financial relationships that could be construed as a potential conflict of interest.

Publisher's note

References

Acosta, J., Uchupi, E., Muñoz, A., Herranz, P., Palomo, C., Ballesteros, M.ZEE Working Group (2004). "Geologic evolution of the Canarian Islands of Lanzarote, Fuerteventura, Gran Canaria and La Gomera and comparison of landslides at these Islands with those at tenerife, La Palma and El Hierro," Marine Geophysical Researches 0, 1–38. doi: 10.1007/1-4020-4352-X_1

Adey, W. H., and McKibbin, D. (1970). Studies on the maerl species *Phymatolithon calcareum* (Pallas) nov. comb. and *Lithothamnion corallioides* crouan in the ria de vigo. *Botanica Marina* 13, 100–106.

Afonso-Carrillo, J. (2021). Las algas coralinas (Rhodophyta) ante la acidificación del océano con especial referencia a las islas canarias. *Rev. Scientia Insularum* 4, 145–204. doi: 10.25145/j.SI.2021.04.08

Afonso-Carrillo, J., and Gil-Rodríguez, M. C. (1982). Sobre la presencia de un fondo de "maerl" en Islas Canarias. *Collectanea Botanica* 13, 703–708.

Aguirre, J., Braga, J. C., and Bassi, D. (2017). "Rhodoliths and rhodolith beds in the rock record," in *Rhodolith/Maërl beds: a global perspective. coastal research library*, vol. vol. 15 . Eds. R. Riosmena-Rodríguez, W. Nelson and J. Aguirre (Cham: Springer). doi: 10.1007/978-3-319-29315-8_5

Ávila, S. P., Madeira, P., da Silva, C. M., Cachão, M., Landau, B., Quartau, R., et al. (2008). Local disappearance of bivalves in the Azores during the last glaciation. *J. Quaternary Sci.* 23, 777–785.

Ávila, S. P., Melo, C., Sá, N., Quartau, R., Rijsdijk, K., Ramalho, R. S., et al. (2019). Towards a "Sea-level sensitive marine Island biogeography" model: the impact of glacio-eustatic oscillations in global marine Island biogeographic patterns. *Biol. Rev.* 94 (3), 1116–1142.

Ávila, S. P., Melo, C., Silva, L., Ramalho, R., Quartau, R., Hipólito, A., et al. (2015a). A review of the MIS 5e highstand deposits from Santa Maria Island (Azores, NE atlantic): palaeobiodiversity, palaeoecology and palaeobiogeography. *Quaternary Sci. Rev.* 114, 126–148.

Ávila, S. P., Ramalho, R., Habermann, J., Quartau, R., Kroh, A., Berning, B., et al. (2015b). Palaeoecology, taphonomy, and preservation of a lower pliocene shell bed (coquina) from a volcanic oceanic Island (Santa Maria Island, Azores, NE Atlantic Ocean). *Palaeogeography Palaeoclimatology Palaeoecol.* 430, 57–73.

Azorin-Molina, C., Menendez, M., McVicar, T. R., Acevedo, A., Vicente-Serrano, S. M., Cuevas, E., et al. (2017). Wind speed variability over the Canary Islands 1948-2014: focusing on trend differences at the land-ocean interface and below-above the trade-wind inversion layer. *Climate Dynamics* 50, 4061–4081.

Basso, D., Babbini, L., Kaleb, S., Bracchi, V. A., and Falace, A. (2016). Monitoring deep Mediterranean rhodolith beds. *Aquat. Conservation: Mar. Freshw. Ecosyst.* 26, 549–561.

Bogaard, P. (2013). The origin of the Canary Island Seamount Province – new ages of old seamounts. *Sci. Rep.* 3, 2107.

Bosence, D. W. J. (1983). Coralline algae from the Miocene of Malta. *Paleontology* 26, 147–173.

Braga, J. C., Bosence, D. W. J., and Steneck, R. S. (1993). New anatomical characters in fossil coralline algae and their taxonomic implications. *Palaeontology* 36, 535–547.

Brandt, D. S. (1989). Taphonomic grades as a classification for fossiliferous assemblages and implications for paleoecology. *Palaios* 4, 303–309.

Cabioch, J. (1974). Un fond de maerl de l'Archipel de Madère et son peuplement végétal. *Bull. la Société Phycologique France* 19, 74–82.

Casillas, R., and Torres, J. M. (2011). *Inventario de recursos vulcanológicos de fuerteventura* (Cabildo de Fuerteventura), 155 p.

Coello, J., Cantagrel, J.-M., Hernán, F., Fúster, J.-M., Ibarrola, E., Ancochea, E., et al. (1992). Evolution of the eastern volcanic ridge of the Canary Islands based on new K-AR data. *J. Volcanology Geothermal Res.* 53, 251–274.

Cronquist, A. (1960). The divisions and classes of plants. *The Botanical Review* 26, 425–482.

Crouan, H. M., and Crouan, P. L. (1867). *Florule du Finistère*. F. Klincksieck, (Paris). x+262pp. doi: 10.5962/bhl.title.11601

Dias, G. T. M., and Villaça, R. C. (2012). Coralline algae depositional environments on the Brazilian Central-South-Eastern shelf. *J. Coast. Res.* 28, 270–279.

Foslie, M. (1908). Die Lithothamnien der Deutschen Südpolar-Expedition. *Deut. Süd. Exp. Botanik* (De Gruyter) 8, 205–220.

Foslie, M. (1909). "Algologiske notiser, VI." *Kongelige norske videnskabers selskabs skrifter*(De Gruyter), 1909 (2) , 1–63.

Foster, M., Amado-Filho, G. M., Kamenos, N. A., Riosmena-Rodríguez, R., and Steller, D. L. (2013). "Rhodoliths and rhodolith beds," in *Smithsonian Contributions to the marine sciences no. 39*. Ed. M. Lange (Smithsonian Institution), pp 143–pp 155. doi: 10.5479/si.1943667X.39

Foster, M., McConnico, L., Lundsten, L., Wadsworth, T., Kimball, T., Brooks, L., et al. (2007). The diversity and natural history of *Lithothamnion muelleri* - *Sargassum horridum* community in the Gulf of California. *Cienc. Marinas* 33, 367–384.

Fredericq, S., Krayesky-Self, S., Sauvage, T., Richards, J., Kittle, R., Arakaki, N., et al. (2019). The critical importance of rhodoliths in the life cycle completion of both macro- and microalgae, and as holobionts for the establishment and maintenance of marine biodiversity. *Front. Mar. Sci.* 5. doi: 10.3389/fmars.2018.00502

Freitas, R., Romeiras, M., Silva, L., Cordeiro, R., Madeira, P., González, J. A., et al. (2019). Restructuring of the "Macaronesia" biogeographic unit: a marine multi-taxon biogeographical approach. *Sci. Rep.* 9, 15792. doi: 10.1038/s41598-019-51786-6

Gonçalves, M., Martinho, P., and Guedes Soares, C. (2020). Wave energy assessment based on a 33-year hindcast for the Canary Islands. *Renewable Energy* 152, 259–269.

Gray, J.E. (1864). *Handbook of British water-weeds or algae*. R. Hardwicke, (London), 123 .

Guiry, M. D., and Guiry, G. M. (2022). *World-wide electronic publication* (Galway: National University of Ireland). Available at: https://www.algaebase.org. 21st of February, 2022.

Haroun, R. J., Gil-Rodríguez, M. C., Díaz de Castro, J., and Prud'homme van Reine, W. F. (2002). A checklist of the marine plants from the Canary Islands (central eastern Atlantic Ocean). *Botanica Marina* 45, 139–169.

Hernández-Kantún, J. J., Hall-Spencer, J. M., Grall, J., Adey, W., Rindi, F., Maggs, C. A., et al. (2017). "North Atlantic rhodolith beds," in *Rhodolith/Maërl beds: a global perspective. coastal research library*, vol. vol. 15 . Eds. R. Riosmena-Rodríguez, W. Nelson and J. Aguirre (Cham: Springer). doi: 10.1007/978-3-319-29315-8_10

Hrabovský, J., Basso, D., and Doláková, N. (2016). Diagnostic characters in fossil coralline algae (Corallinophycidae: Rhodophyta) from the Miocene of southern Moravia (Carpathian Foredeep, Czech Replubic). *J. Systematic Palaeontology* 14, 499–525.

Irvine, L. M., and Chamberlain, Y. M. (1994). "Seaweeds of the British Isles," in *Rhodophyta, part 2B corallinales, hildenbrandiales*, vol. vol. 1. (London: HMSO), 276 pp.

Ishijima, W. (1933). On three species of corallinaceae lately obtained from the Megamiyama Limestone, Sagara District, Prov. *Totomi Japan. Japanese J. Geology Geogr.* 11, 27–30.

Ishijima, W. (1938). New species of calcareous algae from several Tertiary and later limestones from various localities of the Ryukyu Islands. *Japanese J. Geology Geogr.* 15, 13–16.

John, D. M., Prud'homme van Reine, W. F., Lawson, G. W., Kostermans, T. B., and Price, J. H. (2004). A taxonomic and geographical catalogue of the seaweeds of the western coast of Africa and adjacent Islands. *Beihefte zur Nova Hedwigia* 127, 1–339.

Johnson, M. E., Baarli, B. G., Cachão, M., da Silva, C. M., Ledesma-Vázquez, J., Mayoral, E. J., et al. (2012). Rhodoliths, uniformitarianism, and Darwin: Pleistocene and Recent carbonate deposits in the Cape Verde and canary Archipelagos. *Palaeogeography Palaeoclimatology Palaeoeology* 329-330, 83–100.

Johnson, M. E., Baarli, B. G., da Silva, C. M., Cachão, M., Ramalho, R. S., Ledesma-Vázquez, J., et al. (2013). Coastal dunes with high content of rhodolith (coralline red algae) bioclasts: Pleistocene formations on Maio and São Nicolau in the Cape Verde Archipelago. *Aeolian Res.* 8, 1–9.

Johnson, M. E., Uchman, A., Costa, P. J. M., Ramalho, R. S., and Ávila, S. P. (2017a). Intense hurricane transport sand onshore: example from the Pliocene Malbusca section on Santa Maria Island (Azores, Portugal). *Mar. Geology* 385, 244–249. doi: 10.1016/j.margeo.2017.02.002

Johnson, M. E., Ledesma-Vázquez, J., Ramalho, R. S., da Silva, C. M., Rebelo, A. C., Santos, A., et al. (2017b). "Taphonomic range and sedimentary dynamics of modern and fossil rhodolith beds: Macaronesian realm (North Atlantic Ocean)," in *Rhodolith/Maërl beds: A global perspective. coastal research library*, vol. 15 . Eds. R. Riosmena-Rodríguez, W. Nelson and J. Aguirre (Springer), 368 p. doi: 10.1007/978-3-319-29315-8_9

Kato, A, Baba, M., and Suda, S. (2011). Revision of the Mastophoroideae (Corallinales, Rhodophyta) and polyphyly in nongeniculate species widely distributed on Pacific coral reefs. *Journal of Phycology* 47 (3), 662–672.

Le Gall, L., and Saunders, G. W. (2007). A nuclear phylogeny of the Florideophyceae (Rhodophyta) inferred from combined EF2, small subunit and large subunit ribosomal DNA: establishing the new red algal subclass Corallinophycidae. *Molecular Phylogenetics and Evolution* 43, 1118–1130.

Martin, C. S., Giannoulaki, M., De Leo, F., Scardi, M., Salomidi, M., Knittweis, L., et al. (2014). Coralligenous and maërl habitats: predictive modelling to identify their spatial distributions across the Mediterranean Sea. *Sci. Rep.* 4, 5073. doi: 10.1038/srep05073

Masselink, G., Hughes, M., Knight, J., and Houser, C. (2011). "Sediments, boundary layers and transport," in *Introduction to coastal processes and geomorphology*. Eds. R. Davidson-Arnott and B. Bauer (Cambridge University Press).

Meireles, R. P., Quartau, R., Ramalho, R., Madeira, J., Rebelo, A. C., Zanon, V., et al. (2013). Depositional processes on oceanic Island shelves – evidence from storm-generated neogene deposits from the mid-north Atlantic. *Sedimentology* 60, 1769–1785.

Mendoza, M. L., and Cabioch, J. (1998). Étude comparée de la reproduction de *Phymatolithon calcareum* (Pallas) adey & McKibbin et *Lithothamnion coralliodes* (P. & H. Crouan) P. & H. Crouan (Corallinales, Rhodophyta), et reconsidérations sur la définition des genres. *Can. J. Bot.* 76, 1433–1445.

Nelson, W. A., Sutherland, J. E., Farr, T. J., Hart, D. R., Neill, K. F., Kim, H. J., and Yoon, H. S. (2015). Multi-gene phylogenetic analyses of New Zealand coralline algae: Corallinapetra Novaezelandiae gen. et sp. nov. and recognition of the Hapalidiales ord. nov. *Journal of Phycology* 51 (3), 454–468.

Otero-Ferrer, F., Cosme, M., Tuya, F., Espino, F., and Haroun, R. (2020). Effect of depth and seasonality on the functioning of rhodolith seabeds. *Estuarine Coast. Shelf Sci* 235, 106579. doi: 10.1016/j.ecss.2019.106579

Pardo, C., López, L., Peña, V., Hernández-Kantún, J. J., Le Gall, L., Bárbara, I., et al. (2014). A multilocus species delimitation reveals a striking number of maërl species in the OSPAR region. *PloS One* 9, e104073.

Prud'homme van Reine, W. F., Haroun, R. J., and Kostermans, L. B. T. (2005). "Checklists on seaweeds in the Atlantic Ocean and in the Cape Verde Archipelago," in *IV simpósio fauna e flora das ilhas atlânticas, Praia 9-13 setembro 2002* (Praia, Ilha de Santiago, República de Cabo Verde: Ministério do Ambiente, Agricultura e Pescas), 13–26.

Quartau, R., Madeira, J., Mitchell, N. C., Tempera, F., Silva, P. F., and Brandão, F. (2016). Reply to comment by Marques et al. on "The insular shelves of the Faial-Pico Ridge (Azores Archipelago): A morphological record of its evolution". *Geochemistry Geophysics Geosystems* 17, 633–641.

Quartau, R., Tempera, F., Mitchell, N. C., Pinheiro, L. M., Duarte, H., Brito, P. O., et al. (2012). Morphology of the Faial Island shelf (Azores): The interplay between volcanic, erosional, depositional, tectonic and mass-wasting processes. *Geochemistry Geophysics Geosystems* 13, Q04012. doi: 10.1029/2011GC003987

Quartau, R., Trenhaile, A. S., Mitchell, N. C., and Tempera, F. (2010). Development of volcanic insular shelves: Insights from observations and modelling of Faial Island in the Azores Archipelago. *Mar. Geology* 275, 66–83.

Ramalho, R. S., Quartau, R., Trenhaile, A. S., Mitchell, N. C., Woodroffe, C. D., and Ávila, S. P. (2013). Coastal evolution on volcanic oceanic Islands: A complex interplay between volcanism, erosion, sedimentation, sea-level change and biogenic production. *Earth-Science Rev.* 127, 140–170.

Rasser, M. W., and Piller, W. E. (1999). Application of neontological taxonomic concepts to late Eocene Alpine Foreland Basin in Upper Austria: component analysis, facies, and palecology. *Facies* 42, 59–92.

Rebelo, A. C., Johnson, M. E., Quartau, R., Rasser, M. W., Melo, C. S., Neto, A. I., et al. (2018). Modern rhodoliths from the insular shelf of Pico in the Azores (Northeast Atlantic Ocean). *Estuarine Coast. Shelf Sci.* 210, 7–17.

Rebelo, A. C., Johnson, M. E., Rasser, M. W., Silva, L., Melo, C. S., and Ávila, S. P. (2021). Global biodiversity and biogeography of rhodolith-forming species. *Front. Biogeography* 13 (1), e50646. doi: 10.21425/F5FBG50646

Rebelo, A. C., Rasser, M. W., Kroh, A., Johnson, M. E., Ramalho, R. S., Melo, C., et al. (2016). Rocking around a volcanic Island shelf: Pliocene rhodolith beds from

Malbusca, Santa Maria Island (Azores, NE Atlantic). *Facies* 62, 22. doi: 10.1007/s10347-016-0473-9

Reyes, J., Sansón, M., and Afonso-Carrillo, J. (2005). *Flora y vegetaciòn marina. Algas y sebas. Patrimonio natural de la isla de Fuerteventura, Cabildo de Fuerteventura*. Ed. O. Rodríguez Delgado (Tenerife: Gobierno de Canarias y Centro de la Cultura Popular Canaria), 117–140.

Riosmena-Rodríguez, R. (2017). "Natural history of rhodolith/maërl beds: their role in near-shore biodiversity and management," in *Rhodolith/maërl beds: a global perspective*. Eds. R. Riosmena-Rodríguez, W. Nelson and J. Aguirre (Cham: Coastal Research Library, Springer), 3–26. doi: 10.1007/978-3-319-29315-8_1

Rodriguez-Martin, J., Cruz-Perez, N., and Santamarta, J. C. (2022). Maritime climate in the Canary Islands and its implications for the construction of coastal infrastructures. *Civil Eng. Journal-Tehran* 8, 24–32.

Roettig, C. B., Kolb, T., Wolf, D., Baumgart, P., Richter, C., Schleicher, A., et al. (2017). Complexity of Quaternary aeolian dynamics (Canary Islands). *Palaeogeography Palaeoclimatology Palaeoecol.* 472, 146–162.

Roettig, C. B., Kolb, T., Zöller, L., Zech, M., and Faust, D. (2020). A detailed chrono-stratigraphical record of canarian dune archives - interplay of sand supply and volcanism. *J. Arid Environments* 183, 104240.

Rosas-Alquicira, E. F., Riosmena-Rodríguez, R., Couto, R. P., and Neto, A. I. (2009). New additions to the Azorean algal flora, with ecological observations on rhodolith formations. *Cahiers Biologie Mar.* 50, 143–151.

Rusu, E., and Onea, F. (2016). Estimation of the wave energy conversion efficiency in the Atlantic Ocean close to the European Islands. *Renewable Energy* 85, 687–703.

Sañé, E., Chiocci, F. L., Basso, D., and Martorelli, E. (2016). Environmental factors controlling the distribution of rhodoliths: An integrated study based on seafloor sampling, ROV and side scan sonar data, offshore the W-Pontine Archipelago. *Continental Shelf Res.* 129, 10–22.

Sciberras, M., Rizzo, M., Mifsud, J. R., Camilleri, K., Borg, J. A., Lanfranco, E., et al. (2009). Habitat structure and biological characteristics of a maerl bed off the northeastern coast of the Maltese Islands (central Mediterranean). *Mar. Biodiversity* 39, 251–264.

Setchell, W. A. (1943). Mastophora and the Mastophoreae: genus and subfamily of Corallinaceae. *Proceedings of the National Academy of Science of the United States of America* 29, 127–135.

Sewell, A. A., Johnson, M. E., Backus, D. H., and Ledesma-Vázquez, J. (2007). Rhodolith detritus impounded by a coastal dune on Isla Coronados, Gulf of California. *Cienc. Marinas* 33, 483–494.

Silva, P. C., Basson, P. W., and Moe, R. L. (1996). *Catalogue of the benthic marine algae of the Indian ocean* Vol. 79 (University of California Publications in Botany), 1–1259.

Silva, P. C., Meñez, E. G., and Moe, R. L. (1987). Catalog of the benthic marine algae of the Philippines. *Smithsonian Contributions to Mar. Sci.* 27, 1–179. doi: 10.5479/si.1943667X.27.1

Silva, P. C., and Johansen, H. W. (1986). A reappraisal of the order Corallinales (Rhodophyceae). *British Phycological Journal* 21, 245–254.

Spalding, M. D., Fox, H. E., Allen, G. R., Davidson, N., Ferdaña, Z. A., Finlayson, M., et al. (2007). Marine ecoregions of the world: A bioregionalization of coastal and shelf areas. *BioScience* 57, 573–583.

Steiner, C., Hobson, A., Favre, P., Stampfli, G. M., and Hernandez, J. (1998). Mesozoic sequence of Fuerteventura (Canary Islands): Witness of Early Jurassic sea-floor spreading in the central Atlantic. *Geological Society of America Bulletin* 110 (10), 1304–1317.

Steller, D. L., Riosmena-Rodríguez, R., Foster, M., and Roberts, C. (2003). Rhodolith bed diversity in the Gulf of California: the importance of rhodolith structure and consequences of disturbance. *Aquat. Conservation: Mar. Freshw. Ecosyst.* 13, S5–S20.

Stelzer, P. S., Mazzuco, A. C. A., Gomes, L. E., Martins, J., Netto, S., and Bernardino, A. F. (2021). "Taxonomic and functional diversity of benthic macrofauna associated with rhodolith beds in SE Brazil," in *PeerJ* 9, e11903. doi: 10.7717/peerj.11903

Stillman, C. J. (1999). Giant Miocene landslides and the evolution of Fuerteventura, Canary Islands. *J. Volcanology Geothermal Res.* 94, 89–104.

Taylor, W. R. (1960). *Marine algae of the eastern tropical and subtropical coasts of the americas* (Ann Arbor: The University of Michigan Press), 870 pp.

Teichert, S. (2014). Hollow rhodoliths increase Svalbard's shelf biodiversity. *Sci. Rep.* 4, 6972. doi: 10.1038/srep06972

Townsend, R. A., and Huisman, J. M. (2018) Coralline algae. In: *Algae of Australia. Marine benthic algae of north-western Australia. 2. Red Algae*. Ed. Huisman, J.M. (Canberra: CSIRO Publishing), 86–146.

Troll, V. R., and Carracedo, J. C. (2016). *The geology of the Canary Islands* (Elsevier), 621 pp. doi: 10.1016/C2015-0-04268-X

Wettstein, R. R. (1901). *Handuch der systematischen Botanik*. (Deuticke, Leipzig) 1, 201

Wilson, S., Blake, C., Berges, J. A., and Maggs, C. (2004). Environmental tolerances of free-living coralline algae (maerl): implications for European marine conservation. *Biol. Conserv.* 120, 279–289.

Woelkerling, W. J., Irvine, L. M., and Harvey, A. S. (1993). Growth-forms in non-geniculate coralline red algae (Corallines, Rhodophyta). *Aust. Systematical Bot.* 6, 277–293.

Womersley, H. B. S., and Bailey, A. (1970). Marine algae of the Solomon Islands. *Philos. Trans. R. Soc. London B. Biol. Sci.* 259, 257–352.

Wynne, M. J. (2017). A checklist of benthic marine algae of the tropical and subtropical western Atlantic: fourth revision. *Nova Hedwigia Beiheft* 145, 1–202.

Zhao, Z., Mitchell, N. C., Quartau, R., Moreira, S., Rusu, L., Melo, C., et al. (2022). Wave influenced deposition of carbonate-rich sediment on the insular shelf of Santa Maria Island, Azores. *Sedimentology* 69, 1547–1572. doi: 10.1111/sed.12963

Frontiers in Earth Science

Investigates the processes operating within the major spheres of our planet

Advances our understanding across the earth sciences, providing a theoretical background for better use of our planet's resources and equipping us to face major environmental challenges.

Discover the latest Research Topics

See more →

Frontiers

Avenue du Tribunal-Fédéral 34
1005 Lausanne, Switzerland
frontiersin.org

Contact us

+41 (0)21 510 17 00
frontiersin.org/about/contact